The Pennsylvania State University

The Graduate School

Department of Biochemistry and Molecular Biology

CHARACTERIZATION AND MECHANISTIC STUDIES OF *ESCHERICHIA COLI* LIPOYL SYNTHASE: A MEMBER OF THE "RADICAL SAM" FAMILY OF ENZYMES

A Thesis in

Biochemistry and Molecular Biology

by

Robert M. Cicchillo

Submitted in Partial Fulfillment
of the Requirements
for the Degree of

Doctor of Philosophy

December 2006

The thesis of Robert M. Cicchillo was reviewed and approved* by the following:

Squire J. Booker
Associate Professor of Biochemistry and Molecular Biology
Thesis Advisor
Chair of Committee

Joseph M. Bollinger
Associate Professor of Biochemistry and Molecular Biology
Associate Professor of Chemistry

Carsten Krebs
Assistant Professor of Biochemistry and Molecular Biology
Assistant Professor of Chemistry

Ming Tien
Professor of Biochemistry and Molecular Biology

Michael T. Green
Assistant Professor of Chemistry

Robert A. Schlegel
Professor of Biochemistry and Molecular Biology
Head of the Department of Biochemistry and Molecular Biology

*Signatures are on file in the Graduate School

ABSTRACT

Lipoic acid (6,8-thioctic acid) is an essential cofactor in several multienzyme complexes that are involved in energy metabolism, such as the pyruvate dehydrogenase complex, the 2-oxoketoglutarate dehydrogenase complex, the branched-chain oxo-acid dehydrogenase complex, and the glycine cleavage system. The biosynthesis of this cofactor involves the insertion of two sulfur atoms into two completely unactivated carbon atoms of protein bound octanoyl groups. Lipoyl synthase, the protein thought to catalyze sulfur insertion, has been cloned and purified by immobilized metal affinity chromatography. Indeed, lipoyl synthase belongs to a superfamily of enzymes that use S-adenosyl-L-methionine (AdoMet) and iron sulfur clusters to generate high-energy carbon-centered radicals that are intermediates in catalysis. Proteins that are members of this superfamily have a conserved iron sulfur cluster-binding motif arranged in a CX_3CX_2C configuration. Lipoyl synthase deviates from other members in this class in that it contains an additional cysteine-rich motif (CX_4CX_5C). We have shown, through site-directed mutagenesis, UV-visible spectroscopy, EPR spectroscopy, and Mössbauer spectroscopy, that the active enzyme contains two [4Fe-4S] clusters that are coordinated by the cysteines that lie within these two motifs. We have also demonstrated that the synthesis of one molecule of lipoic acid requires the consumption of two equivalents of AdoMet. Consistent with this premise, we have provided evidence for hydrogen atom abstraction by a 5'-deoxyadenosyl radical. Substitution of unlabeled substrate with deuterated substrate allowed for the detection of 5'-dA with one deuterium at position five. Recently we have obtained experimental evidence through isotope labeling studies

that the sulfur atoms inserted into protein-bound octanoyl groups derive from lipoyl synthase itself.

In vitro studies using deuterated substrates have shown that thiolation at C-6 precedes thiolation at C-8. Quantification of 5'-dA over time has allowed for the determination of the rate constants associated with hydrogen atom abstraction and subsequent sulfur insertion. Sulfur insertion at C-6 proceeds with a rate constant of 0.250 ± 0.009 min^{-1} while insertion at C-8 follows at 0.096 ± 0.018 min^{-1}.

TABLE OF CONTENTS

LIST OF FIGURES

LIST OF TABLES

ACKNOWLEDGEMENTS

I would like to start off by thanking my family for whom this dissertation is dedicated to (Mom, Dad, Lisa and Paul, and Grandparents, Bill and Mary Alice Wood and Alexander and Florence Cicchillo). This achievement would not have been possible without their unconditional love and support for me. I would like to thank God for giving me the strength to persevere and accomplish the various goals throughout my life. I would also like to thank my high school chemistry teacher Mr. Thomas Voitus for sparking my enthusiasm in science especially chemistry. I would like to acknowledge Mr. David Deibel for his friendship and encouragement to pursue a Masters degree in chemistry at Youngstown State University. A special thanks to Dr. Peter Norris, my Masters degree mentor, for believing in my ability and supporting me during my graduate studies. It was through his teaching ability and guidance (disciplinary actions) that facilitated my acceptance into Ph.D. school. I would especially like to thank Dr. Brian Scott Freeze for being my best friend and colleague (now). Scott has always been one of my greatest supporters and truly has defined the meaning of best friend. I would like to thank all of my friends who have been along for the ride, Dr. Anthony Rozzo, Dr. Tom Zak, Dr. Danny Yun, Dr. Lana Salah, David Coehlo, Jocelyn Edathil (M.D./Ph.D. soon), Dr. Michael T. Green, Rachel Behan (Dr. to be), Keri and David Stone, John and Anita Novosel, Brian P. Voitus, Brian and Marcy Barnes, the Costello family, and the Minchin family. I would like to thank Dr. Natasha Nesbitt, my labmate at PSU, for being supportive when things looked gloomy in State College (you are free now). I would especially like to thank Dr. David Iwig and Cindy Iwig for providing me a home away

from home at Penn State, also the newest addition to the Iwig family little Grace. Dave and I entered and exited Penn State almost simultaneously. I hope that Dave can say I helped him as much as he helped me-that would be a tremendous feat-thanks Dave. I would like to acknowledge the members of my Ph.D. committee, Dr. Joseph Marty Bollinger, Dr. Carsten Krebs, Dr. Michael T. Green, and Dr. Ming Tien for their support throughout the entire process especially at the end. I would also like to thank Carsten and Marty for not only being outstanding mentors but for also being great friends (you too Ava). I would like to thank a very special person in my life Dr. Maria R. Manzoni whose unconditional love and support has enabled me to achieve in the most difficult times-especially the last two years-thanks Maria-love you. Finally, thanks to my Ph.D. advisor Dr. Squire J. Booker for whom all of the work in my dissertation is attributed to. You have enabled me to think scientifically in a way that I never thought I could. Your vast knowledge in almost every aspect of science has been an invaluable tool in the mentoring process. I feel privileged to have worked in your lab. Thanks for being a great friend in tough times.

Chapter 1

Introduction

α-Lipoic acid (1,2-dithiolane-3-pentanoic acid or thioctic acid) is an essential sulfur-containing metabolic cofactor that is required for the activity of several multienzyme complexes that are involved in energy metabolism [1]. It is an eight carbon fatty acid with sulfur atoms at positions C6 and C8 (Figure 1.1A**)**. The sulfurs at these positions participate in a redox cycle consisting of the reduced (dihydrolipoyl) and oxidized (disulfide containing) forms (Figure 1.1B). When oxidized, a unique 1,2-dithiolane ring is formed, which serves as the biologically active electron acceptor during oxidative decarboxylation reactions.

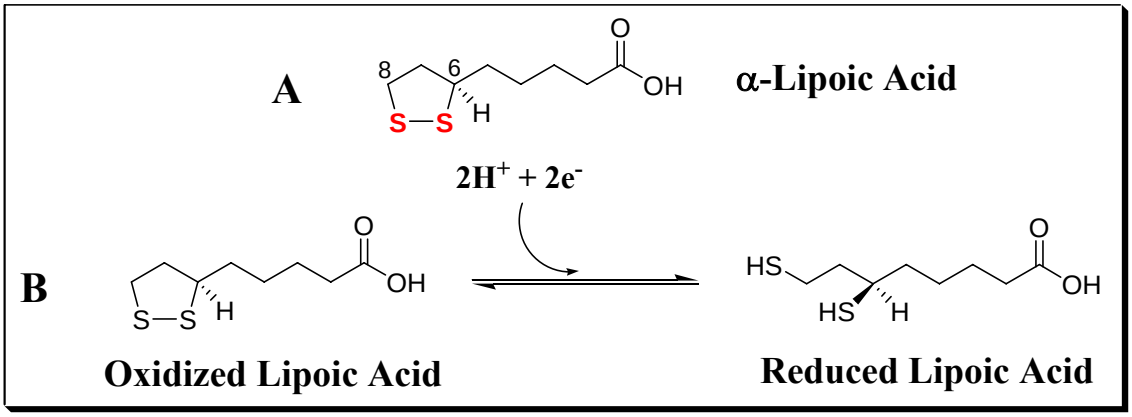

Figure 1.1: α-Lipoic acid (A). Redox cycling of the 1,2-dithiolane ring (B).

1.1 Acetate Replacing Factor: Discovery of Lipoic Acid

Lipoic acid was initially discovered in the latter part of the 1940s by several independent laboratories. In early studies the cofactor had been deemed "acetate-replacing factor," because it aided bacterial growth in organisms such as *Lactobacillus acidophilus*, which could not survive under conditions devoid of acetate [2]. Other laboratories had demonstrated the necessity of lipoic acid for the oxidation of pyruvate to acetate and carbon dioxide, which led to another trivial name, "pyruvate oxidation factor" [3]. The combined efforts of Lester Reed and the Eli Lilly industrial group led to the first isolation of crystalline acetate-replacing/pyruvate oxidation factor in the early 1950s. Astonishingly, it was estimated that 10 tons of beef liver residue led to the purification of 30 mg of crystalline lipoic acid [4]. Distinct physical characteristics, such as solubility in fat solvents, acidity, and involvement in the formation of acetate through the oxidative decarboxylation of pyruvate, led to the naming of the compound as "α-lipoic acid" [5].

Molecular and structural information on the yellow crystals immediately followed. Initial examination of the cofactor gave positive results for sulfide, while a nitroprusside assay for disulfides was negative. Treatment with sodium cyanide resulted in a positive nitroprusside test, indicating the presence of a disulfide [4, 6]. The molecular formula, $C_8H_{14}O_2S_2$, was determined by elemental analysis and electrochemical titration experiments. A titratable group having a pK_a of 4.76 was also observed, corresponding to an aliphatic carboxyl group that is separated from any unsaturation or polar groups by at least two methylene groups. X-ray data along with infrared spectroscopy and polarographic studies revealed that lipoic acid behaves similarly to an aliphatic chain containing a cyclic disulfide. Treatment of the lipoic acid

with raney nickel, a desulfurating metal, yielded n-caprylic acid (octanoic acid). The above data seemed to be consistent with a cyclic disulfide that was derived from 4,8-, 5,8-, or 6,8-, dimercapto-*n*-caprylic acid [4]. The chemical nature of the biologically active cofactor was confirmed by comparisons to a chemically synthesized thioctic acid racemate [7]. The 1,2-dithiolane ring or 5-membered cyclic disulfide of lipoic acid has been observed in the UV-visible region, having an absorption maxima at 330 nm with a molar extinction coefficient of ~ 150 M^{-1} cm^{-1} [8].

α-Lipoic acid has one chiral center, located at carbon six. Synthesis of the optical isomers, (±)-α-lipoic acid, was first achieved at Merck and Co. and facilitated the determination of the absolute configuration at this carbon by Mislow in 1956 [9, 10]. Direct comparisons of certain physical properties of 3-(±)-thioloctanedioic acids to those of known (±)-methyloctanedioic acids were used to provide insight into the stereochemistry of (±)-lipoic acid. Previous work had shown that the physical characteristics of sulfhydryl derivatives behave isomorphously to those of the methyl derivatives [11].

1.2 Nature of Protein-Bound Lipoate and Lipoyl-Dependent Complexes

Lipoic acid is found in most prokaryotic and eukaryotic organisms, where it functions in the oxidative decarboxylation of various α-ketoacids and in glycine catabolism. The pyruvate dehydrogenase complex (PDC) has served as a paradigm in studies on multienzyme complexes that use lipoic acid in catalysis, but it is also ubiquitous in the α-ketoglutarate dehydrogenase (KDC), branched-chain 2-oxo-acid dehydrogenase (BCODC), and acetoin dehydrogenase (ADC) complexes as well as the glycine cleavage system (GCS) [12, 13]. The first three complexes are all involved in the

oxidative decarboxylation of α-keto acids to their appropriate products while the glycine cleavage system catalyzes the conversion of glycine to ammonia and carbon dioxide with concomitant transfer of the α-carbon to tetrahydrofolate (THF), yielding N^5, N^{10}-methylene tetrahydrofolate [13].

The essential physiological role of lipoic acid was first demonstrated in experiments observing the catabolism of α-ketobutyrate, β-methyl-α-ketobutyrate, and β-methyl-α-ketovalerate in *Streptococcus faecalis* cells that were grown on medium lacking lipoic acid [14, 15]. These studies revealed that the "pyruvate oxidation factor" or lipoic acid was required for decarboxylation of pyruvate. It also appeared that the complexes involved in oxidative decarboxylation contained a noticeable amount of "bound" lipoate [15, 16]. Evidence for a participating lipoyl cofactor was further substantiated by utilizing the enzyme lipoamidase, which cleaves the amide bond created between the carboxylate moiety of lipoic acid and the epsilon amino group of a lysine residue, liberating free lipoate [17, 18]. Inactivation and loss of decarboxylation activity was observed upon treatment with lipoamidase [19]. The activity was only restored when the complex was treated with lipoate, ATP, and "lipoic acid activating-system".

Incorporation of $^{35}S_2$-lipoic acid into the pyruvate dehydrogenase complex and the α-ketoglutarate dehydrogenase complex has provided further insight into the exact structure of the tethered lipoyl group. The radioactively labeled complexes were oxidized with performic acid and partially hydrolyzed with hydrochloric acid for 3 hours at 105 ^{o}C. The hydrolysates were treated with ninhydrin and compared to synthetic standards. The radioactive compound was shown to be N^{ϵ}-(6,8-disulfooctanoyl)-L-lysine, confirming the presence of a covalent lipoylysine group in the complexes [20, 21].

In its functional form, lipoic acid is always tethered covalently in an amide linkage *via* its carboxylate moiety to the ε-amino group of a conserved lysine residue located on a specific protein component of one the previously mentioned complexes [22]. The bound lipoyl group creates a long (14 Å) flexible swinging arm that facilitates the shuttling of intermediates between successive active sites (Figure 1.2) [1]. The transfer of the intermediates through these complexes is concomitant with the reduction of the disulfide bond of the lipoyl-cofactor. The reduced cofactor is subsequently reoxidized by a flavin-dependent dehydrogenase, which enables the complex to perform multiple turnovers.

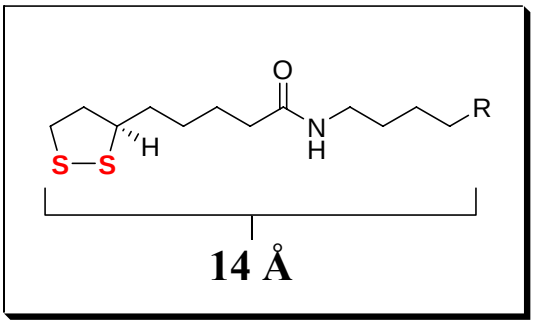

Figure 1.2: Functional form of lipoic acid as a bound lipoylysine group.

Pyruvate Dehydrogenase, α-Ketoglutarate Dehydrogenase, and Acetoin Dehydrogenase Complexes

Pyruvate is oxidatively decarboxylated to an essential metabolic intermediate, acetyl-CoA, which is shuttled into the citric acid cycle and is also used in fatty acid

biosynthesis. The function of the bound lipoyl cofactor has been rigorously dissected by many laboratories [19] [23-25]. The PDC contains three major subunits E1, E2, and E3, which catalyze the conversion of pyruvate to CO_2 and acetyl-CoA (Figure 1.3). The individual subunits are present in multiple copies, giving rise to one very large complex once assembled (~5-14 MDa). The E1 protein, a thiamine pyrophosphate (TPP)-dependent enzyme, catalyzes two distinct reactions; the first is the decarboxylation of pyruvate and the second is the transfer of the hydroxyethyl group to the lipoyl cofactor, forming a thioacetyl intermediate. The lipoyl appendage, as previously mentioned, is covalently attached to a conserved lysine residue contained within the E2 subunit (dihydrolipoyl acetyltransferase). The E2 subunit catalyzes a transthioesterification between the modified lipoyl group and CoA, forming acetyl-CoA. The resulting dihydrolipoyl group is reoxidized to its functional form by E3, a flavin adenine dinucleotide (FAD) containing dihydrolipoyl dehydrogenase (Figure 1.3) [26, 27].

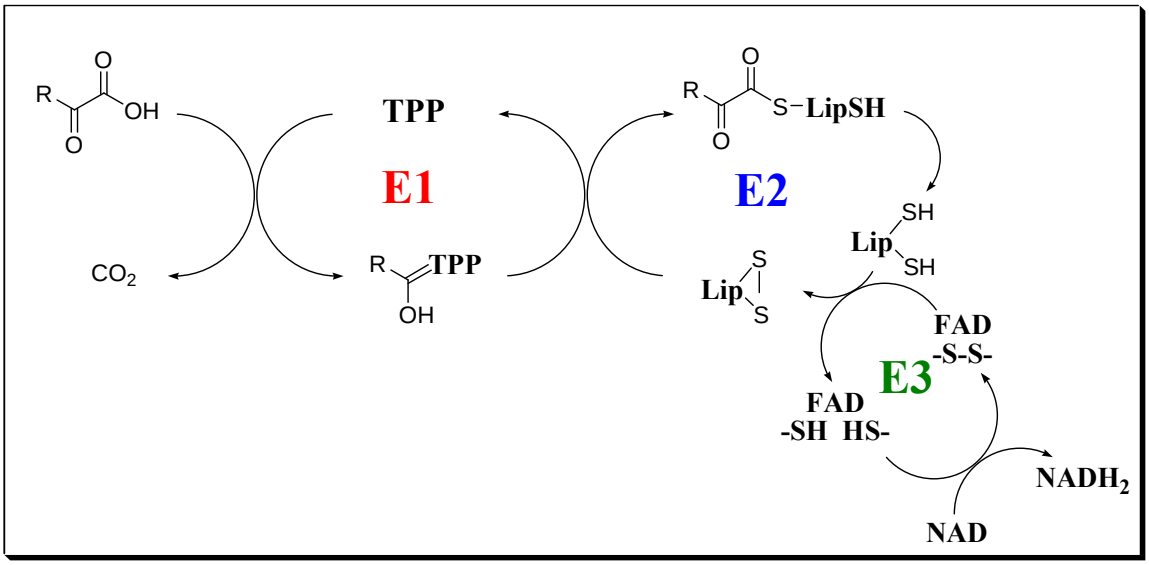

Figure 1.3: General reaction scheme for the PDC, KDC, BCODC, and ADC.

The α-ketoglutarate dehydrogenase complex catalyzes the conversion of α-ketoglutarate to succinyl-CoA and carbon dioxide, one of the reactions of the citric acid cycle. The subunits of the KDC parallel those of the PDC wherein three major components are required for a functional complex. The E3 components of the PDC and the KDC are identical and are encoded by the same gene whereas E1 and E2 of the KDC are encoded by different genes whose protein products have essentially the same function as their homologues in the PDC.

Acetoin dehydrogenase is another multienzyme complex that requires the lipoyl cofactor. Certain bacteria can utilize acetoin (3-hydroxy-2-butanone) as an alternative carbon source, converting it into acetaldehyde and acetyl-CoA. Genes that encode homologues to E1, E2, and E3 of the PDC and KDC are typically expressed when these bacteria are grown in media containing acetoin. Similarly to the PDC and KDC, E1 is a TPP-dependent acetoin dehydrogenase, E2 is a dihydrolipoamide acetyltransferase, and E3 is a dihydrolipoamide dehydrogenase [28, 29].

Glycine Cleavage System

Unlike the PDC and KDC complexes, the glycine cleavage system is composed of loosely associated proteins that require a lipoyl cofactor in catalysis. The GCS is found in a broad spectrum of organisms, ranging from bacteria and fungi to plants and mammals [30-32]. Early studies on the anaerobic bacteria *Diplococcus glycinophilus* and *Peptococcus glycinophilus* provided insight into the catabolism of glycine catalyzed by the GCS. Four proteins (P, H, T, and L) were identified that are absolutely required for the reversible transformation of glycine to ammonia, carbon dioxide, and N^5, N^{10}-

methylene tetrahydrofolate (Figure 1.4) [33-36]. The P-protein binds a pyridoxal-5'-phosphate (PLP) cofactor and catalyzes the decarboxylation of glycine [37, 38]. The remaining aminomethylene moiety is then transferred to one of the sulfur atoms on the lipoyl cofactor, which is attached to a lysine residue on the H-protein [39-43]. The T-protein catalyzes the scission of the C-N bond, liberating ammonia with concomitant transfer of the methylene group (α-carbon of glycine) to tetrahydrofolate producing N^5, N^{10}-methylene tetrahydrofolate, which plays a key role in one carbon metabolism in the cell [41, 44]. Finally the reoxidation of the lipoyl cofactor is catalyzed by the FAD-dependent L-protein (lipoyl dehydrogenase) [35]. This is accomplished *via* a disulfide exchange reaction similar to the one that occurs between the E2 and the E3 subunits of the PDC, with reoxidation of the FAD-dependent subunit by NAD^+.

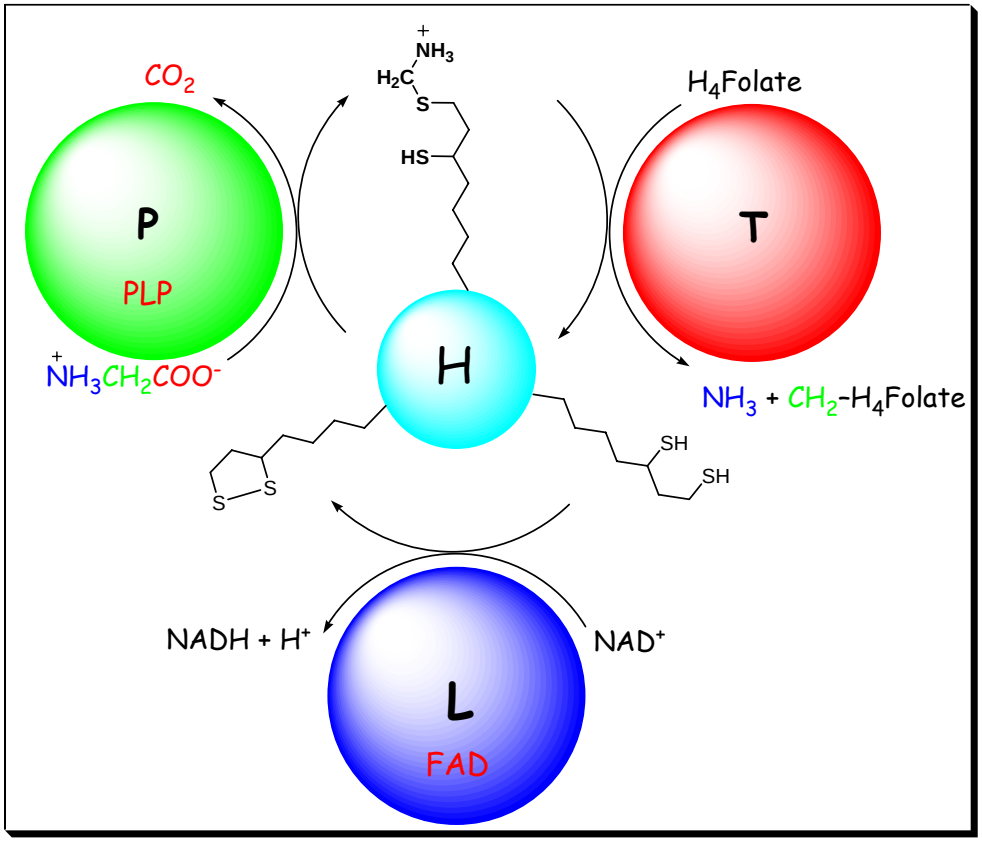

Figure 1.4: Reaction scheme for the glycine cleavage system.

1.3 Post-translational Modification of Proteins with Lipoic Acid

The mechanisms by which proteins are modified with exogenous lipoic acid have recently begun to be illuminated. The pathways of lipoylation in bacteria and plants appear to be similar, while those in mammals are slightly different. Mammals have a lipoate activating enzyme, which catalyzes the ATP-dependent production of a lipoyl-AMP intermediate. This intermediate in turn is a substrate for lipoyltransferase, which completes the transfer of lipoate to a conserved lysine residue on lipoyl accepting proteins [45, 46].

Escherichia coli employs two complementary pathways for the incorporation of an intact lipoyl cofactor. The first is an exogenous pathway, wherein lipoic acid from the environment is taken up into the cell *via* vitamin transporters and attached to lipoyl acceptor proteins by lipoate protein ligase A (LplA) [47], [48]. Initial studies by Reed and coworkers in *Streptococcus faecalis* and *E. coli* provided evidence for a two step process for protein lipoylation involving a lipoyl-AMP intermediate [49]. In *E. coli*, studies using transposon mutagenesis led to the identification of the gene that encodes LplA [50, 51]. Bacterial strains with null mutations in *lplA* were capable of lipoic acid uptake but were unable to incorporate it into the appropriate apoproteins [50]. LplA catalyzes the ATP-dependent activation of the carboxylate of lipoic acid, generating lipoyl-AMP. A subsequent nucleophilic attack by the ε-amino group of the target lysine residue results in the formation of an amide bond with concomitant release of AMP (Figure 1.5). Further studies revealed that lipoyl-AMP is a true intermediate and that its formation is reversible [52].

Interestingly, overexpression of a fragmented *Bacillus stearothermophilus* PDC-E2 domain (residues 1-85), in medium lacking lipoate, resulted in either unlipoylated (80%) or putatively octanoylated (4%) proteins. Similarly, overexpression of the same protein in an *E. coli* mutant, that was deficient in *de novo* lipoic acid biosynthesis, resulted in octanoylation of lipoyl domains. These findings indicating that LplA could use octanoic acid as well as lipoic acid as a substrate; however, the octanoylated proteins were not converted to lipoylated proteins [53, 54]. Cells with an *lplA* null mutation were also able to incorporate radioactive lipoic acid and octanoic acid into the acceptor proteins; although the incorporation was noticeably lower than that of wild type,

indicating a secondary pathway of lipoylation (octanoylation) [50, 51, 55, 56]. A second gene was identified that encodes a lipoyl (octanoyl)-acyl carrier protein:protein-*N*-lipoyltransferase, designated LipB, which catalyzes the transfer of lipoyl (octanoyl) chains from lipoyl(octanoyl)-ACP to various apo acceptor proteins (Figure 1.5) [57]. LipB was found to regulate the incorporation of endogenously synthesized octanoate and lipoate into apoproteins such as the E2 subunits of the PDC and KDC. Various laboratories have demonstrated that endogenously synthesized octanoic acid is provided in the form of the octanoyl-acyl carrier protein (octanoyl-ACP), an intermediate in fatty acid biosynthesis [58-60]. All of the aforementioned apoprotein domains ($E2_{PDC}$, H-Protein, and $E2_{KDC}$) can serve as the second substrate for LipB. The mechanism by which this acyl transfer takes place has remained elusive. Recent studies have shown that the LipB reaction proceeds through a covalent acyl-enzyme intermediate in which cysteine 169 on LipB becomes modified with the octanoyl group before formation of the amide bond on the acceptor protein [61]. The octanoyl-LipB intermediate was shown to be chemically competent in the forward (octanoyl-E2) and reverse reactions (octanoyl-ACP).

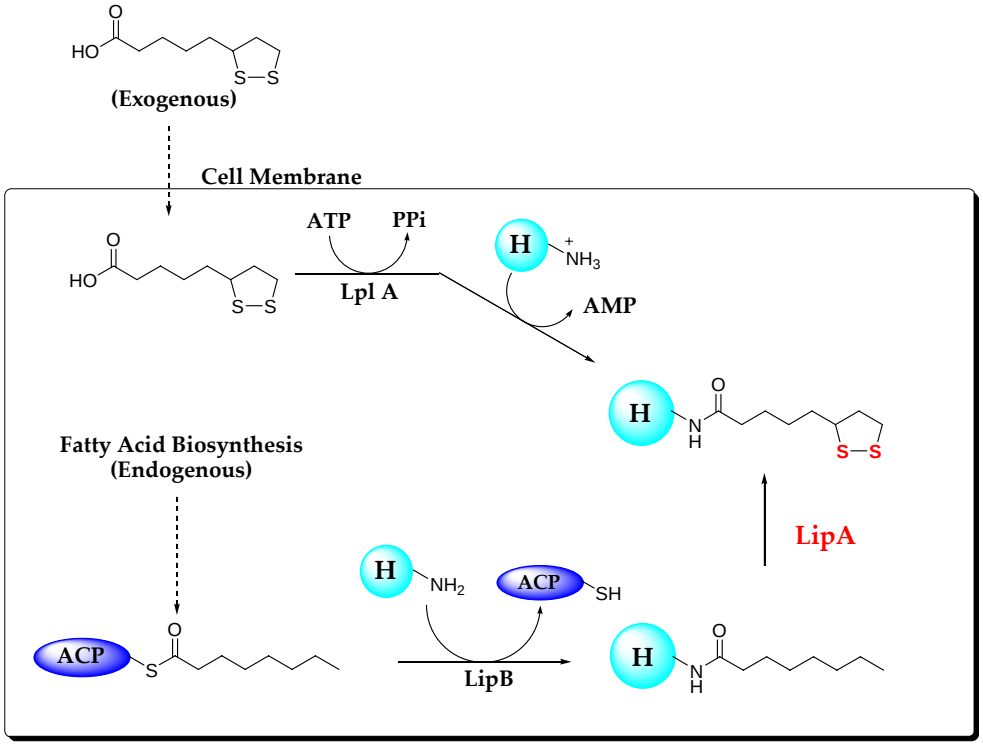

Figure 1.5: Exogenous and endogenous pathways for the incorporation of lipoic acid in *E. coli*.

1.4 Biotin Biosynthesis: A Paradigm for Lipoic Acid Studies

Biotin was originally isolated from egg yolk in the mid 1930s, but the pathway by which biotin is biosynthesized remained ambiguous until the late 1960s. The biotin biosynthetic pathway was elucidated through many biochemical and genetic experiments and was shown in *E. coli* to require the action of four separate enzymes that are encoded by genes within the biotin biosynthetic operon (*bioABFCD*) [62]. BioF, an 8-amino-7-oxopelargonic acid (AOP) synthase, catalyzes the formation of the primary carbon backbone of biotin from L-alanine and pimeloyl-CoA, and requires PLP as a cofactor [63,

64]. The resulting AOP is converted into 7,8-diamino pelargonic acid (DAPA) via a SAM-dependent transamination reaction catalyzed by BioA [65-67]. In the penultimate step of biotin biosynthesis DAPA becomes a substrate for the *bioD* gene product, a dethiobiotin synthetase which requires ATP and CO_2 to complete the formation of the ureido ring [63]. The transformation of dethiobiotin into biotin, catalyzed by BioB, is the final step in biotin biosynthesis but also the most chemically intriguing in the entire pathway. The formation of the thiophane ring requires the formation of two carbon-sulfur bonds at saturated positons, C-1 and C-4 of dethiobiotin (now referred to as C-6 and C-9) (Figure 1.6). The structure of biotin had been known for almost thirty years before attempts were made to understand this mechanistically difficult final step.

Early *in vivo* feeding studies performed in *Aspergillus niger* using dethiobiotin that was tritiated at various positions indicated that the conversion of dethiobiotin into biotin may proceed with the loss of at least four hydrogen atoms [68]. These experiments were expanded on by the Parry group, wherein sites implicated in hydrogen atom loss were specifically labeled with tritium and subsequently combined with [1-^{14}C]-dethiobiotin for use in double mixing experiments [69]. The results provided direct evidence for the removal of only two hydrogen atoms in dethiobiotin, one from each of the carbons (C6 and C9) that are subsequently bonded to the sulfur atom of the thiophane ring. Significant loss of tritium at C5, C7, and C8 in dethiobiotin was not observed, ruling out the possibility of desaturation [70].

The stereochemistry of sulfur introduction into dethiobiotin was also assessed by *in vivo* feeding studies with stereospecifically labeled substrate [71]. The absolute stereochemistry of biotin at C6 is known to be *S* and loss of tritium occurs only when the

pro-S hydrogen atom is labeled, indicating that the reaction takes place with retention of stereochemistry [70, 72].

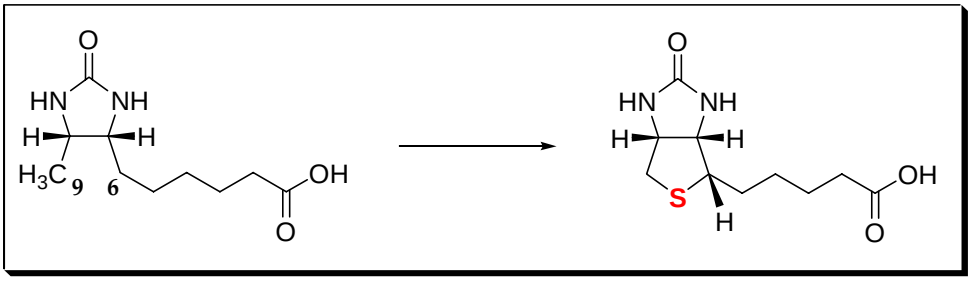

Figure 1.6: Conversion of dethiobiotin into biotin.

It had been suggested that intermediate hydroxylation may provide a method by which the saturated carbons at C-6 and C-9 become activated for sulfur insertion; biological hydroxylation reactions at saturated carbons were previously shown to occur with retention of stereochemistry [73]. The Emoto and Marquet laboratories had investigated the ability of various hydroxylated forms of dethiobiotin to serve as precursors to biotin. *In vivo* feeding studies using strains of *E. coli* that are defective in biotin biosynthesis revealed that 6-hydroxy, 9-hydroxy, and 6,9-dihydroxydethiobiotin do not support growth [74, 75]. These results corroborate the studies of the Parry laboratory in which sulfur insertion into dethiobiotin was shown to proceed with retention of stereochemistry suggesting that hydroxylation and subsequent displacement by a sulfur nucleophile is an unlikely pathway.

The observation that hydroxylated analogs of dethiobiotin did not serve as direct precursors in the biotin biosynthetic pathway prompted studies using monothiolated analogs. It was thought that analogs containing sulfhydryl groups at C-6 and C-9 could serve as precursors to biotin if direct sulfur insertion into dethiobiotin was the operative

mechanism [76]. Preliminary studies using an *E. coli* mutant, C124 which is devoid of a functional DAPA aminotransferase and is subsequently auxotrophic for biotin, showed that growth was promoted when 9-mercaptodethiobiotin (9-DTBSH) and (*6R*)-6-mercaptodethiobiotin were supplemented [77, 78]. When (*6S*)-6-mercaptodethiobiotin was provided in the media the bacteria were unable to grow. It was not understood how the incorrect positional isomer at C-6 could support growth (biotin is known to be of the *S* configuration at C-6). At this time the authors could not rule out some desulfurization mechanism prior to biotin formation. In a separate study, *Bacillus sphaericus* resting cells had been shown, *via* a microbiological assay, to produce biotin from radiolabeled [^{35}S]-9-mercaptodethiobiotin provided as its disulfide [77]. It is noteworthy to mention that the amount of biotin produced from the administration of this compound was 10-fold less than the biotin produced from the normal substrate, dethiobiotin. In contrast to previous work, (*6R*)-6-mercaptodethiobitoin and (*6S*)-6-mercaptodethiobiotin were not converted into biotin. The data supported 9-mercaptodethiobiotin as a direct precursor to biotin; however, the compound could not be isolated from the bacterial system [77].

Studies on the biotin biosynthetic pathway in plant cells showed that an intermediate, originally called “compound A”, accumulated and coeluted with 9-mercaptodethiobiotin using anion-exchange HPLC [79]. When [^{14}C]-dethiobiotin was given to growing cells, radioactivity was detected in compound A and biotin. These results support previous conclusions that a monothiolated compound can serve as an intermediate in the biosynthesis of biotin and that the reaction catalyzed by biotin synthase may be a two step process [77]. It should be noted that recent results from the Marquet lab, using highly purified BioB under well-defined assay conditions, have

indicated that 9-mercaptodethiobiotin can be used as a substrate. The amount and rate at which biotin is produced from 9-mercaptodethiobiotin and dethiobiotin were shown to be comparable. In both cases the amount of biotin produced per mol of biotin synthase in the assay never exceeded one. The K_m for this substrate was found to be 20-fold greater than that of dethiobiotin. It was concluded that the rate determining step followed the formation of a common intermediate from both DTB and 9-DTBSH [80].

The origin of the sulfur atom in the thiophane ring of biotin has been addressed to some extent *in vivo*. Methionine sulfoxide, methionine, as well as some sulfur containing salts (Na_2S, $NaHSO_3$, Na_2SO_4, albeit much more poorly), could serve as sources of sulfur in biotin. When ^{35}S-methionine was used in similar studies, radioactive biotin could be detected. Other small molecules that were not used as sulfur donors were cysteine, cystine, methionine sulfone, S-methylthioadenosine, choline sulfate, and glutathione [70]. In stark contrast, the Shive laboratory showed in multiple studies that the sulfur atom from L-[^{35}S]-cystine is incorporated into biotin with the same specific activity [81, 82].

The bioB gene from *E. coli* was originally sequenced in 1988, but the conversion of dethiobiotin into biotin by cell-free extracts was not shown until 1992 [62, 83]. In this study optimum activity required fructose 1,6-bisphophate, Fe^{2+}, SAM, NADPH, KCl, and the substrate dethiobiotin [83]. Partial purification of the enzyme resulted in the loss of activity, leading to speculation that crude extract components were necessary for reconstitution of BioB activity. Birch and coworkers subsequently showed that flavodoxin/flavodoxin oxidoreductase, a physiological reducing system, was also required for activity in cell-free extracts [84]. Other small molecule components that

were obligatory for the reaction were SAM, cysteine, NADPH, TPP, and either asparagine, aspartate, glutamine or serine [84].

Soon after the requirements for activity were established, investigations into the stoichiometry of SAM in the reaction were undertaken. Using radiolabeled starting materials and monitoring methionine or 5'-deoxyadenosine (5'-dA) formation, the Marquet and Savoy laboratories independently demonstrated that at least two equivalents of SAM were required for the production of one molecule of biotin [85, 86]. Interestingly, the Savoy laboratory showed that the previously mentioned intermediate could be isolated and introduced into another assay where it was capable of being converted into biotin. This suggested that one equivalent of SAM was used to generate the intermediate while the second equivalent of SAM completed the formation of biotin [85]. It was postulated that the intermediate could be a monothiolated form of dethiobiotin but the isolated compound had a different R_f value than that of 9-mercaptodethiobiotin by thin layer chromatography (TLC).

It was proposed that BioB-dependent reductive cleavage of SAM into methionine and 5'-dA was similar to three other SAM-dependent enzymes, namely pyruvate formate-lyase activating enzyme (PFL-AE), lysine 2,3-aminomutase (LAM), and anaerobic ribonucleotide reductase activating enzyme (ARR-AE) [87-90]. All of these proteins catalyze the removal of a hydrogen atom from a chemically inert C-H bond to initiate catalysis [86]. Similar to studies initially carried out on LAM, the Marquet laboratory provided evidence for direct hydrogen atom abstraction from dethiobiotin, presumably by a 5'-deoxyadenosyl radical (5'-dA•), using various deuterated substrates [91]. The 5'-dA produced during the BioB reaction was isolated by high-performance liquid

chromatography (HPLC) and analyzed for its deuterium content by mass spectrometry. Although the percentage of deuterium contained within the total 5'-dA changed as a function of the substrate used, the total number of deuterons incorporated never exceeded one. When 6,9-[$^2H_5$]-dethiobiotin, 9-[$^2H_3$]-dethiobiotin, and 6(S)-[$^2H_1$],9-[$^2H_1$]-dethiobiotin were used as substrates, 5'-dA was found to have 32%, 18%, and 17% deuterium incorporation respectively. When 6(R)-[$^2H_1$],9-[$^2H_1$]-dethiobiotin was used as a substrate little deuterium (~5%) was detected in 5'-dA, which is consistent with previous work supporting the stereospecific removal of the *pro-S* hydrogen atom [70]. One discrepancy the authors did not address was that the total amount of biotin formed when the incorrect (*6-R*) isomer was used was similar to that formed when protiated dethiobiotin was used. This is somewhat puzzling due to the near background levels of deuterium incorporation into 5'-dA. Despite these inconsistencies, the results conform to a mechanism in which direct hydrogen atom abstraction from positions C-6 and C-9 of dethiobiotin occurs. This mechanism contrasts with those of PFL-AE and ARR-AE, in which protein glycyl radicals, generated on cognate enzymes, are formed in the SAM-dependent reaction.

A large number of *bioB* genes from many different species were sequenced by the early 1990s. Sequence alignments of these proteins revealed the presence of two highly conserved sequences; the first was a cysteine triad in a CXXXCXXC configuration, while the second was contained within a YNHNL motif [76]. Biotin synthase was purified to homogeneity from various species soon after these initial characterizations, and the pure enzymes from *E. coli*, *Bacillus sphaericus*, and *Arabidopsis thaliana* were the first to be characterized spectroscopically [92-94]. In all cases the proteins were

purified under aerobic conditions. Initial characterization of the *E. coli* protein by the Flint group revealed two separate species by native gel electrophoresis, a dimer (~104 kDa) and a monomer (~82 kDa). The monomer was shown to bind 2 iron atoms, and contained 2 acid-labile sulfurs, while the dimer contained approximately one equivalent of each. The enzyme was red in color and had unique UV-visible characteristics with absorption bands at 330 nm, 420 nm, 453 nm, and 540 nm, which are common for 2Fe-2S clusters in the +2 oxidation state. Treatment of the protein with excess sodium dithionite led to a gradual decrease in the UV-visible absorption spectrum at 300 nm and 453 nm, and concomitant production of an electron paramagnetic resonance (EPR) signal that is characteristic of S = 1/2 $[2Fe\text{-}2S]^{+}$ clusters. It was also shown that prolonged treatment with dithionite at room temperature led to the loss of iron from the protein [92].

A defined *in vitro* assay was also developed to analyze these two forms of BioB. The activity of both monomeric BioB and dimeric BioB was determined by incubating each form with crude extract from a strain of *E. coli* that lacked a functional *bioB* gene. At various time points the reaction was stopped by heating and the solution was centrifuged. The supernatants were analyzed for biotin production using a microbiological assay. The activity of the native dimer was approximately half that of the monomer, although it could be converted into monomer upon treatment with Fe^{3+} and S^{2-}, which resulted in an increase in activity. Experiments were also performed to investigate the cofactors and small molecules required for activity; it was found that turnover was completely dependent on iron, SAM, NADPH, and to a smaller extent KCl. In contrast to the earlier studies by Ifuku et al., which concluded that fructose 1,6-

bisphosphate stimulates activity in cell-free extracts, the activity of the purified enzyme was unaffected by its inclusion [83]. It was noted as well that activity was low and far from catalytic, and most likely reflected the requirement of other proteins/cofactors yet to be identified from the crude extract. The authors suggested, for the first time, the possible role of the Fe-S center as a sulfur donor, on the basis of its instability. This instability was proposed to lead to the release of sulfur which could then be utilized during catalysis. If this were the case, the cluster would need to be regenerated for multiple turnovers to occur, again leading to the noticeably low amount of activity detected *in vitro*.

Independent studies from the Marquet laboratory confirmed that highly purified BioB from *B. sphaericus* could bind a 2Fe-2S cluster although, the enzyme was deficient in iron and sulfide (1 Fe/monomer and 0.7 S^{2-}/monomer) [93]. The protein had UV-visible absorption spectra similar to that of the *E. coli* enzyme with features at 330 nm and 453 nm. The authors demonstrated, using a microbiological assay, that the enzyme was inactive, even in the presence of low molecular weight cofactors (NADPH, SAM, L-cysteine, and DTT). The addition of crude lysate induced the production of biotin from dethiobiotin. Mejean *et al.* subsequently showed that cell-free extracts could be replaced with 5-deazaflavin and light; purified BioB was active with SAM, 5-deazaflavin and light alone. These results were similar to those obtained with PFL-AE, LAM, and ARR-AE, again suggesting that BioB belongs to the family of enzymes that require SAM and Fe-S clusters to perform catalysis [93, 95, 96].

A few years later the gene from *A. thaliana* was cloned and overexpressed in *E. coli*. The purified protein, a homodimer, was shown to contain a [2Fe-2S] cluster,

analogous to the enzymes from *E. coli* and *B. sphaericus* [94]. The enzyme ran as a monomer by SDS-PAGE and had an approximate molecular weight of 44 kDa, in contrast to its bacterial counterparts which are monomers of 39 kDa. The plant gene was shown to have a 41 amino acid extension at the N-terminus, which is thought to be involved in mitochondrial targeting and give rise to the increase in molecular weight.

The Marquet group, in addition to characterizing the 2Fe-2S center in BioB, explored the ability of various reaction components to serve as the sulfur source. Experiments using [^{35}S]-SAM had previously shown that the sulfur atom in biotin was not derived from the cofactor [97]. By contrast, addition of [^{35}S]-cysteine to cell-free extracts resulted in the production of [^{35}S]-biotin at low levels. To further investigate the potential of cysteine to act as the sulfur donor, reactions were run with crude extract and with 5-deazaflavin as the reducing sources. The presence of crude extract was found to facilitate the incorporation of ^{35}S into biotin, which is consistent with previous results. Radioactivity could be not detected in biotin when 5-deazaflavin and light were used to provide reducing equivalents to the enzyme. These results in combination with the radiolabeled SAM study suggested that the sulfur atom in biotin may be derived from the enzyme itself, an idea that had also been proposed by the Flint laboratory [92, 93].

Further studies on sulfur incorporation into dethiobiotin, using *B. sphaericus* BioB, revealed that the addition of $FeCl_3$ and Na_2S increased the yield of biotin produced in the assay by 3-4 fold [98]. The authors suggested that if the sulfur in biotin is derived from the Fe-S center, addition of iron and sulfur can reconstitute the cluster, therefore activating the enzyme for subsequent turnover. Addition of $Na_2{}^{34}S$ in this manner resulted in the formation of biotin that contains 40% of the heavy isotope. The authors

also generated BioB devoid of the Fe-S cluster by treatment with excess sodium dithionite and EDTA. This form of the protein could then be chemically reconstituted with $FeCl_3$ and $Na_2{}^{34}S$ to give a protein that was spectroscopically similar to the as-isolated protein. The ^{34}S labeled enzyme, presumably in the Fe-S cluster, was capable of producing biotin that contains 67% ^{34}S in the thiophane ring. The deviation from 100% incorporation was attributed to possible sulfide exchange processes within the Fe-S cluster. Similar ^{34}S incorporation percentages were also observed with the *E. coli* enzyme [98].

Gibson *et al.* also showed that sulfur could be mobilized from BioB itself and incorporated into biotin [99]. BioB was grown and overexpressed as previously described, except that upon induction, either [^{35}S]-cysteine, $Na_2{}^{35}S$, or [^{35}S]-methionine was added to the media. Growth under these conditions yielded protein that, when partially purified, was labeled with ^{35}S (cysteine residues, methionine residues, and sulfide). [^{35}S]-biotin was produced at significant amounts (1.2%) only when $Na_2{}^{35}S$ and [^{35}S]-cysteine were added to growing cultures. Enzyme isolated from cells grown on [^{35}S]-methionine resulted in meager amounts of radiolabeled biotin (0.008%). When all three components were added to growing cultures the percentage increased by 20-fold (0.15%).

The Marquet laboratory has also been successful in reconstituting biotin synthase from apo-protein and sulfur mobilized by the action of the NifS and rhodanese enzymes [100]. The *nif* operon from *Azotobacter vinladii* has been shown to encode genes involved in Fe-S cluster biogenesis. In particular, NifS, a cysteine desulfurase, mobilizes sulfur from cysteine, and presents it in the form of an enzyme-bound persulfide [101].

Rhodanese also generates an enzyme bound persulfide from thiosulfate, which can be passed to a sulfur-acceptor [102]. Reconstitution reactions were carried out as previously described except that sodium sulfide was replaced with cysteine and NifS, or thiosulfate, DTT, and rhodanese. The spectroscopic and analytical properties, as well as the activity of reconstituted apo-proteins were nearly identical to that of native enzyme. These results bolstered the hypothesis that sulfur, ultimately from cysteine, can be incorporated into BioB (presumably in the form of a 2Fe-2S cluster) and subsequently biotin.

Iron-Sulfur Clusters of Biotin Synthase

After initial characterization of the Fe-S cluster of BioB, effort was focused on understanding the Fe-S cluster content and possible role of the Fe-S cluster in catalysis. Various spectroscopic techniques have been used to characterize the nature of the metallocofactor associated with active BioB. Using a combination of UV-vis, EPR, variable-temperature magnetic circular dichroism (VTMCD), and resonance Raman (RR) spectroscopies, Duin *et al.* provided evidence for multiple cluster states of BioB [103]. Aerobically purified BioB was shown to bind one S = 0 $[2Fe\text{-}2S]^{2+}$ cluster per monomer. This protein was then treated with sodium dithionite in the presence of 60% (v/v) glycerol or ethylene glycol under anaerobic conditions, which afforded $[4Fe\text{-}4S]^{2+}$ clusters. This represents one of the first cases in which stoichiometric 2-$[2Fe\text{-}2S]^{2+}$ to $[4Fe\text{-}4S]^{2+}$ cluster conversions have been observed. The $[2Fe\text{-}2S]^{2+}$ clusters were not reduced upon sodium dithionite addition; and the $[4Fe\text{-}4S]^{2+}$ cluster could be reduced to the S = 1/2 state only in the presence of glycerol. It was proposed, based on the Fe-S cluster interconversion, that addition of dithionite induced dimerization of BioB with a

bridging [4Fe-4S] cluster at the interface. Interestingly, biotin formation catalyzed by BioB-$[2Fe\text{-}2S]^{2+}$, BioB-$[4Fe\text{-}4S]^{2+}$, and BioB-$[4Fe\text{-}4S]^{+}$ were the same within experimental error. The authors proposed that dimerization could occur under the reducing anaerobic environment of the assay and that the catalytically relevant form of BioB contains one [4Fe-4S] cluster. Mössbauer studies performed by an independent group verified the interconversion of the Fe-S clusters of BioB upon reduction with dithionite in the presence of glycerol [104].

Spectroscopic studies from the Fontecave laboratory provided further insight into the Fe-S configuration of *E. coli* BioB [105]. The enzyme was isolated aerobically and stripped of all the iron that was bound to the as-purified enzyme by anaerobic treatment with 5-deazaflavin, light, and EDTA. Apo-BioB was then chemically reconstituted with iron and sulfide in the presence of dithiothreitol (DTT). Acid-labile sulfide and metal analysis revealed that the protein contained 3.7-4.2 Fe and S atoms per polypeptide. The UV-visible spectrum gave a broad absorption band with a maximum around 420 nm, indicating the presence of Fe-S clusters. Mössbauer and EPR spectroscopies showed the presence of $4Fe\text{-}4S^{2+/+}$ clusters. The cluster was sensitive to oxygen and was shown to degrade to a $2Fe\text{-}2S^{2+}$ center. EPR power saturation and temperature studies indicated the presence of an enzyme that primarily contains a $[4Fe\text{-}4S]^{+}$ center. Collectively, the data presented in this study argued against the formation of a bridging [4Fe-4S] cluster at a dimer interface and suggested that BioB that is reconstituted under strict anaerobic conditions binds 1-[4Fe-4S] cluster per monomer. Previous observations of [2Fe-2S] clusters bound to BioB were proposed to be a direct result of aerobic manipulations.

The [4Fe-4S] containing BioB was also observed by Ugulava et al. during dithionite reduction in the absence or presence of ethylene glycol [106]. UV-vis and EPR spectroscopies revealed that iron dissociates and rebinds during this reductive incubation. In fact, the BioB dimer, upon incubation with excess $FeCl_3$, S^{2-}, and DTT, was shown to accommodate 2-$[4Fe\text{-}4S]^{2+}$ clusters. These clusters are readily converted to 2-$[4Fe\text{-}4S]^{+}$ clusters upon dithionite treatment. It was suggested at this time that the active form of the enzyme contains two 4Fe-4S clusters per dimer and that one monomer catalyzes the first C-S bond formation and the other monomer catalyzes the second, to complete thiophane ring formation.

Jarrett and co-workers soon showed that BioB can also bind 2-[2Fe-2S] clusters/monomer and that the clusters were readily discernable by electrochemical titration [107]. Chemical reconstitution of the protein in the presence of dithionite led to the production of 2-[4Fe-4S] clusters/monomer. These clusters were not readily resolved by their redox potentials but are electrochemically distinct. More importantly, this study demonstrated that under assay conditions, in the absence of dethiobiotin, the relevant form of the protein contains 1-[2Fe-2S] cluster and 1-[4Fe-4S] cluster per monomer. To show this, BioB dimer containing 2Fe-2S clusters was incubated with the physiological reducing system, SAM, DTT, $FeCl_3$, and Na_2S. After 30 min the protein was reisolated anaerobically and was analyzed by UV-vis. Interestingly, the absorption spectrum contained characteristics of 2Fe-2S (330 nm and 460 nm) centers in combination with 4Fe-4S centers (410 nm). Fe/S analysis showed the protein isolated from the reaction mixture binds ~5.8 iron and ~6.2 sulfur atoms per monomer. It was proposed, based on the above information and electrochemical titrations, that the mixed cluster state would

be the predominant form of BioB under *in vivo* conditions. Mössbauer studies from the same group would later verify that BioB can accommodate the mixed cluster state in each monomer [108]. The Johnson group proposed, using whole cell Mössbauer and EPR, that BioB contains Fe-S clusters in the $[2Fe\text{-}2S]^{2+}$ configuration. The authors posited that the $[2Fe\text{-}2S]^{2+}$ cluster is a result of overexpression of BioB under aerobic conditions. Recent detailed spectroscopic analyses from the Johnson and Huynh laboratories corroborated the hypothesis, initially set forth by Jarrett and co-workers, which supports the mixed cluster state of BioB as the most active form [109].

E. coli BioB is known to contain eight conserved cysteine residues, of which three (C53, C57, and C60) are in the CXXXCXXC motif which is common to radical-SAM enzymes. To probe the importance of these residues in catalysis, Hewitson *et al*. prepared variant enzymes in which each of the cysteines was independently replaced by alanine [110]. The variants were then analyzed for their abilities to ligate Fe-S clusters and to convert dethiobiotin into biotin. Results indicated that each of the variants, when chemically reconstituted, can contain ~3-4 equivalents of iron and sulfide per monomer. The iron and sulfide content decreased by a factor of two upon exposure to air, consistent with the degradation of 4Fe-4S clusters to 2Fe-2S clusters that had been reported previously. Wild type activity was observed only with two of the variants (C276A and C288A), whereas no detectable activity was observed for the other six variants. EPR data confirmed the presence of S = 1/2 $[4Fe\text{-}4S]^{+}$ clusters only in the variants with cysteine residues other than those in the CXXXCXXC motif. Mössbauer analysis of the reconstituted C53A variant revealed two quadrupole doublets characteristic of a mixture of diamagnetic [2Fe-2S] and [4Fe-4S] clusters. The mixed cluster state was readily

converted into a homogenous $[2Fe\text{-}2S]^{2+}$ containing protein upon exposure to air for 1 hour. Collectively, six cysteines were shown to be required for catalysis; C53, C57, C60, C97, C128, and C188.

Deconvolution of the Fe-S cluster content and configuration of BioB soon led to studies that were aimed at using spectroscopy to analyze the state of the Fe-S centers under turnover conditions. The active state of BioB had been suggested to contain one [2Fe-2S] cluster and one [4Fe-4S] cluster [106, 108]. This form of the protein was analyzed following single turnover by UV-visible spectroscopy [111]. The BioB dimer was shown to promote formation of 2 equivalents of biotin dependent on the presence of dethiobiotin, SAM, and the physiological reducing system. BioB in the mixed cluster state produced rate constants that were ~100 fold higher than those for any other cluster form. Under the conditions of the assay the [4Fe-4S] remained unchanged while the absorption attributed to the [2Fe-2S] center absorption diminished. Importantly, it was demonstrated that biotin formation and the loss of the UV absorbance at 460 nm occurr with similar rate constants of 0.03 min^{-1}. Based on these studies Jarrett and co-workers proposed that, *in vitro*, the 2Fe-2S cluster served as the sulfur donor (Figure 1.7). The possibility of an Fe-S cluster serving as the sulfur donor has been suggested previously [92, 93].

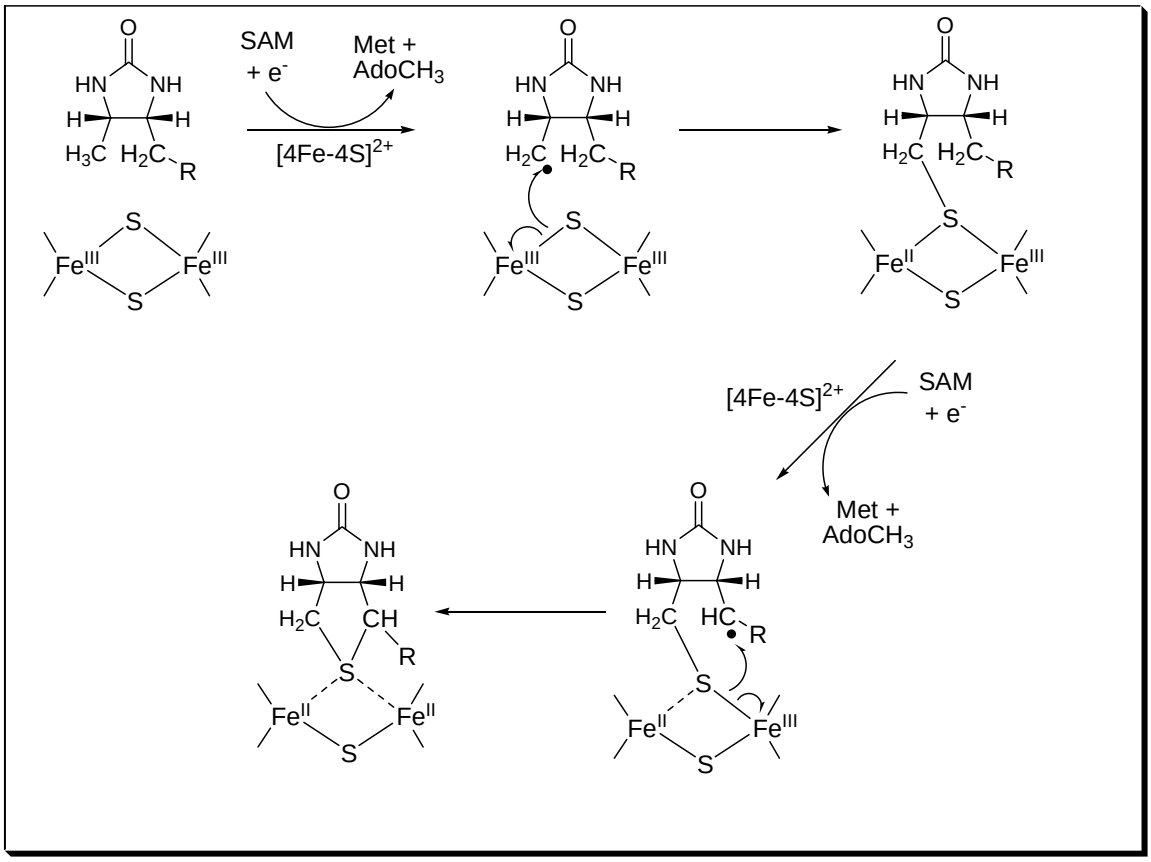

Figure 1.7: Proposed Role of the [2Fe-2S] Cluster in Biotin Biosynthesis (Adapted from Ugulava *et al.* 2001)

Mössbauer studies have recently confirmed the work of the Jarrett laboratory [112]. Bui *et al.* have demonstrated that a partially purified fraction (ammonium sulfate fractionation between 25% and 45%) of BioB containing a 2Fe-2S cluster can be converted into a mixed cluster state, binding one $[2Fe\text{-}2S]^{2+}$ cluster and one $[4Fe\text{-}4S]^{2+}$ cluster [104, 112]. This conversion can be achieved under a reducing environment which resembles the assay conditions. Reactions were performed in the absence and presence of dethiobiotin using the physiological reducing system. When dethiobiotin is added the $[4Fe\text{-}4S]^{2+}$ cluster composition remains constant while the percentage iron contributing to

the $[2Fe\text{-}2S]^{2+}$ cluster decreases by a factor of two. The decrease in the Mossbauer absorption from the $[2Fe\text{-}2S]^{2+}$ cluster is concomitant with an increase in the amount of a high-spin Fe^{3+} species (~21% of the total iron), which appears as a broad paramagnetic absorption along the baseline.

The role of the 2Fe-2S cluster has recently been interrogated by the Huynh and Johnson laboratories using Mössbauer and EPR spectroscopies [113]. Results similar to those of Jarrett and Marquet were obtained. The $[2Fe\text{-}2S]^{2+}$ cluster was observed to be degraded during the reaction while the 4Fe-4S cluster remained intact. In contrast to Jarrett, the cluster degraded with a 10-fold faster initial rate when compared to the rate of biotin formation. The authors suggested that this deviation in rate is possible if the rate determining step follows cluster degradation. One other anomaly in the Huynh study was the formation of a paramagnetic 2Fe-2S cluster during the reaction. It was proposed that the diamagnetic 2Fe-2S cluster may decay *via* reduction.

Proteins belonging to the "Radical SAM" family of enzymes all contain the CXXXCXXC consensus sequence that is thought to be involved in the ligation of a [4Fe-4S] cluster that is required for catalysis [114]. Site-directed mutagenesis studies suggest that C53, C57, and C60 in *E. coli* BioB, the cysteines within the radical SAM motif, are involved in 4Fe-4S cluster ligation [115]. Ollagnier-de Choudens *et al.* set out to provide evidence for the involvement of the 4Fe-4S cluster in catalysis. The reductive cleavage of SAM was observed by monitoring the S = 1/2 EPR signal as a function of methionine formation (one of the by-products of SAM cleavage). The loss of the $[4Fe\text{-}4S]^{+}$ cluster EPR signal paralleled the rate of methionine formation [116]. BioB containing the diamagnetic form of the 4Fe-4S cluster did not form methionine upon addition of SAM.

Oddly, the $[4Fe\text{-}4S]^{+}$-mediated reduction of SAM by BioB did not require the presence of dethiobiotin. The variant proteins, devoid of thiolate ligands in the cluster binding motif, were not capable of catalyzing cleavage of SAM.

Mössbauer, RR, and EPR data supporting the interaction of the [4Fe-4S] cluster of BioB with SAM were provided by the Johnson laboratory. The protein was interrogated in the absence and presence of SAM. Resonance Raman data show the shift in stretching modes from 338 (without SAM) to 342, indicating non cysteinyl ligation to iron. The Mössbauer spectrum was observed to broaden in the presence of SAM giving rise to altered parameters. Finally, cryoreduction of BioB at 77K in the absence of SAM shows a nearly axial spectrum (g = 2, 1.937, and 1.937). The spectrum becomes rhombic upon the addition of SAM with g-values of 2, 1.928, and 1.854. The authors concluded that, as in PFL-AE, SAM binds in close proximity to a unique iron site within the [4Fe-4S] cluster [117, 118].

A fundamental question concerning the reduction of SAM in the absence of dethiobiotin arose from the studies of the Fontecave laboratory. Jarrett had proposed that the production of a high-energy 5'-dA radical has the potential to be deleterious to the system in the absence of substrate [119]. This thought prompted studies to understand the method by which BioB controls SAM-dependent radical formation. Microdialysis experiments revealed that binding of dethiobiotin occurs only in the presence of SAM and that optimal binding occurs when BioB is in the mixed cluster state ($[2Fe\text{-}2S]^{2+}$/$[4Fe\text{-}4S]^{2+}$). It was shown that 0.77 equivalents of SAM and 0.51 equivalents of dethiobiotin can bind per BioB monomer. Equilibrium dialysis studies confirmed that SAM binding is enhanced in the presence of dethiobiotin. In the absence of dethiobiotin the K_d for

SAM is ~100 μM. Incubation of the enzyme with dethiobiotin prior to SAM addtion dramatically decreases the K_d to 2.3 μM. Interestingly, the binding of dethiobiotin could not be detected in the absence of SAM. The binding of SAM results in a decrease in absorbance at 410 nm which were used to analyze the kinetics of binding by stopped-flow UV-visible spectroscopy. The stopped-flow results indicate that dimeric BioB, in the absence of dethiobiotin, binds weakly to one molecule of SAM and slowly to a second molecule with similar affinity (K_d = 100 μM, k_{on} = 10 M^{-1} s^{-1}). When dethiobiotin is added to the reaction the binding of the second molecule of SAM occurs with a high affinity and ~45-fold faster (K_d = 1-5 μM, 450 M^{-1} s^{-1}). In the absence of SAM, binding of dethiobiotin is not observed, indicating an ordered binding event where at least one SAM binds before association of dethiobiotin. The results indicate that the binding of SAM is intimately tied to presence/absence of dethiobiotin and suggest a specific level of control over the abortive formation of high-energy 5'-deoxyadenosyl radicals.

A provocative study from the Fontecave laboratory in 2002 provided evidence suggesting that BioB, in addition to catalyzing sulfur insertion into a saturated carbon, is a pyridoxal 5'-phosphate (PLP)-dependent cysteine desulfurase [120]. The authors postulate that sulfur from cysteine can be mobilized by BioB itself and subsequently be used as the source of sulfur in the formation of biotin. Reconstituted BioB incubated with L-cysteine and DTT showed slow formation of alanine. This activity was greatly stimulated (~5-fold) by the addition of PLP. BioB was subsequently shown to bind ~0.7-1 mol of PLP/polypeptide. Alanine formation was lost in reactions where BioB and/or L-cysteine were omitted. Mechanistic dissection of cysteine desulfurases has shown that they contain a conserved cysteine residue that is required for the formation of the

persulfide intermediate. Site-directed mutagenesis studies have previously shown that six cysteines in BioB are required for the production of biotin. C53, C57, and C60 are thought to coordinate the $[4Fe\text{-}4S]^{+}$ cluster which is responsible for mediating the reductive cleavage of SAM [110]. It has been suggested by Ugulava *et al*. that C97, C128, and C188 could be ligands to the 2Fe-2S cluster [107]. The variant proteins were analyzed for their ability to produce alanine in the same manor as wild-type. C97A and C128A variants could produce only minimal amounts of alanine (5% with resects to wild-type), while C188A retained 70% of the cysteine desulfurase activity. Although it had not been determined, C97 or C128 were suggested to be possible sites of the enzyme-bound persulfide. From the experiments the authors suggested two possible routes for the incorporation of sulfur liberated by the cysteine desulfurase activity of BioB. Both pathways depend on the initial generation of a carbon-centered radical via hydrogen atom abstraction from C-6 or C-9 by a 5-dA radical. The enzyme then generates, by cysteine desulfurase activity, an enzyme-bound persulfide. The mechanisms bifurcate at this point where in one scenario the bound persulfide quenches the radical directly or in the second scenario the sulfur could be utilized in the biogenesis of the 2Fe-2S cluster.

Further mechanistic studies on the PLP-dependent BioB revealed that "multiple turnovers" could be achieved if the enzyme is isolated after one round of turnover, reisolated from the reaction mixture and supplemented with fresh assay components (PLP, SAM, DTT, dethiobiotin, cysteine, NADPH, flavodoxin, and flavodoxin oxidoreductase) [121]. The authors suggested that the low turnover seen in most BioB reactions is due to inhibition by a compound that builds up over the time course of the reaction. To test this possibility various by-products of the reaction were evaluated for

their ability to inhibit BioB, including; methionine, $NADP^+$, and 5'-dA. Only 5'-dA was shown to inhibit BioB reactivity, giving maximal inhibition at 1.5 equivalents. More recent *in vivo* studies from the Cronan laboratory provide evidence for the inhibitory effects of 5'-dA [122]. It was shown that *E. coli* strains lacking a functional *pfs* gene, which encodes a 5'-methylthioadenosine (MTA)/S-adenosylhomocysteine (SAH) nucleosidase, accumulate 5'-dA and cannot convert dethiobiotin into biotin (Pfs was shown to act on 5'-dA *in vitro* and *in vivo*). Growth of the *Δpfs* strain could be observed only upon addition of biotin to the media. These results suggested that a functional nucleosidase, such as Pfs, is required to alleviate inhibition under physiological conditions.

Johnson and coworkers recently re-evaluated work from the Fontecave laboratory that suggested that BioB can bind PLP and subsequently catalyze the desulfurization of L-cysteine [120]. In stark contrast to earlier studies, the 4Fe-4S cluster containing BioB did not bind PLP under similar reconstitution procedures [109]. The time-dependent formation of alanine and sulfide was monitored at 25°C over 2.5 hours. The production of alanine was analyzed *via* a coupled assay using alanine dehydrogenase. Alanine was not formed at levels above the limits of detection of the assay (~5 μM). Approximately $4S^{2-}$/BioB could be detected during the time course but its production was not dependent on the presence of PLP.

1.5 Lipoic Acid Biosynthesis

In the mid-1960s, largely unpublished results from the Reed laboratory suggested that octanoic acid was a likely precursor to lipoate [4, 123]. More definitive *in vivo* feeding studies from the laboratories of Ronald Parry and Robert White demonstrated that isotopically labeled octanoic acid served as the carbon backbone from which lipoic acid is derived [70, 124]. Further studies from the Parry laboratory provided specific mechanistic insight into the incorporation of sulfur atoms into C-6 and C-8 of octanoic acid. Substrates containing tritium at positions C-5, C-6, C-7 (racemic mixtures), and C-8 were synthesized and were mixed with ^{14}C-octanoic acid, and the ratio of ^{3}H/^{14}C in isolated lipoic acid was used to analyze for hydrogen atom abstraction. Minimal loss of tritium was observed with substrates labeled in the 5 and 7 positions, indicating that desaturation is unlikely along the pathway to sulfur insertion. Minimal loss of tritium at C-8 was also observed, and was attributed to a substantial isotope effect at this position. Lipoic acid has a chiral center at C-6, and feeding of [1-^{14}C-6(*RS*)-^{3}H]-octanoic acid to *E. coli* resulted in isolates of lipoic acid that had 50% of the original tritium content, suggesting the stereospecific removal of one hydrogen atom. The synthesis of stereospecifically labeled [1-^{14}C-6(*R*)-^{3}H]- and [1-^{14}C-6(*S*)-^{3}H]-octanoic acids showed that incorporation of sulfur at position C-6 proceeds with the removal of only the *pro-R* hydrogen atom [125]. Results demonstrated that only 10.9% of the initial tritium content remained in the isolated lipoic acid when the R-isomer was used. This study in combination with later studies with deuterated substrates revealed that the incorporation of sulfur at C-6 occurs with inversion of stereochemistry, since the biologically active form of lipoic acid was known to be of the *R* configuration [124, 125].

A mechanism that readily accounts for the observed inversion of stereochemistry in the formation of lipoic acid suggests intermediate hydroxylation at C-8 and C-6, followed by activation and a polar nucleophilic displacement by an appropriate sulfur nucleophile [70, 126]. To address this possibility various hydroxylated and monothiolated compounds were tested for their ability to serve as *in vivo* precursors to lipoic acid (Figure 1.8). 6-Hydroxy, 8-hydroxy, and 6,8-dihydroxyoctanoic acids were not converted into lipoic acid, while 6-mercapto and 8-mercaptooctanoic acid could serve as precursors to lipoic acid (2-5% and 19-28% respectively) [126].

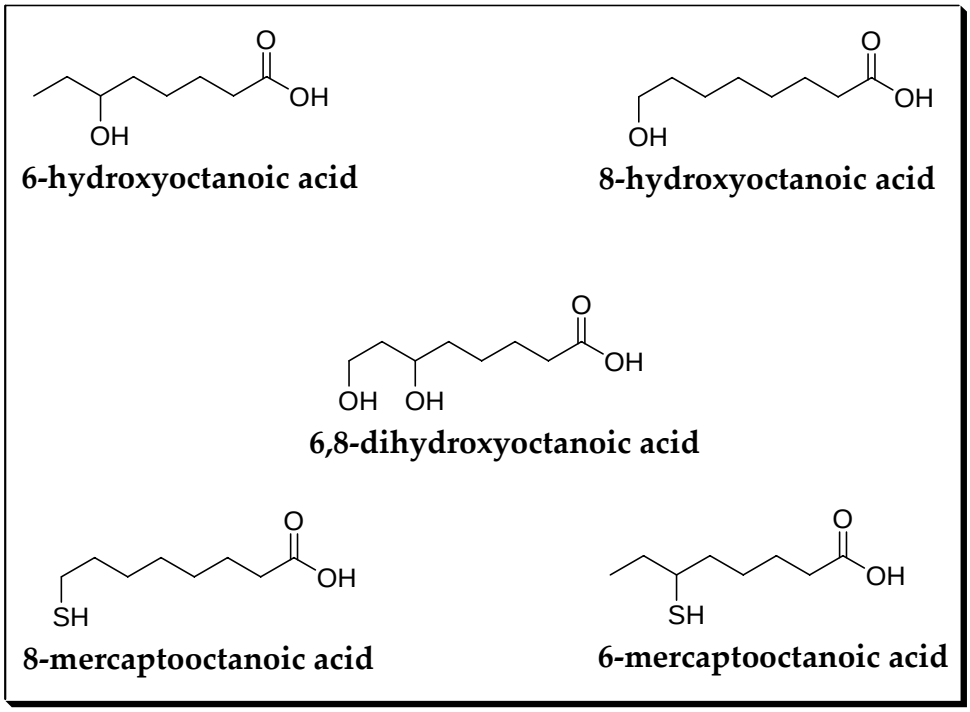

Figure 1.8: Potential intermediates in the biosynthesis of lipoic acid.

In an effort to test for the intermediacy of monothiolated intermediates, feeding studies were performed with two *E. coli* lipoic acid auxotrophs (W1485-lip2 and JRG33-lip9). PCR amplification of the chromosomal DNA showed that each auxotroph

contained G/C to A/T single mutations. The specific point mutations resulted in a Ser→Phe conversion in W1485-lip2 and a Glu→Lys conversion in JRG33-lip9 [127]. Work from the White laboratory had previously shown that wild-type *E. coli* can convert 6-mercaptooctanoic acid and 8-mercaptooctanoic acid into lipoic acid [126]. Growth studies revealed that 8-mercaptooctanoic acid could support growth of both *lipA* auxotrophes but 6-mercaptooctanoic acid could not [127]. Around the same time, Cronan and co-workers demonstrated that *lipA* insertion mutants had the ability to utilize both monothiolated compounds. In those studies growth was substantially greater when 8-mercaptooctanoic acid was used in the medium (a 17 fold excess of 6-mercaptooctanoic acid was required to achieve the same growth level). These results, in combination with earlier isotope studies, led to several possible mechanistic routes to lipoic acid formation. In one case the *lipA* gene product was responsible for at least the insertion of sulfur into C-6 of lipoic acid while the activity of another enzyme was not ruled out for the incorporation of the second sulfur. The fact that the *lip-2* variant growth was greater than the *lip-9* variant, when supplemented with 8-thiooctanoic acid, led the authors to believe that the *lip-2* mutation prevents C-S bond formation at position eight while allowing for C-S bond formation at position six. Lastly, it was proposed that it is more likely that one enzyme is responsible for the formation of both C-S bonds but the lip-9 mutant led to the production of a protein with a greatly diminished capacity to perform sulfur insertion [127].

Identification of the *lipA* Gene

In 1968 Herbert and Guest created *E. coli* mutants that were auxotrophic for lipoic acid (initially called *lip*$^-$ mutants), and used them to map the *lip* locus within the *E. coli* genome. These bacteria were shown to lack 2-oxoacid dehydrogenase activity and required acetate /succinate or glucose/lipoic acid supplementation [128]. Recent studies showed that overexpression of E2 of the PDC in either of the mutant strains produced exclusively octanoylated proteins [54]. Complementation and transposon mutagenesis experiments demonstrated that the previously described *lip* mutants (*lip-2* and *lip-9*) were in fact defective in a gene that is now called *lipA*. Similar genetic manipulations uncovered another gene essential for lipoic acid biosynthesis, *lipB*, which was derived from the same locus [13].

At a similar time a gene responsible for the biosynthesis of lipoic acid was identified in *Saccharomyces cerevisiae* [129]. Sequence analysis demonstrated that the gene, designated as *lip5*, is similar to *E. coli lipA*. Moreover, the *lip5* gene was able to complement strains of *E. coli* that were deficient in lipoic acid biosynthesis. The N-terminus contained an 83-amino acid extension that was not present in *E. coli lipA*, and was determined to be a mitochondrial targeting sequence. All of the gene products required for lipoic acid biosynthesis in eukaryotes are known to be localized to the mitochondria [12]. The acyl carrier protein had previously been implicated in the biosynthesis of lipoic acid in *E. coli* [51]. Interestingly, deletion of the *ACP1* gene in *S. cerevisiae*, which encodes the mitochondrial acyl carrier protein, leads to a dramatic decrease in lipoic acid content (5-10% of wild-type) [59]. Subsequently, LipA homologues have been identified in the mitochondria of mammals and plants as well as

plant plastids [60, 130, 131]. All of the identified genes, like *S. cerevisiae*, were shown to complement *E. coli lipA* mutants [132].

Initial sequencing and annotation of the genes involved in lipoic acid biosynthesis (*lipA* and *lipB*) in *E. coli* was conducted by the laboratories of Gary Ashley and John Cronan [56, 133] and showed that LipA was 40% similar and 17% identical to BioB, the product of the *bioB* gene in *E. coli*. Interestingly, the sequences of both proteins contained a cluster of cysteine residues organized in a CTRRCPFC triad, and it was suggested that this motif could represent a possible site for metal binding, such as an iron-sulfur cluster [56, 133].

1.6 Biophysical Characterization of Lipoyl Synthase

Initial expression of the *lipA* gene product (LipA) yielded overproduced protein that was primarily in insoluble aggregates. The aggregates could be resolubilized by treatment with guanidine-HCl, and the resulting protein was judged to be ~80% pure by gel electrophoresis [56]. LipA was eventually purified to homogeneity independently in the laboratories of Michael Marletta and Marc Fontecave [134, 135]. Fontecave and co-workers showed that nearly all the overexpressed protein was produced in inclusion bodies. After centrifugation, the insoluble fraction was treated with 6 M guanidine-HCl and subjected to gel filtration chromatography. The enzyme was subsequently refolded and dialyzed into buffer lacking guanidine-HCl. Reconstitution of the enzyme was achieved by incubating the enzyme under argon with DTT, Na_2S, and $Fe(NH_4)_2(SO_4)_2$. LipA from both the soluble and insoluble fraction of the crude extract was noted to have a dark reddish-brown color. Quantitative analyses showed that LipA binds 0.56

Fe/protein in the as-isolated form and 2.3 Fe/protein in the reconstituted form, which compared favorably with the analysis performed by Busby et al. [134, 135]. Resonance Raman (RR), UV-visible, and electron paramagnetic resonance (EPR) spectroscopies were used to verify the quantitative Fe/S analyses, indicating that under various conditions LipA can bind [2Fe-2S] or [4Fe-4S] clusters [134, 135]. Additional EPR studies showed that the [2Fe-2S] centers on LipA could be converted to $[4Fe\text{-}4S]^{+}$ clusters upon reduction with sodium dithionite [135]. It was postulated that monomeric LipA containing a [2Fe-2S] center can dimerize upon reduction leading to the formation of a [4Fe-4S] cluster at the interface [134].

A more detailed spectroscopic analysis of LipA in which the enzyme was stripped of iron by treatment with dithionite and ethylenediaminetetraacetic acid (EDTA) and then reconstituted under anaerobic conditions. This method afforded a protein that contained approximately 3.7-4.2 atoms of iron and sulfide per polypeptide. A combination of the analytical data with UV-visible, EPR, and Mössbauer spectroscopies indicated the presence of one [4Fe-4S] cluster per protein [105].

The spectroscopic properties of aerobically isolated LipA resemble those of biotin synthase (BioB), pyruvate-formate lyase activating enzyme (PFL-AE), lysine 2,3-aminomutase (LAM) and anaerobic ribonucleotide reductase activating enzyme (ARR-AE), all of which contain the CXXXCXXC consensus sequence, which is thought to ligate the Fe-S cluster [103, 136-138]. Like LipA, these proteins are capable of binding [4Fe-4S] clusters under certain conditions. In most cases, exposure to oxygen led to the formation of [2Fe-2S] and [3Fe-4S] clusters as degradation products.

1.7 In Vitro Studies of Lipoyl Synthase

Although the *lipA* gene was identified and cloned in 1992, it wasn't until 2000 that the isolated protein was shown to function *in vitro*. This was partly attributable to the instability of LipA, especially in the presence of oxygen, but also to the unknown nature of the protein's substrate [70]. *In vivo*, octanoic acid can serve as a precursor to lipoic acid; however, *in vitro* it was not a substrate for LipA. Genetic and biochemical studies from Cronan and Bourguignon laboratories suggested the involvement of the acyl carrier protein (ACP) in the formation of the lipoyl cofactor, allowing for Cronan and Marletta to establish the first *in vitro* assay [51, 139]. Work primarily from Cronan and co-workers had elucidated the various pathways of lipoic acid incorporation *in vivo* (exogenous vs. endogenous) [57]. The endogenous pathway provided evidence for the involvement of the acyl carrier protein (ACP) in formation of lipoylated proteins in various multienzyme complexes. The combined efforts of the Cronan and Marletta labs led to the first detection of LipA activity *in vitro* [140]. Hexahistidine tagged (His-tagged) LipA was overexpressed and purified to homogeneity from *E. coli* cells. Activation of apo-lipoyl PDC domains was used to assay a functional LipA protein. The assay required the presence of octanoyl-ACP, LipB, LipA, an apoacceptor protein (e.g. E2), SAM, and the physiological reducing system: flavodoxin, flavodoxin oxidoreductase, and nicotinamide adenine dinucleotide phosphate (NADPH). It was presumed that octanoyl-ACP served as the substrate for LipA although lipoyl-ACP was never detected in the assay. Only the lipoylated acceptor protein was detected by mass

spectrometry. Product formation was minimal, suggesting that LipA, like BioB, is not capable of catalyzing multiple turnovers *in vitro*.

Recent studies showed that d_{15}-octanoyl domains build up in the cells containing null mutations in the *lipA* gene. Restoration of a functional *lipA* gene *via* bacteriophage transfection, showed the transformation of the d_{15}-octanoyl domains into lipoyl domains. This observation that LipA could act directly on octanoylated domains of dehydrogenase complexes [141]. These results were confirmed *in vitro* using octanoylated-KGDH and octanoylated-PDH domains as substrates for LipA. The progress of the reaction was monitored by the formation of 5'-dA from SAM and the activity of lipoamide dehydrogenase, which requires a functional lipoyl cofactor for catalysis. These results contradicted earlier studies that implicated octanoyl-ACP as the substrate and now unequivocally demonstrated that octanoylated acceptor domains serve as the substrate for LipA [141].

1.8 X-ray Crystallographic Studies of Radical SAM Proteins

The identification and characterization of enzymes requiring SAM and iron to catalyze reactions is occurring at a profound pace. Indeed, a bioinformatics study has indicated that these enzymes constitute a superfamily containing over 600 members termed the "radical SAM" superfamily [114]. All of the enzymes share the CXXXCXXC motif, or a closely related motif, and share a common mechanistic feature, in which Fe-S clusters and SAM are required to generate a 5'-dA• that is an obligate intermediate in catalysis. The proteins characterized to date require at least one [4Fe-4S]

cluster, SAM, and a reducing equivalent to function *in vitro*. The reduced state of the Fe-S cluster has been shown to be the one that is catalytically relevant [87-89].

Oxygen-Independent Coproporphyrinogen III Oxidase (HemN)

Within the past three years crystal structures of four radical SAM enzymes have been reported. The first, coproporhyrinogen III oxidase (HemN) from *E. coli*, was crystallized by the Schubert laboratory to a resolution of 2.07 Å (Figure 1.9)[142]. The protein was co-crystallized anaerobically with SAM present but in the absence of substrate. The overall structure of the HemN is an $(\alpha\beta)_6$ three-quarter barrel which has many similarities to triose-phosphate isomerase (TIM) $(\alpha\beta)_8$ full-barrel domain. HemN contains two distinct domains, a large N-terminal domain and a smaller C-terminal domain, that are connected by a loop of α-helices and three antiparallel β-sheets.

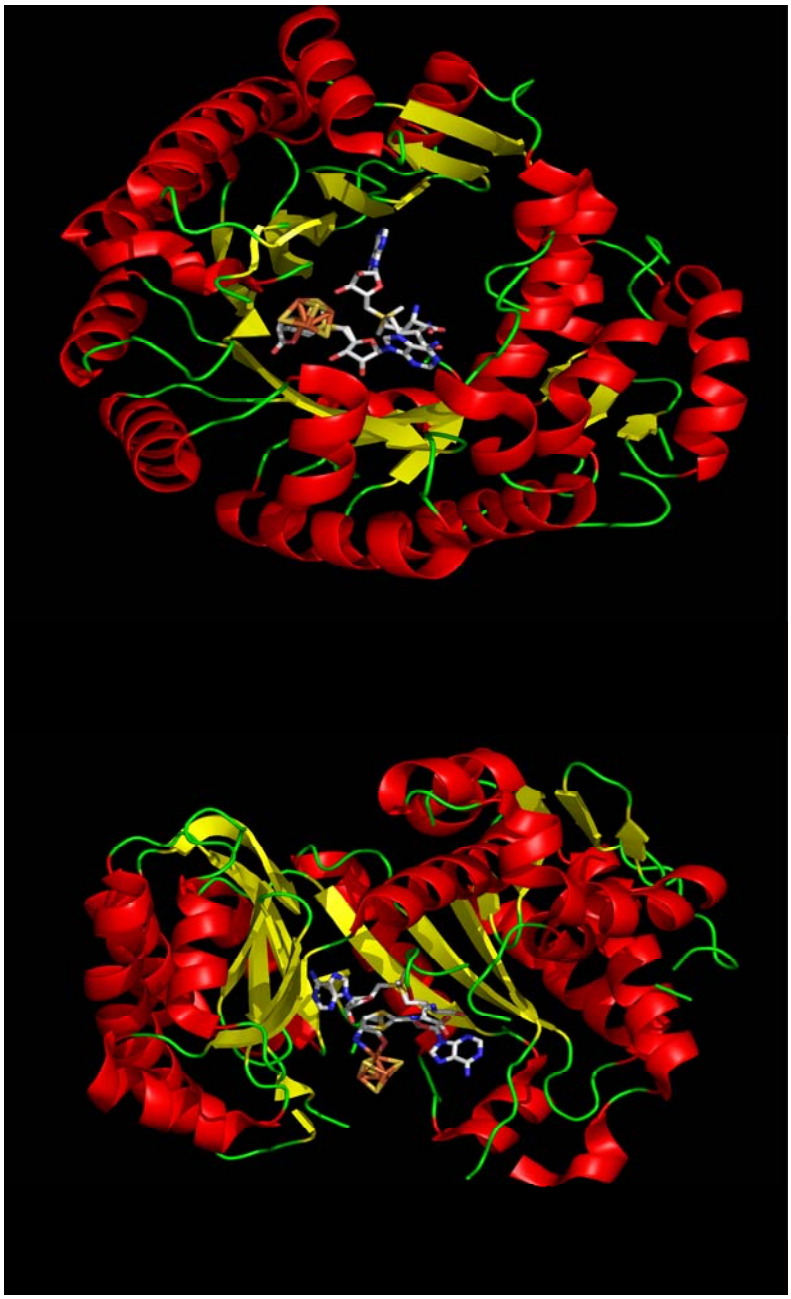

Figure 1.9: Crystal structure of HemN on a top view (top) and a side view (bottom).

The anaerobically purified enzyme is monomeric and was shown to bind one 4Fe-4S cluster *via* three cysteinyl ligands which lie in the prototypical radical SAM motif (CXXXCXXC) [143, 144]. Mössbauer spectroscopy previously revealed the presence of

a unique iron site that is perturbed in the presence of SAM [144]. The crystal structure confirmed spectroscopic and site-directed mutagenesis studies implicating C62, C66, and C69 as cluster ligands, while the unique iron site is ligated by the amine and one of the carboxylate oxygens from the methionine moiety of SAM. The sulfonium atom of cluster-bound SAM is also oriented close to the unique iron site at approximately 3.5 Å. Many conserved residues are involved in hydrogen bonding to the 3' and 4' hydroxyl groups on the ribose ring of SAM while aromatic residues are found in close proximity to the adenine ring. Interestingly, HemN binds a second molecule of SAM which is juxtaposed to the first. Previous site-directed mutagenesis studies show that Y56 is important in catalysis and binding of the Fe-S cluster [143]. The crystal structure reveals a π-stacking interaction with the adenine ring of the second molecule of SAM and the tyrosine residue. The three cofactors are located in a pocket centered within the larger N-terminal domain (residues 36-364). The N-terminal domain forms the barrel and is comprised of 12 β-sheets, three of which are orientated antiparallel to each other. The β-sheets are surrounded by α-helicies and are part of continuous α/β repeats. The authors suggest that the C-terminal domain, primarily composed of α-helicies, could serve to cover the substrate binding site excluding it from solvent.

Mechanistic studies have demonstrated that radical SAM proteins require the injection of an electron into the 4Fe-4S cluster to initiate catalysis. Electrons can be provided by the physiological reducing system flavodoxin/flavodoxin oxidoreductase reductase and NADPH. The 4Fe-4S cluster of HemN is located a mere 6-7 Å from the outer surface. The authors propose that a hydrophobic patch in this region could serve as a binding site for flavodoxin. Modeling studies revealed that docking of flavodoxin

places the flavin cofactor within 8 Å of the 4Fe-4S cluster which is within the range for electron transfer [142].

Biotin Synthase (BioB)

The crystal structure of BioB has also recently been solved in a combined effort from the Drennan and Jarrett laboratories [145]. The structure was resolved to 3.4 Å in the presence of SAM and the substrate, dethiobiotin. BioB is dimeric and adopts a TIM-type ($\alpha\beta_8$) full barrel in contrast to the three-quarter ($\alpha\beta_6$) barrel of the radical SAM protein HemN (Figure 1.10) [142]. The crystal structure shows that each monomer binds a 4Fe-4S cluster, a 2Fe-2S cluster, SAM, and dethiobiotin. The 4Fe-4S cluster is located near the C-terminal end of the barrel and is ~6-7 Å from the outer surface of the protein. As in HemN, the positioning of the 4Fe-4S cluster close to the surface of the protein may optimize transfer of an electron from flavodoxin. Early site-directed mutagenesis studies suggested that the cysteines that lie within the radical SAM motif serve as ligand to the 4Fe-4S cluster [110]. These cysteine residues (C53, C57, and C60) are in fact employed by the enzyme to coordinate three of the iron atoms in the cluster. The fourth iron atom is ligated in an N/O chelate to a nitrogen and oxygen atom from the methionine moiety of SAM. This common feature of radical SAM proteins was first observed spectroscopically in PFL-AE [146-148]. The 2Fe-2S cluster resides at the bottom of the barrel and is ligated by C97, C128, and C188. Unexpectedly, the fourth ligand to the cluster is arginine-260. The authors' note that this type of coordination by arginine has no precedence in biological systems and may be relevant either structurally or catalytically based on its high conservation in biotin synthases.

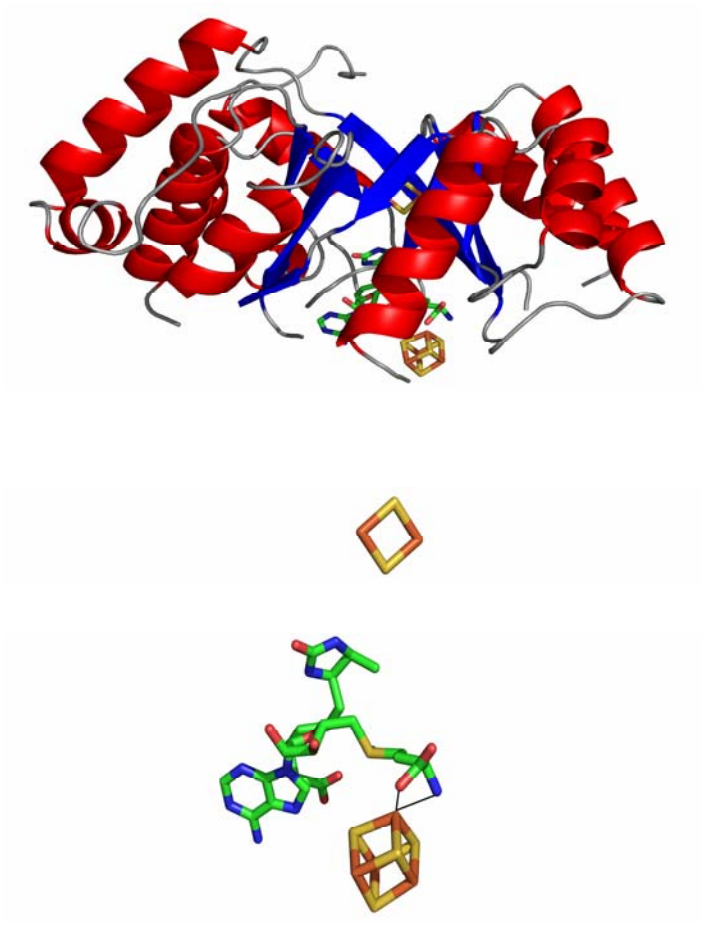

Figure 1.10: Crystal Structure of BioB (top). The bottom figure represents a close-up of the active site without the protein backbone highlighting the coordination of SAM to the unique iron of the 4Fe-4S cluster.

SAM and dethiobiotin are positioned between the 4Fe-4S cluster and the 2Fe-2S cluster (Figure 1.10). The bound SAM molecule stretches across the top of the barrel and has extensive hydrogen bond contacts various β-sheets which subsequently shields it from the environment. It was suggested that this conformation may be important during

the generation of the highly reactive 5'-deoxyadenosyl radical. Dethiobiotin is orientated between SAM and the 2Fe-2S cluster and forms various contacts *via* its carboxylate moiety and ureido ring to the ribose ring and adenine ring of SAM. The authors also highlight the bidentate coordination of the carbonyl oxygen in the ureido ring by asparagine 222 which may aid in positioning of the substrate during hydrogen atom abstraction.

The crystal structure supports a mechanism, first suggested in many biochemical studies, where reductive cleavage of SAM leads to the generation of a 5'-deoxyadenosyl radical that is poised to abstract a hydrogen atom from C-9 of dethiobiotin located 3.9 Å from the 5'-carbon of SAM [149, 150]. The resulting substrate radical is positioned 4.6 Å away from the closest bridging sulfur atom in the 2Fe-2S cluster. This may facilitate radical mediated sulfur atom incorporation into the substrate from the Fe-S cluster. Completion of the thiophane ring can then be achieved by a second round SAM cleavage to yield another 5'-deoxyadenosyl radical which abstracts a hydrogen atom from C-6 (C-6 is located ~ 4.1 Å from the 5'-carbon of SAM).

MoaA: A Radical SAM Enzyme Involved in Molybdenum Cofactor Biosynthesis

Crystallographic studies from the Schindelin laboratory showed that MoaA, like HemN and BioB, shares the overall TIM fold. The protein coexists as a monomer and a dimer in solution and has been crystallized in the absence (2.8 Å) and presence of SAM (2.2 Å) [151]. Like, HemN, the protein is missing two (α/β) units and assumes a (α/β_6) conformation. The N-terminal domain (amino acids 3-323) subsequently forms the core of the incomplete TIM barrel. The C-terminal domain (amino acids 224-329) is

composed of three antiparallel β-sheets which covers the side of the barrel. MoaA binds one 4Fe-4S cluster in the N-terminal domain and one 4Fe-4S cluster in the C-terminus portion of the enzyme. The 4Fe-4S cluster in N-terminus is ligated by three cysteine residues which lie in the CXXXCXXC radical SAM consensus sequence. In the apoprotein the ligand to the fourth atom has not been identified but water has been excluded based on the electron density. When SAM is cocrystallized with MoaA, the amine nitrogen and carboxyl oxygen from SAM form, what is now a classic N/O chelate in this superfamily of enzymes, to the this unique fourth iron site. The C-terminal 4Fe-4S cluster is also bound by three cysteinyl ligands, which lie in a $CX_2CX_{13}C$ motif. The initial crystal structure of MoaA did not have the substrate 5'-GTP present and thus a void was present in the active site between the two Fe-S clusters.

A more recent crystal structure, containing 5'-GTP, revealed that the fourth iron in the C-terminal cluster is in fact ligated to N1 and N2 of the guanine base [152]. The binding of 5'-GTP is enhanced *via* hydrogen bonds in its triphosphate moiety to R17, R71, R192, K69, and K163. A snapshot of the active site subsequent to SAM cleavage was obtained by soaking in sodium dithionite. It is clear from the structure that methionine remains bound to the N-terminal 4Fe-4S cluster in an N/O chelate. 5'-dA was also observed and remained in similar contacts to the protein that SAM does. The electron density about the 5'-carbon becomes disordered indicating a free range of motion may result from scission of the 5'-C-S^+ bond. The substrate/cleavage product containing crystal structure led Hänzelman and Schindelin to propose that potential targets for hydrogen atom abstraction may reside on the C2' (6.3 Å) and C3' (5.3 Å) carbons of the ribose ring. The imidazole C8 carbon from the guanine ring is also within

8.1 Å from the 5'-carbon and may also be involved although large conformational changes maybe required [152].

Lysine-2,3-aminomutase (LAM)

LAM from *Clostridium subterminale* has been characterized in great detail biochemically and spectroscopically by the Frey laboratory [153]. The crystal structure has recently been resolved to 2.1 Å in collaboration with the Ringe laboratory [154]. LAM has many structural and mechanistic similarities to other radical SAM proteins but also deviates significantly utilizing PLP and a catalytic 5'-deoxyadenosyl radical. In solution, the protein has been shown to exist as dimers, tetramers, and hexamers [154]. The protein was crystallized as a homotetramer in the presence of substrate and all cofactors required for turnover, including: L-α-lysine, Se-adenosyl-L-methionine (SeSAM), PLP, zinc ions, and a 4Fe4S cluster. The crystallized complex is suggested to be catalytic upon the injection of a single electron into the 4Fe-4S cluster.

Each individual subunit has a central domain, an N-terminal domain, and a C-terminal domain. LAM follows its predecessors forming an ($\alpha\beta_6$) core in the central domain which resembles the TIM barrel and houses the active site. The N-terminal domain structurally covers the TIM barrel of the adjacent subunit with seven short helicies. Zinc is known to be required for catalysis in LAM, and was found in the crystal structure bound by four cysteine residues. Three cysteines are contributed by one subunit and the fourth cysteine is contributed by the opposing subunit. This zinc-mediated communication between subunits is vital for the assembly of two domain-swapped dimers into the homotetramer.

The active site is composed of SeSAM bound to the 4Fe-4S cluster and L-α-lysine bound in as an external aldimine to PLP. Three iron atoms in the radical SAM cluster are ligated by three cysteine residues (C125, C129, and C132). The methionine moiety of SeSAM coordinates the fourth iron in a typical N/O chelate which was first observed using electron nuclear double resonance (ENDOR) spectroscopy [155].

1.9 Newly Emerging Radical SAM Enzymes

Radical SAM proteins catalyze a diverse range of chemically sophisticated reactions. Within the past five or six years a surge of work has evolved that describes the characterization of new proteins that are contained within this superfamily. The mechanistic complexity is intriguing for many of these enzymes but the roles of the metabolic intermediates formed are even more astounding. These reactions range from the biosynthesis of vital metabolic cofactors and antibiotics to posttranslational modifications such as thiomethylations [114].

Fe-Fe (Fe-only) Hydrogenases

Metal containing hydrogenases exist in two forms: NiFe-containing and Fe-only containing. These metalloenzymes catalyze the reversible oxidation of hydrogen gas to protons. The assembly of the metallocenter (H-cluster) of the Fe-only containing hydrogenase has been studied in some detail. The structure is quite complex and consists of a two iron center connected to a [4Fe-4S] cluster *via* a conserved cysteine residue (Figure 1.11). The 2Fe center is bridged by a unique non-protein dithiolate ligand. Carbon monoxide and cyanide provide two other ligands to each of the iron atoms at the

2Fe center. The dithiolate ligand has putatively been assigned as a dithiopropane or a di(thiomethyl)amine [156] [157]. Mutational analysis identified genes involved in the H-cluster biosynthesis (*hydEFG*) [158]. Sequence alignments demonstrate that *hydE* and *hydG* show similarties to radical SAM proteins containing the CXXXCXXC motif.

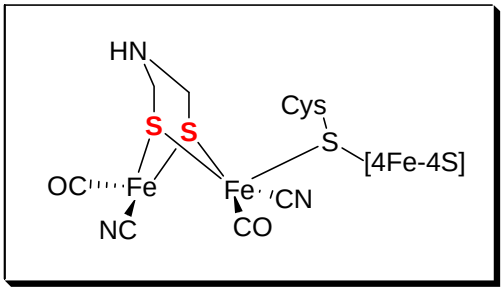

Figure 1.11: Proposed structure of the H-cluster from Fe-only hydrogenases.

The isolation and biophysical characterization of the *hydE* and *hydG* gene products has recently provided evidence that each protein binds at least one [4Fe-4S] cluster and can reductively cleave SAM to 5'-dA [159]. Interestingly, this production occurred in the absence of substrate and was accelerated by the addition of dithiothreitol (DTT). The bridging dithiol moiety is structurally similar to the 1,2-dithiolane ring of lipoic acid, and sulfur insertion *via* LipA/BioB-like reactions into aliphatic precursors has been suggested [158-160].

MiaB: t-RNA Thiomethyltransferase

Another important biological reaction catalyzed by a putative radical SAM protein is a thiomethylation of tRNA. In *E. coli* thiomethylation of *N*-6-isopentyl adenosine in tRNA has been observed and may play an important role in regulation. It has been thought that this base modification requires at least the action of one enzyme, MiaB, and possibly another MiaA. MiaB has been shown to contain the radical SAM

cysteine motif and binds a [4Fe-4S] cluster [161]. The reaction catalyzed by the enzyme(s) is a difficult C-H to C-S bond transformation similar to that of BioB and LipA [162]. Recent evidence suggests that MiaB utilizes SAM in a bifunctional manor where the first molecule of SAM is reductively cleaved via the [4Fe-4S] cluster to yield a high energy 5'-dA• and the second molecule of SAM could then be used more traditionally as a methyl donor. [163]. The sulfur source has been investigated to some extent where reconstituted protein containing a [4Fe-4Se] cluster has been shown to catalyze the incorporation of a selenomethyl group into the nucleoside [163]. These results are similar to studies performed on BioB and LipA where sulfur is thought to be provided by the protein itself therefore the enzyme acts as a catalyst and a substrate *in vitro* [111, 164, 165].

Elp3: Elongator Complex Central Domain

The involvement of a radical SAM protein has even been implicated in transcriptional processes. Elp3 is a subunit of the Elongator complex which is thought to play a vital role in transcription regulation. The protein shows high conservation from archaea to humans. Sequence analysis revealed that the protein has two domains, one that shows high homology to histone acetyltransferases (HATs) and the other to radical SAM proteins [166]. The protein has recently been purified to homogeneity and has a UV-visible spectrum that resembles [4Fe-4S] clusters. EPR spectroscopy confirmed the presence of the Fe-S cluster upon reduction with sodium dithionite. The EPR spectrum is perturbed slightly in the presence of excess SAM suggesting binding of the cofactor in close proximity to the Fe-S center. Although the substrate for Elp3 is unknown, it has been speculated to be involved in histone demethylation

Avilamycin A Biosynthesis

Avilamycin A is a member of the orthosomycin family of antibiotics. This particular family is characterized structurally by a linear heptasaccharide which contains at least one unique spiro-ortholactone linkage [167]. The complex natural product is produced by *Streptomyces viridochromogenes* Tü57 as a secondary metabolite. The active form of the compound has been shown to have a broad spectrum of activity against bacteria that are resistant to vancomycin, methicillin, and penicillin [168]. The cloning of the biosynthetic gene cluster of avilamycin has allowed for a variety of biochemical and genetic experiments to be performed [169]. Gene disruption experiments have shown that the *aviX12* gene is responsible for conferring the compounds bioactivity. Bacteria lacking a functional AviX12 accumulated four derivatives of avilamycin A. The major product, gavibamycin N1, was shown to contain the opposite epimer at C-2 when compared to avialamycin A. These results suggested that the initial monosaccharide building block was not D-mannose but D-glucose and implicated AviX12 as an epimerase. Consequently, these subtle structural differences were shown to lead to a drastic decrease in bioactivity.

Primary sequence analysis revealed a cluster of cysteines arranged in a CXXXCXXC motif which, based on homology, grouped the enzyme in the Radical SAM family of enzymes. A recombinant AviX12 protein engineered with a his-tag was overexpressed in *E. coli* and purified to homogeneity. The aerobically purified protein was shown, using a combination of EPR and UV-visible spectroscopies, to contain a 3Fe-4S cluster [168]. Characterized radical SAM enzymes bind a 4Fe-4S cluster within this conserved cysteine motif. It is the 4Fe-4S cluster configuration that has been shown to be

involved in the binding of SAM which is a required interaction for the generation of a high-energy 5'-dA radical. The 5'-dA radical is then involved in hydrogen atom abstraction from the substrate [170]. The authors suggested that a 5'-dA radical could be involved in hydrogen atom abstraction from the C-2 position of mannose generating a substrate radical intermediate that undergoes epimerization.

1.10 References

1. Reed, L., Multienzyme Complexes. *Acc Chem Res*, 1974. **7**: p. 40-46.
2. Skeggs, H.R., L.D. Wright, E.L. Cresson, G.D.E. MacRae, C.H. Hoffman, D.E. Wolf, and K. Folkers, Disvcovery of a New Acetate-Replacing Factor. *J. Bacteriol.*, 1956. **72**: p. 519-524.
3. Gunsalus, I.C., M.I. Dolin, and L. Struglia, Pyruvic Acid Metabolism. *J Biol Chem*, 1952. **194**(2): p. 849-857.
4. Reed, L.J., I.C. Gunsalus, G.H.F. Schnakenberg, Q.F. Soper, H.E. Boaz, S.F. Kern, and T.V. Parke, Isolation, Characterization and Structure of a-Lipoic Acid. *J Am Chem Soc*, 1953. **75**: p. 1267-1270.
5. Reed, L.J., B.G.D. Busk, I.C. Gunsalus, and G.H.F. Schnakenberg, Crystalline α-Lipoic Acid: A Catalytic Agent Associated with Pyruvate Dehydrogenase. *Science*, 1951. **114**: p. 93.
6. Brockman, J.A.J., E.L.R. Stokstad, E.L. Patterson, J.V. Pierce, M. Macchi, and F.P. Day, Structure of Protogen A. *J Am Chem Soc*, 1952. **74**: p. 1868.

7. Bullock, M.W., Brockman, J.A. Jr., Patterson, E.L., Pierce, J.V., Stokstad, E.L.R., Synthesis of Compounds in the Thioctic Acid Series. *J Am Chem Soc*, 1952. **74**: p. 3455.

8. Barltrop, J.A., P.M. Hayes, and M. Calvin, The Chemistry of 1,2-Dithiolane (Trimethylene Disulfide) as a Model for the Primary Quantum Conversion Act in Photosynthesis. *J Am Chem Soc*, 1954. **76**: p. 4348-4367.

9. Walton, E., A.F. Wagner, L.H. Peterson, F.W. Holly, and K. Folkers, The Synthesis of (+)-a-Lipoic Acid and Its Optical Antipode. *J Am Chem Soc*, 1954. **76**: p. 4748.

10. Mislow, K. and W.C. Meluch, The Stereochemistry of α-Lipoic Acid. *J. Am. Chem. Soc.*, 1956. **78**: p. 5920.

11. Fredga, A., *Arkiv. Kemi Mineral. Geol.*, 1942. **15B**: p. 23.

12. Reed, L.J. and M.L. Hackert, Structure-function relationships in dihydrolipoamide acyltransferases. *J Biol Chem*, 1990. **265**(16): p. 8971-8974.

13. Vanden Boom, T.J., K.E. Reed, and J. J. E. Cronan, Lipoic Acid Metabolism in *Escherichia coli*: Isolation of Null Mutants Defective in Lipoic Acid Biosynthesis, Molecular Cloning and Characterization of the *E. coli lip* Locus, and Identification of the Lipoylated Protein of the Glycine Cleavage System. *J Bacteriol*, 1991. **173**(20): p. 6411-6420.

14. O'Kane, D.J. and I.C. Gunsalus, Pyruvic Acid Metabolism: A Factor Required for Oxidation by Stretococcus faecalis. *J Bacteriol*, 1948. **56**: p. 499-506.

15. Gunsalus, I.C., Oxidative and Transfer Reactions of Lipoic Acid. *Federation Proc.*, 1954. **13**: p. 715-722.

16. Sanadi, D.R., M. Langley, and R.L. Searls, a-Ketoglutaric Dehydrogenase. VI. Reversible Oxidation of Dihydrothioctamide by Diphosphopyridine Nucleotide. *J. Biol. Chem.*, 1959. **234**: p. 178.

17. Suzuki, K. and L.J. Reed, Lipoamidase. *J Biol Chem*, 1963. **238**: p. 4021-4025.

18. Koike, M. and K. Suzuki, Purification and Properties of Lipoamidase. *Methods Enzymol*, 1970. **18**: p. 292-298.

19. Reed, L.J., M. Koike, M.E. Levitch, and F.R. Leach, Studies on the Nature and Reactions of Protein-Bound Lipoic Acid. *J. Biol. Chem.*, 1958. **232**: p. 143-158.

20. Nawa, H., W.T. Brady, M. Koike, and L.J. Reed, Studies on the Nature of Protein-bound Lipoic Acid. *J. Am. Chem. Soc.*, 1960. **82**: p. 896.

21. Koike, M., L.J. Reed, and W.R. Carroll, alpha-Keto acid dehydrogenation complexes. I. Purification and properties of pyruvate and alpha-ketoglutarate dehydrogenation complexes of Escherichia coli. *J. Biol. Chem.*, 1959. **235**: p. 1924.

22. Koike, M. and L.J. Reed, The Role of Protein-Bound Lipoic Acid and Flavin Adenine Dinucleotide. *J Biol Chem*, 1960. **235**: p. 1931-1938.

23. Koike, M. and L.J. Reed, a-Keto acid dehydrogenation Complexes. II. The Role of Protein Bound Lipoic Acid and Flavin Adenine Dinucleotide. *J. Biol. Chem.*, 1960. **235**: p. 1931-1938.

24. Angelides, K.J. and G.G. Hammes, Mechanism of Action of the Pyruvate Dehydrogenase Multienzyme Complex from Escherichia coli. *Proc. Natl. Acad. Sci.*, 1978. **75**: p. 4877-4880.

25. Ambrose-Griffin, M.C., M.C. Danson, W.G. Griffin, G. Hale, and R.N. Perham, Kinetic Analysis of the Role of Lipoic Acid Residues in the Pyruvate Dehydrogenase Multienzyme Complex of Escherichia coli. *Biochem. J.*, 1980. **187**: p. 393-401.

26. Oliver, R.M. and L.J. Reed, *Electron Microscopy of Proteins*. Vol. 2. 1982, London: Academic Press.

27. Perham, R.N., Domains, Motifs, and Linkers in 2-Oxo Acid Dehydrogenase Multienzyme Complexes: A Paradigm in the Design of a Multifunctional Protein. *Biochemistry*, 1991. **30**: p. 8501-8512.

28. Kruger, N., F.B. Oppermann, H. Lorenzl, and A. Steinbuchel, Biochemical and molecular characterization of the Clostridium magnum acetoin dehydrogenase enzyme system. *J Bacteriol*, 1994. **176**(12): p. 3614-30.

29. Priefert, H., S. Hein, N. Kruger, K. Zeh, B. Schmidt, and A. Steinbuchel, Identification and molecular characterization of the Alcaligenes eutrophus H16 aco operon genes involved in acetoin catabolism. *J Bacteriol*, 1991. **173**(13): p. 4056-71.

30. Fujiwara, K., K. Okamura-Ikeda, and Y. Motokawat, Expression of mature bovine H-protein of the glycine cleavage system in *Escherichia coli* and in vitro lipoylation of the apoform. *J Biol Chem*, 1992. **267**: p. 20011-20016.

31. Douce, R., J. Bourguignon, D. Macherel, and M. Neuburger, The Glycine Decarboxylase System in Higher Plant Mitochondria: Structure, Function and Biogenesis. *Biochem Soc Trans*, 1994. **22**: p. 184-188.

32. Okamura-Ikeda, K., Y. Ohmura, K. Fukiwara, and Y. Motokawa, Cloning and nucleotide sequence of the gcv operon encoding the *Escherichia coli* glycine-cleavage system. *Eur J Biochem*, 1993. **216**(2): p. 539-548.

33. Klein, S.M. and R.D. Sagers, Glycine Metabolism. I. Properties of the System Catalyzing the Exchange of Bicarbonate with the Carboxyl Group of Glycine in *Peptococcus glycinophilus*. *J Biol Chem*, 1966. **241**(1): p. 197-205.

34. Klein, S.M. and R.D. Sagers, Glycine Metabolism. II. Kinetic and Optical Studies on the Glycine Decarboxylase System from *Peptococcus glycinophilus*. *J Biol Chem*, 1966. **241**(1): p. 206-209.

35. Klein, S.M. and R.D. Sagers, Glycine Metabolism. III. A Flavin-Linked Dehydrogenase Associated with the Glycine Cleavage System in *Peptococcus glycinophilus*. *J Biol Chem*, 1967. **242**(2): p. 297-300.

36. Klein, S.M. and R.D. Sagers, Glycine Metabolism. IV. Effect of Borohydrine Reduction on the Pyridoxal Phosphate-Containing Glycine Decarboxylase from *Peptococcus glycinophilus*. *J Biol Chem*, 1967. **242**(2): p. 301-305.

37. Fujiwara, K., K. Okamura-Ikeda, and Y. Motokawa, Mechanism of the Glycine Cleavage Reaction. Further Characterization of the Intermediate Attached to H-Protein and of the Reaction Catalyzed by T-Protein. *J Biol Chem*, 1984. **259**(17): p. 10664-10668.

38. Hiraga, K. and G. Kikuchi, THe Mitochondrial Glycine Cleavage System. Purification and Properties of Glycine Decarboxylase from Chicken Liver Mitochondria. *J. Biol. Chem.*, 1980. **255**: p. 11664-11670.

39. Robinson, J.R., S.M. Klein, and R.D. Sagers, Glycine Metabolism. Lipoic Acid as the Prosthetic Group in the Electron Transfer Protein P2 from *Peptococcus glycinophilus*. *J Biol Chem*, 1973. **248**(15): p. 5319-5323.

40. Motokawa, Y. and G. Kikuchi, Glycine Metabolism by Rat Liver Mitochondria. IV. Isolation and Characterization of Hydrogen Carrier Protein, and Essential Factor for Glycine Metabolism. *Arch. Biochem. Biophys.*, 1969. **135**: p. 402-409.

41. Kochi, J.K. and G. Kikuchi, Mechanism of the Reversible Glycine Cleavage Reaction in Arthrobacter globiformis. I. Purification and Function of Protein Components Required for the Reaction. *J. Biochem.*, 1976. **75**: p. 1113-1127.

42. Kochi, J.K. and G. Kikuchi, Mechanism of the Reversible Cleavage Reaction in Arthrobacter globiformis. Function of Lipoic acid in the Cleavage and Synthesis of Glycine. *Arch. Biochem. Biophys.*, 1976. **173**: p. 71-81.

43. Fujiwara, K., K. Okamura-Ikeda, and Y. Motokawa, Hydrogen Carrier Protein from Chicken Liver: Purification, Characterization, and Role of its Prosthetic Group, Lipoic Acid, in the Glycine Cleavage Reaction. *Arch. Biochem. Biophys.*, 1979. **197**: p. 454-462.

44. Motokawa, Y. and G. Kikuchi, Glycine Metabolism by Rat Liver Mitochondria. II. Methylene Tetrahydrofolate as the Direct One Carbon Donor in the Reaction of Glycine Synthesis. *J. Biochem.*, 1969. **65**: p. 71-75.

45. Tsunoda, J.N. and K.T. Yasunobu, Mammalian Lipoic Acid Activating Enzyme. *Arch. Biochem. Biophys.*, 1967. **118**: p. 395-401.

46. Fujiwara, K., S. Takeuchi, K. Okamura-Ikeda, and Y. Motokawa, Purification, Characterization, and cDNA Cloning of Lipoate-Activating Enzyme from Bovine Liver. *J. Biol. Chem.*, 2001. **276**: p. 28819-28823.

47. Leach, F.R., Lipoic Acid Activation: Biosynthesis of Lipoamide (enzyme). *Methods Enzymol.*, 1970. **49**: p. 282-290.

48. Prassad, P.D., H. Wnag, R. Kekuda, T. Fujita, Y.-J. Fei, L.D. Devoes, F.H. Leibach, and V. Ganapathy, Cloning and Functional Expression of cDNA Encoding a Mammalian Sodium-Dependent Vitamin Transporter Mediating the Uptake of Pantothenate, Biotin, and Lipoate. *J. Biol. Chem.*, 1998. **273**: p. 7501-7506.

49. Reed, L.J., F.R. Leach, and M. Koike, Studies on Lipoic Acid-Activating System. *J. Biol. Chem.*, 1958. **232**: p. 123-142.

50. Morris, T.W., K.E. Reed, and J.E. Cronan Jr., Identification of the Gene Encoding Lipoate-Protein Ligase of *Escherichia coli.* Molecular Cloning and Characterization of the *lplA* Gene and Gene Product. *J Biol Chem*, 1994. **269**: p. 16091-16100.

51. Morris, T.W., K.E. Reed, and J. J. E. Cronan, Lipoic Acid Metabolism in *Escherichia coli*: the *lplA* and *lipB* Genes Define Redundant Pathways for Ligation of Lipoyl Groups to Apoprotein. *J Bacteriol*, 1995. **177**(1): p. 1-10.

52. Mitra, S.K. and D.P. Burma, Activation of Lipoic Acid and its Transfer from Free Pool to the Protein-Bound State. *J. Biol. Chem.*, 1965. **240**: p. 4072-4080.

53. Dardel, F., L.C. Packman, and R.N. Perham, Expression in Escherichia coli of a Sub-Gene Encoding the Lipoyl Domain of the pyruvate Dehrdrogenase Complex of Bacillus stearothermophilus. *FEBS*, 1990. **264**: p. 206-210.

54. Ali, S.T., A.J.G. Moir, P.R. Ashton, P.C. Engel, and J.R. Guest, Octanoylation of the Lipoyl Domains of the Pyruvate Dehydrogenase Complex in a Lipoyl-deficient Strain of Escherichia coli. *Molec. Micro.*, 1990. **4**(943-950).

55. Green, D.E., T.W. Morris, G. J., J.E. Cronan Jr., and J.R. Guest, Purification and Properties of the Lipoate Protein Ligase of *Escherichia coli. Biochem J.*, 1995. **309**: p. 853-862.

56. Reed, K.E. and J. J. E. Cronan, Lipoic Acid Metabolism in *Escherichia coli*: Sequencing and Functional Characterization of the *lipA* and *lipB* Genes. *J Bacteriol*, 1993. **175**(5): p. 1325-1336.

57. Jordan, S.W. and J.E. Cronan Jr., The *Escherichia coli* lipB Gene Encodes Lipoyl (Octanoyl)-Acyl Carrier Protein:Protein Transferase. *J Bacteriol*, 2003. **185**(5): p. 1582-1589.

58. Jordan, S.W. and J. J. E. Cronan, A New Metabolic Link. The Acyl Carrier Protein of Lipid Synthesis Donates Lipoic Acid to the Pyruvate Dehydrogenase Complex in *Escherichia coli* and Mitochondria. *J Biol Chem*, 1997. **272**(29): p. 17903-17906.

59. Brody, S., C. Oh, and U.H.E. Schweizer, Mitochondrial Acyl Carrier Protein is Involved in Lipoic Acid Synthesis in *Saccharomyces cerevisiae. FEBS Letters*, 1997. **408**: p. 217-220.

60. Wada, H., D. Shintani, and J. Ohlrogge, Why do Mitochondria Synthesize Fatty Acids? Evidence for Involvement in Lipoic Acid Production. *Proc. Natl. Acad. Sci.*, 1997. **94**: p. 1591-1596.

61. Zhao, S., J.R. Miller, and J.E. Cronan Jr., The Reaction of LipB, the Octanoyl-[Acyl Carrier Protein]:Protein N-Octanoyltransferase of Lipoic Acid Synthesis, Proceeds through an Acyl-Enzyme Intermediate. *Biochemistry*, 2005. **44**: p. 16737-16746.

62. Otsuka, A.J., M.R. Buoncristiani, P.K. Howard, J. Flamm, C. Johnson, R. Yamamoto, K. Uchida, C. Cook, J. Ruppert, and J. Matsuzaki, The *Escherichia coli* Biotin Biosynthetic Enzyme Sequences Predicted from the Nucleotide Sequence of the *bio* Operon. *J Biol Chem*, 1988. **263**: p. 19577-19585.

63. Eisenberg, M.A., Biotin: biogenesis, transport, and their regulation. *Adv Enzymol Relat Areas Mol Biol*, 1973. **38**: p. 317-372.

64. Ploux, O. and A. Marquet, Mechanistic studies on the 8-amino-7-oxopelargonate synthase, a pyridoxal-5'-phosphate-dependent enzyme involved in biotin biosynthesis. *Eur J Biochem*, 1996. **236**: p. 301-308.

65. Pai, C.H., Biosynthesis of biotin: synthesis of 7,8-diaminopelargonic acid in cell-free extracts of Escherichia coli. *J. Bacteriol.*, 1971. **105**: p. 793-800.

66. Stoner, G.L. and M.A. Eisenberg, Purification and properties of 7, 8-diaminopelargonic acid aminotransferase. *J. Biol. Chem.*, 1975. **250**: p. 4029-4036.

67. Stoner, G.L. and M.A. Eisenberg, Biosynthesis of 7, 8-diaminopelargonic acid from 7-keto-8-aminopelargonic acid and S-adenosyl-L-methionine. The kinetics of the reaction. *J. Biol. Chem.*, 1975. **250**: p. 4037-4043.

68. Li, H.C., D.B. McCormick, and L.D. Wright, Conversion of dethiobiotin to biotin in Aspergillus niger. *J. Biol. Chem.*, 1968. **243**: p. 6442-6445.

69. Parry, R.J. and M.G. Kunitani, Biotin biosynthesis. 1. The incorporation of specifically tritiated dethiobiotin into biotin. *J. Am. Chem. Soc.*, 1976. **98**: p. 4024-4026.

70. Parry, R.J., Biosynthesis of Some Sulfur-Containing Natural Products. Investigations of the Mechanism of Carbon-Sulfur bond Formation. *Tetrahedron*, 1983. **39**: p. 1215-1238.

71. Trainor, D.A., R.J. Parry, and A. Gitterman, Biotin Biosynthesis. 2. Stereochemistry of Sulfur Introduction at C-4 of Dethiobiotin. *J Am Chem Soc*, 1980. **102**(4): p. 1467-1468.

72. Trotter, J. and J. Hamilton, The absolute configuration of Biotin. *Biochemistry*, 1966. **5**: p. 713-714.

73. Parry, R.J., *Bioorganic Chemistry*, ed. E.E.v. Tamelen. Vol. II. 1978, New York: Academic Press. 247-242.

74. Frappier, F., G. Guillerm, A.G. Salib, and A. Marquet, On the Mechanism of Conversion of Dethiobiotin to Biotin in Escherichia coli. Discussion of the Occurrence of an Intermediate Hydroxylation. *Biochem Biophys Res Commun*, 1979. **91**(2): p. 521-527.

75. Ohrui, H., N. Sueda, and S. Emoto, *Agric. Biol. Chem.*, 1978. **42**: p. 865.

76. Marquet, A., B.T. Bui, and B. Florentin, *Biosynthesis of Biotin and Lipoic Acid*. Vitamins and Hormones. Vol. 61. 2001, New York: Academic Press.

77. Marquet, A., F. Frappier, G. Guillerm, M. Azoulay, D. Florentin, and J.-C. Tabet, Biotin Biosynthesis: Synthesis and Biological Evaluation of the Putative Intermediate Thiols. *J Am Chem Soc*, 1993. **115**: p. 2139-2145.

78. Even, L., D. Florentin, and A. Marquet, Biotin biosynthesis: Preparation of the postulated intermediate thiol. *Bull. Soc. Chim. Fr.*, 1990. **127**: p. 3571-3578.

79. Baldet, P., H. Gerbling, S. Axiotis, and R. Douce, Biotin biosynthesis in higher plant cells. Identification of intermediates. *Eur. J. Biochem.*, 1993. **217**: p. 479-485.

80. Tse Sum Bui, B., M. Lotierzo, F. Escalettes, D. Florentin, and A. Marquet, Further investigation on the turnover of Escherichia coli biotin synthase with dethiobiotin and 9-mercaptodethiobiotin as substrates. *Biochemistry*, 2004. **43**(51): p. 16432-41.

81. DeMoll, E. and W. Shive, The origin of sulfur in biotin. *Biochem. Biophys. Res. Commun.*, 1983. **110**: p. 243-249.

82. DeMoll, E., R.H. White, and W. Shive, Determination of the Metabolic Origins of the Sulfur and 3'-Nitrogen Atoms in Biotin of Escherichia coli by Mass Spectrometry. *Biochem.*, 1984. **23**(3): p. 558-562.

83. Ifuku, O., J. Kishimoto, S.-I. Haze, M. Yanagi, and S. Fukushima, Conversion of Dethiobiotin to Biotin in Cell-Free Extracts of *Escherichia coli*. *Biosci. Biotech. Biochem.*, 1992. **56**(11): p. 1780-1785.

84. Birch, O.M., M. Fuhrmann, and N.M. Shaw, Biotin Synthase from *Escherichia coli*, an Investigation of the Low Molecular Weight and Protein Components Required for Activity *in Vitro*. *J. Biol. Chem.*, 1995. **270**(32): p. 19158-19165.

85. Shaw, N.M., O.M. Birch, A. Tinschert, V. Venetz, R. Dietrich, and L.-A. Savoy, Biotin Synthase from *Escherichia coli*: Isolation of an Enzyme-Generated Intermediate and Stoichiometry of S-Adenosylmethionine Use. *Biochem. J.*, 1998. **330**: p. 1079-1085.

86. Guianvarc'h, D., D. Florentin, B.T.S. Bui, F. Nunzi, and A. Marquet, Biotin synthase, a New Member of the Family of Enzymes Which Uses S-Adenosylmethionine as a Source of Deoxyadenosyl Radical. *Biochem Biophys Res Commun*, 1997. **236**: p. 402-406.

87. Padovani, D., F. Thomas, A.X. Trautwein, E. Mulliez, and M. Fontecave, Activation of class III ribonucleotide reductase from E. coli. The electron transfer from the iron-sulfur center to S-adenosylmethionine. *Biochemistry*, 2001. **40**: p. 6713-6719.

88. Henshaw, T.F., J. Cheek, and J.B. Broderick, The $[4Fe\text{-}4S]^{+1}$ Cluster of Pyruvate Formate-Lyase Activating Enzyme Generates the Glycyl Radical on Pyruvate Formate-Lyase: EPR-Detected Single Turnover. *J Am Chem Soc*, 2000. **122**: p. 8331-8332.

89. Wu, W., S. Booker, K.W. Lieder, V. Bandarian, G.H. Reed, and P.A. Frey, Lysine 2,3-Aminomutase and *trans*-4,5-Dehydrolysine: Characterization of an Allylic Analogue of a Substrate-Based Radical in the Catalytic Mechanism. *Biochem.*, 2000. **39**: p. 9561-9570.

90. Lieder, K.W., S. Booker, F.J. Ruzicka, H. Beinert, G.H. Reed, and P.A. Frey, S-Adenosylmethionine-Dependent Reduction of Lysine 2,3-Aminomutase and Observation of the Catalytically Functional Iron-Sulfur Centers by Electron Paramagnetic Resonance. *Biochemistry*, 1998. **37**(8): p. 2578-2585.

91. Escalettes, F., D. Florentin, B. Tse Sum Bui, D. Lesage, and A. Marquet, Biotin Synthase Mechanism: Evidence for Hydrogen Transfer from the Substrate into Deoxyadenosine. *J. Am. Chem. Soc.*, 1999. **121**: p. 3571-3578.

92. Sanyal, I., G. Cohen, and D.H. Flint, Biotin Synthase: Purification, Characterization as a [2Fe-2S] Cluster Protein, and in Vitro Activity of the *Escherichia coli bioB* Gene Product. *Biochemistry*, 1994. **33**: p. 3625-3631.

93. Méjean, A., B.T.S. Bui, D. Florentin, O. Ploux, Y. Izumi, and A. Marquet, Highly Purified Biotin Synthase can Transform Dethiobiotin into Biotin in the Absence of any other Protein, in the Presence of Photoreduced Deazaflavin. *Biochem. Biophys. Res. Commun.*, 1995. **217**(3): p. 1231-1237.

94. Baldet, P., C. Alban, and R. Douce, Biotin synthesis in higher plants: purification and characterization of bioB gene product equivalent from Arabidopsis thaliana overexpressed in Escherichia coli and its subcellular localization in pea leaf cells. *FEBS*, 1997. **419**: p. 206-210.

95. Conradt, H., M. Hohmann-Berger, H.P. Hohmann, H.P. Blaschkowski, and J. Knappe, Pyruvate formate-lyase (inactive form) and pyruvate formate-lyase activating enzyme of Escherichia coli: isolation and structural properties. *Arch Biochem Biophys*, 1984. **228**(1): p. 133-42.

96. Bianchi, V., R. Eliasson, M. Fontecave, E. Mulliez, D.M. Hoover, R.G. Matthews, and P. Reichard, Flavodoxin is Required for the Activation of the Anaerobic Ribonucleotide Reductase. *Biochem Biophys Res Commun*, 1993. **197**(2): p. 792-797.

97. Florentin, D., B.T. Bui, A. Marquet, T. Ohshiro, and Y. Izumi, On the mechanism of biotin synthase of Bacillus sphaericus. *C R Acad Sci III*, 1994. **317**(6): p. 485-8.

98. Tse Sum Bui, B., B. Florentin, F. Fournier, O. Ploux, A. Méjean, and A. Marquet, Biotin Synthase Mechanism: On the Origin of Sulphur. *FEBS Lett*, 1998. **440**: p. 226-230.

99. Gibson, K.J., D.A. Pelletier, and S. I. M. Turner, Transfer of Sulfur to Biotin from Biotin Synthase (BioB protein). *Biochem. Biophys. Res. Commun.*, 1999. **254**: p. 632-635.

100. Tse Sum Bui, B., F. Escalettes, G. Chottard, D. Florentin, and A. Marquet, Enzyme-Mediated Sulfide Production for the Reconstitution of [2Fe-2S] Clusters into Apo-Biotin Synthase of *Escherichia coli*: Sulfide Transfer from Cysteine to Biotin. *Eur. J. Biochem.*, 2000. **267**: p. 2688-2694.

101. Jacobson, M.R., K.E. Brigle, L.T. Bennett, R.A. Setterquist, M.S. Wilson, V.L. Cash, J. Beynon, W.E. Newton, and D.R. Dean, Physical and genetic map of the major nif gene cluster from Azotobacter vinelandii. *J Bacteriol*, 1989. **171**(2): p. 1017-27.

102. Agro, A.F., C. Cannella, M.T. Graziani, and D. Cavallini, A possible role for rhodanese: The formation of 'labile' sulfur from thiosulfate. *FEBS Lett*, 1971. **16**(3): p. 172-174.

103. Duin, E.C., M.E. Lafferty, B.R. Crouse, R.M. Allen, I. Sanyal, D.H. Flint, and M.K. Johnson, [2Fe-2S] to [4Fe-4S] Cluster Conversion in *Escherichia coli* Biotin Synthase. *Biochemistry*, 1997. **36**: p. 11811-11820.

104. Tse Sum Bui, B., D. Florentin, A. Marquet, R. Benda, and A.X. Trautwein, Mössbauer Studies of *Escherichia coli* Biotin Synthase: Evidence for Reversible Interconversion between $[2Fe\text{-}2S]^{2+}$ and $[4Fe\text{-}4S]^{2+}$ Clusters. *FEBS Lett*, 1999. **459**: p. 411-414.

105. Ollagnier-de Choudens, S., Y. Sanakis, K.S. Hewitson, P. Roach, J.E. Baldwin, E. Münck, and M. Fontecave, Iron-Sulfur Center of Biotin Synthase and Lipoate Synthase. *Biochemistry*, 2000. **39**: p. 4165-4173.

106. Ugulava, N.B., B.R. Gibney, and J.T. Jarrett, Iron-Sulfur Cluster Interconversions in Biotin Synthase: Dissociation and Reassociation of Iron during Conversion of [2Fe-2S] to [4Fe-4S] Clusters. *Biochemistry*, 2000. **39**: p. 5206-5214.

107. Ugulava, N.B., B.R. Gibney, and J.T. Jarrett, Biotin Synthase Contains Two Distinct Iron–Sulfur Binding Sites: Chemical and Spectroelectrochemical Analysis of Iron–Sulfur Cluster Interconversions. *Biochemistry*, 2001. **40**: p. 8343-8351.

108. Ugulava, N.B., K.K. Surerus, and J.T. Jarrett, Evidence from Mössbauer Spectroscopy for Distinct $[2Fe\text{-}2S]^{2+}$ and $[4Fe\text{-}4S]^{2+}$ Cluster Binding Sites in Biotin Synthase from *Escherichia coli*. *J Am Chem Soc*, 2002. **124**: p. 9050-9051.

109. Cosper, M.M., G.N.L. Jameson, H.L. Hernández, C. Krebs, B.H. Huynh, and M.K. Johnson, Characterization of the cofactor composition of *Escherichia coli* biotin synthase. *Biochemistry*, 2004. **43**: p. 2007-2021.

110. Hewitson, K.S., J.E. Baldwin, N.M. Shaw, and P.L. Roach, Mutagenesis of the Proposed Iron-Sulfur Cluster Binding Ligands in *Escherichia coli* Biotin Synthase. *FEBS Lett*, 2000. **466**: p. 372-376.

111. Ugulava, N.B., C.J. Sacanell, and J.T. Jarrett, Spectroscopic Changes during a Single Turnover of Biotin Synthase: Destruction of a [2Fe–2S] Cluster Accompanies Sulfur Insertion. *Biochemistry*, 2001. **40**: p. 8352-8358.

112. Tse Sum Bui, B., R. Benda, V. Schünemann, D. Florentin, A.X. Trautwein, and A. Marquet, Fate of the $(2Fe\text{-}2S)^{2+}$ Cluster of *Escherichia coli* Biotin Synthase during Reaction: A Mössbauer Characterization. *Biochemistry*, 2003. **42**(29): p. 8791-8798.

113. Jameson, G.N.L., M.M. Cosper, H.L. Hernández, M.K. Johnson, and B.H. Huynh, Role of the [2Fe–2S] cluster in recombinant *Escerhichia coli* biotin synthase. *Biochemistry*, 2004. **43**: p. 2022-2031.

114. Sofia, H.J., G. Chen, B.G. Hetzler, J.F. Reyes-Spindola, and N.E. Miller, Radical SAM, a novel protein superfamily linking unresolved steps in familiar biosynthetic pathways with radical mechanisms: functional characterization using new analysis and information visualization methods. *Nucleic Acids Res*, 2001. **29**(5): p. 1097-1106.

115. Hewitson, K.S., S. Ollagnier-de Choudens, Y. Sanakis, N.M. Shaw, J.E. Baldwin, E. Münck, P.L. Roach, and M. Fontecave, The Iron-Suflur Center of Biotin Synthase: Site-Directed Mutants. *J Biol Inorg Chem*, 2002. **7**: p. 83-93.

116. Ollagnier-de-Choudens, S., Y. Sanakis, K.S. Hewitson, P. Roach, E. Münck, and M. Fontecave, Reductive Cleavage of S-Adenosylmethionine by Biotin Synthase from *Escherichia coli. Biochemistry*, 2002. **277**(16): p. 13449-13454.

117. Cosper, M.M., G.N.L. Jameson, R. Davydov, M.K. Eidsness, B.M. Hoffman, B.H. Huynh, and M.K. Johnson, The [4Fe–4S]2+ Cluster in Reconstituted Biotin Synthase Binds S-Adenosyl-L-methionine. *J Am Chem Soc*, 2002. **124**(47): p. 14006-14007.

118. Krebs, C., W.E. Broderick, T.F. Henshaw, J.B. Broderick, and B.H. Huynh, Coordination of Adenosylmethionine to a Unique Iron Site of the [4Fe–4S] of Pyruvate Formae–Lyase Activating Enzyme: A Mössbauer Spectroscopic Study. *J Am Chem Soc*, 2002. **124**(6): p. 912-913.

119. Ugulava, N.B., K.K. Frederick, and J.T. Jarrett, Control of adenosylmethionine-dependent radical generation in biotin synthase: a kinetic and thermodynamic analysis of substrate binding to active and inactive forms of BioB. *Biochemistry*, 2003. **42**(9): p. 2708-19.

120. Ollagnier-de Choudens, S., E. Mulliez, K.S. Hewitson, and M. Fontecave, Biotin synthase Is a Pyridoxal Phosphate-Dependent Cysteine Desulfurase. *Biochemistry*, 2002. **41**: p. 9145-9152.

121. Ollagnier-de Choudens, S., E. Mulliez, and M. Fontecave, The PLP-dependent biotin synthase from *Escherichia coli*: mechanistic studies. *FEBS Lett*, 2002. **532**: p. 465-468.

122. Choi-Rhee, E. and J.E. Cronan, A nucleosidase required for in vivo function of the S-adenosyl-L-methionine radical enzyme, biotin synthase. *Chem Biol*, 2005. **12**(5): p. 589-93.

123. Reed, L.J., T. Okaichi, and I. Nakanishi, Studies on the Biosynthesis of Lipoic Acid. *Abstr. Int. Synmp. Chem. Nat. Prod. (Kyoto)*, 1964: p. 218-220.

124. White, R.H., Stable Isotope Studies on the Biosynthesis of Lipoic Acid in *Escherichia coli. Biochemistry*, 1980. **19**: p. 15-19.

125. Parry, R.J. and D.A. Trainor, Biosynthesis of Lipoic Acid. 2. Stereochemistry of Sulfur Introduction at C-6 of Octanoic Acid. *J. Am. Chem. Soc.*, 1978. **100**(16): p. 5243-5244.

126. White, R.H., Biosynthesis of Lipoic Acid: Extent of Incorporation of Deuterated Hydroxy- and Thiooctanoic Acids into Lipoic Acid. *J Am Chem Soc*, 1980. **102**: p. 6605-6607.

127. Hayden, M.A., I.Y. Huang, G. Iliopoulos, M. Orozco, and G.W. Ashley, Biosynthesis of Lipoic Acid: Characterization of the Lipoic Acid Auxotrophs *Escherichia coli* W1485-lip2 and JRG33-lip9. *Biochemistry*, 1993. **32**: p. 3778-3782.

128. Herbert, A.A. and J.R. Guest, Biochemical and Genetic Studies with Lysine and Methionine Mutants of Escherichia coli: Lipoic Acid and a-Ketoglutarate Dehydrogenase-less-Mutants. *J. Gen. Microbiol.*, 1968. **53**: p. 363-381.

129. Sulo, P. and N.C. Martin, Isolation and Characterization of LIP5: A Lipoate Biosynthetic Locus of Saccharomyces Cerevisiae. *J. Biol. Chem.*, 1993. **268**: p. 17634-17639.

130. Morikawa, T., R. Yasuno, and H. Wada, Do mammalian cells synthesize lipoic acid? Identification of a mouse cDNA encoding a lipoic acid synthase located in mitochondria. *FEBS Lett.*, 2001. **498**: p. 16-21.

131. Yasuno, R. and H. Wada, The biosynthetic pathway for lipoic acid is present in plastids and mitochondria in Arabidopsis thaliana. *FEBS Lett.*, 2002. **517**: p. 110-114.

132. Cronan, J.E., X. Zhao, and Y. Jiang, Function, attachment and synthesis of lipoic acid in Escherichia coli. *Adv Microb Physiol*, 2005. **50**: p. 103-46.

133. Hayden, M.A., I. Huang, D.E. Bussiere, and G.W. Ashley, The Biosynthesis of Lipoic Acid: Cloning of lip, a Lipoate Biosynthetic Locus of *Escherichia coli*. *J Biol Chem*, 1992. **267**(14): p. 9512-9515.

134. Busby, R.W., J.P.M. Schelvis, D.S. Yu, G.T. Babcock, and M.A. Marletta, Lipoic Acid Biosynthesis: LipA Is an Iron Sulfur Protein. *J Am Chem Soc*, 1999. **121**(19): p. 4706-4707.

135. Ollagnier-de Choudens, S. and M. Fontecave, The Lipoate Synthase from Escherichia coli is an Iron-Sulfur Protein. *FEBS Lett*, 1999. **453**: p. 25-28.

136. Ollagnier, S., C. Meier, E. Mulliez, J. Gaillard, V. Schuenemann, A. Trautwein, T. Mattioli, M. Lutz, and M. Fontecave, Assembly of 2Fe-2S and 4Fe-4S Clusters in Anaerobic Ribonucleotide Reductase from Escherichia coli. *J. Am. Chem. Soc.*, 1999. **121**: p. 6344-6350.

137. Broderick, J.B., R.E. Duderstadt, D.C. Fernandez, K. Wojtuszewski, T.F. Henshaw, and M.K. Johnson, Pyruvate Formate-Lyase Activating Enzyme Is an Iron-Sulfur Protein. *J. Am. Chem. Soc.*, 1997. **119**: p. 7396-7397.

138. Petrovich, R.M., F.J. Ruzicka, G.H. Reed, and P.A. Frey, Characterization of iron-sulfur clusters in lysine 2,3-aminomutase by electron paramagnetic resonance spectroscopy. *Biochemistry*, 1992. **31**: p. 10774-10781.

139. Gueguen, V., D. Macherel, M. Jaquinod, R. Douce, and J. Bourguignon, Fatty acid and lipoic acid biosynthesis in higher plant mitochondria. *J Biol Chem*, 2000. **275**(7): p. 5016-25.

140. Miller, J.R., R.W. Busby, S.W. Jordan, J. Cheek, T.F. Henshaw, G.W. Ashley, J.B. Broderick, J.E. Cronan Jr., and M.A. Marletta, *Escherichia coli* LipA Is a Lipoyl Synthase: In Vitro Biosynthesis of Lipoylated Pyruvate Dehydrogenase Complex from Octanoyl-Acyl Carrier Protein. *Biochemistry*, 2000. **39**: p. 15166-15178.

141. Zhao, S., J.R. Miller, Y. Jiang, M.A. Marletta, and J.E. Cronan Jr., Assembly of the Covalent Linkage Between Lipoic Acid and Its Cognate enzymes. *Chem Biol*, 2003. **10**: p. 1293-1302.

142. Layer, G., J. Moser, D.W. Heinz, D. Jahn, and W.D. Schubert, Crystal structure of coproporphyrinogen III oxidase reveals cofactor geometry of Radical SAM enzymes. *Embo J*, 2003. **22**(23): p. 6214-6224.

143. Layer, G., K. Verfurth, E. Mahlitz, and D. Jahn, Oxygen-independent coproporphyrinogen-III oxidase HemN from Escherichia coli. *J Biol Chem*, 2002. **277**(37): p. 34136-42.

144. Layer, G., K. Grage, T. Teschner, V. Schunemann, D. Breckau, A. Masoumi, M. Jahn, P. Heathcote, A.X. Trautwein, and D. Jahn, Radical S-adenosylmethionine enzyme coproporphyrinogen III oxidase HemN: functional features of the [4Fe-4S] cluster and the two bound S-adenosyl-L-methionines. *J Biol Chem*, 2005. **280**(32): p. 29038-46.

145. Berkovitch, F., Y. Nicolet, J.T. Wan, J.T. Jarrett, and C.L. Drennan, Crystal structure of biotin synthase, an S-adenosylmethionine-dependent radical enzyme. *Science*, 2004. **303**(5654): p. 76-9.

146. Krebs, C., W.E. Broderick, T.F. Henshaw, J.B. Broderick, and B.H. Huynh, Coordination of adenosylmethionine to a unique iron site of the [4Fe-4S] of pyruvate formate-lyase activating enzyme: a Mossbauer spectroscopic study. *J Am Chem Soc*, 2002. **124**(6): p. 912-3.

147. Walsby, C.J., D. Ortillo, B.W. E., J.B. Broderick, and B.M. Hoffman, An Anchoring Role for FeS Clusters: Chelation of the Amino Acid Moiety of S-Adenosylmethionine to the Unique Iron Site of the [4Fe–4S] Cluster of Pyruvate Formate–Lyase Activating Enzyme. *J Am Chem Soc*, 2002. **124**(38): p. 11270-11271.

148. Walsby, C.J., W. Hong, W.E. Broderick, J. Cheek, D. Ortillo, J.B. Broderick, and B.M. Hoffman, Electron-nuclear double resonance spectroscopic evidence that S-adenosylmethionine binds in contact with the catalytically active [4Fe-4S]$^{+}$ cluster of pyruvate formate-lyase activating enzyme. *J. Am. Chem. Soc.*, 2002. **124**(12): p. 3143-3151.

149. Jarrett, J.T., Biotin synthase: enzyme or reactant? *Chem. Biol.*, 2005. **12**: p. 409-410.

150. Lotierzo, M., B.T. Bui, D. Florentin, F. Escalettes, and A. Marquet, Biotin synthase mechanism: an overview. *Biochem. Soc. Trans.*, 2005. **33**: p. 820-823.

151. Hanzelmann, P. and H. Schindelin, Crystal structure of the S-adenosylmethionine-dependent enzyme MoaA and its implications for molybdenum cofactor deficiency in humans. *Proc Natl Acad Sci U S A*, 2004. **101**(35): p. 12870-5.

152. Hanzelmann, P. and H. Schindelin, Binding of 5'-GTP to the C-terminal FeS cluster of the radcial S-adenosylmethionine enzyme MoaA provides insights into its mechanism. *Proc. Natl. Acad. Sci.*, 2006. **103**: p. 6829-6834.

153. Frey, P.A. and O.T. Magnusson, S-Adenosylmethionine: A Wolf in Sheep's Clothing, or a Rich Man's Adenosylcobalamin? *Chem Rev*, 2003. **103**: p. 2129-2148.

154. Lepore, B.W., F.J. Ruzicka, P.A. Frey, and D. Ringe, The x-ray crystal structure of lysine-2,3-aminomutase from Clostridium subterminale. *Proc Natl Acad Sci U S A*, 2005. **102**(39): p. 13819-24.

155. Chen, D., C. Walsby, B.M. Hoffman, and P.A. Frey, Coordination and mechanism of reversible cleavage of S-adenosylmethionine by the [4Fe-4S] center in lysine 2,3-aminomutase. *J Am Chem Soc*, 2003. **125**(39): p. 11788-9.

156. Nicolet, Y., C. Piras, P. Legrand, C.E. Hatchikian, and J.C. Fontecilla-Camps, Desulfovibrio desulfuricans iron hydrogenase: the structure shows unusual coordination to an active site Fe binuclear center. *Structure*, 1999. **7**(1): p. 13-23.

157. Nicolet, Y., A.L. de Lacey, X. Vernede, V.M. Fernandez, E.C. Hatchikian, and J.C. Fontecilla-Camps, Crystallographic and FTIR spectroscopic evidence of changes in Fe coordination upon reduction of the active site of the Fe-only hydrogenase from Desulfovibrio desulfuricans. *J Am Chem Soc*, 2001. **123**(8): p. 1596-601.

158. Posewitz, M.C., P.W. King, S.L. Smolinski, L. Zhang, M. Seibert, and M.L. Ghirardi, Discovery of two novel radical S-adenosylmethionine proteins required for the assembly of an active [Fe] hydrogenase. *J Biol Chem*, 2004. **279**(24): p. 25711-20.

159. Rubach, J.K., X. Brazzolotto, J. Gaillard, and M. Fontecave, Biochemical characterization of the HydE and HydG iron-only hydrogenase maturation enzymes from Thermatoga maritima. *FEBS Lett*, 2005. **579**(22): p. 5055-60.

160. Peters, J.W., R.K. Szilagyi, A. Naumov, and T. Douglas, A radical solution for the biosynthesis of the H-cluster of hydrogenase. *FEBS Lett*, 2006. **580**(2): p. 363-7.

161. Pierrel, F., G.R. Bjork, M. Fontecave, and M. Atta, Enzymatic modification of tRNAs: MiaB is an iron-sulfur protein. *J Biol Chem*, 2002. **277**(16): p. 13367-70.

162. Pierrel, F., H.L. Hernandez, M.K. Johnson, M. Fontecave, and M. Atta, MiaB protein from Thermotoga maritima. Characterization of an extremely thermophilic tRNA-methylthiotransferase. *J Biol Chem*, 2003. **278**(32): p. 29515-24.

163. Pierrel, F., T. Douki, M. Fontecave, and M. Atta, MiaB protein is a bifunctional radical-S-adenosylmethionine enzyme involved in thiolation and methylation of tRNA. *J Biol Chem*, 2004. **279**(46): p. 47555-63.

164. Bui, B.T., D. Florentin, F. Fournier, O. Ploux, A. Mejean, and A. Marquet, Biotin synthase mechanism: on the origin of sulphur. *FEBS Lett*, 1998. **440**(1-2): p. 226-30.

165. Cicchillo, R.M. and S.J. Booker, Mechanistic investigations of lipoic acid biosynthesis in Escherichia coli: both sulfur atoms in lipoic acid are contributed by the same lipoyl synthase polypeptide. *J Am Chem Soc*, 2005. **127**(9): p. 2860-1.

166. Paraskevopoulou, C., S.A. Fairhurst, D.J. Lowe, P. Brick, and S. Onesti, The Elongator subunit Elp3 contains a Fe4S4 cluster and binds S-adenosylmethionine. *Mol Microbiol*, 2006. **59**(3): p. 795-806.

167. Trumtel, M., P. Tavecchia, A. Veyrieres, and P. Sinay, Syntheses of trisaccharide C-D-E and tetrasaccharide B-C-D-E fragments found in orthosomycins. *Carbohydr Res*, 1990. **202**: p. 257-75.

168. Boll, R., C. Hofmann, B. Heitmann, G. Hauser, S. Glaser, T. Koslowski, T. Friedrich, and A. Bechthold, The active conformation of avilamycin A is conferred by AviX12, a radical AdoMet enzyme. *J Biol Chem*, 2006. **281**(21): p. 14756-63.

169. Weitnauer, G., A. Muhlenweg, A. Trefzer, D. Hoffmeister, R.D. Sussmuth, G. Jung, K. Welzel, A. Vente, U. Girreser, and A. Bechthold, Biosynthesis of the orthosomycin antibiotic avilamycin A: deductions from the molecular analysis of

the avi biosynthetic gene cluster of Streptomyces viridochromogenes Tu57 and production of new antibiotics. *Chem Biol*, 2001. **8**(6): p. 569-81.

170. Frey, P.A. and S.J. Booker, Radical Mechanisms of S-adenosylmethionine-Dependent Enzymes. *Adv Protein Chem*, 2001. **58**: p. 1-45.

Chapter 2

Escherichia coli Lipoyl Synthase Binds Two Distinct 4Fe-4S Clusters that are Required for Activity

This chapter was reproduced from Cicchillo, R. M.; Lee, K.-H.; Baleanu-Gogonea, C.; Nesbitt, N. M.; Krebs, C.; Booker, S. J., (2004) Escherichia coli Lipoyl Synthase Binds Two Distinct [4Fe-4S] Clusters per Polypeptide. *Biochemistry*; 43 (37), 11770-11781.

2.1 Abstract

Lipoyl synthase (LS) is a member of a recently established class of metalloenzymes that use S-adenosyl-L-methionine (SAM) as the precursor to a high-energy 5'-deoxyadenosyl 5'-radical (5'-dA•). In the LS reaction, the 5'-dA• is hypothesized to abstract hydrogen atoms from C-6 and C-8 of protein-bound octanoic acid with subsequent sulfur insertion, generating the lipoyl cofactor. Consistent with this premise, two equivalents of SAM are required to synthesize one equivalent of the lipoyl cofactor, and deuterium transfer from octanoyl-d_{15} H-protein of the glycine cleavage system–one of the substrates for LS–has been reported [Cicchillo, R. M., Iwig, D. F.,

Jones, A. D., Nesbitt, N. M., Baleanu-Gogonea, C., Souder, M. G., Tu, L., and Booker, S. J. (2004) *Biochemistry* 43, 6378–6386]. However, the exact identity of the sulfur donor remains unknown. We report herein that LS from *Escherichia coli* can accommodate two [4Fe-4S] clusters per polypeptide, and that this form of the enzyme is relevant to turnover. One cluster is ligated by the cysteine amino acids in the C-X_3-C-X_2-C motif that is common to all radical SAM enzymes, while the other is ligated by the cysteine amino acids residing in a C-X_4-C-X_5-C motif, which is conserved only in lipoyl synthases. When expressed in the presence of a plasmid that harbors an *Azotobacter vinelandii isc* operon that is involved in Fe/S cluster biosynthesis, the as-isolated wild-type enzyme contained 6.9 ± 0.5 irons and 6.4 ± 0.9 sulfides per polypeptide, and catalyzed formation of 0.60 equiv of 5'-deoxyadenosine (5'-dA) per polypeptide and 0.27 equiv of lipoylated H-protein. The C68A-C73A-C79A triple variant, expressed and isolated under identical conditions, contained 3.0 ± 0.1 irons and 3.6 ± 0.4 sulfides per polypeptide, while the C94A-C98A-C101A triple variant contained 4.2 ± 0.1 irons and 4.7 ± 0.8 sulfides per polypeptide. Neither of these variant proteins catalyzed formation of 5'-dA or the lipoyl group. Mössbauer spectroscopy of the as-isolated wild-type protein and the two triple variants indicates that greater than 90% of all associated iron is in the configuration $[4Fe–4S]^{2+}$. When wild-type LS was reconstituted with ^{57}Fe and sodium sulfide, it harbored considerably more iron (13.8 ± 0.6) and sulfide (13.1 ± 0.2) per polypeptide, and catalyzed formation of 0.96 equivalents of 5'-dA and 0.36 equivalents of the lipoyl group. Mössbauer spectroscopy of this protein revealed that only ~67 ± 6% of the iron is in the form of $[4Fe–4S]^{2+}$ clusters, amounting to 9.2 ± 0.4 irons and 8.8 ± 0.1 sulfides, or 2 $[4Fe–4S]^{2+}$ clusters per polypeptide, with the remainder

of the iron occurring as adventitiously bound species. Although the Mössbauer parameters of the clusters associated with each of the variants are similar, EPR spectra of the reduced forms of the cluster show differences in spin concentration and g-values, consistent with each of these clusters as distinct species residing in each of the two cysteine-containing motifs.

2.2 Introduction

Lipoic acid is best known as a required cofactor in several multienzyme complexes that are involved in the oxidative decarboxylation of α-keto acids and glycine. These include the pyruvate dehydrogenase complex (PDC), the α-ketoglutarate dehydrogenase complex (KDC), the branched-chain oxo-acid dehydrogenase complex (BCDC), and the glycine cleavage system (GCS). In each of these systems, the lipoyl cofactor is bound in an amide linkage to the ε-amino group of a conserved lysine residue of the lipoyl-accepting subunit of the respective complex, resulting in a long, 14 Å teather, which allows the cofactor to channel intermediates between successive active sites. In each complex, the active form of the cofactor contains a 1,2-dithiolane ring, which undergoes reduction to the dihydrolipoyl form concomitant with turnover. Lipoamide dehydrogenase, one of the components of the complexes, oxidizes the cofactor back to the cyclic disulfide form with concomitant reduction of nicotinamide adenine dinucleotide (NAD^+) [1-7].

In contrast to the well-known thiamin diphosphate-dependent mechanisms for decarboxylation of α-keto acids by the PDC, KDC, and BCDC [4, 6], the

decarboxylation of glycine by the GCS takes place on the P-protein via a pyridoxal 5'-phosphate (PLP)-dependent reaction. Subsequent to decarboxylation, an aminomethyl group is transferred to the lipoyl cofactor, which resides on a 14 kDa protein called the H-protein. The T-protein catalyzes the cleavage of the amino functionality from the aminomethyl group with concomitant use of the methylene carbon to synthesize N^5,N^{10}-methylenetetrahydrofolate (THF) [2, 3, 8-13].

In *Escherichia coli* and many other organisms, the lipoyl cofactor can be installed by at least two pathways [14]. Lipoate protein ligase (LplA) catalyzes the activation and transfer of free lipoic acid to the relevant lysine accepter [15, 16]. Alternatively, the lipoyl cofactor can be synthesized endogenously [14]. The eight-carbon backbone of the cofactor is created via the fatty acid biosynthetic pathway as an appendage to the acyl carrier protein (ACP) [14, 17]. LipB, a lipoyl(octanoyl)-acyl carrier protein N-lipoyl(octanoyl)transferase [18, 19], catalyzes the transfer of the octanoyl chain from octanoyl-ACP to a target lysine accepter, affording octanoyl-E2, as in the case of the PDC [20]–and by inference, the KDC and BCDC–and octanoyl H-protein, as in the case of the GCS [21]. In the second step, lipoyl synthase (LS) mediates insertion of both sulfur atoms into the C-6 and C-8 positions of the appended alkyl chain (Figure 2.1) [20-22].

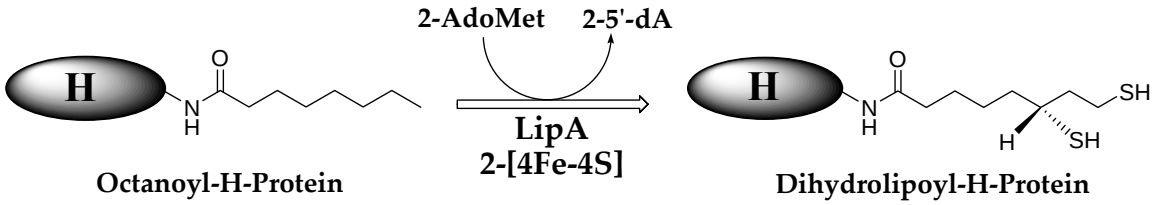

Figure 2.1: Reaction catalyzed by lipoyl synthase.

LS is a member of the radical SAM superfamily of enzymes, which use S-adenosyl-L-methionine (SAM) as a precursor to a 5'-deoxyadenosyl 5'-radical (5'-dA•) [23-26]. In each enzyme system, the 5'-dA• initiates catalysis by abstracting a hydrogen atom from a small-molecule substrate or protein. In the former case, this event triggers turnover. In the latter case, the hydrogen is abstracted from the α-carbon of a target glycine residue, creating a glycyl radical cofactor. All characterized members of the radical SAM superfamily have a C-X_3-C-X_2-C motif, in which the designated cysteine amino acids coordinate a [4Fe–4S] cluster that is requisite for turnover. The cluster serves at least two functions: it acts as the immediate donor of one electron, which is required for the reductive cleavage of SAM to generate the 5'-dA• *[27-30]*, and it acts as a substrate binding determinant, wherein the α-amino and α-carboxylate groups of SAM coordinate in a bidentate fashion to one of the irons [31-37]. The remaining product of SAM cleavage is L-methionine.

In the LS reaction, it is generally believed that the role of the 5'-dA• is to remove hydrogen atoms from the C-6 and C-8 positions of protein-bound derivatives of octanoic acid, allowing for subsequent sulfur insertion [20-22, 38, 39]. Consistent with this premise, 2 equiv of SAM are required to synthesize 1 equiv of the lipoyl cofactor, and deuterium transfer from octanoyl-d_{15} H-protein (OHP) to 5'-deoxyadenosine has been observed [21]. The nature of the immediate sulfur donor is unknown; however, in vitro studies of the LS reaction are consistent with the premise that the protein, itself, provides both sulfur atoms: lipoylated proteins can be synthesized in the absence of added compounds that contain sulfur, except for SAM [21, 22]; and LS catalyzes less than one

turnover in a pseudo first-order kinetic process, consistent with depletion of the sulfur source [21].

There are similarities between LS and biotin synthase (BS), a related radical SAM enzyme that catalyzes the final step in the biotin biosynthetic pathway, the insertion of one sulfur atom between C-6 and C-9 of the substrate, dethiobiotin (DTB) [40-43]. The two proteins from *E. coli* possess 40 % sequence similarity and 17 % sequence identity, and each contains 6 conserved cysteine residues [44-46]. In LS, these residues lie in two defined motifs, the C-X_3-C-X_2-C motif that is common to all radical SAM enzymes, and a C-X_4-C-X_5-C motif, which is conserved only among lipoyl synthases. In BS, the conserved cysteines that are not part of the radical SAM motif are found scattered throughout the entire polypeptide rather than in a short stretch of amino acids. All six of the conserved cysteines in BS are required for turnover [47], and there appears to be universal agreement as to the role of the three residing in the C-X_3-C-X_2-C motif; however, two competing working hypotheses have been advanced regarding the function of the remaining three. On one hand, they are believed to coordinate a [2Fe-2S] cluster that functions in some uncharacterized manner to deliver the sulfur atom in biotin. Consistent with this proposal, a number of laboratories have provided spectroscopic (UV-visible, Mössbauer, EPR, and resonance Raman spectroscopy) and X-ray crystallographic evidence that this cluster form is present in as-isolated (AI) BS, which is inactive, as well as BS that is reconstituted (RCN) to contain a [2Fe-2S] cluster and a [4Fe-4S] cluster, purported to be the active form of the enzyme [48-53]. Moreover, the [2Fe-2S] cluster has been shown to be present in the host bacterium during expression of BS [54, 55], as well as on BS that has been isolated anaerobically [50], suggesting that it is not a

degradation product of the [4Fe-4S] cluster. On the other hand, another laboratory has reported that BS exhibits cysteine desulfurase activity, and that the three remaining cysteines of the protein participate in some uncharacterized manner in liberating sulfur from cysteine and activating it for delivery into dethiobiotin [56]. Consistent with this proposal, a requirement for PLP and the presence of a cysteine persulfide on BS has been demonstrated [56].

In this work we show that LS can accommodate two [4Fe-4S] clusters. One is coordinated by the C-X_3-C-X_2-C motif that is common among radical SAM enzymes, and which is proposed to function in generating the 5'-dA•. The second cluster is housed in the C-X_4-C-X_5-C motif, which is unique to lipoyl synthases. We speculate that this cluster somehow functions to deliver the sulfur that is incorporated into the product. We show that both clusters are required for turnover, and importantly, that formation of product, lipoyl H-protein (LHP), does not require reconstitution of LS.

2.3 Materials and Methods

Materials. All DNA modifying enzymes and reagents were purchased from New England Biolabs (Beverly, MA), as was Vent polymerase and its associated 10X reaction buffer. Oligonucleotide primers for cloning and mutagenesis were obtained from Integrated DNA Technologies (Coralville, IA) or Invitrogen Life Technologies (Carlsbad, CA). Both the Bradford reagent for protein concentration determination and the bovine serum albumin (BSA) standard (2 mg mL^{-1}) were obtained from Pierce

(Rockford, IL). *E. coli* genomic DNA (strain W3110) was obtained from Sigma Corp (St. Louis, MO). All other buffers and common chemicals were reagent grade or better.

^{57}Fe (97-98%) metal was purchased from Pennwood Chemicals (Great Neck, NY). It was washed with $CHCl_3$ and dissolved with heating in an anaerobic solution of 2 N H_2SO_4 (1.5 mol of H_2SO_4 per mol of ^{57}Fe). It was used as is for bacterial growths. For reconstitution experiments, it was first titrated to pH 6.5 with an anaerobic solution of saturated sodium bicarbonate. Routine iron and sulfide analysis was conducted as described previously [57-59].

Spectroscopic methods. UV-visible spectra were recorded using Cary 50 or Cary 300 spectrometers (Varian; Walnut Creek, CA) in combination with the associated WinUV software package. Low-temperature X-band EPR spectroscopy was carried out in perpendicular mode on a Bruker (Billerica, MA) ESP 300 spectrometer equipped with an ER 041 MR microwave bridge and an ST4102 X-band resonator (Bruker). Sample temperature was maintained with an ITC503S temperature controller and an ESR900 liquid helium cryostat (Oxford Instruments; Concord, MA). Spin concentration was determined by double integration of the sample spectrum and comparing the resulting intensity to that of a 1 mM $CuSO_4$ / 10 mM EDTA standard run under identical conditions. General spectral manipulations were carried out using the program IGOR Pro (Wavemetrics; Lake Oswego, OR) on a desktop computer.

Mössbauer spectra were recorded on spectrometers from WEB research (Edina, MN) operating in the constant acceleration mode in a transmission geometry. Spectra were recorded with the temperature of the sample maintained at 4.2 K. For low-field

spectra, the sample was kept inside an SVT-400 dewar from Janis (Wilmington, MA), and a magnetic field of 40 mT was applied parallel to the γ-beam. For high-field spectra, the sample was kept inside a 12SVT dewar (Janis), which houses a superconducting magnet that allows for application of variable magnetic fields between 0 and 8 T parallel to the γ-beam. The quoted isomer shifts are relative to the centroid of the spectrum of a metallic foil of α-Fe at room temperature. Data analysis was performed using the program WMOSS from WEB research.

Recombinant DNA Procedures. The polymerase chain reaction was performed with a Robocycler (Stratagene) temperature cycler. Each amplification reaction contained in a volume of 100 μL: 50 pmol of each primer, 20 nmol of each deoxynucleoside triphosphate, 1 μg of *E. coli* genomic DNA, 1 U of Vent polymerase, and 10 μL of 10X Vent polymerase buffer. After a 5 min denaturation step at 95°C, 35 cycles of the following program were initiated: 1 min at 95 °C, 1 min at 45 °C, and 3 min at 72 °C. All other procedures were carried out by standard methods *[60]*. DNA sequencing was carried out at the Pennsylvania State University Nucleic Acid Facility.

Construction of the C68A–C73A–C79A Triple Variant. The cloning of wild-type LS into expression vector pET-28a has already been described [21]. Single, double, and triple variants of cysteines 68, 73, and 79 were constructed by PCR using the primers listed in Table 2.1 . Initially, a silent *Kpn*I restriction site was engineered into the gene sequence for LS at positions 247-252 by changing a cytosine at position 249 to a thymine, and an adenine at position 252 to a cytosine. These alterations converted the naturally encoded GGC ACA to GGT ACC, with no change in the encoded glycine and

threonine amino acids. The *lipA* gene was amplified in two halves with primer JE001 in combination with primer SB002, and primer JE002 in combination with primer SB004. Subsequent to purification of the resulting fragments and digestion with *Nde*I and *Kpn*I (for the fragment amplified with primers SB004 and JE002) or *Eco*RI and *Kpn*I (for the fragment amplified with primers SB002 and JE001), the two fragments were simultaneously ligated into a pET-28a expression vector that had been digested with *Nde*I and *Kpn*I. The resulting construct was used as the template for construction of the C68A-C73A-C79A triple variant by PCR using primers AS007, AS006, and AS005–all of which spanned the engineered *Kpn*I restriction site–in combination with primer SB004. Construction of the C68A single variant generated the template for construction of the C68A-C73A double variant; the double variant was then used as the template for construction of the C68A-C73A-C79A triple variant. Subsequent to amplification by PCR, the resulting fragments were digested with *Nde*I and *Kpn*I, and simultaneously ligated into pET-28a along with the fragment that was amplified with primers SB002 and JE001.

Table 2.1: Sequence of Primers Used in Cloning and Mutagenesis.

primer	sequence[a]	use
AS005	5′-AAA CGT TGC GGT ACC GTG GTT GAA **CGC** TTC CGC-3′	reverse PCR primer for C79A mutation
AS006	5′-AAA CGT TGC GGT ACC GTG GTT GAA GCA TTC CGC CAG GTT AGG **CGC** GGA GGC-3′	reverse PCR primer for C73A mutation
AS007	5′-AAA CGT TGC GGT ACC GTG GTT GAA GCA TTC CGC CAG GTT AGG GCA GGA GGC TTC CTC **CGC** GAC AGA-3′	reverse PCR primer for C68A mutation
CG002	5′-GTG GGC GAC GTC ACA GAA CGG ACA ACG GCG GGT **AGC** AAT AGC-3′	reverse PCR primer for C94A mutation
JE002	5′-GAG GAT CAT AAA CGT TGC *GGT ACC* GTG GTT GAA GCA TTC CGC-3′	reverse PCR primer for *Kpn*I silent mutation
JE001	5′-GCG GAA TGC TTC AAC CAC *GGT ACC* GCA ACG TTT ATG ATC CTC-3′	forward PCR primer for *Kpn*I silent mutation
AatIIfor	5′-CCG TTC TGT *GAC GTC* GCC CAC GGT CGG CCG-3′	forward PCR primer for *Aat*II silent mutation
AatIIrev	5′-CGG CCG ACC GTG GGC *GAC GTC* ACA GAA CGG-3′	reverse PCR primer for *Aat*II silent mutation
KHL001	5′-CGC CGT **GCT** CCG TTC **GCT** GAC GTC GCC CAC GGT CGG-3′	forward primer for C94A−C98A−C101A triple variant[b]
KHL002	5′-CCG ACC GTG GGC GAC GTC **AGC** GAA CGG **AGC** ACG GCG-3′	reverse primer for C94A−C98A−C101A triple variant[b]
SB004	5′-GCG GCG TC*C ATA TG*A GTA AAC CCA TTG TGA TGG AAC GC-3′	forward PCR primer for cloning lipoyl synthase
SB002	5′-GCC G*GA ATT C*TT ACT TAA CTT CCA TCC CTT TCG C-3′	reverse PCR primer for cloning lipoyl synthase

[a] Italic-type bases designate engineered restriction sites, while bold-type bases designate altered codons. [b] Mutagenesis carried out using QuikChange kit from Stratagene in combination with the C94A template.

Construction of the C94A-C98A-C101A Triple Variant. A silent *Aat*II restriction site was engineered into the *lipA* gene at positions 304–309 by converting a thymine at position 309 to a cytosine. This alteration converted the naturally encoded GAC GTT to GAC GTC, with no change in the encoded valine amino acid. The *lipA* gene was amplified in two halves with primer AatIIfor in combination with SB002, and primer AatIIrev in combination with SB004. Subsequent to purification of the resulting fragments and digestion with *Nde*I and *Kpn*I (for the fragment amplified with primers SB004 and AatIIrev) or *Eco*RI and *Kpn*I (for the fragment amplified with primers SB002 and AatIIfor), the two fragments were simultaneously ligated into pET-28a that had been digested with *Nde*I and *Kpn*I. The resulting construct was then used as the template for the construction of the C94A single variant using primer CG002–which spanned the engineered *Aat*II restriction site–in combination with primer SB004. For uncharacterized reasons, construction of the double and triple variants was resistant to this strategy. The triple variant was therefore synthesized using the QuikChange site-directed mutagenesis

kit from Stratagene in combination with primers KHL001 and KHL002, and the C94A single variant as template. The procedure was carried out according to the protocol established by the manufacturer, but amended as described by Ramamurthy et al [61]. The expression of both variants was carried out in minimal media and in the presence of plasmid pDB1282 as previously described [21], except that ^{57}Fe was added to the growth media instead of natural abundance iron. The purification and reconstitution of wild-type and variant proteins was carried out as previously described [21], except that ^{57}Fe was used for the reconstitution instead of natural abundance iron.

Extinction Coefficient Determination and Bradford Protein Assay Standardization for LS. Protein concentrations of LS samples were analyzed in triplicate by the Bradford dye-staining procedure (Pierce) with BSA as the standard. Parallel samples were also subjected to quantitative amino acid analysis at the University of Iowa's Molecular Analysis Facility. The average protein concentration obtained from the samples subjected to amino acid analysis was then used to determine a correction factor for the Bradford assay.

Preparation of Mössbauer and EPR Samples. Samples to be analyzed by Mössbauer and EPR spectroscopies were prepared inside of the anaerobic chamber, and contained 200-1300 μM LS. Samples (300 μL final volume) to be analyzed by Mössbauer spectroscopy were frozen with liquid nitrogen inside of small plastic cups. For characterization by EPR, the samples (250 μL final volume) were first treated with 2 mM sodium dithionite at ambient temperature for ~2 min, placed in EPR tubes (2 mm

i.d.), and frozen in liquid nitrogen. All steps associated with preparing the samples were conducted inside of a Coy Laboratory Products (Grass Lake, MI) anaerobic chamber.

2.4 Results

Expression and Purification of Wild-Type and Variant E. coli LS Proteins. All wild-type and variant LS proteins in this study were co-expressed with plasmid pDB1282 in ^{57}Fe-containing M9 minimal media as described previously [21]. Plasmid pDB1282 carries an *A. vinelandii* operon that is believed to be important in the biosynthesis of Fe/S clusters. This operon contains the genes, *iscS*, *iscU*, *iscA*, *hscA*, *hscB*, and *fdx [62-64]*, cloned behind an arabinose inducible promoter in a plasmid that confers ampicillin resistance, while the pET-28a plasmid into which the WT and variant *lipA* genes were cloned confers resistance to kanamycin. The proteins were isolated by immobilized metal affinity chromatography (IMAC) as previously described [21], exploiting the hexahistidine tag that is appended to the N-terminus of each.

Quantitative amino acid analysis was employed to establish an extinction coefficient for as-isolated LS, and to standardize the Bradford protein assay. Because the protein has a propensity to precipitate in the presence of oxygen, which could compromise the accuracy of the result, care was taken to ensure that the solution was indeed homogeneous while transferring it to hydrolysis tubes. In three analyses, performed on two separate occasions, concentrations of the same 4 amino acids were used in conjunction with the published amino acid sequence to quantify the LS concentration subsequent to hydrolysis of the protein. Using a commercially available

BSA standard–the concentration of which was verified by UV-visible spectroscopy ($\varepsilon^{1\%}$ = 6.67)–it was determined that the Bradford protein assay overestimates the concentration of LS by a factor of 1.47 ± 0.27. Determination of the molar absorptivity at 400 nm of the various Fe/S cluster species associated with LS cannot be deduced from UV–visible data alone, but also requires analytical information and analysis by Mössbauer and EPR spectroscopies, which can be used to observe and quantify all of the relevant iron-containing species.

Analytical and Spectroscopic Characterization of AI WT LS. The UV-visible spectrum of LS co-expressed in ^{57}Fe-containing minimal media in the presence of plasmid pDB1282, and purified under anaerobic conditions as described previously [21], is displayed in Figure 2.2A (solid line).

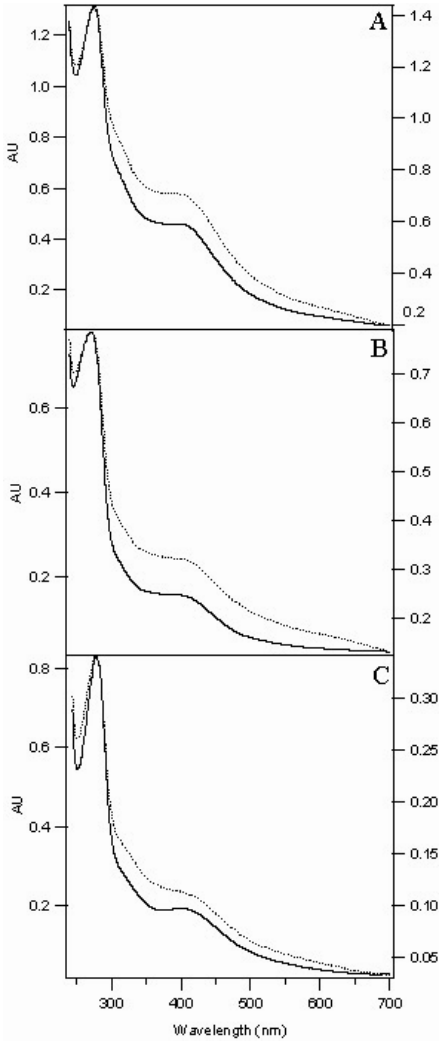

Figure 2.2: UV-visible spectra of (A) WT LS, (B) 94-98-101, and (C) 68-73-79. In each case, the solid line represents the as-isolated sample, while the dashed line represents the reconstituted sample. Sample concentrations were 21.2 μM for AI WT LS, 17.2 μM for RCN WT LS, 13.0 μM for AI 94-98-101, 9.08 μM for RCN 94-98-101, 19.8 μM for AI 68-73-79, and 6.25 μM for RCN 68-73-79. For each spectrum, the secondary Y-axis corresponds to the absorbance for the reconstituted proteins.

In addition to the peak at 280 nm, the spectral envelope contains a small shoulder at 330 nm, and a broad peak at 400 nm, which tails out beyond 700 nm. These features, as well as the dark brown color of the protein, are consistent with the presence of Fe/S

clusters. Although it is difficult to predict accurately the type of clusters associated with the protein solely from UV-visible spectroscopy, the spectrum is distinct from that of AI BS, as well as the reconstituted form of the protein that gives rise to turnover [48-52, 65]. In particular, the UV-visible spectrum of LS lacks the telltale features of $[2Fe\text{-}2S]^{2+}$ clusters, a broad peak at ~460 nm, as well as the shoulder at ~550 nm that is sometimes observed [50, 65-68]. The protein shown in Figure 3.2A (solid line) contained 6.9 ± 0.5 equiv of Fe and 6.4 ± 0.9 equiv of S^{2-} per polypeptide. This stoichiometry is a little less than two-fold greater than that previously reported for WT LS [22, 39, 64], as well as that which we observe when the protein is isolated from an expression host that does not contain the accessory plasmid (data not shown). Consistent with the greater stoichiometry of Fe and S^{2-} associated with LS, the A_{280}/A_{400} ratio in this preparation is 2.88. The A_{280}/A_{400} ratio of AI LS purified in the absence of plasmid pDB1282 is typically ~4.

The Mössbauer spectrum of a sample of AI WT LS recorded at 4.2 K in an externally applied magnetic field (40 mT) oriented parallel to the γ-beam is shown in Figure 2.3A. It shows two broad lines at –0.12mm/s and +1.04 mm/s, which belong to a quadrupole doublet having parameters (isomer shift δ = 0.46 mm/s and quadrupole splitting parameter ΔE_Q = 1.16 mm/s) that are typical of $[4Fe\text{–}4S]^{2+}$ clusters. Because the width of the lines is rather large, the spectrum was analyzed assuming two quadrupole doublets of equal intensity, yielding the following parameters: isomer shifts $\delta(1)$ = 0.45 mm/s and $\delta(2)$ = 0.46 mm/s, and quadrupole splitting parameters $\Delta E_Q(1)$ = 0.98 mm/s and $\Delta E_Q(2)$ = 1.30 mm/s. These two quadrupole doublets account for 97 ± 3% of the

total intensity of the spectrum, and the associated parameters are typical of $[4Fe–4S]^{2+}$-containing proteins. In order to corroborate this assignment, a spectrum of this sample was recorded at 4.2 K in an 8 T magnetic field (Figure 3.3B). $[4Fe–4S]^{2+}$ clusters have diamagnetic ground states, and therefore, it is expected that the magnetic field experienced by the ^{57}Fe nuclei would equal the externally applied field (8 T). The solid line overlaid with the experimental data in Figure 3.3B is a theoretical spectrum using the parameters obtained from the 40 mT spectrum (asymmetry parameters $\eta(1) = 0.5$ and $\eta(2) = 0.6$) and assuming a diamagnetic ($S = 0$) ground state. We note that detection of small amounts of $[2Fe–2S]^{2+}$ clusters, which typically exhibit a quadrupole doublet with $\delta \approx 0.28$ mm/s and $\Delta E_Q \approx 0.6$ mm/s, is difficult. Including a third quadrupole doublet with parameters typical of $[2Fe–2S]^{2+}$ clusters does not improve the quality of the fit significantly. Furthermore, the parameters of the $[4Fe–4S]^{2+}$ component are essentially the same, and no more than 5 % of the total intensity is in the form of $[2Fe–2S]^{2+}$ clusters. We therefore conclude that this sample contains at most 5 % of the iron in the form of $[2Fe–2S]^{2+}$ clusters. A previous Mössbauer study of LS revealed the presence of $[4Fe–4S]^{2+}$ and $[2Fe–2S]^{2+}$ clusters in RCN WT LS [69]. The reported spectrum has a discernable shoulder at ca. 0.6 mm/s, indicative of the high-energy line of the spectrum of $[2Fe–2S]^{2+}$ clusters. We do not see this feature in our spectrum of AI WT LS, which indicates that the percentage of $[2Fe–2S]^{2+}$ clusters in our preparation of LS is smaller.

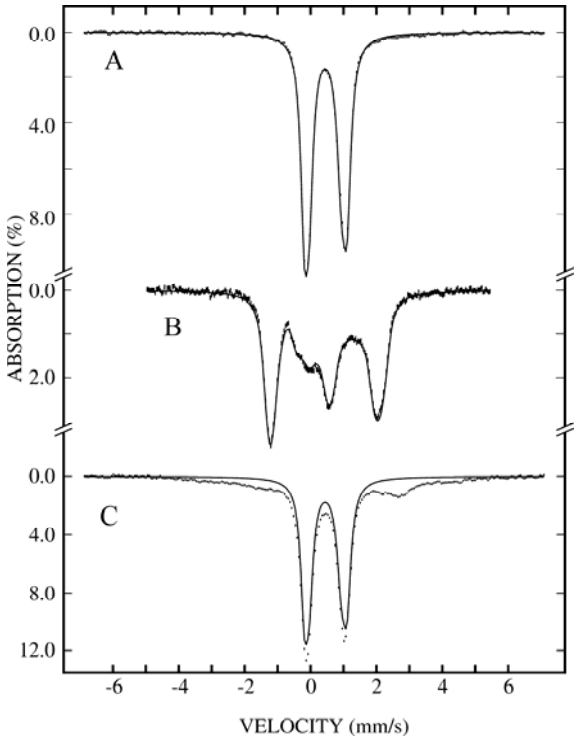

Figure 2.3: Mössbauer spectra of WT AI LS recorded at 4.2 K in an externally applied field (oriented parallel to the γ-beam) of (A) 40 mT and (B) 8 T. The solid line overlaid with the experimental data (hashed marks) are simulations representing the contribution from the $[4Fe–4S]^{2+}$ clusters using the parameters given in the text. The Mössbauer spectrum of WT RCN LS recorded at 4.2 K in an externally applied filed (oriented parallel to the γ-beam) of 40 mT is shown in (C). The simulation of the $[4Fe–4S]^{2+}$ clusters, scaled to 70% of the total intensity of spectrum (C) is shown as a solid line.

The EPR spectrum of an identical sample of AI, ^{57}Fe-grown LS reveals the presence of a small amount (14 μM, 0.03 equiv or 1.5 % of the total Fe) of a $[3Fe–4S]^{+}$ cluster. This type of cluster gives rise to fairly broad and magnetically split Mössbauer spectra when recorded at 4.2 K in a 40 mT external magnetic field, and therefore this small amount is not detectable in the spectrum in Figure 3.3A [70]. By combining Mössbauer and EPR spectroscopic results with iron and sulfide quantification on the exact same proteins, it can be concluded that AI WT LS contains 1.7 ± 0.2 $[4Fe–4S]^{2+}$

and 0.03 $[3Fe–4S]^{+}$ clusters, consistent with the presence of two distinct [4Fe–4S] cluster binding sites in each polypeptide.

Analytical and Spectroscopic Characterization of RCN WT LS. Upon reconstitution of AI WT LS with ^{57}Fe, the concentrations of iron and sulfide that elute with the desalted protein increase enormously to 13.8 ± 0.6 Fe and 13.1 ± 0.2 S^{2-} per polypeptide. Concomitant with the increase in iron and sulfide content is a change in the UV-visible spectrum of the protein (Figure 3.1A, dashed line); the region of the spectrum that is characteristic of the Fe/S cluster has increased in amplitude, although no distinct features that would suggest the presence of other cluster forms are observed. In addition, the A_{280}/A_{400} ratio has decreased to 2.04, suggestive of incorporation of additional Fe/S-containing species. As detailed below, we employed Mössbauer spectroscopy to determine the configuration and stoichiometry of these additional Fe/S-containing species.

The Mössbauer spectrum of this sample, recorded at 4.2 K and 40 mT, is shown in Figure 3.3C. In addition to the two peaks associated with the broad quadrupole doublet emanating from the $[4Fe–4S]^{2+}$ clusters, there is a broad component extending from –5 mm/s to +5 mm/s, with a pronounced broad absorption at ~2.8 mm/s. The broad features may originate from paramagnetic Fe/S cluster species, and/or from adventitiously bound ^{57}Fe. The EPR spectrum of this sample (data not shown) reveals that it contains an insignificantly small amount of $[3Fe–4S]^{+}$ clusters; $[2Fe–2S]^{+}$ and $[4Fe–4S]^{+}$ species are not observed. $[3Fe\text{-}4S]^{0}$ clusters could potentially also give rise–at least in part–to the broad features. They have an S = 2 ground state and exhibit a significant spin expectation value, even in small externally applied magnetic fields,

giving rise to magnetically split Mössbauer spectra [71]. In the absence of an external magnetic field, however, the spectrum associated with $[3Fe–4S]^0$ clusters collapses into quadrupole doublets. We recorded the 4.2 K zero-field spectrum of RCN WT (data not shown), and it is identical to that of the spectrum obtained at 4.2 K and 40 mT. Therefore, the broad feature is attributed to adventitiously bound iron. Deconvolution of the Mössbauer spectrum reveals that 67 ± 6% of the total Fe is in the form of $[4Fe–4S]^{2+}$ clusters. The relative amount of this component has a larger uncertainty because the exact shape of the spectral contribution from adventitiously bound iron is not known. These results, when combined with iron and sulfide analysis, suggest that reconstituted LS contains 2.3 ± 0.3 $[4Fe–4S]^{2+}$ clusters per polypeptide, again consistent with the presence of two distinct Fe/S cluster binding sites per polypeptide.

Analytical and Spectroscopic Characterization of the C94A-C98A-C101A Triple Variant. The UV-visible spectrum of the AI C94A-C98A-C101A triple variant (94-98-101), expressed and purified similarly to the WT protein, is displayed in Figure 3.1B (solid line). The overall spectral envelope is quite similar to that of WT LS, displaying the same distinctive features at 330 and 400 nm, but not displaying features that are indicative of $[2Fe\text{-}2S]^{2+}$ clusters. Analysis for iron and sulfide yielded 4.2 ± 0.1 equiv of Fe, and 4.7 ± 0.8 equiv of S^{2-} per polypeptide, consistent with the premise that one of the [4Fe–4S] cluster binding sites has been removed. However, upon reconstitution with iron and sulfide, the UV-visible spectrum of the triple variant changes significantly (Figure 3.1B, dashed line), shifting from an A_{280}/A_{400} ratio of 5 in the as-isolated sample to 2.5 in the reconstituted sample, suggesting that additional Fe/S-containing species are incorporated despite deleting one of the presumed cluster binding motifs.

The Mössbauer spectrum of AI 94-98-101, recorded at 4.2 K and 40 mT, is shown in Figure 2.4A. It is nearly identical to the spectrum of WT LS, and a fit of the experimental spectrum to two quadrupole doublets yields the following parameters: $\delta(1)$ = 0.44 mm/s, $\delta(2)$ = 0.46 mm/s, $\Delta E_Q(1)$ = 1.00 mm/s, and $\Delta E_Q(2)$ = 1.33 mm/s. This component accounts for 97 ± 3 % of the total ^{57}Fe in this sample, indicating that nearly all of the iron in the sample is in the configuration $[4Fe–4S]^{2+}$. Additionally, AI 94-98-101 is EPR silent, indicating that the paramagnetic cluster types, $[2Fe–2S]^{+}$, $[4Fe–4S]^{+}$ and $[3Fe–4S]^{+}$ are not present. Spectral analysis in combination with iron and sulfide analysis therefore indicates that AI 94-98-101 contains 1.0 ± 0.1 $[4Fe–4S]^{2+}$ cluster per polypeptide.

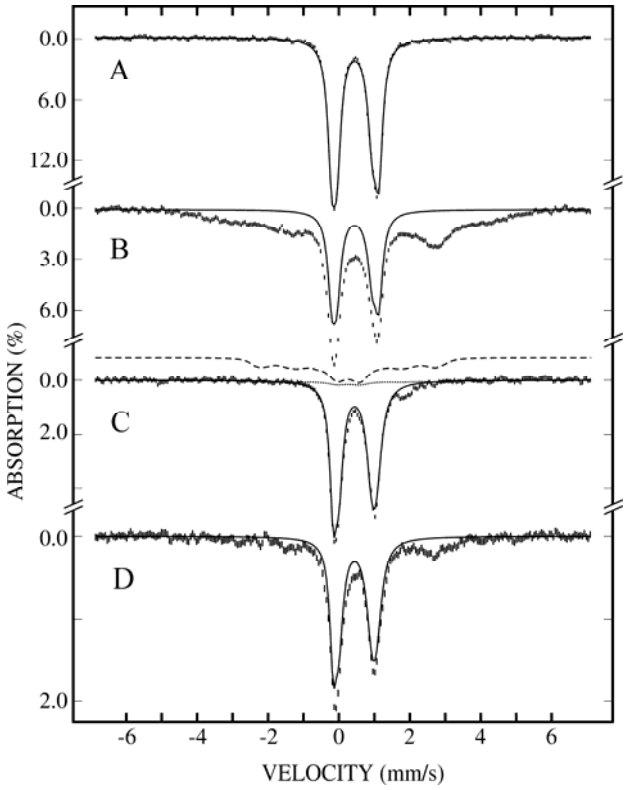

Figure 2.4: Mössbauer spectra, recorded at 4.2 K in an externally applied 40 mT magnetic field of (A) AI 94-98-101, (B) RCN 94-98-101, (C) AI 68-73-79, and (D) RCN 68-73-79. The solid lines are simulations of the $[4Fe–4S]^{2+}$ cluster component, using the parameters in the text. The dotted line in (C) is a theoretical simulation of the $[3Fe–4S]^{+}$ cluster scaled to 8% of the total intensity of the experimental spectrum. The dashed line in (C) is the same simulation of the $[3Fe–4S]^{+}$ cluster component, magnified 5-fold for clarity.

The Mössbauer spectrum of RCN 94-98-101 is displayed in Figure 3.4B. The spectrum shows, in addition to the two lines at –0.12 mm/s and +1.04 mm/s of the $[4Fe–4S]^{2+}$ cluster, a broad absorption extending from –5 mm/s to +5 mm/s. The shape of this component is similar to that observed in the spectrum of reconstituted WT LS. Again, the reconstituted triple variant is EPR silent at 13 K, demonstrating the absence of paramagnetic Fe/S cluster types. Therefore, the broad absorption is attributed to adventitiously bound Fe. Deconvolution of the spectrum reveals that 38 ± 6 % of the

total absorption is contributed by the subspectrum of the $[4Fe–4S]^{2+}$ cluster. This percentage in combination with iron and sulfide analysis indicates an overall stoichiometry of 1.0 ± 0.2 $[4Fe–4S]^{2+}$ clusters per 94-98-101 polypeptide. Importantly, reconstitution of the triple variant does not increase the content of $[4Fe–4S]^{2+}$ clusters per polypeptide, strongly corroborating the hypothesis that cysteines 94, 98, and 101 of WT LS coordinate a [4Fe–4S] cluster.

Analytical and Spectroscopic Characterization of the C68A-C73A-C79A Triple Variant. The UV-visible spectrum of the AI C68A-C73A-C79A triple variant (68-73-79), expressed and purified similarly to the WT protein, is displayed in Figure 3.1C (solid line). Again, the overall spectral envelope is similar to that of WT LS, possessing the same distinctive features at 330 and 400 nm, but not displaying features that are indicative of [2Fe-2S] clusters. Analysis for iron and sulfide yielded 3.05 ± 0.15 equiv of Fe, and 3.64 ± 0.41 equiv of S^{2-} per polypeptide, enough only to support formation of one $[4Fe–4S]^{2+}$ cluster per polypeptide. The UV-visible spectrum of the AI triple variant when compared to that of the AI WT protein is consistent with this premise. The A_{280}/A_{400} ratio is 4.36, which is similar to that for 94-98-101. Upon reconstitution of AI 68-73-79, the associated UV-visible spectrum changes only mildly, displaying an A_{280}/A_{400} ratio of 3, which is consistent with the changes in iron and sulfide content (4.8 ± 0.1 equiv of Fe and 3.6 ± 0.2 equiv of S^{2-}).

The Mössbauer spectrum of the AI 68-73-79, recorded at 4.2 K and 40 mT, is shown in Figure 3.4C. It shows three features: two prominent peaks at –0.1 mm/s and +1.0 mm/s, indicating the presence of $[4Fe–4S]^{2+}$ clusters, and a broad peak at +1.8 mm/s, which tails out to ~3 mm/s. We speculate that this peak originates from

adventitiously bound iron, or from $[3Fe–4S]^0$ clusters. As discussed previously, the spectral features of $[3Fe–4S]^0$ clusters collapse in zero-field to quadrupole doublets, allowing them to be identified in such a manner. The zero-field spectrum of AI 68-73-79 is identical to the 40 mT spectrum, indicating that the sample does not contain $[3Fe–4S]^0$ clusters. We therefore assign the broad feature to adventitiously bound iron.

The EPR spectrum of AI 68-73-79 (data not shown) reveals the presence of a small amount (10 μM or 0.08 equiv, which corresponds to 8% of the total Fe in the sample) of $[3Fe–4S]^+$ clusters. For the deconvolution of the Mössbauer spectrum we approximate the contribution of the $[3Fe–4S]^+$ clusters by using the simulation of the $[3Fe–4S]^+$ clusters observed in pyruvate formate–lyase activating enzyme (PFL-AE), which is another member of the radical SAM superfamily [72]. The simulation of the $[3Fe–4S]^+$ clusters, scaled to 8% of the total intensity, is shown as a dotted line overlaid with the experimental data in Figure 3.4C. For clarity, we also show the spectrum of this component magnified 5-fold as a dashed line above the spectrum in Figure 3.4C. For the analysis of the Mössbauer spectrum of AI 68-73-79, we removed the contribution of the $[3Fe–4S]^+$ cluster from the raw data, and fitted the resulting spectrum to two quadrupole doublets, representing the $[4Fe–4S]^{2+}$ clusters. This analysis yields the following parameters: $\delta(1) = 0.46$ mm/s, $\delta(2) = 0.45$ mm/s, $\Delta E_Q(1) = 0.92$ mm/s, and $\Delta E_Q(2) = 1.22$ mm/s, accounting for 93 ± 6 % of the total iron in this sample. This percentage in combination with results from iron and sulfide analysis indicates that there are 0.7 ± 0.1 $[4Fe–4S]^{2+}$ clusters per polypeptide associated with AI 68-73-79.

The spectrum of the RCN 68-73-79 is shown in Figure 3.4D. In addition to the two prominent lines that are contributed by the $[4Fe–4S]^{2+}$ cluster, there is a broad

absorption extending from ca. –3 mm/s to +3 mm/s. Again, we attribute this absorption to adventitiously bound iron, since the sample is EPR-silent. The $[4Fe–4S]^{2+}$ cluster component can be simulated using the same parameters that were used to simulate that of AI 68-73-79, and were found to correspond to 70 % of the total intensity. This percentage in combination with iron and sulfide analysis results in a stoichiometry of 0.8 ± 0.2 $[4Fe–4S]^{2+}$ clusters per polypeptide. These results are in full agreement with our hypothesis that cysteines 94, 98, and 101 ligate one [4Fe–4S] cluster, while cysteines 68, 73, and 79 ligate another. We point out that the addition of the Mössbauer spectra of AI 68-73-79 LS (Figure 3.4C) and AI 94-98-101 LS (Figure 3.4A) in a 1:1 ratio closely resembles that of AI WT LS (Figure 3.3A).

Determination of extinction coefficients at 400 nm of WT and Variant Lipoyl Synthases. We have used a combination of analytical methods and Mössbauer spectroscopy to determine the stoichiometry of the various Fe/S-containing species present in the samples of AI and RCN WT and variant LSs. Our finding that the iron in all three AI samples is almost exclusively (>93%) in the form of $[4Fe\text{-}4S]^{2+}$ clusters allows a fairly accurate determination of their extinction coefficients at 400 nm. From the protein concentration of AI WT LS (2.1×10^{-5} M) determined from the corrected Bradford protein assay, the absorbance at 400 nm (0.461), and the stoichiometry of $[4Fe\text{-}4S]^{2+}$ clusters per polypeptide (1.7 ± 0.2) as determined from analytical methods and Mössbauer analysis, we calculate an average ε_{400} of 12,800 ± 1,500 M^{-1} cm^{-1} for each of the $[4Fe\text{-}4S]^{2+}$ clusters. The same analysis yields ε_{400} = 13,900 ± 2,000 M^{-1} cm^{-1} for AI 68-73-79 LS and ε_{400} = 12,200 ± 1,200 M^{-1} cm^{-1} for AI 94-98-101 LS. These values fall into the range of molar absorptivities that have been observed for peptide-ligated [4Fe–

$4S]^{2+}$ model complexes in organic solvents, for which ε_{400} values of 12,100 to 17,500 M^{-1} cm^{-1} have been reported [66, 67].

EPR spectroscopy of WT, 68-73-79, and 94-98-101 LS. The EPR spectrum of AI WT LS, reduced in the presence of 2 mM sodium dithionite, is shown in Figure 2.5A (solid line). The spectrum, which was obtained at 13 K and 5 mW power, exhibits a pseudo-axial signal that is broad and distorted, with a g-tensor that is approximated by the principal values $g_{\parallel} = 2.03$ and $g_{\perp} = 1.93$. Additionally, there is a shoulder at g = 1.99. The EPR spectrum of the dithionite-reduced RCN WT LS is also shown in Figure 2.5A (dotted line), and exhibits features that are quite similar to that of the as-isolated protein, if not identical. Spin quantification using a Cu-EDTA standard indicated that both signals accounted for 0.08 to 0.09 equiv of spin per equiv of polypeptide. In addition, both signals were of maximum intensity at 13 K, and diminished greatly in intensity at temperatures above 40 K at 5 mW power (data not shown), consistent with the presence of $[4Fe\text{-}4S]^{+}$ clusters.

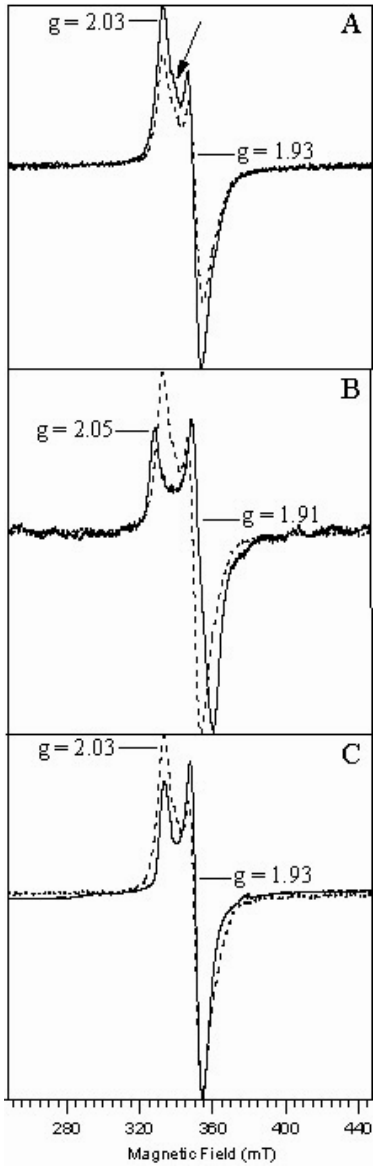

Figure 2.5: EPR spectra of WT LS (A), 94-98-101 (B), and 68-73-79 (C). (A) The solid line represents the as-isolated protein (423 μM), while the dashed line represents the reconstituted protein (344 μM). In B (1.3 mM protein) and C (395 μM protein), the solid line represents as-isolated triple variants, while the dashed line is scaled overlay of the WT protein for comparison. Each sample was incubated at room temperature in the presence of 2 mM sodium dithionite for ~2 min before freezing in liquid nitrogen. Conditions of measurement were: microwave power, 5 mW; receiver gain, 2 x 10^4; modulation amplitude, 10 G; temperature, 13 K; microwave frequency, 9.48 GHz.

The EPR spectrum of dithionite-reduced AI 94-98-101 is shown in Figure 2.5B (solid line); the spectrum of dithionite-reduced WT LS is also displayed (dotted line) for comparison. The spectrum, which was recorded on a 1.3 mM sample of the triple variant, is visibly weak in intensity, and accounts only for less than 0.001 equiv of spin per polypeptide, indicating that the C-X_4-C-X_5-C cluster is not readily reduced in the presence of 2 mM dithionite. The shape of the spectrum is different from that of the WT protein, exhibiting more axial character with g-tensor principal values that are approximated by $g_{\|} = 2.05$ and $g_{\perp} = 1.91$.

The EPR spectrum of dithionite-reduced AI 68-73-79 is shown in Figure 2.5C (solid line); the spectrum of dithionite-reduced WT LS is also displayed (dotted line). This spectrum (4C, solid line) better approximates that of WT LS than that of 94-98-101, displaying a g-tensor with principal values that are approximated by $g_{\|} = 2.03$ and $g_{\perp} = 1.93$. Interestingly, the shoulder at g = 1.99 is absent, which may reflect small conformational differences of the radical SAM [4Fe–4S] cluster in WT LS and 68-73-79. We also note that the EPR spectrum of WT LS may also be perturbed as a consequence of dipolar coupling between the two $[4Fe–4S]^{+}$ clusters. The overall low yield of reduction, however, would result in only a small fraction of WT LS that would have both [4Fe–4S] clusters reduced, suggesting that the feature at g = 1.99 is not attributable to dipolar coupling. The spectrum of AI 68-73-79 also resembles that of the reduced activating proteins of *E. coli* anaerobic ribonucleotide reductase (ARR) and PFL [30, 73], as well as reduced BS [69]. This is consistent with the premise that cysteines 94, 98, and 101 coordinate the Fe/S cluster that resides in the radical SAM motif.

Turnover of WT and Variant Lipoyl Synthases. Wild-type LS and the two triple variants were assayed for their ability to cleave SAM and synthesize LHP from the OHP substrate as described in a previous publication [21]. As shown in Table 2, neither of the triple variants was capable of catalyzing formation of LHP or 5'-dA. By contrast, the AI WT enzyme catalyzed formation of 13.6 μM LHP and 30 μM 5'-dA (0.27 and 0.60 equiv per polypeptide, respectively) after 20 min at 37°C, while the reconstituted enzyme catalyzed formation of 17.7 μM LHP and 48 μM 5'-dA (0.36 and 0.96 equiv per polypeptide, respectively). For both AI and RCN enzymes, the formation of both products could be fitted to a first-order kinetic equation, yielding similar rate constants (~0.18 min^{-1}). In addition, the ratio of 5'-dA to LHP, which has been addressed in a previous publication [21], did not differ significantly between the two proteins.

2.5 Discussion

Until recently, the in vitro characterization of the LS reaction has been impeded by the unknown nature of the true substrates for the reaction [20, 21]. Accordingly, given the similarities that the two enzymes share, studies on BS have served as a general model for catalysis by LS. In both systems, the 5'-deoxaydenosyl radicals generated from the cleavage of SAM are believed to remove unactivated hydrogen atoms from the respective substrates to allow for subsequent sulfur insertion. At present, the major issues and points of contention with respect to catalysis by BS relate to cofactor composition of the protein, the exact nature of the immediate sulfur donor, and the chemistry by which the sulfur atom in biotin is inserted.

Studies from Marquet's laboratory provided initial evidence that the source of the sulfur atom in biotin derived from the protein itself, and was most likely an Fe/S cluster [74]. Consistent with this finding, results from Jarrett's laboratory suggested that the "active" form of BS contained two distinct cluster configurations on each polypeptide. A [4Fe–4S] cluster, housed in the C-X_3-C-X_2-C motif, was postulated to interact with SAM in the presence of a suitable reductant to generate the 5'-dA•, while a [2Fe–2S] cluster was proposed to serve as the source of the sulfur that is incorporated into the substrate [48, 75]. This proposal was largely based on the UV-visible spectrum of the protein and the changes observed in the spectrum during turnover. A number of spectroscopic studies on BS, including in vivo Mössbauer experiments [54, 55], as well as Mössbauer, resonance Raman, and crystallographic studies on purified and reconstituted enzyme [34, 49, 50, 65, 76], have confirmed the presence of both Fe/S clusters on active BS. In addition, it has been demonstrated spectroscopically that SAM interacts with the [4Fe-4S] cluster, thus corroborating the proposed role for this cluster in the generation of the 5'-dA• [33]. The premise that active BS contains two distinct cluster types is not universally shared [56, 77]; the mechanism of sulfur insertion from the $[2Fe–2S]^{2+}$ cluster is presently only speculative [48], and indeed there is no compelling evidence that the *intact* [2Fe–2S] cluster is the immediate sulfur donor [50, 65].

In this study, we endeavored to ascertain whether the parallels between BS and LS could be extended to the number of Fe/S clusters per polypeptide as well as their configuration. We employed a combination of spectroscopic methods (Mössbauer, EPR, and UV-visible), analytical methods (iron, sulfide, and protein quantification), and activity assays on WT LS and two triple variants, in which the three cysteine residues

residing in either the C-X_3-C-X_2-C motif or the C-X_4-C-X_5-C motif were changed to alanine. Importantly, all of our studies were carried out on proteins that were expressed in the presence of ^{57}Fe–and sometimes further reconstituted with ^{57}Fe and sulfide–in order to relate the quantity of bound iron to cluster configuration. Our results indicate that LS houses two [4Fe–4S] clusters per polypeptide; one cluster is ligated by the cysteines in the radical SAM C-X_3-C-X_2-C motif, while the other is ligated by the cysteines in the C-X_4-C-X_5-C motif, which is unique to LSs. Perhaps the most significant finding, especially in light of the ongoing studies on BS, is that LS, when isolated anaerobically from cells in which it and the *E. coli* isc operon are co-expressed, is active without in vitro reconstitution. This has also been observed prior to this study, although the amount of turnover was significantly less [22].

In the original characterization of LS it was reported that the AI protein contained 1.8 ± 0.2 equiv of Fe and 2.2 ± 0.4 equiv of S^{2-} per polypeptide [38], while a later characterization of the enzyme, which included assessment of enzymatic turnover, indicated that AI monomeric LS contained 3.4 ± 0.4 equiv of Fe and 4.8 ± 0.8 equiv of S^{2-}, and that AI dimeric LS contained 3.3 ± 0.4 equiv of Fe and 4.2 ± 0.5 equiv of S^{2-} per polypeptide [22]. LS that was purified from inclusion bodies and reconstituted with a 6-fold excess of iron and sulfide was purported to contain 1.8-2.3 equiv of Fe and S^{2-} per polypeptide in one instance [39], and 3.7-4.2 mol of Fe and S^{2-} in the other [69]. Lastly, LS that was isolated from an expression system containing a plasmid that encodes the *E. coli isc* operon was purported to contain 3.4-3.6 equiv of Fe and 2.4 equiv of S^{2-} per polypeptide [64]. In this study, we find that AI WT LS, purified from a similar expression system, but in minimal media containing ^{57}Fe, contains 6.9 ± 0.5 equiv of Fe

and 6.4 ± 0.9 equiv of S^{2-} per polypeptide, almost enough for two [4Fe–4S] clusters in each polypeptide.

Because our stoichiometry depends largely on the ability to quantify protein concentration accurately, we went to significant extents to ensure that our correction factor for the Bradford protein assay was appropriate. We found that the Bradford protein determination method using BSA as a standard overestimates the concentration of LS by a factor of 1.47. In an earlier study it was reported that the same protein assay overestimates the concentration of LS by 92 % [22]. If we were to use that correction factor our Fe and S^{2-} stoichiometry would increase, not decrease, resulting in 9.0 Fe and 8.3 S^{2-} per polypeptide. Moreover, we have addressed the stoichiometry of the LS reaction with respect to SAM usage, and find that each polypeptide catalyzes formation of almost exactly one equiv of 5'-dA in a clean pseudo first-order kinetic process when using a Bradford correction factor of 1.47 [21].

Upon reconstitution of AI WT LS, the quantity of iron and sulfide bound to the protein increases significantly to 13.8 ± 0.6 and 13.1 ± 0.2 per polypeptide; however, Mössbauer spectroscopy reveals that only ~9 irons and sulfides are in the configuration $[4Fe\text{-}4S]^{2+}$, giving rise to 2.3 ± 0.3 per polypeptide with the remainder existing presumably as adventitiously bound species. Importantly, the 1.4-fold increase in the $[4Fe\text{-}4S]^{2+}$ stoichiometry of RCN WT LS as compared to AI WT LS correlates well with the increase in activity of the protein; a 1.6-fold increase in 5'-dA and a 1.3-fold increase in LHP is observed after 20 min at 37 °C.

Importantly, both triple variants, whether reconstituted or not, were completely inactive with respect to formation of 5'-dA and LHP, thus demonstrating that both [4Fe–

4S] clusters are essential for turnover. Our finding that 68-73-79 does not promote reductive cleavage of SAM may be unexpected, since this variant has the C-X_3-C-X_2-C cluster intact, which is the cluster that is proposed to function intimately in generation of the 5'-dA•. Studies by Mulliez et al have demonstrated that reduction of the $[4Fe–4S]^{2+}$ cluster of the activating enzyme (AE) of the ARR is highly coupled to a thermodynamically favorable step, which in that system is generation of the glycyl radical on the ARR [78]. In LS, abstraction of a hydrogen atom from the octanoyl moiety of OHP to afford a primary alkyl radical would not be considered to be suitably downhill; the thermodynamically favorable step would most likely be the subsequent step, which we hypothesize to be the interaction of the alkyl radical with the sulfur donor. We posit that the activated form of the sulfur donor in 68-73-79 is not present.

Recently, it has been shown that the [2Fe–2S] cluster of BS decays during biotin formation [48, 65], suggesting that it is the immediate sulfur donor, or that it is converted into the immediate sulfur donor. We speculate that in LS the cluster that is coordinated by the C-X_4-C-X_5-C motif may play a similar role, somehow supplying the sulfur atoms that are incorporated into the substrate. There is a clear difference between BS and LS, since both clusters in LS are [4Fe–4S] clusters, whereas BS contains one [2Fe–2S] cluster and one [4Fe–4S] cluster. Although BS is typically purified aerobically, wherein only the [2Fe–2S] cluster is present, it was recently shown that this cluster form is also present in vivo and after anaerobic isolation of the protein, suggesting that the [2Fe–2S] cluster of aerobically purified BS is not caused by oxidative damage of a [4Fe–4S] cluster [50, 54, 55]. It is tempting to speculate that the difference in cluster type between BS and LS may reflect the different requirements for sulfur in the respective reactions, in that only

one sulfur atom is required for formation of biotin from dethiobiotin, whereas formation of the lipoyl group requires addition of two sulfur atoms to an octanoyl chain.

In conclusion, we have unambiguously demonstrated that (1) active LS binds two distinct [4Fe–4S] clusters per polypeptide, and (2) both clusters are important for converting OHP to LHP. Furthermore, these results set the stage for more detailed studies to elucidate the functional role of each of the clusters, which are presently ongoing in our laboratories.

2.6 References

1. Biewenga, G.P., G.R.M.M. Haenen, and A. Bast, *An Overview of Lipoate Chemistry*, in *Lipoic Acid in Health and Disease*, G. Zimmer, Editor. 1997, Marcel Dekker, Inc.: New York. p. 1-32.
2. Douce, R., J. Bourguignon, D. Macherel, and M. Neuburger, The Glycine Decarboxylase System in Higher Plant Mitochondria: Structure, Function and Biogenesis. *Biochem Soc Trans*, 1994. **22**: p. 184-188.
3. Pares, S., C. Cohen-Addad, L. Sieker, M. Neuburger, and R. Douce, X-ray Structure Determination at 2.6-Å Resolution of a Lipoate-Containing Protein: The H-Protein of the Glycine Decarboxylase Complex from Pea Leaves. *Proc Natl Acad Sci USA*, 1994. **914**: p. 4850-4853.
4. Reed, L., Multienzyme Complexes. *Acc Chem Res*, 1974. **7**: p. 40-46.

5. Reed, L.J., B.G.D. Busk, I.C. Gunsalus, and G.H.F. Schnakenberg, Crystalline α-Lipoic Acid: A Catalytic Agent Associated with Pyruvate Dehydrogenase. *Science*, 1951. **114**: p. 93.

6. Reed, L.J. and M.L. Hackert, Structure-function relationships in dihydrolipoamide acyltransferases. *J Biol Chem*, 1990. **265**(16): p. 8971-8974.

7. Williams, C.H., *Lipoamide dehydrogenase, glutathionine reductase, thoredoxine reductase and mercuric reductase-family of flavoenzyme transhydrogenases*, in *Chemistry and Biochemistry of Flavoproteins*, F. Müller, Editor. 1992, CRC press: Boca Raton. p. 121-211.

8. Robinson, J.R., S.M. Klein, and R.D. Sagers, Glycine Metabolism. Lipoic Acid as the Prosthetic Group in the Electron Transfer Protein P2 from *Peptococcus glycinophilus*. *J Biol Chem*, 1973. **248**(15): p. 5319-5323.

9. Fujiwara, K. and Y. Motokawa, Mechansm of the Glycine Cleavage Reaction. Steady State Kinetic Studies of the P-Protein-Catalyzed Reaction. *J Biol Chem*, 1983. **258**(13): p. 8156-8162.

10. Klein, S.M. and R.D. Sagers, Glycine Metabolism. III. A Flavin-Linked Dehydrogenase Associated with the Glycine Cleavage System in *Peptococcus glycinophilus*. *J Biol Chem*, 1967. **242**(2): p. 297-300.

11. Klein, S.M. and R.D. Sagers, Glycine Metabolism. II. Kinetic and Optical Studies on the Glycine Decarboxylase System from *Peptococcus glycinophilus*. *J Biol Chem*, 1966. **241**(1): p. 206-209.

12. Klein, S.M. and R.D. Sagers, Glycine Metabolism. I. Properties of the System Catalyzing the Exchange of Bicarbonate with the Carboxyl Group of Glycine in *Peptococcus glycinophilus*. *J Biol Chem*, 1966. **241**(1): p. 197-205.

13. Fujiwara, K., K. Okamura-Ikeda, and Y. Motokawa, Mechanism of the Glycine Cleavage Reaction. Further Characterization of the Intermediate Attached to H-Protein and of the Reaction Catalyzed by T-Protein. *J Biol Chem*, 1984. **259**(17): p. 10664-10668.

14. Morris, T.W., K.E. Reed, and J. J. E. Cronan, Lipoic Acid Metabolism in *Escherichia coli*: the *lplA* and *lipB* Genes Define Redundant Pathways for Ligation of Lipoyl Groups to Apoprotein. *J Bacteriol*, 1995. **177**(1): p. 1-10.

15. Green, D.E., T.W. Morris, G. J., J.E. Cronan Jr., and J.R. Guest, Purification and Properties of the Lipoate Protein Ligase of *Escherichia coli. Biochem J.*, 1995. **309**: p. 853-862.

16. Morris, T.W., K.E. Reed, and J.E. Cronan Jr., Identification of the Gene Encoding Lipoate-Protein Ligase of *Escherichia coli.* Molecular Cloning and Characterization of the *lplA* Gene and Gene Product. *J Biol Chem*, 1994. **269**: p. 16091-16100.

17. Jordan, S.W. and J. J. E. Cronan, A New Metabolic Link. The Acyl Carrier Protein of Lipid Synthesis Donates Lipoic Acid to the Pyruvate Dehydrogenase Complex in *Escherichia coli* and Mitochondria. *J Biol Chem*, 1997. **272**(29): p. 17903-17906.

18. Jordan, S.W. and J. J. E. Cronan, Biosynthesis of Lipoic Acid and Posttranslational Modification with Lipoic Acid in *Escherichia coli. Methods Enzymol*, 1997. **279**: p. 176-183.

19. Jordan, S.W. and J.E. Cronan Jr., The *Escherichia coli* lipB Gene Encodes Lipoyl (Octanoyl)-Acyl Carrier Protein:Protein Transferase. *J Bacteriol*, 2003. **185**(5): p. 1582-1589.

20. Zhao, S., J.R. Miller, Y. Jiang, M.A. Marletta, and J.E. Cronan Jr., Assembly of the Covalent Linkage Between Lipoic Acid and Its Cognate enzymes. *Chem Biol*, 2003. **10**: p. 1293-1302.

21. Cicchillo, R.M., D.F. Iwig, A.D. Jones, N.M. Nesbitt, C. Baleanu-Gogonea, M.G. Souder, L. Tu, and S.J. Booker, Lipoyl Synthase Requires Two Equivalents of S-Adenosyl-L-Methionine to Synthesize One Equivalent of Lipoic Acid. *Biochemistry*, 2004. **43**: p. 6378-6386.

22. Miller, J.R., R.W. Busby, S.W. Jordan, J. Cheek, T.F. Henshaw, G.W. Ashley, J.B. Broderick, J.E. Cronan Jr., and M.A. Marletta, *Escherichia coli* LipA Is a Lipoyl Synthase: In Vitro Biosynthesis of Lipoylated Pyruvate Dehydrogenase Complex from Octanoyl-Acyl Carrier Protein. *Biochemistry*, 2000. **39**: p. 15166-15178.

23. Frey, P.A. and O.T. Magnusson, S-Adenosylmethionine: A Wolf in Sheep's Clothing, or a Rich Man's Adenosylcobalamin? *Chem Rev*, 2003. **103**: p. 2129-2148.

24. Frey, P.A. and S. Booker, *Radical Intermediates in the Reaction of Lysine 2,3-Aminomutase*, in *Advances in Free Radical Chemistry*, S.Z. Zard, Editor. 1999, JAI Press Inc.: Stamford, CT. p. 1-43.

25. Cheek, J. and J.B. Broderick, Adenosylmethionine-dependent iron-sulfur enzymes: versatile clusters in a radical new role. *J Biol Inorg Chem*, 2001. **6**(3): p. 209-226.

26. Sofia, H.J., G. Chen, B.G. Hetzler, J.F. Reyes-Spindola, and N.E. Miller, Radical SAM, a novel protein superfamily linking unresolved steps in familiar biosynthetic pathways with radical mechanisms: functional characterization using new analysis and information visualization methods. *Nucleic Acids Res*, 2001. **29**(5): p. 1097-1106.

27. Henshaw, T.F., J. Cheek, and J.B. Broderick, The $[4Fe\text{-}4S]^{+1}$ Cluster of Pyruvate Formate-Lyase Activating Enzyme Generates the Glycyl Radical on Pyruvate Formate-Lyase: EPR-Detected Single Turnover. *J Am Chem Soc*, 2000. **122**: p. 8331-8332.

28. Lieder, K.W., S. Booker, F.J. Ruzicka, H. Beinert, G.H. Reed, and P.A. Frey, S-Adenosylmethionine-Dependent Reduction of Lysine 2,3-Aminomutase and Observation of the Catalytically Functional Iron-Sulfur Centers by Electron Paramagnetic Resonance. *Biochemistry*, 1998. **37**(8): p. 2578-2585.

29. Ollagnier-de-Choudens, S., Y. Sanakis, K.S. Hewitson, P. Roach, E. Münck, and M. Fontecave, Reductive Cleavage of S-Adenosylmethionine by Biotin Synthase from *Escherichia coli*. *Biochemistry*, 2002. **277**(16): p. 13449-13454.

30. Ollagnier, S., E. Mulliez, P.P. Schmidt, R. Eliasson, J. Gaillard, C. Deronzier, T. Bergman, A. Gräslund, P. Reichard, and M. Fontecave, Activation of the Anaerobic Ribonucleotide Reductase from *Escherichia coli*. The Essential role of the Iron-Sulfur Center for S-adenosylmethionine Reduction. *J Biol Chem*, 1997. **272**(39): p. 24216-24223.

31. Krebs, C., W.E. Broderick, T.F. Henshaw, J.B. Broderick, and B.H. Huynh, Coordination of Adenosylmethionine to a Unique Iron Site of the [4Fe–4S] of Pyruvate Formae–Lyase Activating Enzyme: A Mössbauer Spectroscopic Study. *J Am Chem Soc*, 2002. **124**(6): p. 912-913.

32. Chen, D., C. Walsby, B.M. Hoffman, and P.A. Frey, Coordination and mechanism of reversible cleavage of S-adenosylmethionine by the [4Fe-4S] center in lysine 2,3-aminomutase. *J Am Chem Soc*, 2003. **125**(39): p. 11788-9.

33. Cosper, M.M., G.N.L. Jameson, R. Davydov, M.K. Eidsness, B.M. Hoffman, B.H. Huynh, and M.K. Johnson, The [4Fe–4S]2+ Cluster in Reconstituted Biotin Synthase Binds S-Adenosyl-L-methionine. *J Am Chem Soc*, 2002. **124**(47): p. 14006-14007.

34. Berkovitch, F., Y. Nicolet, J.T. Wan, J.T. Jarrett, and C.L. Drennan, Crystal Structure of Biotin Synthase, an S-Adenosylmethionine-Dependent Radical Enzyme. *Science*, 2004. **303**: p. 76-79.

35. Walsby, C.J., D. Ortillo, B.W. E., J.B. Broderick, and B.M. Hoffman, An Anchoring Role for FeS Clusters: Chelation of the Amino Acid Moiety of S-Adenosylmethionine to the Unique Iron Site of the [4Fe–4S] Cluster of Pyruvate

Formate–Lyase Activating Enzyme. *J Am Chem Soc*, 2002. **124**(38): p. 11270-11271.

36. Walsby, C.J., W. Hong, W.E. Broderick, J. Cheek, D. Ortillo, J.B. Broderick, and B.M. Hoffman, Electron-nuclear double resonance spectroscopic evidence that S-adenosylmethionine binds in contact with the catalytically active $[4Fe\text{-}4S]^{+}$ cluster of pyruvate formate-lyase activating enzyme. *J. Am. Chem. Soc.*, 2002. **124**(12): p. 3143-3151.

37. Layer, G., J. Moser, D.W. Heinz, D. Jahn, and W.D. Schubert, Crystal structure of coproporphyrinogen III oxidase reveals cofactor geometry of Radical SAM enzymes. *Embo J*, 2003. **22**(23): p. 6214-6224.

38. Busby, R.W., J.P.M. Schelvis, D.S. Yu, G.T. Babcock, and M.A. Marletta, Lipoic Acid Biosynthesis: LipA Is an Iron Sulfur Protein. *J Am Chem Soc*, 1999. **121**(19): p. 4706-4707.

39. Ollagnier-de Choudens, S. and M. Fontecave, The Lipoate Synthase from Escherichia coli is an Iron-Sulfur Protein. *FEBS Lett*, 1999. **453**: p. 25-28.

40. Parry, R.J., Biosynthesis of Some Sulfur-Containing Natural Products. Investigations of the Mechanism of Carbon-Sulfur bond Formation. *Tetrahedron*, 1983. **39**: p. 1215-1238.

41. Marquet, A., Enzymology of carbon-sulfur bond formation. *Curr Opin Chem Biol*, 2001. **5**: p. 541-549.

42. Fontecave, M., E. Mulliez, and S. Ollagnier-de Choudens, Adenosylmethionine as a Source of 5'-Deoxyadenosyl Radicals. *Curr Opin Chem Biol*, 2001. **5**: p. 506-511.

43. Jarrett, J.T., The Generation of 5'-Deoxyadenosyl Radicals by Adenosylmethionine-Dependent Radical Enzymes. *Curr Opin Chem Biol*, 2003. **7**: p. 174-182.

44. Hayden, M.A., I. Huang, D.E. Bussiere, and G.W. Ashley, The Biosynthesis of Lipoic Acid: Cloning of lip, a Lipoate Biosynthetic Locus of *Escherichia coli*. *J Biol Chem*, 1992. **267**(14): p. 9512-9515.

45. Reed, K.E. and J. J. E. Cronan, Lipoic Acid Metabolism in *Escherichia coli*: Sequencing and Functional Characterization of the *lipA* and *lipB* Genes. *J Bacteriol*, 1993. **175**(5): p. 1325-1336.

46. Otsuka, A.J., M.R. Buoncristiani, P.K. Howard, J. Flamm, C. Johnson, R. Yamamoto, K. Uchida, C. Cook, J. Ruppert, and J. Matsuzaki, The *Escherichia coli* Biotin Biosynthetic Enzyme Sequences Predicted from the Nucleotide Sequence of the *bio* Operon. *J Biol Chem*, 1988. **263**: p. 19577-19585.

47. Hewitson, K.S., S. Ollagnier-de Choudens, Y. Sanakis, N.M. Shaw, J.E. Baldwin, E. Münck, P.L. Roach, and M. Fontecave, The Iron-Suflur Center of Biotin Synthase: Site-Directed Mutants. *J Biol Inorg Chem*, 2002. **7**: p. 83-93.

48. Ugulava, N.B., C.J. Sacanell, and J.T. Jarrett, Spectroscopic Changes during a Single Turnover of Biotin Synthase: Destruction of a [2Fe–2S] Cluster Accompanies Sulfur Insertion. *Biochemistry*, 2001. **40**: p. 8352-8358.

49. Ugulava, N.B., K.K. Surerus, and J.T. Jarrett, Evidence from Mössbauer Spectroscopy for Distinct $[2Fe\text{-}2S]^{2+}$ and $[4Fe\text{-}4S]^{2+}$ Cluster Binding Sites in Biotin Synthase from *Escherichia coli*. *J Am Chem Soc*, 2002. **124**: p. 9050-9051.

50. Cosper, M.M., G.N.L. Jameson, H.L. Hernández, C. Krebs, B.H. Huynh, and M.K. Johnson, Characterization of the cofactor composition of *Escherichia coli* biotin synthase. *Biochemistry*, 2004. **43**: p. 2007-2021.

51. Duin, E.C., M.E. Lafferty, B.R. Crouse, R.M. Allen, I. Sanyal, D.H. Flint, and M.K. Johnson, [2Fe-2S] to [4Fe-4S] Cluster Conversion in *Escherichia coli* Biotin Synthase. *Biochemistry*, 1997. **36**: p. 11811-11820.

52. Sanyal, I., G. Cohen, and D.H. Flint, Biotin Synthase: Purification, Characterization as a [2Fe-2S] Cluster Protein, and in Vitro Activity of the *Escherichia coli bioB* Gene Product. *Biochemistry*, 1994. **33**: p. 3625-3631.

53. Tse Sum Bui, B., D. Florentin, A. Marquet, R. Benda, and A.X. Trautwein, Mössbauer Studies of *Escherichia coli* Biotin Synthase: Evidence for Reversible Interconversion between $[2Fe\text{-}2S]^{2+}$ and $[4Fe\text{-}4S]^{2+}$ Clusters. *FEBS Lett*, 1999. **459**: p. 411-414.

54. Cosper, M.M., G.N.L. Jameson, M.K. Eidsness, B.H. Huynh, and M.K. Johnson, Recombinant *Escherichia coli* Biotin Synthase is a $[2Fe–2S]^{2+}$ Protein in Whole Cells. *FEBS Lett*, 2002. **529**: p. 332-336.

55. Benda, R., B. Tse Sum Bui, V. Schünemann, D. Florentin, A. Marquet, and A.X. Trautwein, Iron–Sulfur Clusters of Biotin Synthase In Vivo: A Mössbauer Study. *Biochemistry*, 2002. **41**: p. 15000-15006.

56. Ollagnier-de Choudens, S., E. Mulliez, K.S. Hewitson, and M. Fontecave, Biotin synthase Is a Pyridoxal Phosphate-Dependent Cysteine Desulfurase. *Biochemistry*, 2002. **41**: p. 9145-9152.

57. Beinert, H., Micro Methods for the Quantitative Determination of Iron and Copper in biological Material. *Methods Enzymol*, 1978. **54**: p. 435-445.

58. Beinert, H., Semi-micro Methods for Analysis of Labile Sulfide and of Labile Sulfide plus Sulfane Sulfur in Unusually Stable Iron-Sulfur Proteins. *Anal Biochem*, 1983. **131**: p. 373-378.

59. Kennedy, M.C., T.A. Kent, M. Emptage, H. Merkle, H. Beinert, and E. Münck, Evidence for the Formation of a Linear [3Fe-4S] Cluster in Partially Unfolded Aconitase. *J Biol Chem*, 1984. **259**(23): p. 14463-14471.

60. Sambrook, J., E.F. Fritsch, and T. Maniatis, *Molecular Cloning: A Laboratory Manual*. 2nd ed, ed. M. Ferguson. Vol. 3. 1989, Plainview, New York: Cold Spring Harbor Laboratory Press.

61. Ramamurthy, V., S.L. Swann, J.L. Paulson, C.J. Spedaliere, and E.G. Mueller, Critical Aspartic Acid Residues in Pseudouridine Synthases. *J Biol Chem*, 1999. **274**(32): p. 22225-22230.

62. Frazzon, J. and D.R. Dean, Formation of iron–sulfur clusters in bacteria: an emerging field in bioinorganic chemistry. *Curr Opin Chem Biol*, 2003. **7**: p. 166-173.

63. Frazzon, J., J.R. Fick, and D.R. Dean, Biosynthesis of iron–sulphur clusters is a complex and highly conserved process. *Biochem Soc Trans*, 2002. **30**(4): p. 680-685.

64. Kriek, M., L. Peters, Y. Takahashi, and P.L. Roach, Effect of iron–sulfur cluster assembly proteins on the expresssion of *Escherichia coli* lipoic acid synthase. *Protein Expr Purif*, 2003. **28**: p. 241-245.

65. Jameson, G.N.L., M.M. Cosper, H.L. Hernández, M.K. Johnson, and B.H. Huynh, Role of the [2Fe–2S] cluster in recombinant *Escerhichia coli* biotin synthase. *Biochemistry*, 2004. **43**: p. 2022-2031.

66. Nakamura, A. and N. Ueyama, *Iron–Sulfur Models of Protein Active Sites*, in *Encyclopedia of Inorganic Chemistry*, R.B. King, Editor. 1994, John Wiley & Sons: Chichester. p. 1883-1896.

67. Holm, R.H. and J.A. Ibers, *Synthetic Analogues of the Active Sites of Iron–Sulfur Proteins*, in *Iron-Sulfur Proteins*, W. Lovenberg, Editor. 1977, Academic Press: New York.

68. Orme-Johnson, W.H. and N.R. Orme-Johnson, *Iron-sulfur proteins: The problem of determining cluster type.*, in *Iron-Sulfur Proteins*, T.G. Spiro, Editor. 1982, John Wiley & Sons: New York.

69. Ollagnier-de Choudens, S., Y. Sanakis, K.S. Hewitson, P. Roach, J.E. Baldwin, E. Münck, and M. Fontecave, Iron-Sulfur Center of Biotin Synthase and Lipoate Synthase. *Biochemistry*, 2000. **39**: p. 4165-4173.

70. Kent, T.A., B.H. Huynh, and E. Münck, Iron–sulfur proteins: spin-coupling model for three-iron clusters. *Proc Natl Acad Sci U S A*, 1980. **77**(11): p. 6574-6576.

71. Papaefthymiou, V., J.J. Girerd, J.J.G. Moura, E. Moura, and E. Münck, Mössbauer study of D. gigas ferredoxin II and spin-coupling model for Fe_3S_4 cluster with valence delocalization. *J Am Chem Soc*, 1987. **109**: p. 4703-4710.

72. Krebs, C., T.F. Henshaw, J. Cheek, B.H. Huynh, and J.B. Broderick, Conversion of 3Fe–4S to 4Fe–4S Clusters in Native Pyruvate Formate-Lyase Activating

Enzyme: Mössbauer Characterization and Implications for Mechanism. *J Am Chem Soc*, 2000. **122**(50): p. 12497-12506.

73. Külzer, R., T. Pils, R. Kappl, J. Hüttermann, and J. Knappe, Reconstitution and Characterization of the Polynuclear Iron-Sulfur Cluster in Pyruvate Formate-Lyase-Activating Enzyme. *J Biol Chem*, 1998. **273**(9): p. 4897-4903.

74. Tse Sum Bui, B., B. Florentin, F. Fournier, O. Ploux, A. Méjean, and A. Marquet, Biotin Synthase Mechanism: On the Origin of Sulphur. *FEBS Lett*, 1998. **440**: p. 226-230.

75. Ugulava, N.B., B.R. Gibney, and J.T. Jarrett, Biotin Synthase Contains Two Distinct Iron–Sulfur Binding Sites: Chemical and Spectroelectrochemical Analysis of Iron–Sulfur Cluster Interconversions. *Biochemistry*, 2001. **40**: p. 8343-8351.

76. Tse Sum Bui, B., R. Benda, V. Schünemann, D. Florentin, A.X. Trautwein, and A. Marquet, Fate of the $(2Fe\text{-}2S)^{2+}$ Cluster of *Escherichia coli* Biotin Synthase during Reaction: A Mössbauer Characterization. *Biochemistry*, 2003. **42**(29): p. 8791-8798.

77. Ollagnier-de Choudens, S., E. Mulliez, and M. Fontecave, The PLP-dependent biotin synthase from *Escherichia coli*: mechanistic studies. *FEBS Lett*, 2002. **532**: p. 465-468.

78. Mulliez, E., D. Padovani, M. Atta, C. Alcouffe, and M. Fontecave, Activation of Class II Ribonucleotide Reductase by flavodoxin: A Protein Radical-Driven Electron Transfer to the Iron–sulfur Center. *Biochemistry*, 2001. **40**: p. 3730-3736.

Chapter 3

Reaction Stoichiometry and Mechanistic Investigations into the Formation of Lipoic Acid in *Escherichia coli*

This chapter was reproduced, with slight modifications, from Cicchillo, R. M.; Iwig, D. F.; Jones, A. D.; Nesbitt, N. M.; Baleanu-Gogonea, C.; Souder, M. G.; Tu, L.; Booker, S. J., (2004) Lipoyl Synthase Requires Two Equivalents of S-Adenosyl-L-methionine To Synthesize One Equivalent of Lipoic Acid. *Biochemistry*; 43(21); 6378-6386.

3.1 Abstract

Lipoyl synthase (LipA) catalyzes the formation of the lipoyl cofactor, which is employed by several multienzyme complexes for the oxidative decarboxylation of various α-keto acids, as well as the cleavage of glycine into CO_2, and NH_3, with transfer of its α-carbon to tetrahydrofolate, generating N^5,N^{10}-methylenetetrahydrofolate. In each case, the lipoyl cofactor is tethered covalently in an amide linkage to a conserved lysine residue located on a designated lipoyl-bearing subunit of the complex. Genetic and biochemical studies have suggest that lipoyl synthase is a member of a newly established class of metalloenzymes that use S-adenosyl-L-methionine (AdoMet) as a source of a 5'-deoxyadenosyl radical (5'-dA•), which is an obligate intermediate in each reaction. These enzymes contain iron–sulfur clusters, which provide an electron during the cleavage of AdoMet, allowing formation of L-methionine in addition to the primary radical. Recently, one substrate for lipoyl synthase has been shown to be the

octanoylated derivative of the lipoyl-bearing subunit (E_2) of the pyruvate dehydrogeanse complex [Zhao, S., Miller, J. R., Jian, Y., Marletta, M. A., and Cronan Jr, J. E. (2003) *Chem Biol 10*, 1293-1302]. Herein, we show that the octanoylated derivative of the lipoyl-bearing subunit of the glycine cleavage system (H-Protein) is also a substrate for LipA, substantiating the conclusion that the cofactor is synthesized on its target protein. Moreover, we show that the 5'-dA• acts directly on the octanoyl substrate, as evidenced by deuterium transfer from [d_{15}-octanoyl]H-protein. Our data also indicate that 2 equiv of AdoMet are cleaved irreversibly in forming 1 equiv of [lipoyl]H-Protein, and are consistent with a model in which two LipA proteins are required to synthesize one lipoyl group.

Interestingly, lipoyl-H protein could not be detected when [d_{15}-octanoyl]H-protein was used as the substrate indicating that there is a significant observed isotope effect on hydrogen atom abstraction from either C-6 or C-8. To address which C–D bond is associated with the high isotope effect, we synthesized [8-$^2H_3$-octanoyl]–H protein, and [6,6-$^2H_2$-octanoyl]–H protein and assessed formation of 5'-dA and lipoyl-H protein using these specifically labeled substrates. Rate constants for the removal of hydrogen atoms from both positions were determined by quantifying the amount of 5'-deoxyadenosine. Comparison plots indicate that the observed isotope effect arises from the C-8 position and suggests that sulfur insertion at C-6 precedes insertion at C-8. In addition, the dependence of isotope incorporation in the substrate on the rate constants for 5'-dA formation indicates that cleavage of SAM is highly coupled to hydrogen atom abstraction and presumably formation of carbon–sulfur bonds.

3.2 Introduction

Lipoyl synthase (LipA) catalyzes the insertion of sulfur atoms into the 6 and 8 positions of protein-bound derivatives of octanoic acid, forming the corresponding lipoyl derivative (Figure 3.1) [1, 2]. When attached to its appropriate acceptor protein, the lipoyl cofactor plays a central role in the oxidative decarboxylation of glycine and several α-keto acids, which is catalyzed by large multisubunit complexes such as the glycine cleavage system (GCS), the pyruvate dehydrogenase complex (PDC), the α-ketoglutarate dehydrogenase complex (KDC), and the branched chain oxo-acid dehydrogenase complex (BCDC) [3, 4]. In each of these complexes, the lipoyl cofactor is bound covalently in an amide linkage to the ε-amino group of a target lysine residue on the lipoyl-bearing subunit. This linkage creates a long and flexible appendage that enables the cofactor to deliver intermediates between successive active sites among the subunits of each complex. Analysis of available sequence information from a number of organisms indicates that lipoyl synthases are found among the bacteria, eukarya, and archaea kingdoms, and are present in *Homo sapien*, *Arabidopsis thaliana*, *Sacchromyces cerevisiae*, and both gram-positive and gram-negative bacteria.

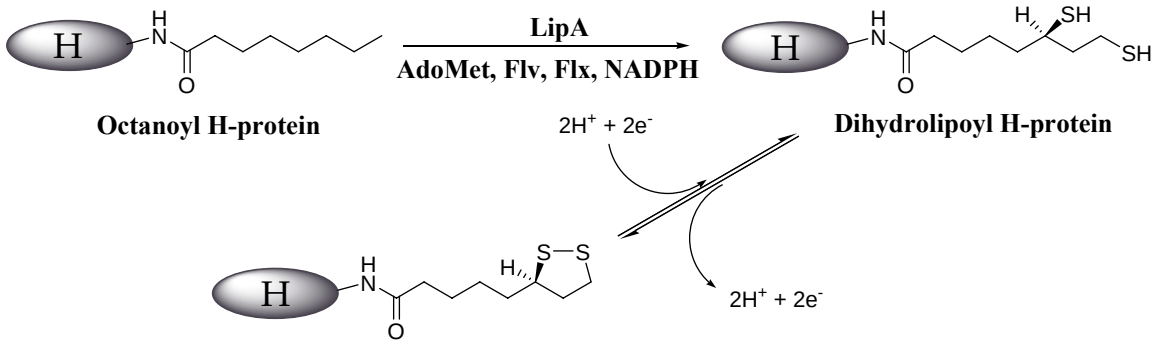

Figure 3.1**:** Reaction Catalyzed by Lipoyl Synthase.

Despite success in elucidating the multiple functions of the lipoyl cofactor in the multienzyme complexes that require it, the unraveling of the pathway by which it is biosynthesized has been challenging. In vivo feeding studies in *Escherichia coli*, initiated as early as 1964, indicated that octanoic acid could serve as a precursor to lipoic acid, requiring removal of only two hydrogens during the transformation, one from C-6 and one from C-8, which are those that are replaced by sulfur insertion [5-7]. It is the *pro*-R-hydrogen that is removed from C-6; however, sulfur insertion ensues with inversion of configuration at this position. The intrinsic inertness of the octanoyl substrate prompted speculation of the involvement of radical intermediates in the reaction. One hypothesis suggested intermediate hydroxylation, followed by activation of the hydroxyl groups and their subsequent displacement with sulfur-derived nucleophiles. The particularly satisfying aspect of the proposal was that it would readily account for the observed inversion of configuration that takes place at C-6, if hydroxylation occurred with retention of configuration. However, in vivo feeding studies with [8-$^2H_2$]-8-hydroxyoctanoic acid, [6(RS)-^{2}H]-6-hydroxyoctanoic acid, and [8-$^2H_2$]-(±)-6,8-dihydroxyoctanoic acid indicated that neither of the compounds was converted into lipoic acid. By contrast, [8-$^2H_2$]-8-thiooctanoic acid was readily converted into lipoic acid, while [6(RS)-^{2}H]-6-thiooctanoic acid was converted 10-20% as efficiently as the former compound [8].

A number of parallels can be drawn between LipA and biotin synthase (BioB), which catalyzes a similar reaction. Biotin is formed by insertion of one sulfur atom between C-6 and C-9 of dethiobiotin, and also requires removal of two unactivated hydrogen atoms. As described for lipoic acid biosynthesis, the corresponding

hydroxylated derivatives of dethiobiotin are not intermediates in the reaction, whereas the thiol-containing derivatives are [5, 9-11]. In stark contrast to lipoic acid biosynthesis, sulfur insertion at C-6 of dethiobiotin takes place with retention of configuration [10].

Recent genetic, bioinformatics, and biochemical studies indicate that lipoyl synthases belong to a newly defined superfamily of metalloenzymes that use S-adenosyl-L-methionine (AdoMet) as a precursor to a 5'-deoxyadenosyl radical (5'-dA•) [2, 12-14]. In each case, the role of the 5'-dA• is to abstract a hydrogen atom from a protein or small-molecule substrate, either generating a cofactor, or initiating a radical-dependent reaction that leads to the formation of the appropriate product [15]. Enzymes within this "Radical SAM" superfamily contain a conserved CXXXCXXC motif, wherein the noted cysteine amino acids coordinate a [4Fe–4S] cluster that is requisite for turnover. In its reduced state ($[4Fe–4S]^{+1}$), it supplies an electron that is necessary for cleavage of AdoMet, generating methionine as a byproduct in addition to the 5'-dA• [16-19]. A second cysteine-containing motif (CXEAXCXNXXEC) is present only in lipoyl synthases, and in analogy to biotin synthase–a related Radical SAM enzyme–is speculated to coordinate an additional iron–sulfur (FeS) cluster that functions as the sulfur donor in the reaction in some uncharacterized manner [20-23].

Radical SAM enzymes have been categorized into three classes [15]. In class I enzymes, AdoMet acts as a true cofactor; its cleavage is readily reversible, and one molecule can support multiple turnovers. In class II enzymes, AdoMet is cleaved irreversibly; however, the 5'-dA• simply abstracts a hydrogen atom from a conserved glycine amino acid on a cognate protein, creating a glycyl-radical cofactor that can support multiple turnovers. Lipoyl and biotin synthases have tentatively been assigned to

class III. These enzymes are believed to consume at least one equiv of AdoMet for each equiv of product that is produced. The stoichiometry of AdoMet usage has been addressed in the BioB reaction; however, conflicting conclusions were reached. Results of one study were consistent with a requirement of 2 equiv of AdoMet per equiv of biotin synthesized [24], while the results of a second study indicated that only one equiv of AdoMet was required to synthesize biotin [25]. Herein we describe, for the first time, experiments that address the stoichiometry of AdoMet usage by *E. coli* LipA, and conclude that irreversible cleavage of one AdoMet is required for *each* of the two hydrogen atoms that are removed from the substrate. Subsequently, synthesis of substrates that are specifically deuterated at positions C-6 and C-8 reveals that the first sulfur is installed at C-6.

3.3 Materials and Methods

Materials. Adenine, 5'-deoxyadenosine (5'-dA), DL-6,8-thioctic (DL-lipoic) acid, caprylic (*n*-octanoic) acid, porcine heart lipoamide dehydrogenase (LDH), sodium sulfide (nonahydrate), nicotinamide adenine dinucleotide (NAD^+), reduced nicotinamide adenine dinucleotide phosphate (NADPH), tris-(2-carboxyethyl)phosphine (TCEP), L-(+)-arabinose, ferric chloride, (trimethylsilyl) diazomethane (2M solution) were purchased from Sigma Corp (St. Louis, MO). [d_{15}, 98%]Octanoic acid was purchased from Cambridge Isotope Laboratories (Andover, MA). [8,8,8-d_3, 99.7%]Octanoic acid was purchased from CDN Isotopes (Pointe-Claire, Canada). Coomassie blue dye-binding

reagent, N-methyl-N-trimethylsilyltrifluoroacetamide (MSTFA) and bovine serum albumin (BSA) standard were purchased from Pierce (Rockford, IL).

Synthesis of 6,6-d_2-octanoic acid. The synthesis of 6,6-d_2-octanoic acid was achieved in two parts. [6-^{2}H]-6-hydroxyoctanoic acid was synthesized according to the methods of White except that 6-oxooctanoic acid was first converted to its methyl ester with methanol and sulfuric acid prior to sodium borodeuteride reduction [8]. The resulting racemic alcohol, methyl [6-^{2}H]-6-hydroxyoctanoate, was converted to 6,6-d_2-octanoic acid following the method of Dakoji *et al.* for the synthesis of [3-^{2}H] butanoic acid [26]. The chloroform layer from the Jones oxidation was rotovaped to give colorless oil. Thin layer chromatography (TLC) in 1:1 ethyl acetate/hexane showed a clean spot that ran with the same R_f as authentic octanoic acid. GC-MS analysis of the corresponding methyl ester gave rise to the parent ion M = 160 m/z and M-31 (-OMe) at 129 m/z. MS (ESI-) calculated for $C_8H_{13}D_2O_2$ (M-H) 145.21, found 145.31. The oil was dissolved in 50 mM HEPES pH 7.5 and added directly to the LplA reaction for the synthesis of 6,6-*d2*-octanoyl H-protein.

Synthesis of Acyl-H protein Substrates. The attachment of octanoic, [d_{15}]-octanoic, 8,8,8-d_3-octanoic, and 6,6-d_2-octanoic acids to the H protein of *E. coli* was performed enzymatically using *E. coli* LplA (lipoate protein ligase). Typical reactions were carried out in a total of 50 mL and contained: 50 mM HEPES pH = 7.5, 5 mM $MgCl_2$, 5 mM ATP, 500 μM substrate, 200 μM apo-H protein, and After completion of the reaction mixture was diluted in 20 mM potassium phosphate buffer pH = 7.2 and loaded onto a DE-52 column equilibrate in the same buffer. Subsequet to loading the column was washed with 250 mL of the same buffer containing 180 mM NaCl. The

product was eluted from the column using a 250 x 250 mL linear gradient that increased the NaCl concentration from 180 mM to 450 mM. Fractions containing protein were collected based on their absorbance at 280 nm. The pooled fractions were concentrated in an Amicon stirred cell to 1 mL using a 3,000 kDa molecular weight cut-off membrane. The protein was taken into the anaerobic chamber and exchanged into 50 mM HEPES, pH 5.7, 200 mM KCl, 10% glycerol by anaerobic gel-filtration chromatography (G-25). Aliquots of each protein were analyzed by reversed phase (C_{18}) HPLC to verify that they were homogeneous, and also by LC-MS to confirm the correct compound.

(S,S) S-adenosyl-L-methionine was synthesized using AdoMet synthetase (E.C. 2.5.1.6), and purified as described elsewhere (Iwig and Booker). *E. coli* lipoyl transferase (LplA) [27], and the H-protein of the *E. coli* GCS [4, 28] were cloned into the *Nde*I site of expression vector pET-28a, which causes the proteins to be expressed with an N-terminal 6X-histidine tag that is separated from the ATG start codon of each protein by a linker of 10 amino acids. *E. coli* genes for flavodoxin (Flv) [29] and flavodoxin reductase (Flx) [30] were cloned into the intein-based expression vector pTYB1 (New England Biolabs, Beverly, MA), and purified by affinity chromatography. The isolated proteins contained no amino acids that were not part of the natural gene sequence. Details of the cloning and purification of all of these proteins will be provided elsewhere [31].

UV-visible spectra were recorded using Cary 50 or Cary 300 spectrometers (Varian; Walnut Creek, CA) in combination with the associated WinUV software package. HPLC was carried out on an Agilent (Foster City, CA) 1100 HPLC System,

which included an autosampler and a variable wavelength detector. Data collection and analysis were performed with the associated ChemStation software package.

Expression of LipA. The *lipA* gene was amplified from *E. coli* genomic DNA (W3110) using polymerase chain reaction (PCR) technology, and cloned into expression vector pET-28a, producing plasmid pMGS10. Details of the actual cloning will be described elsewhere [31]. An overnight culture of *E. coli* BL21(DE3) containing plasmids pMGS10 and pDB1282 was used to inoculate 16 L of M9 minimal media [32] containing kanamycin (50 μg mL^{-1}) and ampicillin (100 μg mL^{-1}). The cultures, which were evenly distributed among four 6-L Erlenmeyer flasks, were allowed to grow at 37°C. At an optical density (660 nm; OD_{660}) of 0.3, solid L-(+)-arabinose was added to each flask at a final concentration of 0.05%. At an OD_{660} of 0.6, solid IPTG and ferric chloride were added to each flask at final concentrations of 200 μM and 50 μM, respectively. The cultures were allowed to incubate further at 37°C for 4 h, upon which they were cooled in an ice–water bath and harvested by centrifugation at 10,000xg for 10 min at 4°C. Typical yields were 50-60 g of frozen cell paste, which was stored in a liquid nitrogen dewar until ready for use.

Reconstitution of LipA. LipA was purified by immobilized metal affinity chromatography (IMAC) using a Ni-NTA solid support. All steps were carried out inside of an anaerobic chamber obtained from Coy Laboratory Products, Inc. (Grass Lake, MI) under an atmosphere of N_2 and H_2 (95% / 5%), wherein the O_2 concentration was maintained below 1 ppm via the use of palladium catalysts. Details of the purification will be described elsewhere [20]. Reconstitution of LipA with iron and sulfide was carried out in the anaerobic chamber using anaerobic buffers and solutions. A typical

reconstitution reaction contained in a final volume of 2 mL: 100 μM LipA and 8-fold molar excesses of $FeCl_3$ and Na_2S. LipA was initially treated with 5 mM DTT for 10 min on ice, followed by addition of $FeCl_3$. Finally, Na_2S was added drop wise over 10 min, and the mixture was allowed to stir gently on ice for an additional 4 h. The solution was placed in air-tight centrifuge tubes, removed from the anaerobic chamber, and centrifuged at 20,000xg for 20 min at 4°C to remove precipitate. The samples were brought back into the anaerobic chamber, and the supernatants were removed and exchanged into Buffer D (50 mM HEPES, pH 7.5, 100 mM KCl, 10% glycerol, and 10 mM $MgCl_2$) by gel-filtration.

Assay for 5'-dA and Lipoyl-H Protein (LHP). The time-dependent formation of 5'-dA and LHP was determined simultaneously using the same assay mixture. The assay contained in a final volume of 540 μL: 50 mM Na-Hepes, pH 7.5, 20 μM Flv, 5 μM Flx, 1 mM NADPH, 100 μM octanoyl-H protein (OHP), 700 μM AdoMet, 50 μM LipA, and 1 mM L-tryptophan. The reaction was initiated by addition of AdoMet subsequent to incubation of the other components of the assay mixture at 37°C for 5 min. For the quantification of 5'-dA, 25-μL aliquots of the assay mixture were removed at designated times and added to 25 μL of 2 N H_2SO_4 to quench the reaction. Precipitated proteins were pelleted by centrifugation, and a 10-μL aliquot of the supernatant was analyzed by reverse phase (C_{18}) HPLC. Solvent A consisted of 0.4% trifluoroacetic acid (TFA) titrated to pH 1.76 with triethylamine (TEA), while solvents B and C consisted of 100% acetonitrile and 100% methanol. The column was equilibrated in 95% solvent A–5% solvent C, and eluted for 5 min under the same conditions after sample injection. Over the following 10 min, solvent B was increased linearly to 50%, while solvent C was

increased to 30%. Under these conditions and a flow rate of 1 mL min^{-1}, AdoMet eluted at 3.1 min, adenine eluted at 4.5 min, 5'-dA eluted at 6.8 min, methylthioadenosine eluted at 11.1 min, and the tryptophan internal standard (IS) eluted at 12.9 min. The concentration of 5'-dA was then determined from a calibration curve of known concentrations of 5'-dA that was run under identical conditions, using the IS to correct for subtle volume changes between sample injections.

For the quantification of LHP, 100-μL aliquots were removed from the assay mixture and loaded directly onto Nick™ pre-poured gel-filtration columns (Amersham Biosciences; Piscataway, NJ) equilibrated in Buffer D, and eluted in a volume of 400 μL according to the manufacturer's specifications. Each assay was carried out at 22°C, and contained in final volume of 1.1 mL: 50 mM Na-HEPES, pH 7.5, 8 mM TCEP, 2 mM NAD^+, 0.9 μM LDH, and varying amounts of the Nick™ column eluate. Assays were initiated by addition of LDH subsequent to pre-incubation at 22°C, and were monitored by an increase in absorbance at 340 nm (ε_{340} = 6220 M^{-1} cm^{-1}). The concentration of LHP was then determined from a standard curve (0–5 μM) of known concentrations of LHP generated under identical conditions.

GC-MS analysis of 5'-dA. Assays were carried out as described above, except that [d_{15}-octanoyl]H-Protein was substituted for unlabeled substrate. The 5'-dA produced at each time point was isolated by HPLC as described above, and the solvent was removed in vacuo. Pyridine (50 μL) and MSTFA (100 μL) were added to the remaining pellet, and the mixture was heated at 100°C for 1 h. The resulting trimethylsilyl derivative of 5'-dA was injected onto a Hewlett Packard 5972 GC-MS without further purification. Separation of the derivatized products was carried out as described

previously [33] using a J&W DB-5 capillary column (30 m length x 0.25 mm bore x 0.25 μm film thickness).

3.4 Results

Expression and purification of LipA. *E. coli* LipA was cloned into a pET-28a expression vector, and co-transformed into *E. coli* BL21(DE3) along with plasmid pDB1282. Plasmid pDB1282 confers ampicillin resistance, and contains an *E. coli* operon that is involved in the biosynthesis of FeS clusters cloned behind an arabinose-inducible promoter. These genes include *iscS*, *iscU*, *iscA*, *hscB*, *hscA* and *fdx*. The *iscS* gene encodes a cysteine desulfurase, which activates the sulfur of L-cysteine for use in the formation of FeS clusters. The *iscU* and *iscA* genes are believed to encode proteins that serve as scaffolds for the construction of precursors to mature FeS clusters, while the *hscB* and *hscA* proteins encode molecular chaperones that are believed to facilitate incorporation of the FeS clusters into the apo-protein. Finally, the fdx gene encodes a ferrodoxin that is believed to be involved in maintaining electron balance during formation of the FeS cluster [34]. The co-expression of *E. coli* LipA under similar conditions has already been reported; the accessory proteins supported a greater yield of soluble protein, which also contained greater amounts of iron and sulfide [35]. We obtained very similar results, which are described in detail elsewhere [20].

LipA was purified under anaerobic conditions by IMAC. Amino acid analysis indicated that the Bradford reagent, using a commercially available BSA standard, overestimates the protein concentration by a factor of 1.45. This number is in agreement

with a previous assessment of the protein concentration [36], but differs a bit from a subsequently reported correction factor, wherein the assay was determined to overestimate the concentration of LipA by almost a factor of 2 [2, 36].

Assay of E. coli LipA. In vitro studies of LipA have been hampered by uncertainty in the identity of the substrates for the reaction. Recent studies indicate that the protein acts on octanoyl derivatives of the target lysine residue of lipoyl-accepting proteins [37, 38]. We employed the octanoyl derivative of the H-Protein of the *E. coli* GCS as our model substrate because of the ease in which its extent of lipoylation can be quantified. The assay is based on the ability of the lipoylated form of the H-Protein to mediate reduction of NAD^+ by dihydrolipoamide dehydrogenase at the expense of TCEP, which allows the extent of lipoylation to be determined spectrophotometrically by measuring the rate of NADH formation and comparing the value to a standard curve of graded concentrations of LHP [39]. Under the conditions described in Materials and Methods, the assay gives a linear response from 0–10 μM LHP.

The cleavage of AdoMet to generate a 5'-dA requires the input of one electron, which often can be satisfied by dithionite or 5-deazaflavin plus light. In the *E. coli* cell, the electron is supplied by NADPH via the flavodoxin / flavodoxin reductase reducing system. In the presence of the in vivo reducing system, 50 μM of reconstituted LipA catalyzed formation of 18 μM LHP after 20 min at 37°C, while the as-isolated protein catalyzed formation of 14 μM. In the absence of LipA, AdoMet, or NADPH, 3.4 μM, 5.21 μM, and 6 μM of LHP was detected, respectively. The product detected in the absence of LipA is attributed to small amounts of contaminating LHP in our OHP stock solution. The slight excess above background produced in the absence of AdoMet is

attributed to a fraction of the protein that is isolated with AdoMet bound, while the slight excess produced in the absence of NADPH is attributed to partially reduced forms of flavodoxin and flavodoxin reductase in the assay. Similar behavior with respect to AdoMet and NADPH has been observed previously in studies of LipA [2] and BioB [40], respectively. In all experiments, detected amounts of LHP that were not dependent on LipA were subtracted from the observed concentrations.

Stoichiometry of 5'-dA to LHP. In Figure 3.2, curves depicting the LipA-dependent formation of LHP (closed circles) and 5'-dA (open circles) are displayed as a function of time. Both processes can be fitted to a first-order kinetic equation, allowing extraction of rate constants of 0.175 ± 0.010 min^{-1} for formation of LHP (solid line) and 0.144 ± 0.005 min^{-1} for formation of 5'-dA (dashed line). The amplitudes of each fit reveal the maximum amount of product formed in each first-order process, indicating 50.5 μM 5'-dA, which corresponds to 1.01 equiv with respect to LipA, and 18.4 μM LHP, which corresponds to 0.378 equiv. The concentrations of LHP and 5'-dA formed at each time point are given in Table 2.1, the ratio of the two varying from 2.4 at early time points, to 2.7 at later time points. These ratios can be rationalized by a model in which 2 equiv of both AdoMet and LipA are required to synthesize LHP from OHP if a given fraction of 5'-dA results from non-productive cleavage of AdoMet. From this model, the maximum concentration of LHP that can be synthesized from 50 μM LipA is 25 μM, suggesting that only 74% of our LipA is configured to react productively upon cleavage of AdoMet. Using this constraint, as well as the assumption that the rate constant for productive cleavage of AdoMet must be as large as the rate constant for formation of LHP, the trace for total 5'-dA formation can be reconstructed from two simultaneous

first-order processes: one with an amplitude (A) of 37 μM 5'-dA and a rate constant (k) of 0.175 min^{-1}, and one with A = 13 μM 5'-dA and k = 0.092 min^{-1}. Table 3.1 and Figure 2.2 (closed triangles) show that the computed values for 5'-dA agree well with the observed values. The slower first-order rate constant that is actually observed for 5'-dA production (0.144 min^{-1}) results from fitting biphasic behavior to a single exponential.

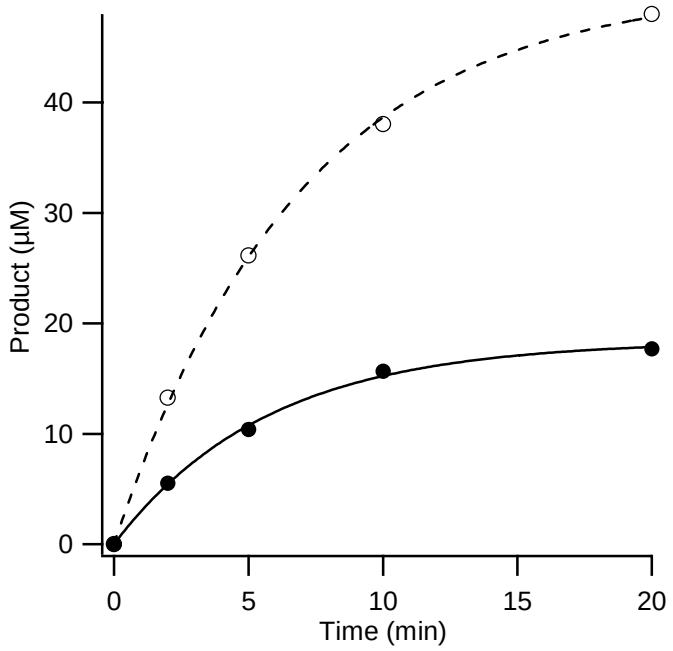

Figure 3.2: Time-dependent production of LHP (closed circles) and 5'-dA (open circles). The reaction was carried out as described in Materials and Methods, and contained 50 μM reconstituted LipA, 100 μM OHP, 20 μM Flv, 5 μM Flx, and 700 μM AdoMet. At each time point, the concentration of LHP that was attributed to contamination of the OHP substrate was subtracted from the observed concentration of LHP before plotting the value. Computed values of 5'-dA (closed triangles) were calculated by assuming two pathways for its formation, one in which k = 0.175 min^{-1} and A = 37 μM, and one in which k = 0.092 min^{-1} and A = 13 μM.

Table 3.1: Time-dependent Formation of 5'-dA and LHP[a]

Time (min)	5'-dA (μM) (Observed)	5'-dA (μM) (Computed)[b]	LHP (μM)	Ratio 5'-dA / LHP
0	0	0	0	–
2	13.2	13.1	5.54	2.38
5	26.1	26.4	10.4	2.51
10	38.0	38.4	15.7	2.42
20	48.0	46.8	17.7	2.71

[a]Data are from a single time course. [b]Derived from computing 5'-dA by assuming two independent processes: one with $k = 0.175$ min^{-1} and A = 37 μM, and one with $k = 0.092$ min^{-1} and $A = 13$ μM.

Direct hydrogen-atom abstraction by 5'-dA•. In order to show that the 5'-dA• acts directly on the substrate, [d_{15}-octanoyl]H-Protein was substituted for unlabeled substrate, and 5'-dA was isolated, derivatized, and analyzed for its deuterium content by GC-MS. We posited that if a single molecule of AdoMet mediates insertion of both sulfur atoms into the octanoyl group, an increase in two atomic mass units (amu) should be observed, since removal of hydrogen atoms from C-6 and C-8 are a prerequisite for sulfur insertion [7]. By contrast, if insertion of both sulfur atoms were mediated by two different AdoMet molecules, an increase in only one amu should be observed. The mass spectral fragmentation behavior of TMS derivatives of 5'-dA has been reported [33]; the relevant m/z value is 260, which corresponds to the sugar–after loss of the adenine base–

minus a proton. Chromatograms for four unique m/z values (260, 261, 262, and 263) were collected in single-ion monitoring mode for reactions containing both unlabeled and labeled substrates. The ratios of the m/z values for the unlabeled sample allowed correction for contamination from natural abundance isotopic distribution at each m/z value for the labeled sample.

In Table 3.2, the extent of deuterium incorporation into 5'-dA is displayed at several fixed times. Over the course of 60 min, a total of 38.6 μM 5'-dA was formed, which is noticeably lower than that obtained at 20 min in the presence of unlabeled substrate (48 μM). Also, at each time point, significant amounts of nondeuterated 5'-dA were observed, the fraction thereof increasing as a function of time; however, the dideuterated product was not detected. Because it was necessary to correct for contamination from natural abundance isotopic distribution, the limit of detection at m/z = 262 was ~2-3% of the magnitude of the base peak (m/z = 261). Unexpectedly, our assay did not detect significant amounts of LHP above the background level, suggesting that there is a significant isotope effect against removing a hydrogen atom from either C-6 or C-8. Curves depicting the time-dependent production of total 5'-dA (solid line), monodeuterated 5'-dA (dashed line), and unlabeled 5'-dA (dotted line) are shown in Figure 3.3. Fits of each curve to a first-order kinetic equation yield $k = 0.058 \pm 0.005$ and $A = 38.7 \pm 1.15$ for total 5'-dA, $k = 0.068 \pm 0.005$ and $A = 29.7 \pm 0.613$ for monodeuterated 5'-dA, and $k = 0.028 \pm 0.004$ and $A = 11.3 \pm 1.25$ for unlabeled 5'-dA.

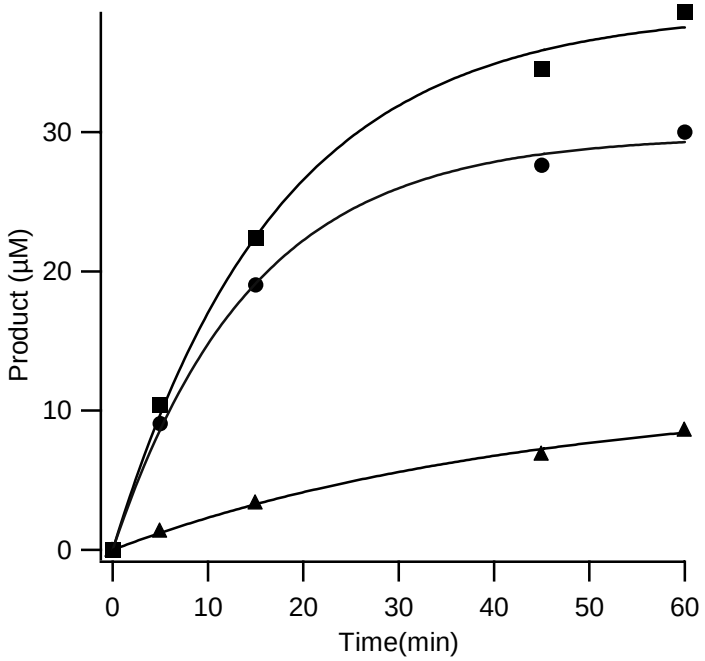

Figure 3.3: Time-dependent production of total 5'-dA (closed squares), monodeuterated 5'-dA, and unlabeled 5'-dA. The reaction was carried out as described in Materials and Methods, and contained 50 μM reconstituted LipA, 100 μM [octanoyl-d_{15}]H-Protein, 20 μM Flv, 5 μM Flx, and 700 μM AdoMet. At each time point, 5'-dA was isolated by HPLC, and its deuterium content was assessed by GC-MS after proper derivatization.

Table 3.2: Time-dependent Deuterium Incorporation into 5'-dA[a]

Time (min)	Total [5'-dA] (μM)	[5'-dA]-d_0 (μM)	[5'-dA]-d_1 (μM)	[5'-dA]-d_0 (% of Total)
0	0	–	–	–
5	10.45	1.38	9.07	13.2
15	22.42	3.40	19.0	15.2
45	34.53	6.92	27.61	20.0
60	38.63	8.63	30.0	22.3

[a]Data are from a single time course in the presence of [d_{15}-octanoyl]H-Protein. Only monodeuterated and unlabeled 5'-dA detected.

LC-MS Analysis of the LipA Reaction. LC-MS analysis of protein products was carried out to confirm that LHP indeed was not synthesized in the presence of OHP-d15. The mass spectrum of unlabeled OHP is shown in Figure 3.4A and displays a peak (1) with a molecular mass of 15971 Da, which is the molecular mass predicted by the amino acid composition of the H-protein plus the octanoyl moiety. After incubation of 100 μM OHP with 50 μM LipA at 37 °C for 60 min in the presence of other required components of the assay, a peak at a molecular mass of 16033 Da appears (3), which corresponds to the exact molecular mass of the H-protein plus an oxidized lipoyl group (Figure 3.4B). A shoulder is also apparent (2) and displays a molecular mass of 16003 Da, which is consistent with a thiooctanoyl group appended to the H-protein. This shoulder is not present in the OHP substrate. In the presence of OHP-d15, the peak at 15971 Da shifts 15

amu (Figure 3.4C) to 15986 Da, confirming that peak 1 is indeed OHP. However, no peak was observed at a molecular mass of 16046 Da, which would correspond to LHP-d13. The shoulder (2), however, has shifted to a molecular mass of 16016 Da, which is consistent with a monothiolated species. LC-MS was also carried out on V8-protease digests of the H-protein isolated from the reaction containing OHP-d15, which allows a more accurate determination of the mass and relative amounts of all octanoyl species because of the smaller size of the fragment subjected to analysis. The monothiolated species was confirmed and estimated to be ~15-20% of the starting substrate (data not shown).

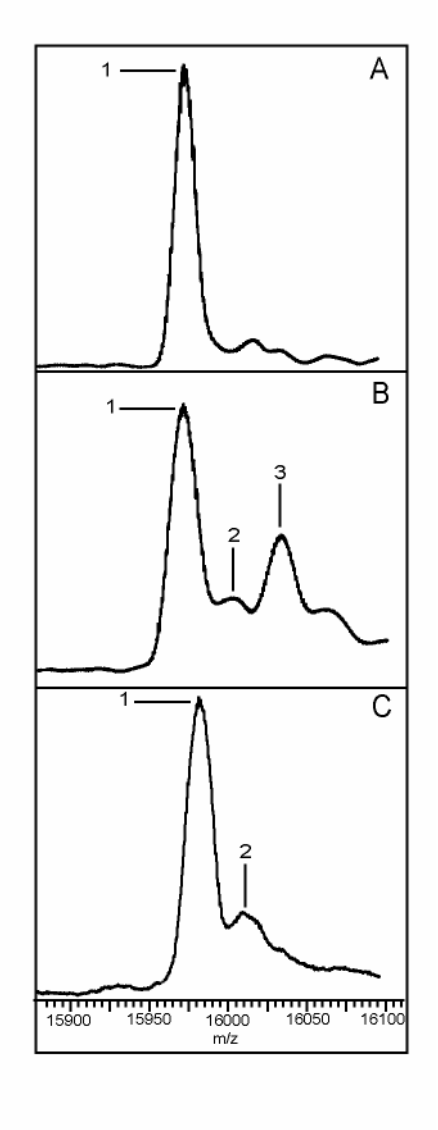

Figure 3.4: LC-MS Analysis of the Lipoyl Synthase Reaction

Turnover in the Presence of [d_{15}]-Octanoyl-H-Protein, 8,8,8-d_3-Octanoyl H-Protein, and 6,6-d_2-Octanoyl-H-Protein. Turnover in the presence of [d_{15}]-octanoyl-H-protein leads to a significant isotope effect on hydrogen atom abstraction at C-6 or C-8. To assess which C-D bond gives rise to the observed isotope effect we synthesized 8,8,8-d_3-octanoyl-H protein, and 6,6-d_2-octanoyl-H protein, and used them as substrates in the LipA reaction. Reactions with labeled substrates were carried out under conditions that were similar to those in which unlabeled octanoyl-H protein was employed, except that the reaction times were extended to 40 min. In the presence of the physiological reducing system and unlabeled octanoyl-H protein (Figure 3.5A, diamonds), the formation of 5'-dA is best fitted to a consecutive A→B→C reaction, affording rate constants of 0.250 ± 0.009 min^{-1} and 0.0903 ± 0.018 min^{-1} for the first and second phases, respectively. In the presence of [d_{15}]-octanoyl-H protein (Figure 3.5A, triangles), the same fit affords rate constants of 0.098 ± 0.003 min^{-1} and 0.081 ± 0.013 min^{-1}, and an overall amplitude that is roughly 1/2 of that obtained with unlabeled substrate. When 8,8,8-d_3-octanoyl-H protein is employed as substrate, the first phase (0.296 ± 0.068 min^{-1}) closely matches the first phase observed in the presence of unlabeled substrate; however, the rate constant for the second phase (0.0316 ± 0.0234 min^{-1}) is considerably smaller (Figure 3.5, circles). In addition, assay determinations for lipoyl-H protein found that none (< 1 μM) was produced, and very little 5'-dA was isolated that contained deuterium. These results indicate that deuterium abstraction from C-8 follows abstraction from C-6, and proceeds with the significant isotope effect. We postulate that the slow phase that is observed corresponds to abortive cleavage as is seen in Figure 3.3 (triangles). Last, when 6,6-d_2-octanoyl-H protein is used as substrate , the rate constant for the first phase (0.092 ±

0.0041 min^{-1}) closely matches that obtained in the presence of [d_{15}]-octanoyl-H protein, but the rate constant for the second phase (0.096 ± 0.018 min^{-1}) is three-fold greater, indicating that the first phase corresponds to hydrogen atom abstraction from C-6, while the second phase corresponds to hydrogen atom abstraction from C-8. We can also calculate an isotope effect for hydrogen abstraction from C-6 of ~2.7.

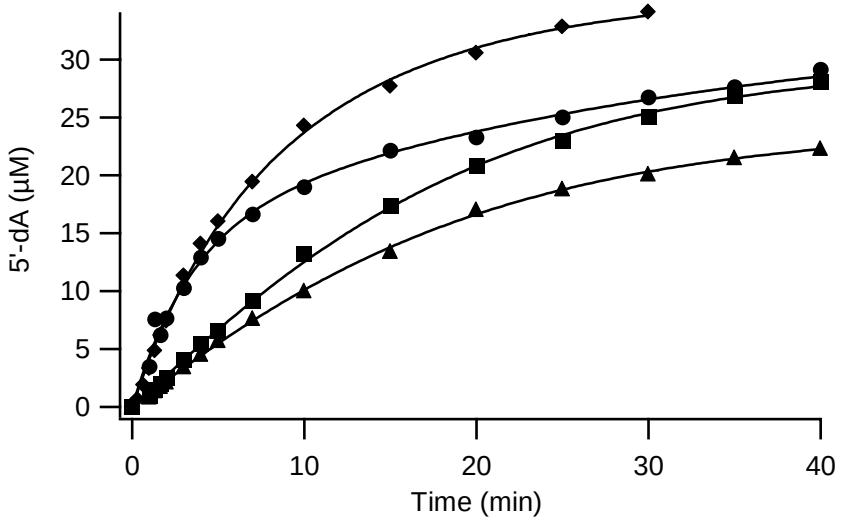

Figure 3.5: LipA-dependent 5'-dA formation from deuterated substrates. Reactions were run in the presence of the physiological reducing system (Flavodoxin/Flavodoxin Reductase/NADPH). Reactions were run in the presence of octanoyl-H protein (diamonds), 8,8,8-d_3-octanoyl-H protein (circles), d_{15}-octanoyl-H protein (triangles), and 6,6-d_2-octanoyl-H protein (squares)

3.5 Discussion

Lipoyl and biotin synthases belong to a unique subclass of Radical SAM enzymes in which the proteins, themselves, serve both as catalyst and substrate [41, 42]. Consequently, they are unable to catalyze multiple turnovers in the absence of a suitable system for regenerating the active sulfur donor. Indeed, BioB catalyzes no more than one

turnover, even after 4 h at 37°C [25, 40, 42], while LipA has been reported to catalyze formation of no more than 0.05 equiv of product after 15 min at 37°C [2]. Herein, we report that reconstituted LipA can catalyze formation of 0.38 equiv of LHP with an apparent first-order rate constant of 0.175 min^{-1} in the presence of the physiological reducing system. This rate constant, though slow, compares favorably with the rate constant (0.07 min^{-1}) for BioB-catalyzed sulfur insertion into dethiobiotin under similar conditions [40].

Stoichiometry of the Lipoyl Synthase Reaction. Clearly, the stoichiometry of 5'-dA to LHP at each time point is consistent with a model in which 2 equiv of AdoMet are required to synthesize one equiv of LHP from OHP. If only one AdoMet were used to synthesize LHP from OHP, it would be expected that a much larger fraction of the 5'-dA at each time point would be produced with a slower rate constant, since >50% would derive from abortive processes. In order to minimize nonproductive cleavage of AdoMet, our studies were carried out in the absence of DTT, and with the physiological reducing system. The observed stoichiometry is surprisingly similar to that obtained in one of the two studies that addressed the stoichiometry of AdoMet usage in the BioB reaction [24], and suggests that the abortive cleavage of AdoMet in each system might derive from some innate reactivity associated with this class of enzymes.

We had hoped to address the stoichiometry of AdoMet usage in the LipA reaction by simply counting the number of deuterium atoms in isolated 5'-dA when perdeuterated OHP is substituted for unlabeled OHP. Although no dideuterated 5'-dA was detected, which would support usage of 1 AdoMet per LHP synthesized from OHP; unexpectedly, LHP also was not detected. In vivo feeding studies in *E. coli* have shown that there is a

significant intramolecular isotope effect against removing tritium from [8-^{3}H]octanoic acid during the synthesis of lipoic acid, which might explain our failure to observe LHP in our in vitro assay. The effect of isotopic substitution at C-6 has not yet been addressed in a quantitative manner. Nevertheless, monodeuterated 5'-dA is indeed formed with a rate constant that is ≥ 0.06 min^{-1}, which is not insignificant when compared to the rate constant for LHP formation in the presence of unlabeled substrate. Abstraction of this deuterium from substrate is either unrelated to LHP formation, or represents a slower pathway to LHP formation. We prefer the latter hypothesis since it has been shown that [U-^{2}H]octanoic acid can be converted into lipoic acid in vivo [6, 38]. If this rate constant corresponds to sulfur insertion at C-6, then its magnitude would be $\geq$0.06 min^{-1} in the presence of unlabeled substrate.

Sulfur Insertion at C-6 Precedes that of C-8. We had hoped to address the stoichiometry of AdoMet usage in the LipA reaction by simply counting the number of deuterium atoms in isolated 5'-dA when perdeuterated OHP is substituted for unlabeled OHP. Although no dideuterated 5'-dA was detected, which would support usage of one AdoMet per LHP synthesized from OHP; unexpectedly, LHP also was not detected. A closer analysis of the maximum amount of 5'-dA-d_1 produced (30 μM) indicates that it is a little greater than one-half of that produced in the presence of unlabeled substrate (50 μM), suggesting that a hydrogen atom is removed from either C-6 or C-8 but not from both carbons. *In vivo* feeding studies have shown that there is a significant intramolecular isotope effect involving abstraction of a tritium atom from [8-^{3}H]-octanoic acid during the synthesis of lipoic acid, which implies the C-8 C-D bond as the one that is difficult to cleave. To address which C-D bond displays the large isotope effect on

cleavage, we synthesized 8,8,8-d_3-octanoyl-H protein and 6,6-d_2-octanoyl-H protein and used them as substrates in the LipA reaction along with [d_{15}]-octanoyl-H protein. In each instance the production of 5'-dA as a function of time can be fitted satisfactorily only to a sequential (A→B→C) reaction, in which hydrogen atom abstraction at C-6 must precede hydrogen atom abstraction at C-8. Fits to parallel processes, wherein the probability of hydrogen atom abstraction at C-6 or C-8 is dependent upon the associated relevant rate constants, do not adequately reproduce the rate constants obtained from one substrate to another. The observation that in presence of 8,8,8-d_3-octanoyl-H protein the rate constant for the first phase of 5'-dA production is almost identical to the rate constant observed for the first phase in the presence of OHP, suggests that the first phase involves removal of the hydrogen atom from C-6. The observed isotope effect of 2.7 on the first phase, when using 6,6-d_2-octanoyl-H protein as the substrate, further substantiates this assignment.

The kinetics of 5'-dA formation in the presence of labeled substrates also uncovers another interesting aspect of the reaction; the productive cleavage of AdoMet is coupled to hydrogen atom abstraction from the substrate. This is best demonstrated in the presence of 6,6-d_2-octanoyl-H protein as the substrate, which affords an isotope effect of 2.7 on the first phase of 5'-dA production. Similar kinetic coupling has been observed in enzymes that employ adenosylcobalamin (coenzyme-B_{12}) in catalysis, another cofactor that serves as a precursor to an obligate 5'-dA• intermediate. In coenzyme-B_{12}-dependent reactions, the 5'-dA• is generated upon simple homolysis of the Co-C-5' bond, also producing cob(II)alamin, which has distinct UV-visible features, and which is EPR active. In glutamate mutase, isotope effects of 28 and 25 are observed on cob(II)alamin formation in the presence of the substrates, deuterated L-glutamate and deuterated L-

threo-3-methylaspartate, respectively [43]. Substitution of [CD_3]-methylmalonyl-CoA for unlabeled substrate resulted in an isotope effect of >20 on formation of Co-C bond in the reaction catalyzed by methylmalonyl-CoA mutase, while in ethanolamine ammonia lyase the isotope effect on cob(II)alamin formation is ≥10 when using [1,1-^{2}H]-ethanolamine as the substrate, and ~3 when using [1,1-$^2H_2$]-S-2-aminopropanol as the substrate [44]. In each system, the isotope effect on Co-C cleavage arises from an unfavorable equilibrium between the intact cofactor and the products of homolysis, which does not allow detectable amounts of hydrogen-abstracting species to accumulate. As the 5'-dA• is depleted by hydrogen atom abstraction from the substrate, additional cob(II)alamin is formed during the re-establishment of equilibrium conditions.

In LipA, several unfavorable steps precede generation of 5'-dA. Formation of the reduced Fe-S cluster is unfavorable, since no reduced cluster is ever observed in the presence of flavodoxin/flavodoxin reductase reducing system. In addition, the one-electron reduction of AdoMet is believed to be unfavorable, as is cleavage of AdoMet to generate the 5'-dA•. Since substrate radicals have not yet been observed in either BioB or LipA, their generation is either not sufficiently favorable thermodynamically, or their generation is concerted with, or highly coupled to, sulfur insertion. This observed kinetic coupling in a radical SAM enzyme further showcases the similarities between nature's only known cofactors that function to generate 5'-deoxyadenosyl radicals.

3.6 References

1. Hayden, M.A., I.Y. Huang, G. Iliopoulos, M. Orozco, and G.W. Ashley, Biosynthesis of Lipoic Acid: Characterization of the Lipoic Acid Auxotrophs *Escherichia coli* W1485-lip2 and JRG33-lip9. *Biochemistry*, 1993. **32**: p. 3778-3782.
2. Miller, J.R., R.W. Busby, S.W. Jordan, J. Cheek, T.F. Henshaw, G.W. Ashley, J.B. Broderick, J.E. Cronan Jr., and M.A. Marletta, *Escherichia coli* LipA Is a Lipoyl Synthase: In Vitro Biosynthesis of Lipoylated Pyruvate Dehydrogenase Complex from Octanoyl-Acyl Carrier Protein. *Biochemistry*, 2000. **39**: p. 15166-15178.
3. Reed, L.J. and M.L. Hackert, Structure-function relationships in dihydrolipoamide acyltransferases. *J Biol Chem*, 1990. **265**(16): p. 8971-8974.
4. Vanden Boom, T.J., K.E. Reed, and J. J. E. Cronan, Lipoic Acid Metabolism in *Escherichia coli*: Isolation of Null Mutants Defective in Lipoic Acid Biosynthesis, Molecular Cloning and Characterization of the *E. coli lip* Locus, and Identification of the Lipoylated Protein of the Glycine Cleavage System. *J Bacteriol*, 1991. **173**(20): p. 6411-6420.
5. Parry, R.J., Biosynthesis of Some Sulfur-Containing Natural Products. Investigations of the Mechanism of Carbon-Sulfur bond Formation. *Tetrahedron*, 1983. **39**: p. 1215-1238.

6. White, R.H., Stable Isotope Studies on the Biosynthesis of Lipoic Acid in *Escherichia coli*. *Biochemistry*, 1980. **19**: p. 15-19.

7. Parry, R.J., Biosynthesis of Lipoic Acid. 1. Incorporation of Specifically Tritiated Octanoic Acid into Lipoic Acid. *J Am Chem Soc*, 1977. **99**(19): p. 6464-6466.

8. White, R.H., Biosynthesis of Lipoic Acid: Extent of Incorporation of Deuterated Hydroxy- and Thiooctanoic Acids into Lipoic Acid. *J Am Chem Soc*, 1980. **102**: p. 6605-6607.

9. Frappier, F., G. Guillerm, A.G. Salib, and A. Marquet, On the Mechanism of Conversion of Dethiobiotin to Biotin in Escherichia coli. Discussion of the Occurrence of an Intermediate Hydroxylation. *Biochem Biophys Res Commun*, 1979. **91**(2): p. 521-527.

10. Trainor, D.A., R.J. Parry, and A. Gitterman, Biotin Biosynthesis. 2. Stereochemistry of Sulfur Introduction at C-4 of Dethiobiotin. *J Am Chem Soc*, 1980. **102**(4): p. 1467-1468.

11. Marquet, A., F. Frappier, G. Guillerm, M. Azoulay, D. Florentin, and J.-C. Tabet, Biotin Biosynthesis: Synthesis and Biological Evaluation of the Putative Intermediate Thiols. *J Am Chem Soc*, 1993. **115**: p. 2139-2145.

12. Hayden, M.A., I. Huang, D.E. Bussiere, and G.W. Ashley, The Biosynthesis of Lipoic Acid: Cloning of lip, a Lipoate Biosynthetic Locus of *Escherichia coli*. *J Biol Chem*, 1992. **267**(14): p. 9512-9515.

13. Reed, K.E. and J. J. E. Cronan, Lipoic Acid Metabolism in *Escherichia coli*: Sequencing and Functional Characterization of the *lipA* and *lipB* Genes. *J Bacteriol*, 1993. **175**(5): p. 1325-1336.

14. Sofia, H.J., G. Chen, B.G. Hetzler, J.F. Reyes-Spindola, and N.E. Miller, Radical SAM, a novel protein superfamily linking unresolved steps in familiar biosynthetic pathways with radical mechanisms: functional characterization using new analysis and information visualization methods. *Nucleic Acids Res*, 2001. **29**(5): p. 1097-1106.

15. Frey, P.A. and S.J. Booker, Radical Mechanisms of S-adenosylmethionine-Dependent Enzymes. *Adv Protein Chem*, 2001. **58**: p. 1-45.

16. Henshaw, T.F., J. Cheek, and J.B. Broderick, The $[4Fe\text{-}4S]^{+1}$ Cluster of Pyruvate Formate-Lyase Activating Enzyme Generates the Glycyl Radical on Pyruvate Formate-Lyase: EPR-Detected Single Turnover. *J Am Chem Soc*, 2000. **122**: p. 8331-8332.

17. Lieder, K.W., S. Booker, F.J. Ruzicka, H. Beinert, G.H. Reed, and P.A. Frey, S-Adenosylmethionine-Dependent Reduction of Lysine 2,3-Aminomutase and Observation of the Catalytically Functional Iron-Sulfur Centers by Electron Paramagnetic Resonance. *Biochemistry*, 1998. **37**(8): p. 2578-2585.

18. Ollagnier-de-Choudens, S., Y. Sanakis, K.S. Hewitson, P. Roach, E. Münck, and M. Fontecave, Reductive Cleavage of S-Adenosylmethionine by Biotin Synthase from *Escherichia coli. Biochemistry*, 2002. **277**(16): p. 13449-13454.

19. Ollagnier, S., E. Mulliez, P.P. Schmidt, R. Eliasson, J. Gaillard, C. Deronzier, T. Bergman, A. Gräslund, P. Reichard, and M. Fontecave, Activation of the Anaerobic Ribonucleotide Reductase from *Escherichia coli*. The Essential role of the Iron-Sulfur Center for S-adenosylmethionine Reduction. *J Biol Chem*, 1997. **272**(39): p. 24216-24223.

20. Cicchillo, R.M., K.-H. Lee, C. Baleanu-Gogonea, N.M. Nesbitt, C. Krebs, and S.J. Booker, Escherichia coli lipoyl synthase binds two distinct [4Fe–4S] clusters per polypeptide. *Biochemistry*, 2004. **43**: p. 11770-11781.

21. Berkovitch, F., Y. Nicolet, J.T. Wan, J.T. Jarrett, and C.L. Drennan, Crystal Structure of Biotin Synthase, an S-Adenosylmethionine-Dependent Radical Enzyme. *Science*, 2004. **303**: p. 76-79.

22. Ugulava, N.B., B.R. Gibney, and J.T. Jarrett, Biotin Synthase Contains Two Distinct Iron–Sulfur Binding Sites: Chemical and Spectroelectrochemical Analysis of Iron–Sulfur Cluster Interconversions. *Biochemistry*, 2001. **40**: p. 8343-8351.

23. Tse Sum Bui, B., B. Florentin, F. Fournier, O. Ploux, A. Méjean, and A. Marquet, Biotin Synthase Mechanism: On the Origin of Sulphur. *FEBS Lett*, 1998. **440**: p. 226-230.

24. Guianvarc'h, D., D. Florentin, B.T.S. Bui, F. Nunzi, and A. Marquet, Biotin synthase, a New Member of the Family of Enzymes Which Uses S-Adenosylmethionine as a Source of Deoxyadenosyl Radical. *Biochem Biophys Res Commun*, 1997. **236**: p. 402-406.

25. Ollagnier-de Choudens, S., E. Mulliez, and M. Fontecave, The PLP-dependent biotin synthase from *Escherichia coli*: mechanistic studies. *FEBS Lett*, 2002. **532**: p. 465-468.

26. Dakoji, S., I. Shin, K.P. Battaile, J. Vockley, and H.W. Liu, Redesigning the active-site of an acyl-CoA dehydrogenase: new evidence supporting a one-base mechanism. *Bioorg Med Chem*, 1997. **5**(12): p. 2157-64.

27. Morris, T.W., K.E. Reed, and J.E. Cronan Jr., Identification of the Gene Encoding Lipoate-Protein Ligase of *Escherichia coli.* Molecular Cloning and Characterization of the *lplA* Gene and Gene Product. *J Biol Chem*, 1994. **269**: p. 16091-16100.

28. Okamura-Ikeda, K., Y. Ohmura, K. Fukiwara, and Y. Motokawa, Cloning and nucleotide sequence of the gcv operon encoding the *Escherichia coli* glycine-cleavage system. *Eur J Biochem*, 1993. **216**(2): p. 539-548.

29. Osborne, C., L.-M. Chen, and R.G. Matthews, Isolation, Cloning, Mapping, and Nucleotide Sequencing of the Gene Encoding Flavodoxin in *Escherichia coli. J Bacteriol*, 1991. **173**(5): p. 1729-1737.

30. Bianchi, V., P. Reichard, R. Eliasson, E. Pontis, M. Krook, H. Jörnvall, and E. Haggard-Ljungquist, *Escherichia coli* Ferredoxin $NADP^+$ Reductase: Activation of *E. coli* Anaerobic Ribonucleotide Reduction, Cloning of the Gene (*fpr*), and Overexpression of the Protein. *J Bacteriol*, 1993. **175**(6): p. 1590-1595.

31. Cicchillo, R.M., N.M. Nesbitt, C. Gogonea, and S.J. Booker, Characterization of *Escherichia coli* Lipoyl Synthase. *In preparation*, 2004.

32. Sambrook, J., E.F. Fritsch, and T. Maniatis, *Molecular Cloning: A Laboratory Manual*. 2nd ed, ed. M. Ferguson. Vol. 3. 1989, Plainview, New York: Cold Spring Harbor Laboratory Press.

33. Reimer, M.L.J., T.D. McClure, and K.H. Schram, Differentiation of Isomeric 2'-, 3'- and 5'-Deoxynucleosides by Electron Ionization and Chemical Ionization-linked Scanning Mass Spectrometry. *Biomed Env Mass Spectrom*, 1989. **18**: p. 533-542.

34. Frazzon, J., J.R. Fick, and D.R. Dean, Biosynthesis of iron–sulphur clusters is a complex and highly conserved process. *Biochem Soc Trans*, 2002. **30**(4): p. 680-685.

35. Kriek, M., L. Peters, Y. Takahashi, and P.L. Roach, Effect of iron–sulfur cluster assembly proteins on the expresssion of *Escherichia coli* lipoic acid synthase. *Protein Expr Purif*, 2003. **28**: p. 241-245.

36. Busby, R.W., J.P.M. Schelvis, D.S. Yu, G.T. Babcock, and M.A. Marletta, Lipoic Acid Biosynthesis: LipA Is an Iron Sulfur Protein. *J Am Chem Soc*, 1999. **121**(19): p. 4706-4707.

37. Booker, S.J., Unvraveling the Pathway of Lipoic Acid Biosynthesis. *Chem Biol*, 2004. **11**: p. 10-12.

38. Zhao, S., J.R. Miller, Y. Jiang, M.A. Marletta, and J.E. Cronan Jr., Assembly of the Covalent Linkage Between Lipoic Acid and Its Cognate enzymes. *Chem Biol*, 2003. **10**: p. 1293-1302.

39. Gueguen, V., D. Macherel, M. Neuburger, C. Saint Pierre, M. Jaquinod, P. Gans, R. Douce, and J. Bourguignon, Structural and Functional Characterization of H Protein Mutants of the Glycine Decarboxylase Complex. *J Biol Chem*, 1999. **274**(37): p. 26344-26352.

40. Ugulava, N.B., C.J. Sacanell, and J.T. Jarrett, Spectroscopic Changes during a Single Turnover of Biotin Synthase: Destruction of a [2Fe–2S] Cluster Accompanies Sulfur Insertion. *Biochemistry*, 2001. **40**: p. 8352-8358.

41. Fontecave, M., S. Ollagnier-de Choudens, and E. Mulliez, Biological Radical Sulfur Insertion Reactions. *Chem Rev*, 2003. **103**(6): p. 2149-2166.

42. Marquet, A., Enzymology of carbon-sulfur bond formation. *Curr Opin Chem Biol*, 2001. **5**: p. 541-549.

43. Marsh, E.N. and D.P. Ballou, Coupling of cobalt-carbon bond homolysis and hydrogen atom abstraction in adenosylcobalamin-dependent glutamate mutase. *Biochemistry*, 1998. **37**(34): p. 11864-72.

44. Bandarian, V. and G.H. Reed, Isotope effects in the transient phases of the reaction catalyzed by ethanolamine ammonia-lyase: determination of the number of exchangeable hydrogens in the enzyme-cofactor complex. *Biochemistry*, 2000. **39**(39): p. 12069-75.

Chapter 4

Mechanistic Investigations of Lipoic Acid Biosynthesis in *Escherichia coli*

This Chapter was reproduced with slight modifications from Cicchillo, R. M.; Booker, S. J., (2005) Mechanistic Investigations of Lipoic Acid Biosynthesis in *Escherichia coli*: Both Sulfur Atoms in Lipoic Acid are Contributed by the Same Lipoyl Synthase Polypeptide. *J. Am. Chem. Soc.*; (Communication); 2005; 127(9); 2860-2861.

4.1 Abstract

It has been proposed that during catalysis by lipoyl synthase (LipA) the 5'-dA• abstracts hydrogen atoms from C-6 and C-8 of the octanoyl chain, allowing for subsequent sulfur insertion by a mechanism involving carbon-centered radicals [1-3]. We have demonstrated that the formation of one lipoyl cofactor requires the cleavage of two molecules of SAM, consistent with two rounds of hydrogen atom abstraction. Subsequent labeling of the substrate with deuterium resulted in the formation of deuterated 5'-dA, implicating the 5'-dA• in catalysis [2]. We have also established, using various spectroscopic and analytical techniques, that formation of the observed product requires the presence of two 4Fe-4S clusters [4]. One of the 4Fe-4S clusters is bound in a CX_3CX_2C motif that is common to all radical SAM proteins, while the second cluster is found in a CX_4CX_5C motif that is conserved among lipoyl synthases. Although the

cofactor content and reaction stoichiometry have been addressed, the mechanism of sulfur insertion remains enigmatic. Herein we demonstrate that like BioB, LipA serves as a catalyst and a substrate *in vitro*. LipA produced in *E. coli* that is cultured in media containing $Na_2{}^{34}S$ as the sole sulfur source catalyzed the formation of ^{34}S-lipoic acid in an in vitro assay that lacks other potential sulfur donors, indicating that the sulfurs are derived from the protein itself. In in vitro assays containing approximately stoichiometric concentrations of ^{34}S-LipA and ^{32}S-LipA the majority of the lipoic acid formed contained two sulfur atoms of the same isotopic composition (either ^{34}S-^{34}S or ^{32}S-^{32}S), indicating that both sulfurs are derived from one LipA polypeptide. This finding implies that freely dissociating monothiolated species are not intermediates in lipoic acid biosynthesis. We therefore evaluated the ability of 8-mercaptooctanoyl-H protein and 6(RS)-mercaptooctanoyl-H protein to serve as substrates for LipA *in vitro*. Although the formation of the lipoyl product could not be detected, 5'-dA was observed, suggesting that the monothiolated species do bind to the enzyme. This binding was confirmed by EPR spectroscopy, which revealed slight perturbations of the signal contributed by the $[4Fe–4S]^{+}$ cluster upon incubation with the substrates. We subsequently provide preliminary evidence that suggests that the *in vivo* formation of the lipoyl cofactor from 6- or 8–mercaptooctanoic acid is not catalyzed by LipA, but by another protein with similar substrate specificity—presumably BioB.

4.2 Introduction

Lipoyl synthase (LipA) catalyzes the final step in the *de novo* biosynthesis of the lipoyl cofactor, which is the insertion of two sulfur atoms into positions C-8 and C-6 of protein-bound octanoyl groups (Figure 4.1) [5, 6]. Genetic and recent biochemical studies indicate that the enzyme is a member of a newly characterized superfamily of metalloproteins that utilize a $[4Fe–4S]^{+}$ cluster to reductively fragment S-adenosyl-L-methionine (SAM) into L-methionine and a 5'-deoxyadenosyl radical (5'-dA•) [1, 7-9]. This high-energy radical then initiates catalysis by abstracting a key hydrogen atom from the appropriate position on a small-molecule substrate, or creates a stable glycyl radical cofactor cofactor by abstracting a hydrogen atom from the α-carbon of a glycine residue on a cognate protein [10]. In the LipA reaction, the octanoyl acyl chain substrate is attached covalently in an amide linkage to a conserved lysine residue on the protein that is to bear the lipoyl cofactor, indicating that the cofactor is constructed "on site" [2, 6]. In *Escherichia coli*, three proteins are known to house the lipoyl cofactor: the H protein of the glycine cleavage system, and the E2 subunits of the pyruvate and α-ketoglutarate dehydrogenase complexes [11].

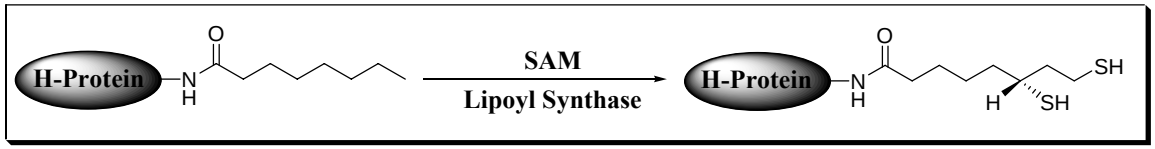

Figure 4.1: Reaction catalyzed by Lipoyl Synthase

Recent studies have provided strong evidence that the active form of LipA contains two [4Fe–4S] clusters per polypeptide. One of the clusters is coordinated by

cysteines residing in the CX_3CX_2C motif that is common to all radical SAM enzymes, while the other cluster is coordinated by cysteines residing in a CX_4CX_5C motif, which is found only among lipoyl synthases [4]. The presence of two distinct iron–sulfur clusters on LipA is reminiscent of biotin synthase (BioB), in which the active form of the enzyme is proposed to contain a [2Fe–2S] cluster in addition to the [4Fe–4S] cluster that interacts with SAM [12]. The reaction mechanisms of the two enzymes are presumably similar, given the similarities in reaction type and primary structures (32% sequence similarity) [7]; although, BioB catalyzes the insertion of only one sulfur atom–between C-6 and C-9 of dethiobiotin–while LipA catalyzes the insertion of two sulfur atoms into the octanoyl chain. Although there is not yet conclusive evidence that the additional cluster provides the sulfur in each enzyme system, it is tempting to speculate that the different configurations of the additional cluster somehow relate to the number of sulfur atoms that are mobilized during catalysis.

Prior to the cloning of the *lipA* gene and establishment of its protein product as a member of the radical SAM superfamily, a general understanding of how the cofactor was constructed with respect to bond-making and bond-breaking events was limited. Elegant *in vivo* feeding studies from several laboratories did, however, illuminate certain important aspects of the chemistry. It was clear that the cofactor is constructed upon an intact eight-carbon fatty acid backbone, since [1-^{14}C]-octanoic acid could serve as a precursor to lipoic acid [13, 14]. In addition, feeding of various specifically tritiated forms of octanoic acid to *E. coli* followed by isolation of lipoic acid demonstrated that the only hydrogens that are removed during sulfur insertion are the ones that are replaced by the sulfur atoms, and that at C-6, which is prochiral, the 6 *pro-R* hydrogen is removed

[15]. The additional finding that sulfur is inserted at C-6 with inversion of configuration led to the suggestion that lipoic acid formation might take place *via* intermediate hydroxylation. Hydroxylation at C-6 with retention of configuration, followed by activation of the hydroxyl group and displacement with the appropriate sulfur nucleophile by an S_N2 mechanism would readily explain the observed inversion of configuration. However, further isotopic studies showed that [6(RS)-$^2H_1$]-6-hydroxy-, [8-$^2H_2$]-8-hydroxy-, and [8-$^2H_2$]-(±)-6,8-dihydroxyoctanoic acids were not converted to lipoic acid *in vivo* [15, 16]. By contrast, when [6(RS)-$^2H_1$]-6-mercaptooctanoic and [8-$^2H_2$]-8-mercaptooctanoic acids were administered, lipoic acid was produced, suggesting that monothiolated species are formed in the reaction [16]. The study revealed that [8-$^2H_2$]-8-mercaptooctanoic acid was incorporated ~10-times more efficiently than [6(RS)-$^2H_1$]-6-mercaptooctanoic acid. This observation suggested that sulfur insertion at C-8 may precede insertion at C-6.

The ability of 6-mercaptooctanoic acid or 8-mercaptooctanoic acid to serve as *in vivo* precursors to lipoic acid was also evaluated using two *E. coli* mutants, W1485-lip2 and JRG33-lip9, which are auxotrophic for lipoic acid [17]. Neither W1485-*lip2* nor JRG33-lip9 was able to grow in media containing 6-mercaptooctanoic acid or octanoic acid. By contrast, W1485-*lip2* was able to grow on 8-mercaptooctanoic acid, while growth by JRG33-*lip9* was 20-fold less efficient in the presence of the same compound. These results, in combination with the stable isotope studies, suggested that LipA is responsible for the insertion of both sulfur atoms into octanoic acid and that sulfur insertion at C-8 may precede insertion at C-6 [17].

Similar studies have been performed on BioB, an enzyme that also catalyzes the formation of C-S bonds. Feeding studies with isotopically labeled precursors showed that biotin formation proceeds without desaturation or intermediate hydroxylation, and that removal of the *pro-S* hydrogen from C-6 proceeds with retention of stereochemistry [15, 18]. Interestingly, 9-mercaptodethiobiotin promoted the formation of biotin in *Bacillus sphaericus* resting cells, while (6R)-6-mercaptodethiobiotin and (6S)-6-mercaptodethiobiotin did not [19]. Use of 9-[^{34}S]- or 9-[^{35}S]-mercaptodethiobiotin led to the production of biotin that retained 80% of the starting heavy isotopes, suggesting that 9-mercaptodethiobiotin is a potential intermediate along the biotin biosynthetic pathway [19]. Some evidence for the formation of the monothiolated intermediate emerged from isotopic feeding studies using lavender cells that were supplemented with $Na_2{}^{35}SO_4$ [20]. A compound that was chromatographically similar to 9-mercaptodethiobiotin was isolated from the cells and contained radioactivity. Reintroduction of the compound into cells that lacked $Na_2{}^{35}SO_4$ led to the formation of [^{35}S]-biotin. In contrast to lavender cells, the putative monothiolated intermediate was not released into culture in bacterial systems, suggesting that it is not freely dissociating and may remain bound to the enzyme [19, 21]. Recent studies in a well defined *in vitro* system have shown that purified BioB can transform 9-mercaptodethiobiotin into biotin with a similar rate to that of dethiobiotin [22]. Collectively, *in vivo* studies on the biosynthesis of biotin and lipoic acid support mechanisms in which monothiolated intermediates are formed during the reactions.

As previously mentioned, BioB and LipA each bind an additional Fe-S cluster. Biotin synthase binds a 2Fe-2S cluster through three conserved cysteine residues and one conserved arginine residue [23]. The amino acids involved in ligating the 2Fe-2S cluster

are not arranged in any particular compact motif. By contrast, LipA binds a second 4Fe-4S cluster in a CX_4CX_5C motif that is conserved among lipoyl synthases. The role of the additional cluster in LipA has not been established.

Seminal *in vitro* studies indicated that cysteine and SAM were not the immediate source of sulfur in biotin, but for the first time implicated the enzyme itself as the sulfur donor [24, 25]. Subsequent studies revealed that reconstitution of the 4Fe-4S cluster in BioB with Fe, $Na_2{}^{34}S$, and a reductant led to the incorporation of the heavy sulfur isotope into biotin [26]. The authors speculated that the sulfur incorporated into biotin may have been derived from the reconstituted Fe-S cluster. Similar studies, supporting this model, showed that BioB isolated from cultures grown in the presence of ^{35}S-cysteine and ^{35}S-sulfide could catalyze the formation of ^{35}S-biotin [27].

Multiple biochemical and spectroscopic studies have also suggested that the sulfur incorporated into the thiophane ring of biotin may be derived from an Fe-S cluster [28, 29]. UV-visible and Mössbauer spectroscopies have shown that the 2Fe-2S cluster is degraded during the time course of the reaction [12, 30, 31]. Recently, resonance Raman spectroscopy was used to verify the presence of a 2Fe-2Se cluster on BioB, which was generated by reconstitution of the enzyme with sodium selenide. This form of the enzyme catalyzed the production of Se-biotin, supporting the use of the 2Fe-2S cluster as an "S" donor [32].

In this study we provide direct evidence that the sulfur atoms in lipoic acid are derived from the protein itself and that both sulfurs are mobilized from one LipA polypeptide. In contrast to early *in vivo* studies, we demonstrate that protein-bound monothiolated intermediates are not kinetically competent precursors for the construction

of the lipoyl cofactor. While not conclusive, we posit that BioB may be responsible for the observed *in vivo* conversion of 8-mercaptooctanoic into lipoic acid. In addition, preliminary *in vitro* studies suggest that BioB-mediated formation of 5'-dA (hydrogen atom abstraction) from 8-mercaptooctanoic acid occurs with similar rate constants to those of dethiobiotin.

4.3 Materials and Methods

Materials. All DNA modifying enzymes and reagents were purchased from New England Biolabs (Beverly, MA), as was Vent polymerase and its associated 10X reaction buffer. Oligonucleotide primers for cloning were obtained from Integrated DNA Technologies (Coralville, IA) or Invitrogen Life Technologies (Carlsbad, CA). Both the Bradford reagent for protein concentration determination and the bovine serum albumin (BSA) standard (2 mg mL^{-1}) were obtained from Pierce (Rockford, IL). *E. coli* genomic DNA (strain W3110) was obtained from Sigma Corp (St. Louis, MO). All other buffers and common chemicals were reagent grade or better. $Na_2{}^{34}S$ was prepared from elemental ^{34}S-sulfur (99%) obtained from Trace Sciences International (Richmond Hill, ON, Canada), using a modification of a previously published procedure [33]. Synthesized $Na_2{}^{34}S$ was analyzed by ICP-MS, which revealed the following isotopic distribution: 0.99% ^{32}S, 1.2% ^{33}S, and 98% ^{34}S. 2-Ethylcyclohexanone was purchased from ChemSampCo (Trenton, New Jersey). 8-Mercaptooctanoic acid (99%) was obtained from Dojindo Laboratories (Kumamoto, Japan). Biotin and dethiobiotin were purchased from Sigma-Aldrich (St. Louis, MO).

Procedures. Routine UV-visible spectra were recorded using Cary 50 or Cary 300 spectrometers (Varian; Walnut Creek, CA) in combination with the associated Win UV software package. Low-temperature X-band EPR spectroscopy was performed in perpendicular mode using a Bruker (Billerica, MA) ESP-300 instrument that contained an ER 041 MR microwave bridge and an ST4102 X-band resonator. An ITC503S temperature controller and an ESR900 liquid helium cryostat, both from Oxford Instruments (Concord, MA), were used to maintain sample temperature. Spin quantification was conducted by integrating the sample spectrum twice, and then comparing its intensity to the intensity of a doubly-integrated spectrum of a 1 mM $CuSO_4$/10 mM EDTA standard that was obtained under identical conditions. General spectral manipulations were carried out using the program IGOR Pro (Wavemetrics; Lake Oswego, OR) on a desktop computer.

Mössbauer spectra were recorded on spectrometers from WEB research (Edina, MN) operating in the constant acceleration mode in a transmission geometry. Spectra were recorded with the temperature of the sample maintained at 4.2 K. For low-field spectra, the sample was kept inside an SVT-400 dewar from Janis (Wilmington, MA), and a magnetic field of 40 mT was applied parallel to the γ-beam. For high-field spectra, the sample was kept inside a 12SVT dewar (Janis), which houses a superconducting magnet that allows for application of variable magnetic fields between 0 and 8 T parallel to the γ-beam. The quoted isomer shifts are relative to the centroid of the spectrum of a metallic foil of α-Fe at room temperature. Data analysis was performed using the program WMOSS from WEB research.

Preparation of Mössbauer and EPR Samples. Samples to be analyzed by Mössbauer and EPR spectroscopies were prepared inside of the anaerobic chamber, and contained 200-500 μM LipA or BioB. Samples (300 μL final volume) to be analyzed by Mössbauer spectroscopy were frozen with liquid nitrogen inside of small plastic cups. For characterization by EPR, the samples (250 μL final volume) were first treated with 2 mM sodium dithionite at ambient temperature for ~2 min, placed in EPR tubes (2 mm i.d.), and frozen in liquid nitrogen. All steps associated with preparing the samples were conducted inside of a Coy Laboratory Products (Grass Lake, MI) anaerobic chamber.

Recombinant DNA Procedures. The polymerase chain reaction was performed with a Robocycler (Stratagene) temperature cycler. Each amplification reaction contained in a volume of 50 μL: 0.2 μM of each primer, 250 μM of each deoxynucleoside triphosphate, 1 μg of *E. coli* genomic DNA, 1 U of Vent polymerase, and 5 μL of 10X Vent polymerase buffer. After a 5 min denaturation step at 95°C, 35 cycles of the following program were initiated: 1 min at 95 °C, 1 min at 55 °C, and 2.5 min at 72 °C. The reaction was subsequently incubated at 72 ^{o}C for 10 min. All other procedures were carried out by standard methods [34]. DNA sequencing was carried out at the Pennsylvania State University Nucleic Acid Facility.

Cloning of Escherichia coli Biotin Synthase. The *bioB* gene was amplified from *E. coli* (strain W3110) genomic DNA by PCR using primers bioB forward (5'-ACA AGC CAT ATG GCT CAC CGC CCA CGC TGG ACA TTG TCG C-3') and bioB reverse (5'-ACT GGA ATT CTC ATA ATG CTG CCG CGT TGT AAT ATT CGT CGG-3'). Primer bioB forward contained an *Nde*I restriction site and the first 28 bases of the *bioB* gene. Primer bioB reverse contained an *Eco*RI restriction site and the last 32 bases of the

bioB gene, including the stop codon. After PCR amplification, the 1041 bp fragment was purified and digested with *Nde*I and *EcoR*I, and inserted into plasmid pET28a (incorporates a 6 x His-tag at the N-terminus) that had been similarly digested. The identity and integrity of the *bioB* gene was verified by DNA-sequencing.

Large-scale Expression of the E. coli lipA Gene, and Production of LipA. An overnight culture of *E. coli* BL21(DE3) containing plasmids pMGS10 and pDB1282 was used to inoculate 16 L of M9 minimal media [34] containing kanamycin (50 μg mL^{-1}) and ampicillin (100 μg mL^{-1}). The cultures, which were evenly distributed among four 6-L Erlenmeyer flasks, were allowed to grow at 37°C. At an optical density (660 nm; OD_{660}) of 0.3, solid L-(+)-arabinose was added to each flask at a final concentration of 0.05%. At an OD_{660} of 0.6, solid IPTG and ferric chloride were added to each flask at final concentrations of 200 μM and 50 μM, respectively. The cultures were allowed to incubate further at 37°C for 4 h, upon which they were cooled in an ice–water bath and harvested by centrifugation at 10,000 xg for 10 min at 4°C. Typical yields were 50-60 g of frozen cell paste, which was stored in a liquid nitrogen dewar until ready for use.

Production of LipA for sulfur incorporation studies was carried out in a modified minimal medium, in which $Na_2{}^{34}S$ or Na_2S (1.35 mM final concentration) was substituted for $MgSO_4$, and $MgCl_2$ was used as the source of magnesium. LipA was then purified according to previously described procedures [2].

Expression of the bioB Gene, and Production and Isolation of BioB. The *E. coli* *bioB* gene was co-expressed with plasmid pDB1282 in ^{57}Fe-containing M9 minimal media as described previously [2]. Plasmid pDB1282 carries an *A. vinelandii* operon that encodes genes known to participate in the biosynthesis of Fe/S clusters. These genes are

iscS, *iscU*, *iscA*, *hscA*, *hscB*, and *fdx* [35-37], and are cloned behind an arabinose inducible promoter. Plasmid pDB1282 confers ampicillin resistance, while the pET-28a plasmid into which the *bioB* gene was cloned confers resistance to kanamycin. BioB was purified by immobilized metal affinity chromatography (IMAC) using a Ni-NTA solid support. All steps were carried out inside of an anaerobic chamber obtained from Coy Laboratory Products, Inc. (Grass Lake, MI) under an atmosphere of N_2 and H_2 (95% / 5%), wherein the O_2 concentration was maintained below 1 ppm via the use of palladium catalysts. Frozen cell paste (30 g) was taken into the anaerobic chamber and suspended at ambient temperature in 100 mL of lysis buffer (50 mM EPPS, pH 8, 500 mM KCl, 10 mM β-mercaptoethanol (BME), and 10 mM imidazole). Lysozyme was then added to a final concentration of 1 mg/mL and the solution was allowed to stir for 20 min. The solution was then cooled to 0^{o}C and the cells were disrupted *via* 4 x 1 minute bursts using a sonicator located within the anaerobic chamber. The lysed cells were placed in sealed tubes and subjected to centrifugation for 1 hour at 50,000 xg at 4^{o}C. After pelleting, the solution was taken back into the anerobic chamber, and the cell-free extract was loaded onto a Ni-NTA column that had been equilibrated in lysis buffer. The column was washed with 100 mL of wash buffer containing 50 mM EPPS, pH 8, 500 mM KCl, 10 mM BME, and 20 mM imidazole. The protein was clearly visible on the column as a dark brown band, which arises from the Fe-S clusters. Elution buffer (50 mM EPPS, pH 8, 500 mM KCl, 10 mM BME, 250 mM imidazole) was added until no brown color remained on the column. The protein was concentrated anaerobically to 2 mL using an Amicon stirred cell that was equipped with a 10 kDa molecular weight cut-off membrane. Imidazole was removed by gel filtration of the protein into 50 mM HEPES pH 7.5,

containing 100 mM KCl, 20% glycerol, and 10 mM dithiothreitol (DTT). The dark brown fraction was divided into 300 μL aliquots and stored in a liquid N_2 dewar. The concentration of BioB was determined by the Bradford protein assay and was subsequently corrected to account for a 10% overestimation as determined by Jarrett co-workers [38].

BioB Activity Determination. The BioB-dependent formation of 5'-dA was determined similarly to that described for LipA [2]. The reaction mixture contained in a final volume of 200 μL: 50 mM Na-HEPES, pH 7.5, 25 μM flavodoxin, 10 μM flavodoxin oxidoreductase, 1 mM NADPH, 200 μM 8-mercaptooctanoic acid or dethiobiotin, 700 μM AdoMet, 50 μM BioB, and 1 mM L-tryptophan. The reaction was incubated at 37°C for 3 min, and turnover was initiated by addition of SAM. Aliquots (25 μL) of the assay mixture were removed at designated times and added to 25 μL of 2 N H_2SO_4 to quench the reaction. Precipitated proteins were pelleted by centrifugation at 10,000 xg, and a 10-μL aliquot of the supernatant was analyzed by reverse phase (C_{18}) HPLC.

Synthesis of $Na_2{}^{34}S$. The synthesis of $Na_2{}^{34}S$ was achieved by a slight modifications to a published procedure [33], and all steps were conducted under a constant flow of nitrogen. A two-neck 250 mL round bottom flask, equipped with a magnetic stir bar, was cooled to -78 °C in a dry ice-acetone bath. Elemental ^{34}S-sulfur (0.5 g) was added to the cooled flask and ammonia gas was passed through the attached Dewar condenser until 75 mL of liquid ammonia accumulated. A two-fold molar excess of sodium metal was added slowly and the reaction was allowed to stir for 30 minutes. The solution was then removed from the dry ice-acetone bath and allowed to warm to

room temperature. The ammonia was evaporated under a stream of nitrogen gas to yield a white precipitate. Isopropanol was then added to quench the excess sodium metal (until blue color dissipates); this was followed by addition of 15 mL of water, which dissolves the resulting white precipitate. The solutions were removed *in vacuo* to yield a white precipitate (NaOH and $Na_2{}^{34}S$). The precipitate was dissolved in a minimal amount of water and the concentration was determined by the method of Beinert [39].

Synthesis of 6-(R,S)-Mercaptooctanoic acid. 6-(*R,S*)-Mercaptooctanoic acid was synthesized from 6-(*R,S*)-hydroxyoctanoic acid by a modification of a previously described procedure [40]. First, 7-ethyloxepanone was synthesized via a Baeyer-Villager oxidation of 2-ethylcyclohexanone as previously described [41]. The purified product (1g, 0.007 mol) was then stirred overnight in 14 mL of 1 M NaOH at 70°C. After acidification with concentrated HCl, the reaction mixture was extracted four times with 20 mL of diethyl ether, and the organic layers were pooled and dried over $MgSO_4$. Upon removal of solvent, the product (6-hydroxyoctanoic acid) appeared as a yellow oil (87% yield), and migrated as one spot by TLC (3:1 hexane/ethyl acetate). The authenticity of the compound was verified by mass spectrometry and ^{1}H and ^{13}C NMR. 6-Hydroxyoctanoic acid (0.98 g, 0.0061 mol) was refluxed with thiourea (0.46 g, 0.0061 mol) and 57% HI in water (2.3 g, 0.0183 mol) for 9 hours. The resulting isothiouronium salt was hydrolyzed to the thiol by addition of 7.3 mL of 2.5 M NaOH with subsequent refluxing for 2 h. The solution was cooled to room temperature and acidified with concentrated HCl. The acidified solution was extracted three times with 20 mL of diethyl ether, and the organic layer was dried over $MgSO_4$. Solvent was removed *in vacuo*, and

the final product was confirmed by ^{1}H NMR and LC-MS ESI^{-} (calculated 176.28, observed 175.0).

Attachment of 6-(R,S)-Mercaptooctanoic and 8-Mercaptooctanoic acids to E. coli H protein. The attachment of 6-(R,S)-mercaptooctanoic and 8-mercaptooctanoic acids to the H protein of *E. coli* was performed enzymatically using *E. coli* LplA as previously described [2]. After completion of the reaction the proteins were exchanged into 50 mM HEPES buffer, pH 7.5, containing 200 mM KCl, and 10% glycerol, by anaerobic gel-filtration chromatography (G-25). Aliquots of each protein were analyzed by reverse phase (C_{18}) HPLC to verify that they were homogeneous; verification of the correct modification was conducted by LC-MS after removal of the modification from the H protein by treatment with lipoamidase.

Characterization of Substrate Binding to Wild-type LipA by EPR Spectroscopy. Samples to be analyzed by EPR spectroscopy were prepared inside of the anaerobic chamber and contained 50 mM HEPES, pH 7.5, 300 μM LipA, 600 μM octanoyl-H protein, 6-(R,S)-mercaptooctanoyl-H protein, or 8-mercaptooctanoyl-H protein, and 600 μM SAM. Samples were treated with 2 mM sodium dithionite at ambient temperature before loading into EPR tubes and freezing in liquid N_2.

GC-MS Analysis of LipA Reactions. Reactions were carried out in a final volume of 2.5 mL as described previously, but contained 0.53 μmol of [^{32}S]- or [^{34}S]-LipA and 0.1 μmol octanoyl-H protein. When reactions contained both [^{32}S]- and [^{34}S]-LipA, each was present at 0.16 μmol. Reactions were incubated at 37 °C for 30 min and then acidified by addition of concentrated HCl to a final concentration of 6.4 M. The acidified solutions were autoclaved for 2 h at 121 °C to liberate lipoic acid from the H-protein, and

then extracted four times with equal volumes of benzene. The benzene extracts were concentrated to 0.5 mL by rotary evaporation, and 1 mL aliquots of (trimethylsilyl)diazomethane (2 M solution in hexanes) and methanol were added to form lipoic acid methyl esters (LAMEs). Derivatizations to form lipoic acid methyl esters (LAMEs) were carried out at room temperature and were typically complete within 30 min. The solution was evaporated to ~50 μL and injected directly onto a Shimadzu QP5000 GC-MS. Sample introduction was *via* splitless injection onto an XTI-5 column (30 m x 0.25 μm; Restek Corporation) and the injection temperature was 250 °C. The initial column temperature was 50 °C, and was held for 1 min after injection before increasing to 180 °C at 15 °C min^{-1}. The temperature was subsequently increased to 275 °C at 5 °C min^{-1}.

4.4 Results

GC-MS Analysis of Lipoic Acid Derived from Reactions Catalyzed by Isotopically Labeled LipA. To show conclusively that the sulfur atoms incorporated into lipoic acid are derived from LipA itself, LipA was produced from *E. coli* grown in minimal medium that contained either $Na_2{}^{32}S$ or $Na_2{}^{34}S$ as the sole sulfur source. Bacterial growth was monitored at 600 nm and the observed doubling times were approximately 45 min to one hour; by contrast, the doubling time of this strain of *E. coli* grown in LB medium under identical conditions was approximately 30 min. Expression of the *lipA* gene as well as the genes harbored by plasmid pDB1282 was carried out as previously described.

Reactions were carried out as described in Materials and Methods, and unnecessary sulfur-containing compounds such as DTT were omitted from the reaction mixture to limit the presence of alternative sources of sulfur. The only other sources of sulfur in the reaction were the HEPES buffer, a sulfonic acid that is quite stable and not physiologically relevant, and SAM, which is known to breakdown only to 5'-dA and L-methionine in this class of enzymes. In contrast to typical LipA assays, the concentration of LipA in these reactions was five-fold greater than that of octanoyl-H protein to ensure adequate conversion of octanoyl-H protein to lipoyl-H protein for GC-MS analysis.

The analysis of oxidized lipoic acid methyl ester (LAME) by GC-MS has previously been described [42]. The relative intensities of the parent ion (m/z = 220), which is approximately 40% of the base peak (m/z = 85), were used to analyze LipA-dependent incorporation of ^{32}S or ^{34}S sulfur into LA by single ion monitoring (SIM) analysis after derivatization with (trimethylsilyl)diazomethane. In Figure 4.2A, the mass spectrum of LAME synthesized from LipA containing natural abundance sulfur is displayed from m/z values of 219 to 228. It is virtually identical to that of commercially available LipA derivatized in the same manner (data not shown). As expected, the base peak corresponds to m/z = 220, and the peaks at m/z values of 221 and 222 (12.2 and 9.01 percent of the base peak, respectively) represent the contribution of ^{13}C and ^{33}S to the M+1 peak, and ^{34}S to the M+2 peak of LAME. In Figure 4B, the mass spectrum of LAME synthesized from [^{34}S]-containing LipA is displayed. The base peak corresponds to m/z = 224, indicating insertion of two ^{34}S atoms, and clearly supporting the premise that the sulfur atoms in LA derive directly from LipA itself. The peak intensities at m/z values of 220, 222, 225, and 226 are higher than what would be expected as a result of

contributions by other relevant isotopes of sulfur (^{32}S and ^{33}S) and carbon (^{13}C). In particular the peak at m/z = 225 is approximately twice the intensity predicted based on other isotopic contributions. We attribute this to adventitious contamination, which appears significant because of the low concentrations of metabolites analyzed. In Figure 4C, the mass spectrum of LAME synthesized from equimolar concentrations of [^{32}S]-LipA and [^{34}S]-LipA is displayed. The two most prominent peaks exhibit m/z values of 220 and 224, indicating that most of the LAME synthesized by LipA contains two sulfur atoms of identical isotope. Again, the peak at m/z = 222 is more intense than what would be expected from analysis of plots in Figures 4A and 4B (observed 19.4% of base peak; calculated 10.9% of base peak). This may reflect a small fraction of liberated monothiolated species that are converted to the intact cofactor at another active site, or it may arise from adventitious contamination. Although, studies presented in this work demonstrate that monothiolated intermediates are not kinetically competent in the formation of the lipoyl cofactor. Additionally, if the Fe-S cluster is indeed serving as the source of sulfur, it is conceivable that sulfide is liberated under turnover conditions. This sulfide could then exchange with bridging sulfides of another Fe-S center in a separate active site, which might be catalyzed by the lipoyl group that is produced during turnover. Subsequent sulfur insertion could then lead to the formation of lipoic acid containing ^{32}S-^{34}S which would increase the intensity of the ion at 222 m/z. The peaks at m/z = 225 and 226 correspond to the predicted intensities after correcting for the contribution by ^{13}C to the product. Ideally, the peaks at m/z = 220 and 224 should be of equal intensity. The deviation most likely reflects a difference in the activity of the two proteins or a slight contamination at m/z = 224. Clearly, however, the ratio of the peaks

at m/z values of 220, 222, and 224, is far from the 1:2:1, respectively, expected for a mechanism in which the monothiolated species are obligatorily released, and are consistent with a mechanism in which both sulfurs must derive from the same polypeptide. A similar result might also arise from a mechanism in which sulfurs derive from different LipA polypeptides that form kinetically stable dimers. However, molecular sieve chromatographic studies conducted under anaerobic conditions indicate that LipA is primarily monomeric (Chapter 5, Figure 5.11).

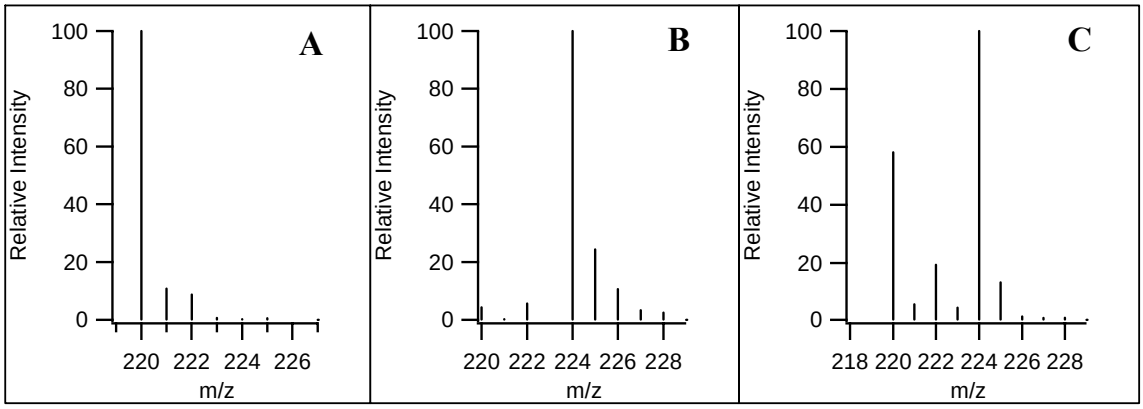

Figure 4.2: Analysis of the lipoyl synthase reaction by GC-MS. Each reaction contained in addition to 0.1 µmol of octanoyl-H Protein, 0.53 µmol of ^{32}S-labeled LipA (Panel A), 0.53 µmol of ^{34}S-labeled LipA (Panel B), or a mixture of ^{32}S-(0.16 µmol) and ^{34}S-labeled (0.16 µmol) lipoyl synthases (Panel C). The reaction conditions and subsequent work-up are described in the Materials and Methods.

Spectroscopic Perturbations of Wild-Type LipA in the Presence of Putative Monothiolated Intermediates. EPR spectroscopy has been used as a qualitative tool to monitor the binding of substrates directly to or in the vicinity of the Fe-S clusters of LipA. To ascertain whether 8-mercaptooctanoyl-H protein or 6-(R,S)-mercaptooctanoyl-H protein bind to LipA, each of the proteins was incubated anaerobically with dithionite-

reduced LipA in the presence or absence of SAM. The corresponding EPR spectra are shown in Figure 4.3. As detailed in Chapter 2, the EPR spectrum of dithionite reduced LipA in the absence of substrates is broad and pseudoaxial, and displays a g-tensor that is approximated by the principal values $g_{\parallel}$ = 2.03 and $g_{\perp}$ = 1.93, consistent with the presence of $[4Fe\text{-}4S]^{+}$ clusters (Figure 4.3A, dashed line). As described in Chapter 5, when LipA is reduced in the presence of SAM alone or octanoyl-H protein alone, the EPR spectrum remains largely unchanged. By contrast, when LipA is reduced in the presence of both SAM and octanoyl-H protein, the corresponding EPR spectrum changes dramatically, which is manifested primarily in a shift of $g_{crossover}$ from 1.92 to 1.88 (Figure 4.3A, red line). Upon reduction of LipA in the presence of SAM and 8-mercaptooctanoyl-H protein (Figure 4.3B, red line) or 6-(R,S)-mercaptooctanoyl-H protein (Figure 4.3C, red line) the corresponding spectra do not exhibit shifts that are as dramatic as that seen in the presence of octanoyl-H protein and SAM (Figures 4.3B and 4.3C, black lines), but they do sharpen significantly, which is consistent with relief of g-strain by reducing conformational flexibility. It is tempting to speculate that the changes observed by EPR derive from a direct interaction between SAM and the Fe/S cluster that is liganded in the radical SAM motif, and that this interaction requires the presence of the substrate, octanoyl-H protein. Consistent with this hypothesis, cleavage of SAM to L-methionine and a 5'-dA• requires the presence of substrate; it does not occur with SAM alone, even in the presence of dithionite. As will be detailed below, both 8-mercaptooctanoyl- and 6-mercaptooctanoyl-H proteins trigger formation of 5'-dA, although their effects on the EPR spectrum of reduced LipA are not as dramatic. It must

be stated, however, that the rate constants for 5'-dA formation are two to three-fold lower in the presence of these putative substrates.

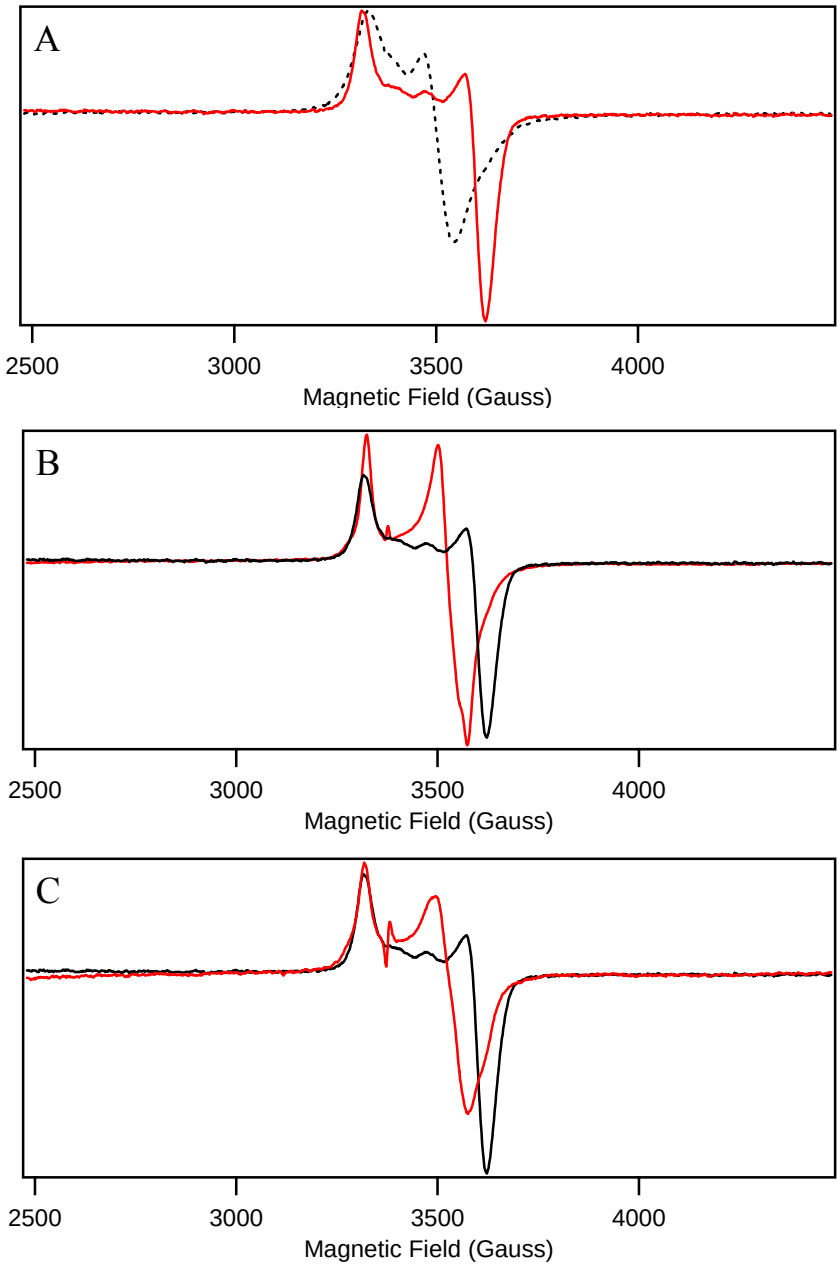

Figure 4.3: Effect of putative monothiolated substrates on the EPR spectrum of LipA. As-isolated wild-type LipA (panel A, dashed line), LipA in the presence of 8-mercaptooctanoyl-H protein (panel B, red line), LipA in the presence of 6-(R,S)-mercaptooctanoyl-H protein (panel C, red line). All samples contained substrates and SAM in a two-fold molar excess over enzyme. Panels B and C also have LipA with octanoyl-H protein and SAM overlaid for comparative purposes (black line).

Activity Determination of Wild-Type LipA in the Presence of Putative Monothiolated Intermediates. The ability of wild-type LipA to catalyze cleavage of SAM and synthesis of lipoyl-H protein was assessed using 8-mercaptooctanoyl-H protein and 6-(R,S)-mercaptooctanoyl-H protein as substrates. As shown in Figure 4.4, both substrates induce time-dependent formation of 5'-dA. The data were fitted to a first-order kinetic process, which allowed for the determination of amplitudes and rate constants. In the presence of 6-(R,S)-mercaptooctanoyl-H protein (dashed line), 5'-dA was formed with a rate constant and amplitude of 0.068 ± 0.002 min^{-1} and 43.775 ± 0.685 μM, respectively. A rate constant of 0.046 ± 0.005 min^{-1} and amplitude of 43.652 ± 3.73 μM were obtained when 8-mercaptooctanoyl-H protein was used as the substrate (solid line). Interestingly, lipoyl-H protein was not observed with either substrate using the lipoamide dehydrogenase assay, which only detects the intact cofactor. In contrast, when octanoyl-H protein was used as the substrate rate constants of 0.14 min^{-1} for 5'-dA and 0.18 min^{-1} for lipoyl-H protein were observed. It is unknown whether other species are generated in the reaction, which might arise from sulfur insertion at other positions of the octanoyl chain.

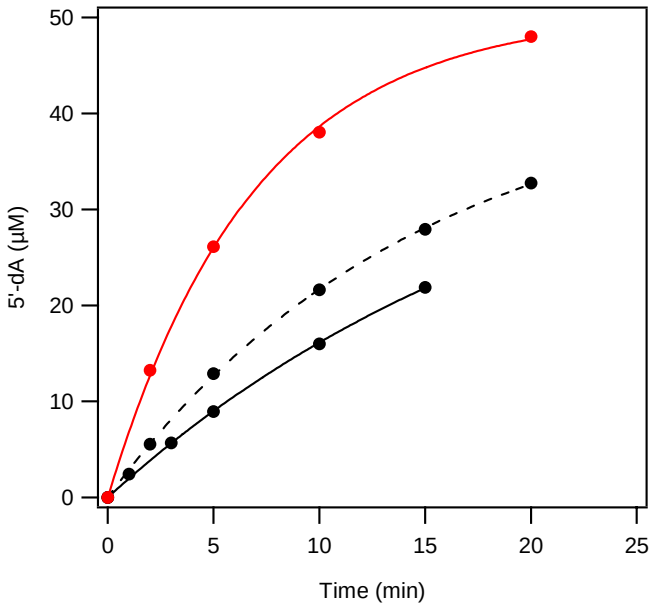

Figure 4.4: Kinetics of 5'-dA formation in the presence of 8-mercaptooctanoyl-H protein (solid line), 6-(R,S)-mercaptooctanoyl-H protein (dashed line), and octanoyl-H protein (red line).

Isolation and Characterization of BioB from E. coli. The *E. colibioB* gene was cloned into plasmid pET-28a such that upon its expression the protein produced would contain an N-terminal hexahistidine tag that is separated from the start codon by a spacer of 10 amino acids. This construct is similar, if not identical, to those that are currently used by others who study BioB [43]. In an attempt to optimize cluster incorporation the *bioB* gene was coexpressed with genes on plasmid pDB1282, which encodes proteins that are involved in Fe/S cluster biogenesis in *Azotobacter vinelandii*. In one *in vivo* Mössbauer study on *E. coli* cells that overproduce BioB, the majority of the protein was found to contain only a 2Fe-2S cluster [44], while in another study the protein was found to contain mixtures of 2Fe-2S and 4Fe-4S clusters both in vivo and in crude lysate [45]. To date, most, if not all, in vitro studies on BioB have been conducted on protein that was purified under aerobic conditions, and then reconstituted to contain a 2Fe-2S cluster and a

4Fe-4S cluster (references). In this study BioB was purified anaerobically using a procedure that is similar to that for the purification of LipA. The purified enzyme was dark brown in color, and its UV-visible spectrum (Figure 4.5A)displayed a broad peak at 460 nm and a shoulder at 330 nm (arrows). These features are similar to those that have been published for anaerobically reconstituted BioB that contains one 2Fe-2S cluster and one 4Fe-4S cluster [38, 46].

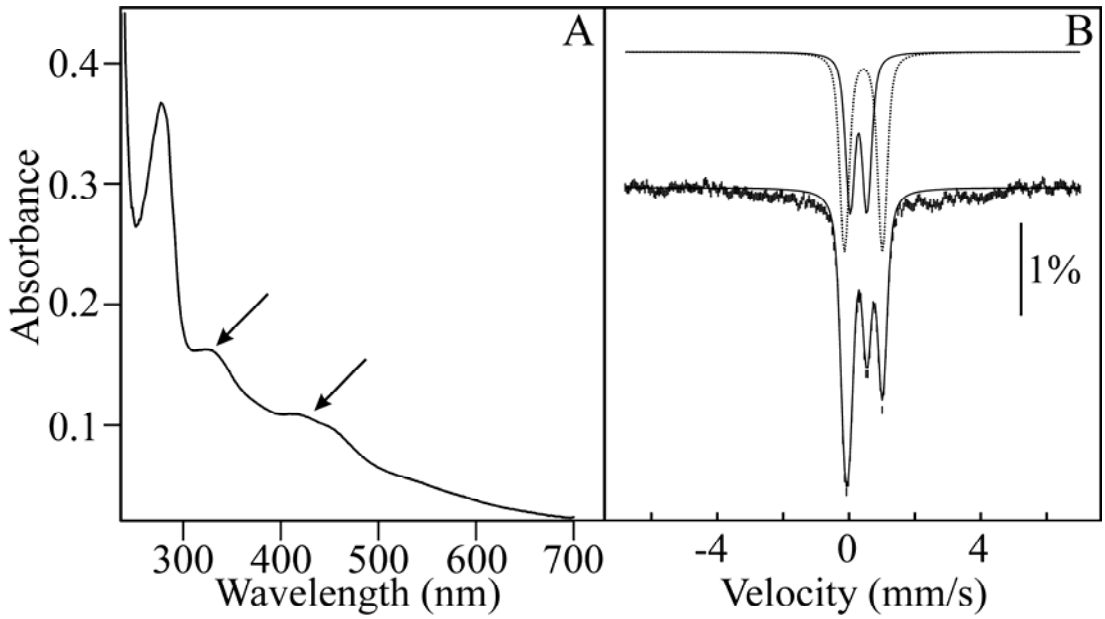

Figure 4.5: Spectroscopic Characterization of As-Isolated BioB. UV-visible spectrum of as-isolated BioB, 5 μM (panel A). The arrows in Panel A highlight absorptions that are characteristic of 2Fe-2S and 4Fe-4S clusters. Panel B, Mössbauer of as-isolated BioB (upper lines are fits to two quadrupole doublets).

The Mössbauer spectrum of as-isolated BioB is shown in Figure 4.6B. It is composed of two quadrupole doublets having isomer shift and quadrupole splitting parameters that are characteristic of $[4Fe\text{-}4S]^{2+}$ (δ = 0.44 mm/s, ΔE_Q = 1.15 mm/s, 47% of the total intensity) and $[2Fe\text{-}2S]^{2+}$ (δ = 0.28 mm/s, ΔE_Q = 0.51 mm/s, 36% of the total intensity) clusters. The relative intensities of the two clusters indicate that they are

present in a ratio of ca. 1-$[2Fe\text{-}2S]^{2+}$ cluster to 0.65 $[4Fe\text{-}4S]^{2+}$ clusters. There have been a number of Mössbauer studies conducted on *E. coli* BioB. Of those that were performed on protein that contained both the [2Fe-2S] and [4Fe-4S] clusters in a single polypeptide, the parameters reported are similar to those obtained herein for BioB isolated under anaerobic conditions. In the initial Mössbauer characterization of this form of BioB, the enzyme was isolated aerobically and contained only a [2Fe-2S] cluster, having the parameters, $\delta = 0.27$ mm/s and $\Delta E_Q = 0.49$ mm/s. It was then reconstituted with $^{57}FeCl_3$, Na_2S, and DTT to contain both the [2Fe-2S] and [4Fe-4S] clusters; the [4Fe-4S] cluster displayed Mössbauer parameters, $\delta = 0.42$ mm/s and $\Delta E_Q = 1.00$ mm/s. In a separate but similar study of reconstituted BioB, the [2Fe-2S] cluster displayed the parameters, $\delta = 0.28$ mm/s and $\Delta E_Q = 0.5$ mm/s, while the [4Fe-4S] cluster was simulated as a composite of two overlapping quadrupole doublets of similar intensities, having the parameters, $\delta(1) = 0.45$ mm/s and $\Delta E_Q(1) = 1.28$ mm/s, and $\delta(2) = 0.44$ mm/s and $\Delta E_Q(2) = 1.03$ mm/s. These parameters are in good agreement with chemically reconstituted BioB and with BioB that had been overexpressed and analyzed from *E. coli* whole cells ($[2Fe\text{-}2S]^{2+}$: $\delta = 0.28$ mm/s and $\Delta E_Q = 0.53$ mm/s, and $[4Fe\text{-}4S]^{2+}$: $\delta = 0.45$ mm/s and $\Delta E_Q = 1.11$ mm/s) [45]. The similarity in parameters between BioB reconstituted/whole cells to have both clusters in a single polypeptide and anaerobically isolated BioB, suggests that these methods afford the same BioB construct.

Turnover of BioB in the Presence of 8-Mercaptooctanoic Acid and Dethiobiotin: Production of 5'-dA. The ability of BioB to catalyze the formation of 5'-dA from dethiobiotin and 8-mercaptooctanoic acid was assessed using as-isolated BioB (no

reconstitution). The data were fitted to a sequential reaction, which takes into account two individual hydrogen atom abstraction steps, each of which affords 5'-dA. Curves depicting the BioB-dependent formation of 5'-dA in the presence of dethiobiotin and 8-mercaptooctanoic acid are represented in Figure 4.6. When dethiobiotin was used as a substrate, 5'-dA was formed in two phases, displaying first order rate constants, k_1 = 0.852 ± 0.089 min^{-1} and k_2 = 0.115 ± 0.015 min^{-1} (Figure 4.7, squares). When 8-mercaptooctanoic acid was substituted for dethiobiotin, first order rate constants of 0.747 ± 0.192 min^{-1} and 0.03 ± 0.001 min^{-1} were obtained (Figure 4.7, circles). The first rate constant, k_1, is similar to that obtained when dethiobiotin is used as a substrate, while the second rate constant, k_2, is ~3.8-fold smaller. Interestingly, when [d_{15}]-octanoyl-H protein was used as a substrate in the LipA reaction, unlabeled 5'-dA formation was observed with a similar rate constant, 0.028 min^{-1} (Chapter 3). We attributed the production of unlabeled 5'-dA to an abortive process not associated with hydrogen atom abstraction from the substrate. The formation of biotin from dethiobiotin or lipoic acid from 8-mercaptooctanoic acid is currently being assessed by LC-MS, which will allow a time-dependent correlation between 5'-dA and the respective products to be made.

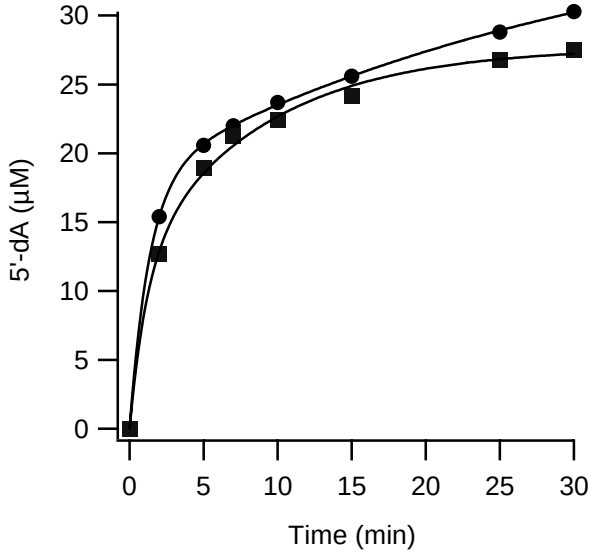

Figure 4.6: Kinetics of 5'-dA formation catalyzed by BioB with dethiobiotin (-■-) and 8-mercaptooctanoic acid (-●-).

4.5 Discussion

We have recently shown that synthesis of one lipoyl cofactor requires the expenditure of two molecules of SAM, and that deuterium from [octanoyl-d_{15}]-H protein is transferred to the resulting 5'-dA [2]. In analogy to BioB, LipA does not catalyze multiple turnovers; 50 μM LipA affords only 18 μM of the lipoyl cofactor over 30 min at 37 °C in a kinetic process that displays an overall pseudo-first order rate constant of 0.175 min^{-1} [2]. Two hypotheses have been envisaged to account for the meager amount of the lipoyl cofactor generated by LipA [2]. The first hypothesis simply supposes that only 36% of the enzyme is capable of generating the lipoyl cofactor. The second supposes that 72% of the enzyme is in an active state; however, each polypeptide contributes only one sulfur atom to the intact cofactor. This scenario would predict that

the maximum concentration of lipoyl cofactor synthesized by LipA could be no higher than one-half of the enzyme concentration, or 25 μM.

The above working hypotheses have been differentiated experimentally. The first hypothesis assumes that both sulfur atoms derive from the same polypeptide. The second hypothesis necessitates that subsequent to insertion of one sulfur atom into the octanoyl chain, the monothiolated intermediate dissociates from the enzyme and binds another LipA polypeptide that is competent for sulfur transfer. Herein, we addressed this issue directly using two differentially labeled forms of LipA, one isolated from minimal medium containing $Na_2{}^{34}S$ (98%) as the only sulfur source, and one isolated from minimal media containing natural abundance Na_2S (^{32}S = 95%) as the only sulfur source. Under turnover conditions, in the absence of extraneous sources of sulfur, and using equimolar concentrations of [^{34}S]-LipA and [^{32}S]-LipA, each synthesized lipoyl cofactor should contain either two atoms of ^{32}S or two atoms of ^{34}S if both sulfurs emanate from the same polypeptide. If each polypeptide contributes only one sulfur atom in the reaction, then the isolated lipoyl cofactor should contain a 1:2:1 ratio of ^{32}S–^{32}S, ^{32}S–^{34}S, and ^{34}S–^{34}S, respectively.

When LipA was overproduced in minimal media containing $Na_2{}^{34}S$ as the only source of sulfur, the isolated lipoic acid methyl ester contained ^{34}S at the same level of isotopic enrichment. The only other source of sulfur in these LipA reactions is SAM, and it is known that L-methionine and 5'-dA are the only products of SAM cleavage. Therefore, this experiment clearly indicates that the sulfur atoms in the LipA reaction derive from LipA itself (Figure 4.2B). We also have found that mixing of [^{34}S]-LipA and [^{32}S]-LipA in stoichiometric amounts prior to initiating the reaction results in formation

of primarily ^{32}S–^{32}S lipoic acid (220 m/z) and ^{34}S–^{34}S lipoic acid (224 m/z) (Figure 4.2C). This indicates that each LipA polypeptide donates both sulfur atoms in each lipoyl product. These results also support a model where free monothiolated species (i.e. 6-(*R,S*)-mercaptooctanoyl-H protein or 8-mercaptooctanoyl-H protein) do not dissociate from the active site of the enzyme; they are bonded to the sulfur donor, and are not released until the second sulfur atom is inserted. This contradicts early isotopic feeding studies by the White laboratory where 8-mercaptooctanoic acid was readily converted into lipoic acid *in vivo* [16]. Similarly, genetic studies performed in the Ashley laboratory showed that a lipoic acid auxotroph (W1485-*lip2*) could grow in the presence of 8-mercaptooctanoic acid [17]. Collectively the two studies suggested that 8-mercatpooctanoic acid could serve as an intermediate in the lipoic acid biosynthetic pathway.

We directly addressed the issue of free monothiolated intermediates in the LipA reaction by synthesizing 6-(*R,S*)-mercaptooctanoyl-H protein as well as 8-mercaptooctanoyl-H protein, and ascertaining whether they are converted into lipoyl–H proteins in vitro. 8-Mercaptooctanoic acid was commercially available, while 6-(R,S)-mercaptooctanoic acid was synthesized by a modification of a previously described procedure. Both compounds were attached to apo-H protein using lipoyl protein ligase (LplA). Both 6-(*R,S*)-mercaptooctanoyl-H protein and 8-mercaptooctanoyl-H protein induced cleavage of SAM to 5'-dA; however the rate constants associated with the process were ~1/3 of that obtained in the presence of octanoyl–H protein (Figure 4.4). In addition, no lipoyl cofactor was detected using the lipoamide dehydrogenase assay. Since SAM is not cleaved in the absence of bound substrate, these results suggest that

both the 8-mercaptooctanoyl and 6-(*R,S*)-mercaptooctanoyl compounds can bind to LipA, presumably in the active site, but they are not converted into product. Consistent with this conclusion, these compounds induce perturbations in the EPR spectra of LipA in the presence of SAM (Figure 4.3B and C). We argue that the putative monothiolated intermediates do not bind productively because the sulfur atom in each compound may be located in the same region of the active site as the sulfur atoms that are inserted into the normal substrate.

It appears that some fundamental differences between the LipA and BioB reactions may have emerged from the findings in this study. Early labeling studies showed that [^{35}S]- or [^{34}S]-9-mercaptodethiobiotin acid can be converted into labeled biotin [47]. Recently Marquet and co-workers demonstrated that 9-mercaptodethiobiotin is used as a substrate by BioB, and that biotin production proceeds with a similar rate constant to that obtained when dethiobiotin is used as a substrate [22]. Since 9-mercaptodethiobiotin has never been isolated from bacterial assay mixtures, it was presumed that the free monothiolated intermediate is never generated; it remains bound, perhaps covalently, to BioB. Formation of biotin from 9-mercaptodethiobiotin was rationalized by a mechanism wherein its thiol group exchanges with a bridging sulfur in the 2Fe-2S cluster. Abstraction of a hydrogen atom from C-6 of the compound then leads to formation of the thiophane ring [22]. The findings in this study contradict those from early *in vivo* feeding studies, and have led us to speculate that another enzyme, namely BioB, which has similar catalytic abilities, could be responsible for the conversion of 8-mercaptooctanoic acid into lipoic acid. It is noteworthy to point out the similarities between the structures of dethiobiotin and 8-mercaptooctanoic acid (Figure 4.8).

Certainly, the ureido ring is a major binding determinant as shown in the crystal structure of BioB [23] but it is conceivable that the active site could readily accommodate a molecule lacking the bulky heterocycle (Figure 4.7). We cloned the *bioB* gene in a pET-derived vector and coexpressed it with plasmid pDB1282, which encodes proteins involved in Fe-S cluster biogenesis. The protein was isolated by affinity chromatography under anaerobic conditions. The UV-visible spectrum of the protein suggested the presence of both $[2Fe–2S]^{2+}$ and $[4Fe–4S]^{2+}$ clusters, which was subsequently confirmed by Mössbauer spectroscopy (Figure 4.6). To our knowledge, this represents the first time that the clusters in BioB have been isolated and characterized in the absence of chemical reconstitution. Using the physiological reducing system, flavodoxin, flavodoxin oxidoreductase, and NADPH, we confirmed the ability of BioB to catalyze cleavage of SAM into 5'-dA, which required the presence of dethiobiotin and 8-mercaptooctanoic acid. By contrast, previous studies showed that BioB that was reduced by 5'-deazariboflavin and light could catalyze the formation of methionine in the absence of substrate [48]. This process as well as the oxidation of the $[4Fe\text{-}4S]^{+}$ cluster were shown to occur with the same rate constant (0.025 ± 0.005 min^{-1}). Interestingly, this rate constant is very similar to those observed for abortive processes in LipA. The authors noted that the rate constant associated with the production of methionine greatly exceeded that of biotin formation.

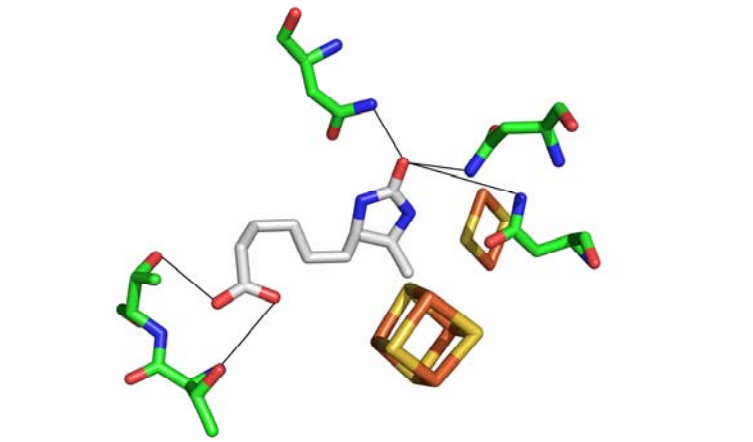

Figure 4.7: Binding of dethiobiotin in the BioB active site. Residues Asn 151, Asn 153, and Asn 222 are in position to form hydrogen bonds to the ureido ring of dethiobiotin, while Thr 292 and Thr 293 are in position to form hydrogen bonds to the carboxylate moiety of dethiobiotin.

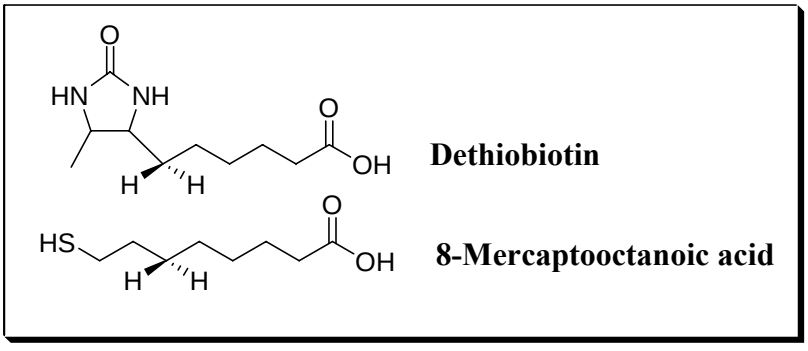

Figure 4.8: Structures of Dethiobiotin and 8-Mercaptooctanoic acid

Further experiments are being carried out to address whether lipoic acid is formed when 8-mercaptooctanoic acid is the substrate. Although we have not directly detected

biotin or lipoic acid, the kinetics of 5'-dA formation are provocative. A model can be constructed from the kinetics of 5'-dA formation, wherein each phase represents removal of one hydrogen atom. The first phase proceeds with similar rate constants regardless of the substrate (~0.7-0.8 min^{-1}). When dethiobiotin is used, the second phase has a rate constant of 0.115 min^{-1}, which could represent removal of the second hydrogen atom, resulting in the formation of the thiophane ring. In contrast, when 8-mercaptooctanoic acid is used as a substrate, the second phase may represent abortive cleavage of SAM, which takes place with a rate constant of ~0.03 min^{-1}. As previously mentioned, this rate constant is similar to those obtained in the LipA reaction in the presence of deuterated substrates that are presumed to be derived from abortive processes. It is conceivable that uncoupled hydrogen atom abstraction occurs when 8-mercaptooctanoic acid is used as a substrate because it lacks the requirement for a second C-S bond forming event.

The results presented in this study further detail the similarities between LipA and BioB, wherein the proteins act as both catalysts and reactants. It seems that like BioB, LipA may mobilize sulfur from the second Fe-S cluster. The crystal structure of BioB has bolstered this argument, wherein SAM and dethiobiotin are found between the 4Fe-4S cluster and the 2Fe-2S cluster (Figure 4.7) [23]. The α-amino group and the carboxylate of SAM are coordinated to a unique iron in the 4Fe-4S cluster while C-9 of dethiobiotin is positioned ~4.5 Å from the closest μ-sulfido sulfur in the 2Fe-2S cluster. Sequence homology has predicted LipA to have a truncated triose phosphate isomerase (TIM) $(\alpha\beta)_6$ fold, similar to lysine 2,3-aminomutase (LAM) and coproporphyrinogen III oxidase (HemN) [49]. Positioning of the octanoyl chain near the second [4Fe-4S] cluster in LipA may facilitate quenching of substrate radicals generated at positions C-6 and C-8.

4.6 References

1. Miller, J.R., R.W. Busby, S.W. Jordan, J. Cheek, T.F. Henshaw, G.W. Ashley, J.B. Broderick, J.E. Cronan Jr., and M.A. Marletta, *Escherichia coli* LipA Is a Lipoyl Synthase: In Vitro Biosynthesis of Lipoylated Pyruvate Dehydrogenase Complex from Octanoyl-Acyl Carrier Protein. *Biochemistry*, 2000. **39**: p. 15166-15178.
2. Cicchillo, R.M., D.F. Iwig, A.D. Jones, N.M. Nesbitt, C. Baleanu-Gogonea, M.G. Souder, L. Tu, and S.J. Booker, Lipoyl Synthase Requires Two Equivalents of S-Adenosyl-L-Methionine to Synthesize One Equivalent of Lipoic Acid. *Biochemistry*, 2004. **43**: p. 6378-6386.
3. Busby, R.W., J.P.M. Schelvis, D.S. Yu, G.T. Babcock, and M.A. Marletta, Lipoic Acid Biosynthesis: LipA Is an Iron Sulfur Protein. *J Am Chem Soc*, 1999. **121**(19): p. 4706-4707.
4. Cicchillo, R.M., K.-H. Lee, C. Baleanu-Gogonea, N.M. Nesbitt, C. Krebs, and S.J. Booker, Escherichia coli lipoyl synthase binds two distinct [4Fe–4S] clusters per polypeptide. *Biochemistry*, 2004. **43**: p. 11770-11781.
5. Booker, S.J., Unvraveling the Pathway of Lipoic Acid Biosynthesis. *Chem Biol*, 2004. **11**: p. 10-12.
6. Zhao, S., J.R. Miller, Y. Jiang, M.A. Marletta, and J.E. Cronan Jr., Assembly of the Covalent Linkage Between Lipoic Acid and Its Cognate enzymes. *Chem Biol*, 2003. **10**: p. 1293-1302.

7. Hayden, M.A., I. Huang, D.E. Bussiere, and G.W. Ashley, The Biosynthesis of Lipoic Acid: Cloning of lip, a Lipoate Biosynthetic Locus of *Escherichia coli*. *J Biol Chem*, 1992. **267**(14): p. 9512-9515.

8. Reed, K.E. and J. J. E. Cronan, Lipoic Acid Metabolism in *Escherichia coli*: Sequencing and Functional Characterization of the *lipA* and *lipB* Genes. *J Bacteriol*, 1993. **175**(5): p. 1325-1336.

9. Sofia, H.J., G. Chen, B.G. Hetzler, J.F. Reyes-Spindola, and N.E. Miller, Radical SAM, a novel protein superfamily linking unresolved steps in familiar biosynthetic pathways with radical mechanisms: functional characterization using new analysis and information visualization methods. *Nucleic Acids Res*, 2001. **29**(5): p. 1097-1106.

10. Frey, P.A. and S.J. Booker, Radical Mechanisms of S-adenosylmethionine-Dependent Enzymes. *Adv Protein Chem*, 2001. **58**: p. 1-45.

11. Vanden Boom, T.J., K.E. Reed, and J. J. E. Cronan, Lipoic Acid Metabolism in *Escherichia coli*: Isolation of Null Mutants Defective in Lipoic Acid Biosynthesis, Molecular Cloning and Characterization of the *E. coli lip* Locus, and Identification of the Lipoylated Protein of the Glycine Cleavage System. *J Bacteriol*, 1991. **173**(20): p. 6411-6420.

12. Ugulava, N.B., C.J. Sacanell, and J.T. Jarrett, Spectroscopic Changes during a Single Turnover of Biotin Synthase: Destruction of a [2Fe–2S] Cluster Accompanies Sulfur Insertion. *Biochemistry*, 2001. **40**: p. 8352-8358.

13. Parry, R.J., Biosynthesis of Lipoic Acid. 1. Incorporation of Specifically Tritiated Octanoic Acid into Lipoic Acid. *J Am Chem Soc*, 1977. **99**(19): p. 6464-6466.

14. White, R.H., Stable Isotope Studies on the Biosynthesis of Lipoic Acid in *Escherichia coli*. *Biochemistry*, 1980. **19**: p. 15-19.

15. Parry, R.J., Biosynthesis of Some Sulfur-Containing Natural Products. Investigations of the Mechanism of Carbon-Sulfur bond Formation. *Tetrahedron*, 1983. **39**: p. 1215-1238.

16. White, R.H., Biosynthesis of Lipoic Acid: Extent of Incorporation of Deuterated Hydroxy- and Thiooctanoic Acids into Lipoic Acid. *J Am Chem Soc*, 1980. **102**: p. 6605-6607.

17. Hayden, M.A., I.Y. Huang, G. Iliopoulos, M. Orozco, and G.W. Ashley, Biosynthesis of Lipoic Acid: Characterization of the Lipoic Acid Auxotrophs *Escherichia coli* W1485-lip2 and JRG33-lip9. *Biochemistry*, 1993. **32**: p. 3778-3782.

18. Frappier, F., G. Guillerm, A.G. Salib, and A. Marquet, On the Mechanism of Conversion of Dethiobiotin to Biotin in Escherichia coli. Discussion of the Occurrence of an Intermediate Hydroxylation. *Biochem Biophys Res Commun*, 1979. **91**(2): p. 521-527.

19. Marquet, A., F. Frappier, G. Guillerm, M. Azoulay, D. Florentin, and J.-C. Tabet, Biotin Biosynthesis: Synthesis and Biological Evaluation of the Putative Intermediate Thiols. *J Am Chem Soc*, 1993. **115**: p. 2139-2145.

20. Baldet, P., H. Gerbling, S. Axiotis, and R. Douce, Biotin biosynthesis in higher plant cells. Identification of intermediates. *Eur. J. Biochem.*, 1993. **217**: p. 479-485.

21. Florentin, D., B.T. Bui, A. Marquet, T. Ohshiro, and Y. Izumi, On the mechanism of biotin synthase of Bacillus sphaericus. *C R Acad Sci III*, 1994. **317**(6): p. 485-8.

22. Tse Sum Bui, B., M. Lotierzo, F. Escalettes, D. Florentin, and A. Marquet, Further investigation on the turnover of Escherichia coli biotin synthase with dethiobiotin and 9-mercaptodethiobiotin as substrates. *Biochemistry*, 2004. **43**(51): p. 16432-41.

23. Berkovitch, F., Y. Nicolet, J.T. Wan, J.T. Jarrett, and C.L. Drennan, Crystal structure of biotin synthase, an S-adenosylmethionine-dependent radical enzyme. *Science*, 2004. **303**(5654): p. 76-9.

24. Méjean, A., B.T.S. Bui, D. Florentin, O. Ploux, Y. Izumi, and A. Marquet, Highly Purified Biotin Synthase can Transform Dethiobiotin into Biotin in the Absence of any other Protein, in the Presence of Photoreduced Deazaflavin. *Biochem. Biophys. Res. Commun.*, 1995. **217**(3): p. 1231-1237.

25. Sanyal, I., G. Cohen, and D.H. Flint, Biotin Synthase: Purification, Characterization as a [2Fe-2S] Cluster Protein, and in Vitro Activity of the *Escherichia coli bioB* Gene Product. *Biochemistry*, 1994. **33**: p. 3625-3631.

26. Tse Sum Bui, B., D. Florentin, F. Fournier, O. Ploux, A. Mejean, and A. Marquet, Biotin synthase mechanism: on the origin of sulphur. *FEBS Lett*, 1998. **440**(1-2): p. 226-30.

27. Gibson, K.J., D.A. Pelletier, and S. I. M. Turner, Transfer of Sulfur to Biotin from Biotin Synthase (BioB protein). *Biochem. Biophys. Res. Commun.*, 1999. **254**: p. 632-635.

28. Jarrett, J.T., Biotin synthase: enzyme or reactant? *Chem Biol*, 2005. **12**(4): p. 409-10.

29. Lotierzo, M., B. Tse Sum Bui, D. Florentin, F. Escalettes, and A. Marquet, Biotin synthase mechanism: an overview. *Biochem Soc Trans*, 2005. **33**(Pt 4): p. 820-3.

30. Tse Sum Bui, B., R. Benda, V. Schünemann, D. Florentin, A.X. Trautwein, and A. Marquet, Fate of the $(2Fe\text{-}2S)^{2+}$ Cluster of *Escherichia coli* Biotin Synthase during Reaction: A Mössbauer Characterization. *Biochemistry*, 2003. **42**(29): p. 8791-8798.

31. Jameson, G.N.L., M.M. Cosper, H.L. Hernández, M.K. Johnson, and B.H. Huynh, Role of the [2Fe–2S] cluster in recombinant *Escerhichia coli* biotin synthase. *Biochemistry*, 2004. **43**: p. 2022-2031.

32. Tse Sum Bui, B., T.A. Mattioli, D. Florentin, G. Bolbach, and A. Marquet, Escherichia coli biotin synthase produces selenobiotin. Further evidence of the involvement of the [2Fe-2S]2+ cluster in the sulfur insertion step. *Biochemistry*, 2006. **45**(11): p. 3824-34.

33. Fehér, F., *"Handbook of Preparative Inorganic Chemistry"*, ed. G. Bauer. Vol. Vol. 1. 1963. 358-360.

34. Sambrook, J., E.F. Fritsch, and T. Maniatis, *Molecular Cloning: A Laboratory Manual*. 2nd ed, ed. M. Ferguson. Vol. 3. 1989, Plainview, New York: Cold Spring Harbor Laboratory Press.

35. Frazzon, J. and D.R. Dean, Formation of iron–sulfur clusters in bacteria: an emerging field in bioinorganic chemistry. *Curr Opin Chem Biol*, 2003. **7**: p. 166-173.

36. Frazzon, J., J.R. Fick, and D.R. Dean, Biosynthesis of iron–sulphur clusters is a complex and highly conserved process. *Biochem Soc Trans*, 2002. **30**(4): p. 680-685.

37. Kriek, M., L. Peters, Y. Takahashi, and P.L. Roach, Effect of iron–sulfur cluster assembly proteins on the expresssion of *Escherichia coli* lipoic acid synthase. *Protein Expr Purif*, 2003. **28**: p. 241-245.

38. Ugulava, N.B., B.R. Gibney, and J.T. Jarrett, Biotin Synthase Contains Two Distinct Iron–Sulfur Binding Sites: Chemical and Spectroelectrochemical Analysis of Iron–Sulfur Cluster Interconversions. *Biochemistry*, 2001. **40**: p. 8343-8351.

39. Beinert, H., Semi-micro Methods for Analysis of Labile Sulfide and of Labile Sulfide plus Sulfane Sulfur in Unusually Stable Iron-Sulfur Proteins. *Anal Biochem*, 1983. **131**: p. 373-378.

40. Frank, R.L. and P.V. Smith, Preparation of mercaptans from alcohols. *J. Am. Chem. Soc.*, 1946. **68**: p. 2103-2104.

41. Woster, P.M., A.Y. Black, K.J. Duff, J.K. Coward, and A.E. Pegg, Synthesis and biological evaluation of S-adenosyl-1,12-diamino-3-thio-9-azadodecane, a multisubstrate adduct inhibitor of spermine synthase. *J Med Chem*, 1989. **32**(6): p. 1300-7.

42. Pratt, K.J., C. Carles, T.J. Carne, and M.J. Danson, Detection of bacterial lipoic acid. A modified gas-chromatographic-mass-spectrometric procedure. *Biochem. J.*, 1989. **258**: p. 749-754.

43. Ugulava, N.B., B.R. Gibney, and J.T. Jarrett, Iron-Sulfur Cluster Interconversions in Biotin Synthase: Dissociation and Reassociation of Iron during Conversion of [2Fe-2S] to [4Fe-4S] Clusters. *Biochemistry*, 2000. **39**: p. 5206-5214.

44. Cosper, M.M., G.N.L. Jameson, M.K. Eidsness, B.H. Huynh, and M.K. Johnson, Recombinant *Escherichia coli* Biotin Synthase is a $[2Fe–2S]^{2+}$ Protein in Whole Cells. *FEBS Lett*, 2002. **529**: p. 332-336.

45. Benda, R., B. Tse Sum Bui, V. Schünemann, D. Florentin, A. Marquet, and A.X. Trautwein, Iron–Sulfur Clusters of Biotin Synthase In Vivo: A Mössbauer Study. *Biochemistry*, 2002. **41**: p. 15000-15006.

46. Cosper, M.M., G.N.L. Jameson, H.L. Hernández, C. Krebs, B.H. Huynh, and M.K. Johnson, Characterization of the cofactor composition of *Escherichia coli* biotin synthase. *Biochemistry*, 2004. **43**: p. 2007-2021.

47. Marquet, A., B.T. Bui, and B. Florentin, *Biosynthesis of Biotin and Lipoic Acid*. Vitamins and Hormones. Vol. 61. 2001, New York: Academic Press.

48. Ollagnier-de-Choudens, S., Y. Sanakis, K.S. Hewitson, P. Roach, E. Münck, and M. Fontecave, Reductive Cleavage of S-Adenosylmethionine by Biotin Synthase from *Escherichia coli*. *Biochemistry*, 2002. **277**(16): p. 13449-13454.

49. Nicolet, Y. and C.L. Drennan, AdoMet radical proteins--from structure to evolution--alignment of divergent protein sequences reveals strong secondary structure element conservation. *Nucleic Acids Res*, 2004. **32**(13): p. 4015-25.

Chapter 5

Spectroscopic Changes Associated with Substrate and Cofactor Binding to Lipoyl Synthase

5.1 Abstract

Lipoyl synthase (LipA), a member of the radical S-adenosyl-L-methionine (SAM) family of enzymes, catalyzes the formation of two consecutive carbon-sulfur bonds at positions C-6 and C-8 of protein-bound octanoyl groups. The insertion of sulfur is thought to be a radical-mediated process initiated by hydrogen atom abstraction. The enzymes within the radical SAM superfamily are identified by the presence of a CX_3CX_2C consensus sequence, wherein the denoted cysteines provide thiolate ligands to an oxygen-sensitive 4Fe-4S cluster. The reduced 4Fe-4S cluster is thought to provide an electron, which is necessary to reductively cleave SAM into L-methionine and a 5'-deoxyadenosyl radical (5'-dA•) intermediate. Spectroscopic studies on pyruvate formate-lyase activating enzyme (PFL-AE), biotin synthase (BioB), and lysine 2,3-aminomutase (LAM), and recent X-ray structures of coproporphyrinogen-III oxidase (HemN), BioB, MoaA, and LAM provided evidence for a specific binding interaction between the methionine moiety of SAM and a unique iron in the 4Fe-4S cluster, wherein the α-amino nitrogen and α-carboxylate oxygen of SAM form an N/O chelate to the open-iron site of the cluster.

We have recently shown that LipA can accommodate two 4Fe-4S clusters and that this state of the enzyme is required for the formation of the lipoyl cofactor [Cicchillo, R. M.; Lee, K.-H.; Baleanu-Gogonea, C.; Nesbitt, N. M.; Krebs, C.; Booker, S. J., (2004) *Biochemistry*; 43 (37), 11770-11781]. One of the Fe-S clusters is bound by three cysteinyl ligands of the shared CX_3CX_2C radical SAM motif, while the second is coordinated by cysteines of a CX_4CX_5C motif, which is conserved only among lipoyl synthases. Using various spectroscopic techniques, we have initiated an investigation of the possible interaction of SAM and octanoyl-H protein with the 4Fe-4S clusters of LipA. Preliminary results indicate that the presence of the substrates does indeed perturb the electronic environment of the 4Fe-4S clusters, primarily the cluster bound in the radical SAM binding site (CX_3CX_2C). The observed spectroscopic changes suggest that LipA, like other radical SAM proteins, shares a common SAM binding mode to the 4Fe-4S cluster. We also demonstrate, in certain instances, that productive binding requires the presence of both SAM and the octanoyl-H protein. This interaction is supported by anaerobic gel filtration data, which demonstrates that LipA and the octanoyl-H protein form a heterodimer in the presence of SAM.

5.2 Introduction

Biochemical, genetic, and bioinformatic studies have demonstrated that LipA is a member of the recently discovered radical SAM superfamily of enzymes [1-3], which is estimated to have over 600 members, and is currently expanding. Various proteins have been shown to be involved in, or are implicated in a myriad of metabolic pathways

ranging from the biosynthesis of antibiotics and cofactors to DNA repair [2, 4]. Most enzymes within this family share a conserved motif of cysteines ordered in a CX_3CX_2C configuration, which serve as ligands to an oxygen-sensitive 4Fe-4S cluster. Characterized members of this family, including PFL-AE, LAM, BioB, and anaerobic ribonucleotide reductase activating enzyme (ARR-AE), have been shown to require a reduced $[4Fe\text{-}4S]^+$ cluster and SAM to initiate catalysis [1, 5-7]. The reduced $[4Fe\text{-}4S]^+$ cluster provides an electron to reductively cleave SAM into methionine and a high-energy 5'-dA•. The 5'-dA• then initiates catalysis by stereoselectively abstracting a hydrogen atom from the substrate. Characterized radical SAM proteins have subsequently been placed into three subclasses, which are delineated by the manner in which SAM is used during catalysis. Class I is represented by LAM along with SPL (spore photoproduct-lyase) and are mechanistically distinct from the other characterized members of the family because SAM is a true cofactor where it is regenerated after each turnover [8]. PFL-AE and ARR-AE represent Class II proteins where SAM is consumed stoichiometrically to generate a catalytic glycyl radical cofactor. Class III enzymes such as BioB and LipA also utilize SAM as a substrate, rather than a cofactor, and SAM consumption parallels the number of hydrogen atoms removed during turnover.

It has been proposed that a specific interaction between the $[4Fe\text{-}4S]^+$ cluster and SAM is required for the generation of the 5'-dA•. Interestingly, the 4Fe-4S cluster coordinated by the CX_3CX_2C motif only has three protein-derived ligands and one unidentified ligand to the fourth iron, presumed to be water. Water coordination to an open ligation site has been observed in the enzyme aconitase, which catalyzes the 4Fe-4S cluster-dependent stereospecific interconversion of citrate and isocitrate. The 4Fe-4S

cluster, as in radical SAM enzymes, is bound by three cysteinyl ligands. ENDOR studies revealed that in the absence of substrate water occupies an open ligation site within the 4Fe-4S cluster [9]. Similar ENDOR studies revealed that when substrate is present the hydroxyl and one carboxylate of isocitrate coordinate to an open ligation site to the Fe-S cluster [10]. Biochemical and spectroscopic data suggest that this iron acts as a lewis acid to facilitate the loss of water.

Early proposals suggested that some portion of SAM may bind to the unique iron site of the 4Fe-4S cluster [8, 11]. Initial spectroscopic evidence for an interaction between SAM and the 4Fe-4S cluster of ARR-AE was provided by Fontecave and co-workers [12]. Simple mixing experiments revealed that the EPR spectrum of sodium dithionite reduced ARR-AE was perturbed in the presence of excess SAM. The signal broadened upon the addition of SAM, becoming more axial, and suggested that binding induces a conformational change in the protein or SAM binds in close proximity to the metallocofactor.

In similar experiments, the incubation of chemically reconstituted PFL-AE with excess SAM or S-adenosyl-homocysteine (SAH) transformed the EPR signal from axial to rhombic ($g = 2.009$, 1.921, and 1.886) [13]. Interestingly, the absence of the substrate pyruvate formate-lyase (PFL), did not prevent the formation of some 5'-dA. This suggested that some abortive cleavage of SAM occurred. SAM binding was shown to require the presence of the Fe-S center. In contrast, the EPR signal of native (non-chemically reconstituted) photoreduced PFL-AE was shown to exhibit a rhombic signal ($g = 2.02$, 1.94, and 1.88) [14]. Incubation of this protein with two molar equivalents of SAM converted the signal to nearly axial ($g = 2.01$, 1.88, and 1.87) [14]. The results

suggested that some unresolved differences exist between the native and reconstituted enzymes.

The Broderick and Huynh laboratories elegantly showed using Mössbauer spectroscopy that SAM binds a unique iron site of the 4Fe-4S cluster in PFL-AE [15]. The specific experiment takes advantage of the intrinsic lability of the 4Fe-4S cluster to oxygen (Figure 5.1). Previous studies showed that anaerobically isolated native PFL-AE primarily contains $[3Fe\text{-}4S]^{+}$ clusters (66% of the total iron) [16]. Mössbauer spectroscopy revealed that the dominating Fe-S center was in the form of $[4Fe\text{-}4S]^{+/+2}$ configuration upon sodium dithionite reduction. Recent studies showed that PFL-AE isolated with a 4Fe-4S cluster containing natural abundance iron could be exposed to air to generate a 3Fe-4S cluster (Figure 5.1) [15]. After gel filtration, the protein was reconstituted with ^{57}Fe in the presence of dithiothreitol (DTT) resulting in the reformation of an EPR silent $[4Fe\text{-}4S]^{2+}$ cluster. Mössbauer analysis revealed that the iron was in the $[4Fe\text{-}4S]^{2+}$ (S = 0) configuration with typical quadrupole splitting and isomer shift values (ΔE_Q = 1.12 mm/s and δ = 0.42 mm/s). The same protein was then incubated with 10-fold excess SAM to probe for interactions with the unique iron site, now isotopically labeled. A significant difference was observed when SAM is added and was highlighted by the change in the isomer shift from δ = 0.42 mm/s to δ = 0.72 mm/s. The quadrupole splitting parameter remained relatively unchanged at a ΔE_Q = 1.15. The entire absorption spectrum could be fit to two quadrupole doublets, the first having the same parameters (ΔE_{Q1} = 1.15 and δ_1 = 0.42 mm/s) of the reconstituted cluster, and the second having the new isomer shift value (ΔE_{Q2} = 1.15 and δ_2 = 0.72 mm/s). The second quadrupole doublet accounted for ~32 % of the total absorption. Collectively, the authors suggested

that the data support a model where SAM binding increases the coordination state of the unique iron site within the cluster [15].

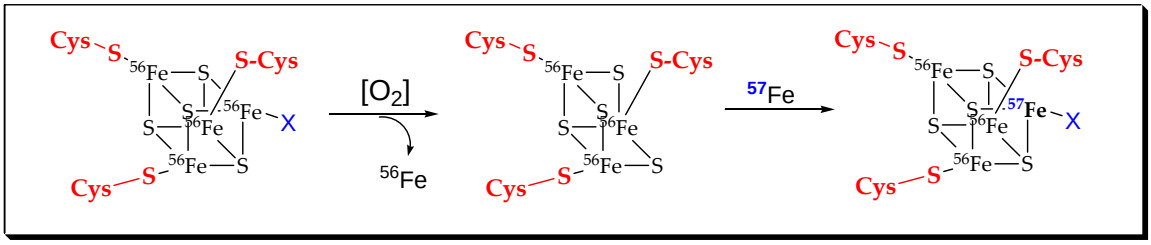

Figure 5.1: ^{57}Fe exchange into the 4Fe-4S cluster of PFL-AE for Mössbauer studies

Electron nuclear double resonance (ENDOR) spectroscopy subsequently identified specific binding interactions of portions of SAM to the 4Fe-4S cluster [14]. Two forms of isotopically labeled SAM were prepared that were specifically labeled with ^{2}H and ^{13}C in the methyl position. These compounds could then act as a sensitive probe to assess the interaction of SAM with the [4Fe-4S]$^{+}$ cluster of PFL-AE. ENDOR samples were prepared anaerobically by photoreducing the enzyme with 5'-deazariboflavin and then were quickly mixed with a two-fold excess labeled SAM ($^{2}H_3C$- or H_3C^{13}-). The corresponding ENDOR spectra revealed substantial ^{2}H and ^{13}C hyperfine coupling interactions. The authors suggested that this strong coupling is a direct result of binding in close proximity to the cluster as opposed to an effect due to remote binding of SAM. Direct measurements of the hyperfine interaction allowed for the determination of distances from the selected isotope in the methyl position from the Fe-S center. The data revealed that the methyl carbon is positioned ~4-5 Å from the Fe-S cluster, while the deuterons are located between 3-3.8 Å away. Cryoreduction experiments later

demonstrated that the interaction of SAM with the reduced $[4Fe\text{-}4S]^{+}$ cluster is identical to the interaction with the oxidized $[4Fe\text{-}4S]^{+2}$ cluster [14].

Although initial ENDOR studies showed that SAM was positioned close to the cluster and Mössbauer data suggested that SAM changed the coordination state of this iron, the role of the unique iron site remained unknown. Therefore, Walsby et al. set out to determine the specific interactions between SAM and the cluster. SAM specifically labeled with ^{17}O and ^{15}N in the methionine moiety was utilized in similar ENDOR experiments [17]. The corresponding spectra revealed significant hyperfine coupling interactions which arise from the interaction of the nuclei with the paramagnetic Fe-S cluster ($A(^{15}N)$ = 5.8 MHz and $A(^{17}O)$ = 12.2 mHz). The ENDOR and Mössbauer data together support a mode of binding where the nitrogen and oxygen atoms from the methionine moiety of SAM are coordinated to the unique iron site of the cluster in an N/O chelate. This coordination was suggested to play a role in "anchoring" SAM to the 4Fe-4S center, priming the complex for one electron transfer (Figure 5.2A) [17].

As in PFL-AE, the specific contacts between SAM and the [4Fe-4S] cluster of LAM were confirmed by ENDOR [18]. Specific labeling of the methionine portion of SAM in the carboxylate with ^{17}O and the amine with ^{15}N led to hyperfine coupling constants in the ENDOR spectra corresponding to the close interaction of the specified nuclei with the $[4Fe\text{-}4S]^{+}$ cluster. The observed hyperfine interactions were comparable to those seen in PFL-AE [17]. Samples that were reduced with sodium dithionite, or samples frozen first and subsequently reduced by cryoreduction afforded similar spectra, indicating that SAM binds to both the +1 and +2 states of the Fe-S cluster. A combination of ENDOR and EXAFS data led to the model shown in Figure 5.1B, which

differs slightly from the proposed model of Walsby et al. for PFL-AE. The model described in LAM accounts for a 2.7 Å Se-Fe interaction observed by Se-EXAFS. This observation suggests that sulfur binds to the open iron site after the reductive cleavage of SAM in the LAM reaction, whereas the sulfonium is proposed to interact with a bridging sulfur in the cluster of PFL-AE.

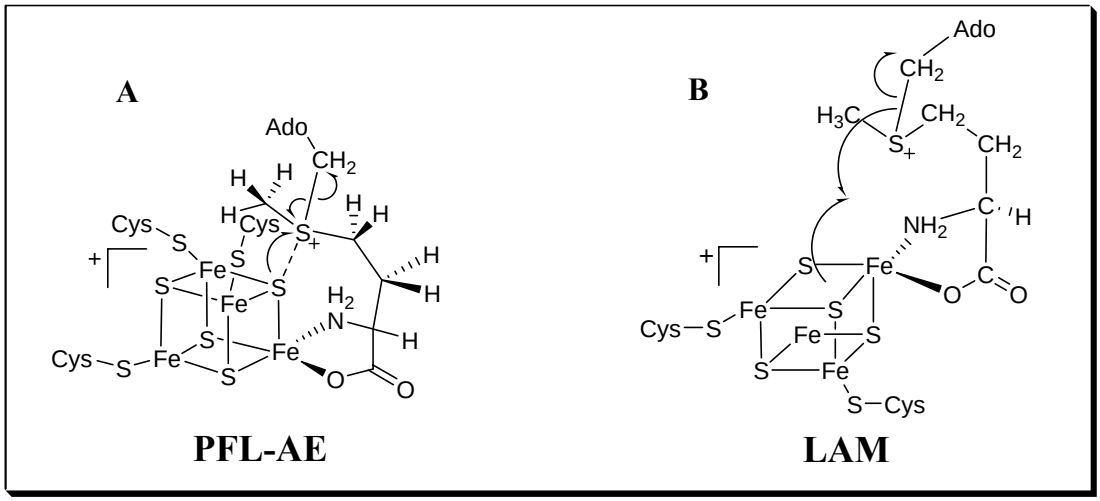

Figure 5.2: "Anchoring" of SAM to the 4Fe-4S clusters of LAM and PFL-AE.

Johnson and co-workers also observed SAM binding to the 4Fe-4S cluster of BioB using resonance Raman (RR), Mössbauer, and EPR spectroscopies. Chemically reconstituted BioB containing one 4Fe-4S cluster per monomer yielded a RR spectrum with characteristic stretching modes at 338 cm^{-1} (major component) and 364 cm^{-1} [19]. The addition of SAM shifted the dominating feature to 342 cm^{-1}, which the authors suggest lies outside of the range for a common 4Fe-4S cluster thiolate ligand. The Mössbauer spectrum of $[4Fe\text{-}4S]^{+2}$-BioB was fit to two quadrupole doublets with parameters, ΔE_{Q1} = 1.21 mm/s and δ_1 = 0.42 mm/s and ΔE_{Q2} = 1.10 mm/s and δ_2 = 0.47

mm/s, for the two mixed-valence iron pairs [19]. Addition of SAM broadened the overall spectrum and shifts the parameters of the second doublet to ΔE_{Q2} = 1.26 mm/s and δ_2 = 0.64 mm/s, which indicated an increase in coordination state that is not from a thiolate ligand. The EPR spectrum of cryoreduced BioB confirmed that SAM binding induced changes in the electronic properties of the cluster. The addition of SAM transforms the overall spectral envelope from axial (g = 2.00, 1.937, and 1.937) to rhombic (g = 2.042, 1.928, and 1.845). Similar changes in EPR spectra were observed in photoreduced samples of PFL-AE [13, 14] . The recently solved crystal structures of HemN, BioB, MoaA, and LAM have cemented the interaction between the 4Fe-4S cluster and SAM that originated from spectroscopic studies [20-24]. The structures unambiguously demonstrate that SAM is coordinated to the unique iron site in the 4Fe-4S center *via* the carboxylate and the amino portion of methionine.

Various spectroscopies have also been used to characterize the reaction catalyzed by BioB. The active form of the enzyme has been suggested to contain one 4Fe-4S cluster and one 2Fe-2S cluster [25]. SAM binding to the 4Fe-4S cluster is thought to facilitate the formation of the 5'-dA•, while the function of the 2Fe-2S cluster remained ambiguous [19, 26]. The origin of the sulfur atom in biotin has been debated for several years. Recent spectroscopic data from multiple groups has implicated the 2Fe-2S cluster as the sulfur donor [27-29]. Another group has posited that BioB can mobilize sulfur from cysteine in a PLP-dependent fashion, and that a protein bound persulfide could serve as the sulfur source [30]. Jarrett and co-workers have demonstrated using UV-visible spectroscopy that biotin formation is accompanied by the destruction of the 2Fe-2S center with comparable rate constants [27]. The reaction was subsequently

characterized by the Marquet laboratory using Mössbauer spectroscopy and showed that the level of the 4Fe-4S cluster remained constant throughout the duration of the assay while 2Fe-2S cluster degradation was concomitant with the formation of high-spin ferric species [28]. Recent Mössbauer experiments from the Johnson laboratory confirmed the early UV-visible and Mössbauer data, although the initial rate constant associated with the loss of the 2Fe-2S cluster was 10-fold faster than that of biotin formation [29].

In this study, using a combination of spectroscopic techniques, we probe the state of the 4Fe-4S clusters of LipA in the presence of substrates and under turnover conditions. We observe spectroscopic perturbations that are maximized, and in some instances only observable, in the presence of both SAM and the octanoyl-H protein. We also demonstrate that these observations require the presence of both 4Fe-4S clusters. We postulate that the interactions are similar to those described for PFL-AE, LAM, and BioB, where SAM is coordinated to a unique iron site within the Fe-S cluster.

5.3 Materials and Methods

Materials. L-selenomethionine, 5'-deoxyadenosine (5'-dA), S-adenosyl-L-homocysteine (SAH), and sodium dithionite were purchased from Sigma Corp (St. Louis, MO). ATP was purchased from MP Biomedicals (Solon, OH). ^{57}Fe (97-98%) metal was purchased from Web Research (Edina, MN). It was washed with $CHCl_3$ and dissolved with heating in an anaerobic solution of 2 N H_2SO_4 (1.5 mol of H_2SO_4 per mol of ^{57}Fe). It was used as is for bacterial growths. Routine iron and sulfide analysis was conducted as described previously. Se-adenosyl-selenomethionine (SeSAM) was synthesized as

previously described using SAM synthetase (E.C. 2.5.1.6) [31]. All enzyme purifications, reconstitutions, analyses, and preparations of substrates were performed as previously described [3, 32].

Low-temperature X-band EPR spectroscopy was carried out in perpendicular mode on a Bruker (Billerica, MA) ESP 300 spectrometer equipped with an ER 041 MR microwave bridge and an ST4102 X-band resonator (Bruker). Sample temperature was maintained with an ITC503S temperature controller and an ESR900 liquid helium cryostat (Oxford Instruments; Concord, MA). Spin concentration was determined by double integration of the sample spectrum and comparing the resulting intensity to that of a 1 mM $CuSO_4$ / 10 mM EDTA standard run under identical conditions. General spectral manipulations were carried out using the program IGOR Pro (Wavemetrics; Lake Oswego, OR) on a desktop computer.

Mössbauer spectra were recorded on spectrometers from WEB research (Edina, MN) operating in the constant acceleration mode in a transmission geometry. Spectra were recorded with the temperature of the sample maintained at 4.2 K. For low-field spectra, the sample was kept inside an SVT-400 dewar from Janis (Wilmington, MA), and a magnetic field of 40 mT was applied parallel to the γ-beam. For high-field spectra, the sample was kept inside a 12SVT dewar (Janis), which houses a superconducting magnet that allows for application of variable magnetic fields between 0 and 8 T parallel to the γ-beam. The quoted isomer shifts are relative to the centroid of the spectrum of a metallic foil of α-Fe at room temperature. Data analysis was performed using the program WMOSS from WEB research.

Preparation of Mössbauer, EPR, and EXAFS Samples. Samples to be analyzed by Mössbauer and EPR spectroscopies were prepared inside of the anaerobic chamber, and contained 200-500 μM LS. Samples (350 μL final volume) to be analyzed by Mössbauer spectroscopy were frozen with liquid nitrogen inside of small plastic cups. For characterization by EPR, the samples (250 μL final volume) were first treated with 2 mM sodium dithionite at ambient temperature for ~2 min, placed in EPR tubes (2 mm i.d.), and frozen in liquid nitrogen. All steps associated with preparing the samples were conducted inside of a Coy Laboratory Products (Grass Lake, MI) anaerobic chamber.

Samples for cryoreduction were prepared as described above and then irradiated at 77 K in the γ-irradiation facility of the Breazeale nuclear reactor at Pennsylvania State University using a ^{60}Co source (35 krad/h); a total dose of 3.6 MRad was applied.

In collaboration with Bob Scott (University of Georgia), Selenium EXAFS data were collected at the Stanford Synchrotron Radiation Laboratory (SSRL). Typical EXAFS samples contained 50 mM HEPES buffer (pH 7.5), between 200-400 μM as-isolated LipA, 400 μM SeSAM or 400 μM seleneomethionine, and 400 μM octanoyl-H protein in a final volume of 65 μL. When included, 5'-dA was added to a final concentration of 3.5 mM. Glycerol was added as needed to 25% (v/v) in all samples. Samples were frozen in the anaerobic chamber immediately after mixing.

Molecular Sieve Chromatography of Reconstituted LipA. All gel filtration experiments were carried out in a COY anaerobic chamber, which contained an ÄKTA FPLC equipped with a HiPrep 16/60 sephacryl S-200 high resolution column (Amersham Biosciences). The column was equilibrated in chilled gel filtration buffer (50 mM HEPES pH 7.5, 100 mM KCl, 315 μM SAM, and 10% glycerol) prior to the running of

samples. Protein standards (cytochrome c (12.4 kDa), carbonic anhydrase (29 kDa), bovine serum albumin (66 kDa), alcohol dehydrogenase (150 kDa), and β-amylase (200 kDa) (SIGMA)) were used to generate a standard curve of graded molecular masses. The molecular mass standards (2-10 mg/mL) along with LipA and octanoyl-H samples (100-200 μM) were developed in gel filtration buffer over the course of 120 min at a flow rate of 1 mL/min. The void volume (V_o) of the column was determined using blue dextran (2,000 kDa). The elution volumes (V_e) of the standards were obtained and the ratios of V_e/V_o were plotted as a function of the log of their respective molecular masses. The standard curve was then used to extrapolate the apparent molecular mass of reconstituted LipA, along with the LipA/octanoyl-H protein complex, based upon their elution volumes.

5.4 Results

Mössbauer Analysis of LipA in the Presence of Substrates. The Mössbauer spectrum of a sample of as-isolated LipA recorded at 4.2 K in an externally applied magnetic field (40 mT) oriented parallel to the γ-beam is shown in Figure 5.3 (hashed marks). The observed absorption lines belong to a quadrupole doublet with parameters that are typical of $[4Fe\text{-}4S]^{2+}$ clusters in the S = 0 ground state (δ = 0.46 mm/s and ΔE_Q = 1.16 mm/s). It is estimated that ~95% of the total absorption arises from $[4Fe\text{-}4S]^{2+}$ species. The spectrum of the as-isolated protein is identical to the spectrum of a sample that was incubated with a 10-fold molar excess of SAM (Figure 5.2, solid line). Addition of the octanoyl-H protein, either in the presence or absence of SAM, also has no affect on

the quadrupole doublet (data not shown). These results suggest that binding in a productive complex to or around the diamagnetic clusters of LipA does not occur, or that binding results in perturbations that are too small to detect.

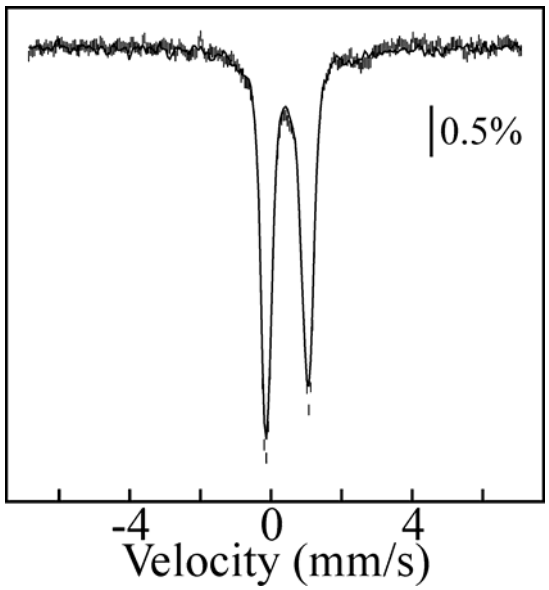

Figure 5.3: As-isolated LipA in the presence (solid line) or absence (hashed marks) of SAM.

Mössbauer Analysis of LipA Under Turnover Conditions. Mössbauer spectroscopy was employed to gain insight into the state of the Fe-S clusters of LipA before and after turnover. Spectra were recorded under turnover conditions using the physiological reducing system (flavodoxin, flavodoxin oxidoreductase, and NADPH) or with sodium dithionite. Reference spectra were recorded either without substrates or without reductant. The reactions were allowed to proceed for 30 min at room temperature (dithionite reduced sample) or at 37^{o}C (physiological reducing system), and were quenched by freezing in liquid nitrogen. The Mössbauer spectra using the physiological reducing system are shown in Figure 5.4 (left panel). Figure 5.4A

corresponds to LipA in the presence of SAM and the octanoyl-H protein. The parameters are identical to those of the as-isolated protein (ΔE_Q = 1.18 ± 0.03 mm/s and δ = 0.46 ± 0.03 mm/s). The quadrupole doublet represents >95% of the total absorbing species in the sample and is characteristic of $[4Fe\text{-}4S]^{2+}$ clusters. The reaction was initiated by the addition of flavodoxin, flavodoxin oxidoreductase, and NADPH, and was quenched after 30 min, resulting in the spectrum shown in Figure 5.3 spectrum B (left panel). The parameters of the quadrupole doublet remain unchanged throughout the duration of the assay while it appears that a small amount (~10%) of high-spin ferrous species develops (Figure 5.3B, arrow).

Reactions were also conducted in the presence of a chemical reductant, sodium dithionite. A control sample was prepared by incubating LipA with SAM and octanoyl-H protein in the absence of dithionite (Figure 5.4C, right panel). The parameters and relative amount of the diamagnetic cluster are identical to those reported in spectrum A (>95% $[4Fe\text{-}4S]^{2+}$ cluster). Reduction of LipA with 5 mM sodium dithionite in the presence of the octanoyl-H protein leads to the spectrum shown in Figure 5.4D. The central quadrupole doublet corresponds to a $[4Fe\text{-}4S]^{2+}$ species (75 ± 5%), while the new broad signal, due to a paramagnetic $[4Fe\text{-}4S]^{+}$ cluster, is observed along the baseline (Figure 5.4D, arrows). It is possible that a small absorption derived from a high-spin ferrous species overlays the $[4Fe\text{-}4S]^{+}$ cluster (Figure 5.4D, right arrow). Turnover was initiated by addition of SAM, and was allowed to proceed for 30 minutes at room temperature (Figure 5.4E, right panel). A quadrupole doublet having the exact same parameters as that in Figure 5.4C remains and represents 85 ± 3% of the absorbing species in the sample indicating that throughout the reaction the $[4Fe\text{-}4S]^{+}$ cluster is

oxidized back to the $[4Fe\text{-}4S]^{2+}$ state. The oxidation is highlighted by the disappearance of the broad feature between -3.5 mm/s and -1 mm/s (Figure 5.4D, left arrow) and is concomitant with the formation of approximately 15% high-spin ferrous species (Figure 5.3E, right arrow).

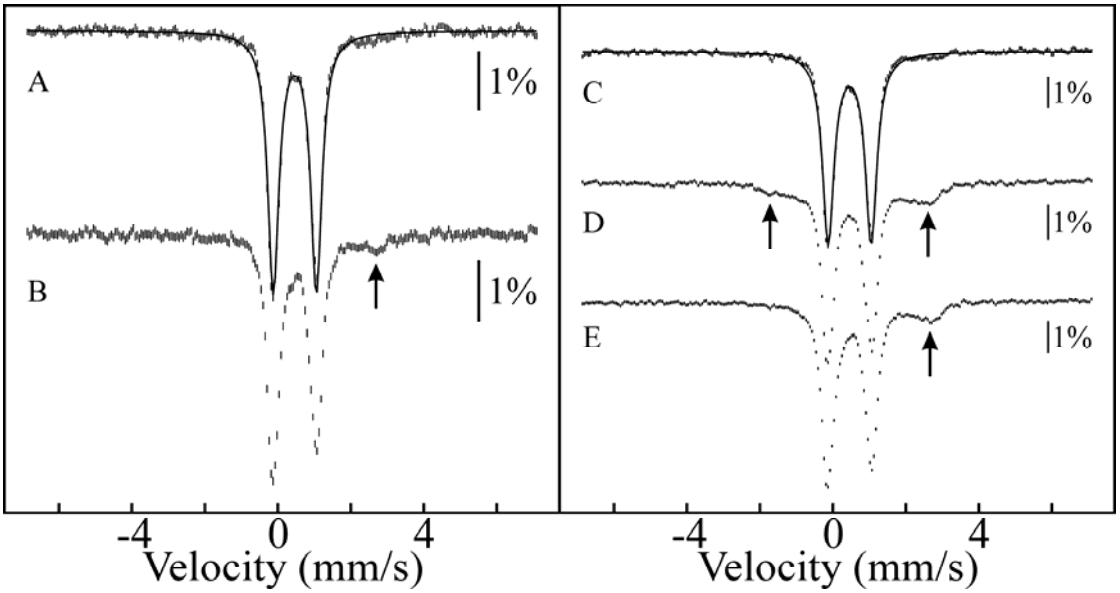

Figure 5.4: Mössbauer spectra of LipA under turnover conditions. Reactions were carried out with the physiological reducing system (left panel); spectrum A represents LipA with the octanoyl-H protein and SAM alone, spectrum B shows the same components in spectrum A except the physiological reducing system is added for 30 min. The right panel represents the sodium dithionite reaction. The right panel shows samples from the reaction with sodium dithionite. Spectrum C (reference spectrum) represents LipA in the presence of SAM and the octanoyl-H protein. Addition of 5 mM dithionite yields spectrum D. Spectrum E is the resulting spectrum after 30 min of turnover with dithionite.

EPR Spectra of Wild-Type LipA in the Presence of Substrates. Studies were performed to examine the affect of SAM and octanoyl-H protein on the EPR spectrum of reduced wild-type LipA. The EPR spectrum of wild-type LipA in the absence of substrates is shown in Figure 5.5 (dashed line). The signal is psuedoaxial with principal g- values centered at 2.03 and 1.93 which are characteristic of a $[4Fe\text{-}4S]^{+}$. Addition of

either SAM or octanoyl-H protein individually has no significant affect on the overall spectral envelope of the reduced cluster (Figure 5.2, solid line).

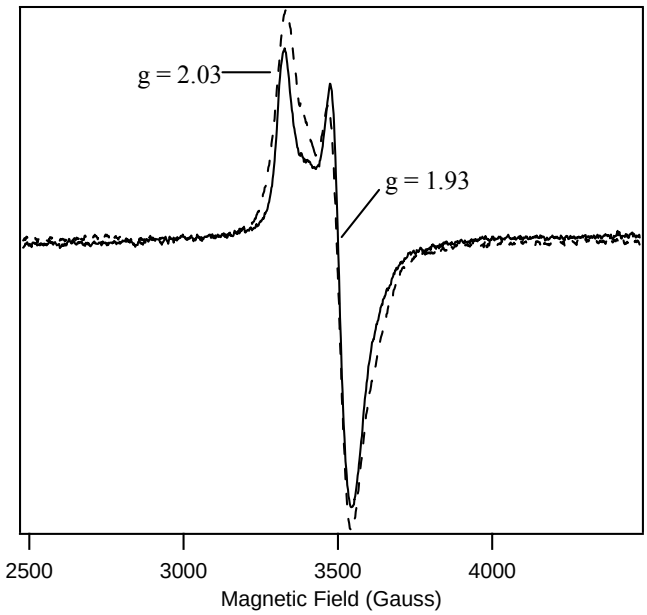

Figure 5.5: LipA reduced with 2 mM sodium dithionite (dashed line). LipA incubated with octanoyl-H protein (solid line). LipA incubated with SAM (not shown, but has an overall spectral envelope that is identical to the sample incubated with the octanoyl-H protein).

By contrast, the overall spectral envelope undergoes a dramatic transformation when reduced LipA is incubated with both substrates. The signal remains axial but is significantly sharpened with a g-value now centered at g = 1.88 (Figure 5.6, solid black line). The perturbation is suggests the presence of both substrates significantly perturbs the electronic environment of the cluster. Similar EPR perturbations have been seen in other radical-SAM proteins such as PFL-AE and ARR-AE. We propose that, as in PFL-AE, this perturbation is due to a direct binding interaction with the $[4Fe\text{-}4S]^{+}$ cluster as opposed to a conformational change in the protein. Spin quantitation revealed that ~20 % of the protein is reduced to the $[4Fe\text{-}4S]^{+}$ state within the first minute (Figure 5.5, red

line). This number corresponds approximately to the amount of active enzyme in any given protein preparation. The total spin decays by a factor of ~2.5 over the time course of the reaction, suggesting that the oxidation of the $[4Fe\text{-}4S]^{+}$ cluster might be coupled to turnover.

To verify that the observed changes in the EPR spectrum were due solely to binding and did not arise from turnover, LipA was incubated with Te-adenosyl-L-methionine (TeSAM), an analogue of SAM that binds to LipA but does not support turnover. The overall spectral envelope of the sample with TeSAM and octanoyl-H protein is almost identical to the sample that contained SAM and octanoyl-H protein, with slight changes in g-values (data not shown).

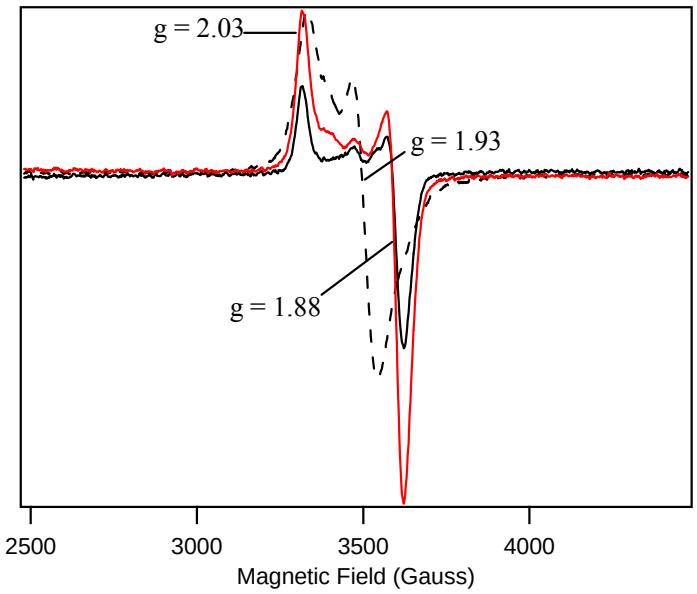

Figure 5.6: As-isolated LipA (dashed line). Dithionite reduced LipA incubated with SAM and octanoyl-H protein for 1 min (red line) or for 30 min (black line).

Spectroscopic and crystallographic studies on various radical-SAM proteins have shown that the sulfonium of bound SAM binds in close contact (~ 4-5 Å) to the 4Fe-4S

cluster [4, 14, 17]. To assess the effect of the positively charged sulfur atom of SAM on the 4Fe-4S cluster of LipA the reduced protein was incubated with octanoyl-H protein and S-adenosyl-L-homocysteine (SAH). The spectrum in Figure 5.7 (solid line) shows that incubation of the enzyme with SAH leads to a shift in g-value, albeit to a lesser extent than with SAM. The effect of the positive charge is uncovered by spin quantitation where, after rapid freezing, only ~7% of the enzyme becomes reduced (20 % with SAM). The sulfonium seems to have a significant role in reduction of the 4Fe-4S cluster. Previous EPR studies on LAM have shown that the presence of SAM or SAH is required to reduce the cluster to the $[4Fe\text{-}4S]^{+}$ state. The data showed that the reduction of the 4Fe-4S cluster was not dependent on the sulfonium center but more likely on other heteroatoms common to SAM and SAH [7]. Our results indicate binding and reduction occur in the presence of SAH but to a lesser extent when compared to SAM.

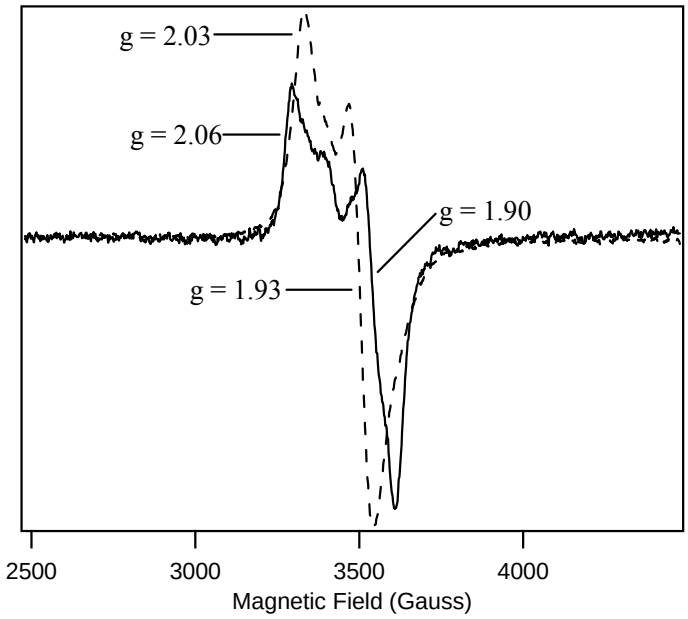

Figure 5.7: As-isolated LipA (dashed line). LipA incubated with SAH and octanoyl-H protein (solid line). For comparative purposes the sample containing SAH was multiplied by a factor of four.

EPR analysis of the LipA C68-73-79A Triple Variant in the Presence of Substrates. Analysis of the C68-73-79A LipA variant by EPR spectroscopy was also conducted. This particular protein retains the ability to bind the 4Fe-4S cluster that lies within the radical-SAM motif but lacks the 4Fe-4S cluster that is implicated in sulfur mobilization. Removal of this cluster abolishes the production of the lipoyl cofactor and the ability to cleave SAM into 5'-dA and methionine [32]. As-isolated C68-73-79A was reduced with 2 mM sodium dithionite in the absence and presence of substrates. The EPR signal in the absence of substrates has been reported and displays g-values that are identical to those of wild-type (Figure 5.7, dashed line) [32]. The simultaneous addition of SAM and the octanoyl-H protein lead to significant sharpening of the signal shifting

$g_{crossover}$ to ~1.89 (Figure 5.8 , solid line). The overall signal remains axial but the shift is not as significant when compared to those of wild-type enzyme (Figure 5.7, red line).

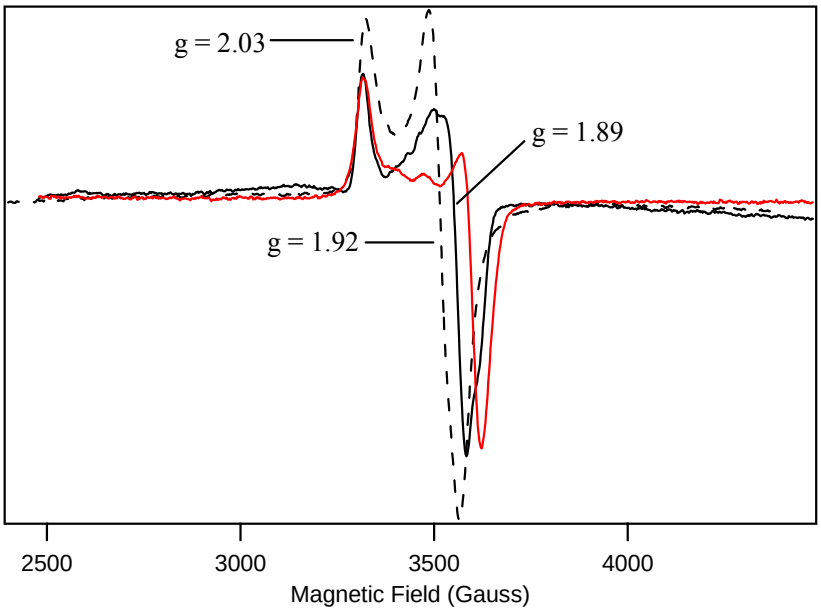

Figure 5.8: EPR spectra of the LipA triple variant C68-73-79A in the absence (dashed line) or presence (solid black line) SAM and the octanoyl-H protein. The red spectrum represents reduced wild-type LipA in the presence of octanoyl-H protein and SAM.

Cryoreduction of LipA in the Presence of SAM and Octanoyl-H Protein. The $[4Fe\text{-}4S]^{+}$ clusters of LipA are dramatically affected by the addition of both substrates. Cryoreduction experiments have shown that SAM can also bind in close proximity to the $[4Fe\text{-}4S]^{+2}$ cluster of native PFL-AE and the form of BioB that contains only the 4Fe-4S cluster [14, 19]. This important experiment revealed that the interaction of SAM with the 4Fe-4S cluster of PFL-AE is independent of oxidation state. Mössbauer and UV-visible spectroscopies have revealed that native LipA contains two 4Fe-4S clusters in the +2 oxidation state [32]. Samples of native enzyme were frozen in the presence or absence of SAM and octanoyl-H protein, and reduction of the Fe-S centers was conducted by

gamma irradiation with a ^{60}Co source (Figure 5.9). A sample of enzyme without substrates, Figure 5.9, red line, produced a weak axial signal, indicating partial reduction of the clusters occurred. The addition of octanoyl-H protein (Figure 5.8, green line), prior to radiolytic reduction lead to only minor changes in the EPR signal. In contrast, samples containing LipA and SAM lead to a significant increase in signal intensity (Figure 5.8, blue line). This is probably due to an increase in reduction potential facilitated by the binding of SAM to the unique iron site within the cluster. Similar results have been seen in LAM where elevated midpoint potentials were observed in the presence of substrates [33]. The affect of the addition of both SAM and the octanoyl-H protein is shown in the black line. The binding of both substrates to one or both of the $[4Fe\text{-}4S]^{+2}$ clusters causes a further increase in the signal intensity and is accompanied by a small shift in $g_{crossover}$ from 1.90 to 1.89. The interaction provides further evidence for the SAM-mediated regulation of redox potential that is affected by the addition of the octanoyl-H protein.

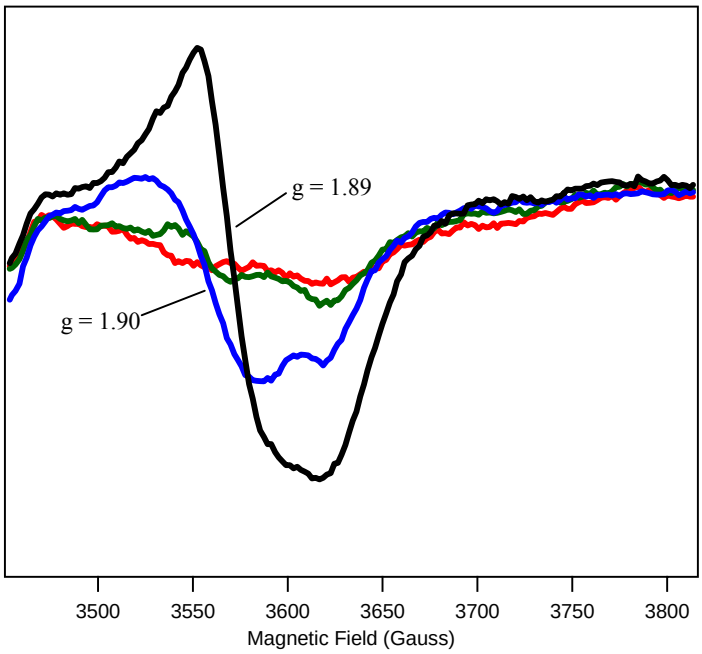

Figure 5.9: EPR spectra of cryoreduced as-isolated LipA (red line). LipA in the presence of octanoyl-H protein (green line), SAM (blue line), or both substrates (black line).

Se-EXAFS Analysis of LipA in the Presence of Substrates and Cleavage Products. XAS analysis was used to ascertain whether methionine coordinates to the Fe-S cluster subsequent to cleavage of SAM. To establish a reference point, control spectra were obtained on samples containing the octanoyl-H protein in the presence of SeSAM or L-selenomethionine and 5'-dA. Spectra were then recorded to investigate the potential binding of these components to wild-type LipA and LipA triple variants. All samples were prepared in the presence of the octanoyl-H protein. Incubation of wild-type LipA with SeSAM gave a Se-edge spectrum that resembled the control (data not shown). The triple variants prepared under the same conditions gave similar results, indicating that simply incubating the proteins with SeSAM does not lead to an observable Se-Fe

interaction with the Fe-S cluster (also observed in LAM). The wild-type and variant proteins were also incubated with L-selenomethionine and 5'-dA, which mimics the SAM cleavage reaction products [34]. The resulting spectra of the variant proteins were once again identical within the uncertainty of the method to the spectra of control samples. Interestingly, the wild-type sample contains a new absorption at 2.7 Å (Figure 5.10, arrow) and, as in LAM, is interpreted as an interaction of the selenium atom in L-selenomethionine and the unique iron site in the 4Fe-4S cluster of LipA. The spectra of LAM (red line) and LipA (blue line) are overlaid in Figure 5.10.

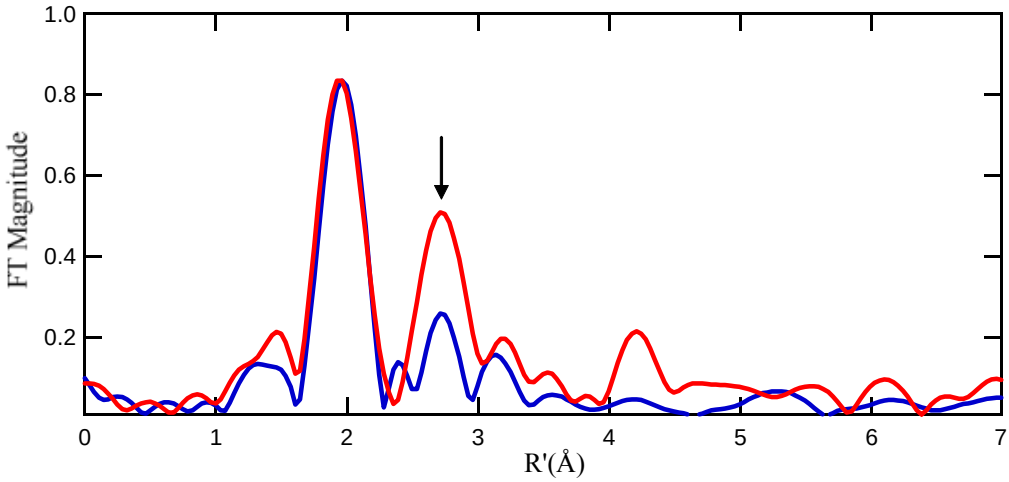

Figure 5.10: Se-EXAFS spectra of as-isolated LipA (blue line) and LAM (red line) incubated with L-selenomethionine and 5'-dA.

Analysis of LipA in the Absence and Presence of Substrates by Anerobic Gel Filtration Chromatography. Molecular sieve chromatography was used to assess the quaternary structure of LipA. When chromatographed alone, LipA has an elution volume of 63.97 mL under the described conditions (Figure 5.11, black line). This corresponds to a molecular weight of approximately 36,700 kDa, which suggests that the protein

migrates as a monomer (calculated: 38, 210 kDa for His-tagged LipA). A large portion of the enzyme also elutes in the void volume of the column and is attributed to soluble aggregates (*Ve* = 39 mL). Octanoyl-H protein runs as a dimer (Figure 5.11 , blue line) by gel filtration with an apparent molecular mass of 25, 983 kDa (Ve = 68.19 mL). Mixing of octanoyl-H protein in a two-fold molar excess over LipA results in the formation of a new absorption at 280 nm. The new peak has an elution volume of 57.13 mL, which corresponds to a molecular mass of 64,233 kDa (Figure 5.11, red line). The corresponding retention time supports the complexation of LipA and the octanoyl-H protein in a heterodimeric complex (arrow). The presence of both proteins was subsequently verified by collecting the peak and running it on a SDS-PAGE gel.

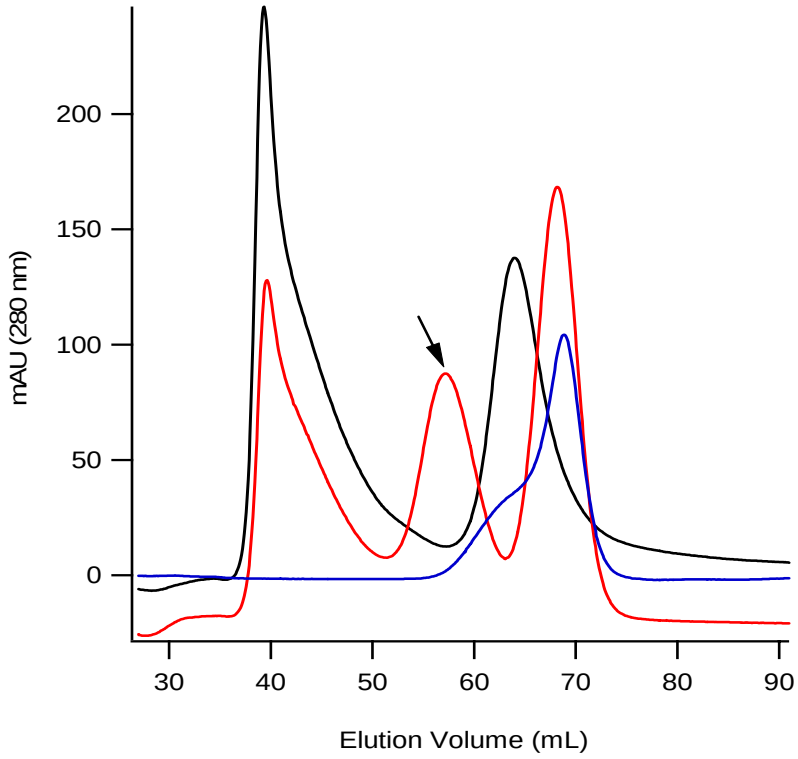

Figure 5.11: Gel filtration chromatography of reconstituted LipA (black line) and the octanoyl-H protein (blue line). The red line represents a 2:1 mixture of octanoyl-H protein and LipA in the presence of SAM.

5.5 Discussion

LipA catalyzes the insertion of sulfur atoms into saturated carbons at positions C-6 and C-8 of protein-bound octanoyl groups. LipA, along with other members of the radical SAM family of enzymes, utilizes one 4Fe-4S cluster and SAM to generate a high-energy 5'-dA•, which is required to initiate catalysis [3, 32]. All characterized radical SAM proteins contain a 4Fe-4S cluster that is bound by three conserved cysteines in the "radical SAM motif" (CX_3CX_2C). The fourth iron is not coordinated by an amino acid from the protein. Like BioB and MoaA, LipA binds a second Fe-S cluster. This Fe-S

cluster is also bound by three cysteinyl ligands and has been shown to be required for production of the lipoyl cofactor. Interestingly, MoaA also binds a second 4Fe-4S cluster by three cysteine residues [22]. The open-iron site has recently been shown to interact with the substrate, 5'-GTP, through N1 and N2 of the guanine ring [23]. By contrast, the second clusters in BioB and LipA have been implicated in the mobilization of sulfur for insertion into substrates [27-29, 32]. While the cofactor content of LipA and BioB have been addressed in some detail, the mechanism of SAM reduction and subsequent formation of the 5'-dA• remains elusive.

Elegant spectroscopic experiments, primarily on PFL-AE and LAM, have shown that the generation of the requisite 5'-dA• is linked to the binding of SAM to a unique iron site in the 4Fe-4S cluster. ENDOR studies on PFL-AE and LAM revealed that the specific contacts made to the unique (non-cysteinyl ligated) iron is through the amino and carboxylate portions of the methionine moiety of SAM [14, 17, 18]. These results confirmed previous Mössbauer studies on PFL-AE and BioB where perturbations were interpreted as an increase in coordination number to the unique iron in the 4Fe-4S clusters [15, 19]. The X-ray crystal structures of HemN, BioB, MoaA, and LAM, are consistent with the results from spectroscopic studies wherein SAM in each case is bound to the unique open-iron site in an N/O chelate [20-22, 24].

Without a crystal structure of LipA we turned to similar spectroscopic techniques to analyze the potential binding of substrates near or to the 4Fe-4S clusters. Unfortunately, simply incubating the enzyme with excess SAM in the presence or absence of octanoyl-H protein does not lead to significant perturbations in the Mössbauer spectrum (Figure 5.2). One possibility is that the interaction of substrates with LipA is

masked by the presence of two 4Fe-4S clusters having identical Mössbauer parameters. Repeating the same experiments using the C68-73-79A triple variant may help to alleviate this problem by removing the second 4Fe-4S cluster while leaving the radical SAM cluster intact. The amount of active enzyme may also contribute to the decreased sensitivity in the experiment. Assays have shown that both sulfurs are derived from one lipoyl synthase polypeptide indicating that ~30-40 % of the enzyme is configured to productively bind substrates in any given preparation. This suggests that only 15% of the total iron may be configured properly to interact with substrates. A final source of variability lies within the percentage of protein that forms soluble aggregates. Removal of damaged protein that retains the ability to bind 4Fe-4S clusters may eliminate contaminating absorptions.

We then chose to monitor potential Fe-S cluster transformations under turnover conditions using ^{57}Fe-labeled LipA. This type of analysis has been performed in multiple studies on BioB where destruction of the 2Fe-2S cluster was observed during turnover. UV-visible spectroscopy showed that destruction of the cluster was concomitant with biotin formation [27]. A recent Mössbauer study showed that the initial rate of biotin formation was an order of magnitude slower than 2Fe-2S destruction [29]. For these studies Mössbauer data were collected, under turnover conditions using the physiological reducing system and with the chemical reductant sodium dithionite. We also have analyzed the LipA reaction under turnover conditions using the physiological reducing system. The Mössbauer spectrum shows a central quadrupole doublet that originates from a diamagnetic [4Fe-4S]+2 cluster, which does not change markedly during turnover;

however ~10% of a ferrous species develops, which we believe is associated with partial cluster degradation.

Similar changes are observed when dithionite is used as reductant. Figure 5.4D was recorded in the absence of SAM and represents t = 0. The central quadrupole doublet in accounts for ~75% of the iron, and is indicative of a diamagnetic $[4Fe–4S]^{2+}$ cluster. The broad background indicted by the arrows derives most likely from a paramagnetic species, which is probably the $[4Fe–4S]^{+}$ cluster. It is also possible that a small absorption deriving from a high-spin ferrous species overlays the spectrum of the $[4Fe–4S]^{+}$ cluster. After 30 min at room temperature, the broad background disappears, leaving behind the central quadrupole doublet, which now accounts for 85% of the total iron, and a signal that is consistent with a ferrous species as is seen in the sample with flavodoxin. In this instance, the ferrous species accounts for ~15% of the total iron. Changes in the EPR spectra of these samples are consistent with what is observed by Mössbauer. In the presence of flavodoxin, nothing is observed except the flavodoxin semiquinone. In the presence of dithionite, we observe only the signal associated with the Fe/S clusters, the intensity of which is reduced upon incubation at room temperature for 30 min under turnover conditions.

The Fe-S clusters of LipA are capable of being reduced to the $[4Fe\text{-}4S]^{+}$ state, which is an S = 1/2 system and is EPR active. Although reduction of the clusters is far from quantitative, we were able to assess the affects of substrates on the paramagnetic centers of the enzyme. EPR is very sensitive and allows for the detection of subtle changes to the electronic environment of the Fe-S clusters. The EPR spectrum of wild-type reconstituted LipA remained fairly axial with no significant changes upon

incubation with two-fold molar excess octanoyl-H protein. Similar results were obtained when the protein was incubated with SAM alone. Incubation of the prereduced enzyme with SAM and the octanoyl-H protein indicates that productive binding to or around the 4Fe-4S clusters of LipA is dependent on the presence of both substrates. This substrate synergy is reminiscent of BioB studies that revealed binding of SAM is enhanced 20-fold when dethiobiotin is present [35]. The overall spectral envelope of LipA in the presence of both substrates remains fairly axial but undergoes a significant shift in $g_{crossover}$ (1.93 to 1.88). The EPR perturbations are similar to those observed in PFL-AE and suggest that substrate binding induces an altered coordination environment to the "radical SAM" cluster [14]. We interpret these changes in the EPR spectra as deriving from the interaction of the α-carboxylate and α-amino groups of SAM (or TeSAM) with the unique iron site in the 4Fe-4S cluster.

We also set out to determine if the oxidation state of the cluster(s) affects the binding of substrates. To examine these interactions, EPR samples were prepared with enzyme in the presence and absence of substrates and subsequently cryoreduced. This technique has been used in ENDOR studies with other radical SAM proteins, such as PFL-AE and LAM, to evaluate the interaction of the $[4Fe\text{-}4S]^{+2}$ cluster and substrates. The data suggest that the interaction of SAM with the unique iron in the 4Fe-4S cluster is independent of oxidation state [18, 36]. Addition of SAM and the octanoyl-H protein independently lead to small perturbations while the presence of both substrates shifts $g_{crossover}$ from ~1.92 to 1.89. These values are in good agreement with binding studies performed with the prereduced cluster in the presence of both substrates. It also appears

that the addition of both substrates increases the intensity of the EPR signal suggesting that substrate synergy also affects cluster reduction.

We then utilized a SAM analog (SAH) to examine the potential effect of the sulfonium center on the electronic environment of the Fe-S clusters. The EPR spectrum remained fairly axial exhibiting a slightly perturbed spectrum ($g = 1.93 \rightarrow g = 1.90$). It is clear from the EPR spectrum that a significantly smaller amount of the $[4Fe\text{-}4S]^{+}$ species is generated in the presence of SAH. These results indicate that the sulfonium atom mediates the redox potential of the cluster through a binding interaction. Similarly, early EPR studies on reconstituted PFL-AE showed that incubation of the enzyme with SAH transforms the signal to rhombic as does SAM with slight changes in the overall line shape [13]. The amount of spin was not calculated for the sample therefore it is unclear whether the reduction of the cluster was diminished. Studies from the Frey laboratory showed that the reduction of the EPR silent $[4Fe\text{-}4S]^{+2}$ cluster was dependent on the presence of SAM [7]. The same study revealed that the reduction of the cluster could also be achieved by incubation of the enzyme with SAH. Interestingly, spin quantitation revealed that SAH mediated the formation of a significantly greater amount of $[4Fe\text{-}4S]^{+}$ cluster; however, recent studies revealed that the midpoint reduction potential of the 4Fe-4S cluster of LAM in the presence of SAH was 30 mV lower than samples containing SAM [33]. The reduction potentials for LipA, in the presence of SAM and/or SAH, have yet to be determined, and therefore make it difficult to assess the subtle differences between the two enzymes.

As previously mentioned, LipA requires the presence of two 4Fe-4S clusters to catalyze the insertion of sulfur into protein-bound octanoyl groups. We posit that the

"radical SAM" cluster (CX_3CX_2C) interacts with SAM to generate a 5'-dA• while the second cluster (CX_4CX_5C) is involved in sulfur mobilization. We assessed the capability of a LipA triple variant (C68-73-79A), which lacks the second cluster, to interact with substrates. Although this protein binds one 4Fe-4S cluster it is incapable of catalyzing the formation of 5'-dA or the lipoyl cofactor. The EPR spectrum is axial with g-values similar to those of as-isolated wild-type protein. The signal narrows slightly upon addition of SAM and the octanoyl-H protein, shifting $g_{crossover}$ from 1.92 to 1.89. The data suggest that, although binding of the substrates to the radical SAM 4Fe-4S cluster can occur in the absence of the second cluster, its presence is electronically and/or structurally important.

The wild-type protein, when incubated with L-selenomethionine and 5'-dA, exhibited an absorption in the fourier transformed EXAFS spectrum which corresponds to a 2.7 Å interaction between selenium and iron. Although the yield of this "post-cleavage" binding complex was much lower than what was seen in LAM studies (~50%), it is consistent with the same interaction [34]. The results suggest that the sulfur of SAM is located in close proximity to the unique iron in the 4Fe-4S cluster and remains coordinated after reductive cleavage occurs [34]. Interestingly, similar EXAFS experiments showed that BioB and PFL-AE did not exhibit the same Se-Fe interaction [37]. The differences were attributed to how each enzyme utilizes SAM. In the mechanism of LAM, SAM is a true cofactor where it is regenerated upon each turnover. In BioB and PFL-AE, SAM is used a cosubstrate where its consumption parallels hydrogen atom abstraction. LipA seems to deviate from PFL-AE and BioB, wherein "LAM-like" Se-Fe interactions are observed. It is noteworthy to point out that the form

of BioB used in the aforementioned study did not contain the 2Fe-2S cluster that is thought to be catalytically essential and therefore makes it difficult to conclude that the lack of a Se-Fe interaction (or a different orientation of the post-cleavage products) arises from mechanistic differences [37].

We have also assessed the interaction of substrates with LipA by gel filtration chromatography. Initial studies suggested that LipA was primarily dimeric containing 4Fe-4S clusters [38]. A small contaminating amount of monomeric LipA was shown to contain 2Fe-2S clusters and led the authors to suggest the possibility that the 4Fe-4S cluster was assembled at a dimer interface [38]. Recent studies by Marletta and co-workers showed that the protein was isolated containing ~70% monomer [1]. We have shown here, using anaerobic gel filtration chromatography that reconstituted LipA exists exclusively as a monomer in solution. Interestingly, incubation of the protein with the octanoyl-H protein, in the presence of SAM, leads to the formation of a protein complex that migrates with a molecular mass that is consistent with the formation of a LipA/octanoyl-H protein heterodimer. These results support spectroscopic studies which suggest a tight complex is formed in the presence of both substrates.

In conclusion, it appears that formation of a productive LipA/substrate complex requires the assembly of both 4Fe-4S clusters as well as the presence of both SAM and the octanoyl-H protein. We are currently evaluating the specific interactions the Fe-S clusters with labeled substrates by ENDOR.

5.6 References

1. Miller, J.R., R.W. Busby, S.W. Jordan, J. Cheek, T.F. Henshaw, G.W. Ashley, J.B. Broderick, J.E. Cronan Jr., and M.A. Marletta, *Escherichia coli* LipA Is a Lipoyl Synthase: In Vitro Biosynthesis of Lipoylated Pyruvate Dehydrogenase Complex from Octanoyl-Acyl Carrier Protein. *Biochemistry*, 2000. **39**: p. 15166-15178.
2. Sofia, H.J., G. Chen, B.G. Hetzler, J.F. Reyes-Spindola, and N.E. Miller, Radical SAM, a novel protein superfamily linking unresolved steps in familiar biosynthetic pathways with radical mechanisms: functional characterization using new analysis and information visualization methods. *Nucleic Acids Res*, 2001. **29**(5): p. 1097-1106.
3. Cicchillo, R.M., D.F. Iwig, A.D. Jones, N.M. Nesbitt, C. Baleanu-Gogonea, M.G. Souder, L. Tu, and S.J. Booker, Lipoyl Synthase Requires Two Equivalents of S-Adenosyl-L-Methionine to Synthesize One Equivalent of Lipoic Acid. *Biochemistry*, 2004. **43**: p. 6378-6386.
4. Nicolet, Y. and C.L. Drennan, AdoMet radical proteins--from structure to evolution--alignment of divergent protein sequences reveals strong secondary structure element conservation. *Nucleic Acids Res*, 2004. **32**(13): p. 4015-25.
5. Henshaw, T.F., J. Cheek, and J.B. Broderick, The $[4Fe\text{-}4S]^{+1}$ Cluster of Pyruvate Formate-Lyase Activating Enzyme Generates the Glycyl Radical on Pyruvate

Formate-Lyase: EPR-Detected Single Turnover. *J Am Chem Soc*, 2000. **122**: p. 8331-8332.

6. Padovani, D., F. Thomas, A.X. Trautwein, E. Mulliez, and M. Fontecave, Activation of class III ribonucleotide reductase from E. coli. The electron transfer from the iron-sulfur center to S-adenosylmethionine. *Biochemistry*, 2001. **40**: p. 6713-6719.
7. Lieder, K.W., S. Booker, F.J. Ruzicka, H. Beinert, G.H. Reed, and P.A. Frey, S-Adenosylmethionine-Dependent Reduction of Lysine 2,3-Aminomutase and Observation of the Catalytically Functional Iron-Sulfur Centers by Electron Paramagnetic Resonance. *Biochemistry*, 1998. **37**(8): p. 2578-2585.
8. Frey, P.A. and S.J. Booker, Radical Mechanisms of S-adenosylmethionine-Dependent Enzymes. *Adv Protein Chem*, 2001. **58**: p. 1-45.
9. Werst, M.M., M.C. Kennedy, H. Beinert, and B.M. Hoffman, 17O, 1H, and 2H electron nuclear double resonance characterization of solvent, substrate, and inhibitor binding to the [4Fe-4S]+ cluster of aconitase. *Biochemistry*, 1990. **29**(46): p. 10526-32.
10. Beinert, H., Iron-sulfur proteins: ancient structures, still full of surprises. *J Biol Inorg Chem*, 2000. **5**(1): p. 2-15.
11. Cheek, J. and J.B. Broderick, Adenosylmethionine-dependent iron-sulfur enzymes: versatile clusters in a radical new role. *J Biol Inorg Chem*, 2001. **6**(3): p. 209-26.
12. Ollagnier, S., E. Mulliez, P.P. Schmidt, R. Eliasson, J. Gaillard, C. Deronzier, T. Bergman, A. Gräslund, P. Reichard, and M. Fontecave, Activation of the

Anaerobic Ribonucleotide Reductase from *Escherichia coli*. The Essential role of the Iron-Sulfur Center for S-adenosylmethionine Reduction. *J Biol Chem*, 1997. **272**(39): p. 24216-24223.

13. Külzer, R., T. Pils, R. Kappl, J. Hüttermann, and J. Knappe, Reconstitution and Characterization of the Polynuclear Iron-Sulfur Cluster in Pyruvate Formate-Lyase-Activating Enzyme. *J Biol Chem*, 1998. **273**(9): p. 4897-4903.
14. Walsby, C.J., W. Hong, W.E. Broderick, J. Cheek, D. Ortillo, J.B. Broderick, and B.M. Hoffman, Electron-nuclear double resonance spectroscopic evidence that S-adenosylmethionine binds in contact with the catalytically active $[4Fe\text{-}4S]^{+}$ cluster of pyruvate formate-lyase activating enzyme. *J. Am. Chem. Soc.*, 2002. **124**(12): p. 3143-3151.
15. Krebs, C., W.E. Broderick, T.F. Henshaw, J.B. Broderick, and B.H. Huynh, Coordination of adenosylmethionine to a unique iron site of the [4Fe-4S] of pyruvate formate-lyase activating enzyme: a Mossbauer spectroscopic study. *J Am Chem Soc*, 2002. **124**(6): p. 912-3.
16. Krebs, C., T.F. Henshaw, J. Cheek, B.H. Huynh, and J.B. Broderick, Conversion of 3Fe–4S to 4Fe–4S Clusters in Native Pyruvate Formate-Lyase Activating Enzyme: Mössbauer Characterization and Implications for Mechanism. *J Am Chem Soc*, 2000. **122**(50): p. 12497-12506.
17. Walsby, C.J., D. Ortillo, B.W. E., J.B. Broderick, and B.M. Hoffman, An Anchoring Role for FeS Clusters: Chelation of the Amino Acid Moiety of S-Adenosylmethionine to the Unique Iron Site of the [4Fe–4S] Cluster of Pyruvate

Formate–Lyase Activating Enzyme. *J Am Chem Soc*, 2002. **124**(38): p. 11270-11271.

18. Chen, D., C. Walsby, B.M. Hoffman, and P.A. Frey, Coordination and mechanism of reversible cleavage of S-adenosylmethionine by the [4Fe-4S] center in lysine 2,3-aminomutase. *J Am Chem Soc*, 2003. **125**(39): p. 11788-9.
19. Cosper, M.M., G.N.L. Jameson, R. Davydov, M.K. Eidsness, B.M. Hoffman, B.H. Huynh, and M.K. Johnson, The [4Fe–4S]2+ Cluster in Reconstituted Biotin Synthase Binds S-Adenosyl-L-methionine. *J Am Chem Soc*, 2002. **124**(47): p. 14006-14007.
20. Berkovitch, F., Y. Nicolet, J.T. Wan, J.T. Jarrett, and C.L. Drennan, Crystal structure of biotin synthase, an S-adenosylmethionine-dependent radical enzyme. *Science*, 2004. **303**(5654): p. 76-9.
21. Layer, G., J. Moser, D.W. Heinz, D. Jahn, and W.D. Schubert, Crystal structure of coproporphyrinogen III oxidase reveals cofactor geometry of Radical SAM enzymes. *Embo J*, 2003. **22**(23): p. 6214-24.
22. Hanzelmann, P. and H. Schindelin, Crystal structure of the S-adenosylmethionine-dependent enzyme MoaA and its implications for molybdenum cofactor deficiency in humans. *Proc Natl Acad Sci U S A*, 2004. **101**(35): p. 12870-5.
23. Hanzelmann, P. and H. Schindelin, Binding of 5'-GTP to the C-terminal FeS cluster of the radcial S-adenosylmethionine enzyme MoaA provides insights into its mechanism. *Proc. Natl. Acad. Sci.*, 2006. **103**: p. 6829-6834.

24. Lepore, B.W., F.J. Ruzicka, P.A. Frey, and D. Ringe, The x-ray crystal structure of lysine-2,3-aminomutase from Clostridium subterminale. *Proc Natl Acad Sci U S A*, 2005. **102**(39): p. 13819-24.

25. Ugulava, N.B., B.R. Gibney, and J.T. Jarrett, Iron-Sulfur Cluster Interconversions in Biotin Synthase: Dissociation and Reassociation of Iron during Conversion of [2Fe-2S] to [4Fe-4S] Clusters. *Biochemistry*, 2000. **39**: p. 5206-5214.

26. Ugulava, N.B., B.R. Gibney, and J.T. Jarrett, Biotin Synthase Contains Two Distinct Iron–Sulfur Binding Sites: Chemical and Spectroelectrochemical Analysis of Iron–Sulfur Cluster Interconversions. *Biochemistry*, 2001. **40**: p. 8343-8351.

27. Ugulava, N.B., C.J. Sacanell, and J.T. Jarrett, Spectroscopic Changes during a Single Turnover of Biotin Synthase: Destruction of a [2Fe–2S] Cluster Accompanies Sulfur Insertion. *Biochemistry*, 2001. **40**: p. 8352-8358.

28. Tse Sum Bui, B., R. Benda, V. Schünemann, D. Florentin, A.X. Trautwein, and A. Marquet, Fate of the $(2Fe\text{-}2S)^{2+}$ Cluster of *Escherichia coli* Biotin Synthase during Reaction: A Mössbauer Characterization. *Biochemistry*, 2003. **42**(29): p. 8791-8798.

29. Jameson, G.N.L., M.M. Cosper, H.L. Hernández, M.K. Johnson, and B.H. Huynh, Role of the [2Fe–2S] cluster in recombinant *Escerhichia coli* biotin synthase. *Biochemistry*, 2004. **43**: p. 2022-2031.

30. Ollagnier-de Choudens, S., E. Mulliez, and M. Fontecave, The PLP-dependent biotin synthase from *Escherichia coli*: mechanistic studies. *FEBS Lett*, 2002. **532**: p. 465-468.

31. Iwig, D.F. and S.J. Booker, Characterization and comparison of the intrinsic reactivities of S-Adenosyl-L-methionine, Se-Adenosyl-L-selenomethionine, and Te-Adenosyl-L-telluromethionine. *In preparation*, 2004.

32. Cicchillo, R.M., K.-H. Lee, C. Baleanu-Gogonea, N.M. Nesbitt, C. Krebs, and S.J. Booker, Escherichia coli lipoyl synthase binds two distinct [4Fe–4S] clusters per polypeptide. *Biochemistry*, 2004. **43**: p. 11770-11781.

33. Hinckley, G.T. and P.A. Frey, Cofactor dependence of reduction potentials for [4Fe-4S]2+/1+ in lysine 2,3-aminomutase. *Biochemistry*, 2006. **45**: p. 3219-3225.

34. Cosper, N.J., S.J. Booker, F. Ruzicka, P.A. Frey, and R.A. Scott, Direct FeS Cluster Involvement in Generation of a Radical in Lysine 2,3-Aminomutase. *Biochem.*, 2000. **39**(51): p. 15668-15673.

35. Ugulava, N.B., K.K. Frederick, and J.T. Jarrett, Control of adenosylmethionine-dependent radical generation in biotin synthase: a kinetic and thermodynamic analysis of substrate binding to active and inactive forms of BioB. *Biochemistry*, 2003. **42**(9): p. 2708-19.

36. Walsby, C.J., D. Ortillo, J. Yang, M.R. Nnyepi, W.E. Broderick, B.M. Hoffman, and J.B. Broderick, Spectroscopic approaches to elucidating novel iron-sulfur chemistry in the "radical-Sam" protein superfamily. *Inorg. Chem.*, 2005. **21**: p. 727-741.

37. Cosper, M.M., N.J. Cosper, W. Honig, J.E. Shokes, W.E. Broderick, J.B. Broderick, M.K. Johnson, and R.A. Scott, Structural Studies of the Interaction of S-Adenosylmethionine with the [4Fe–4S] Clusters in Biotin Synthase and

Pyruvate Formate–Lyase Activating Enzyme. *Protein Sci.*, 2003. **12**: p. 1573-1577.

38. Busby, R.W., J.P.M. Schelvis, D.S. Yu, G.T. Babcock, and M.A. Marletta, Lipoic Acid Biosynthesis: LipA Is an Iron Sulfur Protein. *J Am Chem Soc*, 1999. **121**(19): p. 4706-4707.

Appendix A

L-Serine Deaminase from Escherichia coli Requires a [4Fe-4S] Cluster in Catalysis

This chapter was reproduced from Cicchillo R.M., Baker M.A., Schnitzer E.J., Newman E.B., Krebs C., Booker S.J. (2004) Escherichia coli L-Serine Deaminase Requires a [4Fe-4S] Cluster in Catalysis. *J. Biol Chem*. 279, 32418-25.

A.1 Abstract

L-Serine deaminases catalyze the deamination of L-serine, producing pyruvate and ammonia. Two families of these proteins have been described, and are delineated by the cofactor that each employs in catalysis. These are the pyridoxal 5'-phosphate-dependent deaminases, and the deaminases that are activated in vitro by iron and dithiothreitol. In contrast to the enzymes that employ pyridoxal 5'-phosphate, detailed physical and mechanistic characterization of the iron-dependent deaminases is limited, primarily because of their extreme instability. We report here the characterization of L-serine deaminase from *Escherichia coli*, which is the product of the *sdaA* gene. When purified anaerobically, the isolated protein contains 1.86 ± 0.46 equiv of Fe and 0.670 ± 0.019 equiv of sulfide per polypeptide, and displays a UV-visible spectrum that is consistent with a [4Fe–4S] cluster. Reconstitution of the protein with iron and sulfide generates considerably more of the cluster, and treatment of the reconstituted protein with dithionite gives rise to an axial EPR spectrum, displaying $g_{\parallel}$ = 2.03 and $g_{\perp}$ = 1.93.

Mössbauer spectra of the ^{57}Fe-reconstituted protein reveal that the majority of the iron is in the form of $[4Fe–4S]^{2+}$ clusters, as evidenced by the typical Mössbauer parameters–isomer shift, δ = 0.47 mm/s, and quadrupole splitting ΔEq = 1.14 mm/s–and the diamagnetic (S = 0) ground state. Treatment of the dithionite-reduced protein with L-serine results in a slight broadening of the feature at g = 2.03 in the EPR spectrum of the protein, and a dramatic loss in signal intensity, suggesting that the amino acid interacts directly with the cluster.

A.2 Introduction

L-serine can be deaminated by a variety of enzymes of varying degrees of specificity, producing pyruvate and ammonia (Figure 1.1). As described in the Swiss-Prot database, these enzymes fall into two families, the serine/threonine (S/T)[1] deaminases (EC 4.3.1.19) and the bacterial L-serine deaminases (EC 4.3.1.17). The first of these, the S/T deaminases, require pyridoxal 5'-phosphate (PLP) as a cofactor in catalysis. Enzymes within this family that have been characterized to any significant extent include the mammalian liver L-serine deaminase, which serves a gluconeogenic function [230, 231], and the biosynthetic threonine deaminase (EC 4.3.1.19), which is encoded by the *ilvA* gene of *Escherichia coli*. This enzyme deaminates either serine or threonine [232], and is essential for isoleucine biosynthesis. A second threonine deaminase, the biodegradative enzyme, which is encoded by the *tdcB* gene of *E. coli*, uses the same cofactor, as does D-serine deaminase of *E. coli* (4.2.1.4) [233-235]. Moreover, serine is deaminated by enzymes of varying physiological function, including cystathionine γ-

synthase [236] and the β subunit of tryptophan synthase [237]. The mechanism of all these enzymes is well understood. The role of the PLP cofactor is to facilitate removal of the α-proton of the bound amino acid, allowing for a β-elimination of the hydroxyl group as water. Tautomerization of the resulting α-aminoacrylate results in 2-imino-propionic acid, which is hydrolyzed to ammonia and pyruvate [238].

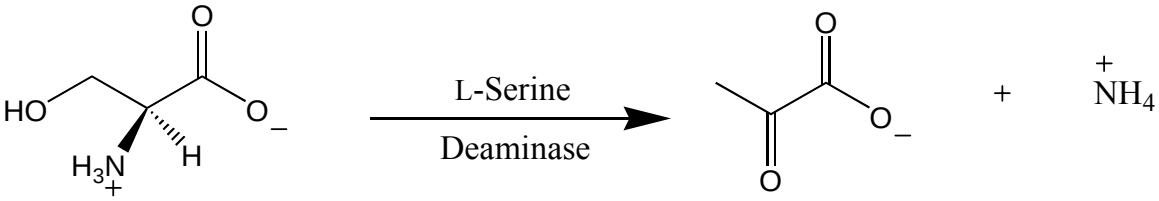

Figure 1.1: Reaction Catalyzed by L-Serine Deaminase

By contrast, the bacterial L-serine deaminases (LSDs) are activated by iron, and are not as well characterized [239, 240]. This family of enzymes is exclusively prokaryotic and widespread in bacteria, although not omnipresent. In fact, many bacteria elaborate one to three LSDs. In *E. coli* these proteins are encoded by the *sdaA*, *sdaB,* and *tdcG* genes [241-243]; the corresponding protein products are designated as LSD1, LSD2, and TdcG, respectively. All three proteins are very similar in primary structure; LSD2 and TdcG exhibit 77 and 78% identity with LSD1. In contrast to LSD1 and LSD2, TdcG is synthesized only during anaerobic growth [241].

The manner in which expression and/or function of these enzymes is regulated is known in some detail, but the mechanism of catalysis is not. LSD1 has been moderately characterized [242, 244, 245]. It contains 454 amino acids, including 9 cysteines [242]. When purified aerobically, the enzyme is inactive until incubated with iron and DTT under aerobic conditions. These characteristics make it very similar to the LSDs from

Clostridium acidiurici [246], *Peptostreptococcus asaccharolyticus* [247], and *Clostridium propionicum* [248], which are all activated in the same manner. Electron paramagnetic resonance (EPR) spectroscopic studies on the *P. asaccharolyticus* enzyme indicate the presence of $[3Fe–4S]^{+}$ clusters [249]. It is believed, however, that the catalytically active form of the enzyme contains a [4Fe–4S] cluster, in light of the striking similarities between the proposed reaction mechanism of the Fe-dependent LSDs and aconitase, which has been studied in detail using a variety of spectroscopic techniques [239, 250]. Herein, we use a variety of spectroscopic methods to show that treatment of LSD1 with iron and sulfide results in formation of a [4Fe–4S] cluster on the protein, and that this state of the protein is essential for catalysis. Reconstituted LSD1 catalyzes the deamination of L-serine with a first-order rate constant (k_{cat}) of 436 s^{-1}, and a K_M value of 2.67 ± 0.25 mM. It will also deaminate L-threonine and L-*allo*-threonine, albeit with greatly reduced efficiency; however, D-serine and L-cysteine are not substrates, but serve as competitive inhibitors. Additionally, analyses of EPR spectra recorded on the dithionite-reduced protein in the presence of various substrates and inhibitors are consistent with a direct role in catalysis for the iron–sulfur (Fe/S) cluster as opposed to a simple structural element.

A.3 Experimental Procedures

Materials. L-serine and dithiothreitol (DTT) were obtained from ICN Biomedicals Inc. L-Threonine, L-cysteine, lactate dehydrogenase (LDH), sodium sulfide

(nonahydrate), molecular weight standards for gel filtration, and ferric chloride were obtained from Sigma (St. Louis, MO). Sodium hydrosulfite (dithionite), potassium ferricyanide, and L-*allo*-threonine were obtained from Aldrich (Milwaukee, WI). Bovine serum albumin (BSA) standard and the Bradford reagent for protein quantification were purchased from Pierce (Rockford, IL). Nicotinamide adenine dinucleotide (reduced form) was obtained from Roche Diagnostics (Indianapolis, IN). Tryptone and yeast extract were obtained from Marcor Development (Carlstadt, NJ) and Biospringer USA (Milwaukee, WI), respectively. ^{57}Fe metal (97-98%) was obtained from Pennwood Chemicals (Great Neck, NY). It was washed with $CHCl_3$, and dissolved with heating in an anaerobic solution of 1 M H_2SO_4 (1.5 mol of H_2SO_4 per mol of ^{57}Fe). Upon dissolution, the pH of the solution was raised to ~4.5 by the addition of solid sodium bicarbonate immediately before the reconstitution procedure.

Spectroscopic Methods. UV-visible spectra were recorded on Cary 50 or Cary 300 spectrometers (Varian, Walnut Creek, CA), employing the associated WinUV software package. The Cary 300 was equipped with a 6 x 6 peltier-thermostattable multicell-holder and an associated temperature controller.

Low-temperature X-band EPR spectra were recorded in perpendicular mode on a Bruker (Billerica, MA) ESP300 spectrometer equipped with an ER 041 MR microwave bridge and a 4102ST resonator. Sample temperature was maintained with an ITC503S temperature controller and an ESR900 liquid helium cryostat (Oxford Instruments, Concord, MA). Spin concentration was determined by double integration of the sample spectrum obtained under non-saturating conditions, and comparing the resulting intensity

to that of a standard (1 mM $CuSO_4$, 10 mM EDTA) obtained under identical conditions. General spectral manipulations were performed on personal computers using the WinEPR software package (Bruker) or the IGOR Pro software package (Wavemetrics, Lake Oswego, USA).

Mössbauer spectra were recorded on spectrometers from WEB research (Edina, MN) operating in the constant acceleration mode in a transmission geometry. Spectra were recorded with the temperature of the sample maintained at 4.2 K. For low-field spectra, the sample was kept inside an SVT-400 dewar from Janis (Wilmington, MA), and a magnetic field of 40 mT was applied parallel to the γ-beam. For high-field spectra, the sample was kept inside a 12SVT dewar (Janis), which houses a superconducting magnet that allows for application of variable magnetic fields between 0 and 8 T parallel to the γ-beam. The quoted isomer shifts are relative to the centroid of the spectrum of a metallic foil of α-Fe at room temperature. Data analysis was performed using the program WMOSS from WEB research.

Analytical Procedures and Assays. Protein concentration was determined by the Bradford dye-staining procedure with bovine serum albumin (BSA) as the standard [251]. As determined in this work, this method overestimates the true concentration of LSD1 by a factor of 1.35. Routine chemical analyses of iron and sulfide were carried out by the methods of Beinert [182-184]. The method of Gill and von Hippel [252] was used to establish an extinction coefficient for apo-LSD1, which in turn was used to correct the Bradford dye-staining protein assay.

Routine gel-filtration of LSD1 was carried out in a Coy Laboratory Products (Grass Lake, MI) anaerobic chamber using Sephadex G-25 resin (Amersham Biosciences; Piscataway, NJ). When it was necessary to concentrate the protein, it was carried out using an Amicon stirred-cell ultrafiltration device (Millipore; Billerica, MA) in combination with a YM-10 membrane, which has a molecular weight cutoff of 10 kDa. Ultrafiltration was carried out inside of the anaerobic chamber by threading the tubing from the nitrogen source through one of the chamber's ports.

Overexpression and Purification of LSD1. A 200-mL overnight culture of *E. coli* BL21(DE3) containing plasmid psdaAH6 in terrific broth (100 μg mL^{-1} ampicillin) was used to inoculate 16 L of the same media, which was divided evenly among four 6-L Erlenmeyer flasks. Plasmid psdaAH6 contains the *sdaA* gene cloned as a fusion construct with a C-terminal 6X histidine tag that is separated from the last amino acid of the protein by a linker of two amino acid residues. The cultures were grown at 37°C with gentle shaking (200 rpm), and induced at an OD_{600} of 0.5 by addition of solid isopropyl-β-D-thiogalactopyranoside (IPTG) to a final concentration of 400 μM. At induction, solid $FeCl_3$ was also added to each flask to a final concentration of 50 μM. Expression of the *sdaA* gene was allowed to proceed for 4 h at 37°C, after which, the cultures were placed in an ice–water bath for 30 min. The bacteria were harvested by centrifugation for 20 min at 10,000xg and 4°C, yielding ~30 g of cells from 16 L of cell culture after freezing in liquid nitrogen.

LSD1 was purified by immobilized metal affinity chromatography (IMAC) using a Ni-NTA matrix (Qiagen; Valencia, CA). All steps were carried out

inside of the anaerobic chamber under an atmosphere of N_2 and H_2 (95% / 5%), wherein the O_2 concentration was maintained below 1 ppm via the use of palladium catalysts. Steps involving centrifugation were carried out outside of the anaerobic chamber; however, samples were loaded into appropriate centrifuge bottles and tightly sealed before removing them. In a typical purification, 30 g of cells were thawed in 60 mL of Buffer A (50 mM HEPES, pH 7.5, 100 mM NaCl, 1 mM DTT, 20 mM imidazole), and allowed to incubate with lysozyme (1 mg mL^{-1}) for 30 min at room temperature. Subsequent to chilling on ice, the cells were lysed by sonic disruption in 4 x 1-min bursts, and the lysate was centrifuged at 50,000xg for 1 h at 4°C. The supernatant was loaded onto a Ni-NTA column (2.5 x 7 cm) that was equilibrated in Buffer A, and the column was washed with 50 mL of Buffer A containing 10% glycerol and 40 mM imidazole. Finally, the protein was eluted with Buffer A containing 10% glycerol and 250 mM imidazole. Fractions that displayed a brown color were pooled and concentrated using an Amicon stirred-cell, and exchanged into Buffer B (50 mM EPPS, pH 8.0, 100 mM NaCl, 10% glycerol, 1 mM DTT) by anaerobic gel filtration. The protein was routinely frozen in small aliquots and stored in liquid N_2 until ready for use.

Reconstitution of Serine Deaminase. Reconstitution of LSD1 with iron and sulfide was carried out inside of the anaerobic chamber with buffers and solutions that were prepared with deoxygenated water. A typical reconstitution reaction contained 100 μM LSD1, and 8-fold molar excesses of $FeCl_3$ and Na_2S in a final volume of 2 mL. The protein was initially treated with a 50-fold molar excess of DTT for 10 min on ice. The $FeCl_3$ was added, and then a solution of Na_2S was added dropwise over 10 min. The

mixture was allowed to stir gently on ice for 4 h in the anaerobic chamber. It was then placed in centrifuge tubes, capped, and centrifuged at 20,000xg for 20 min at 4°C. It was brought back into the anaerobic chamber, and the supernatant was removed and exchanged into Buffer B by anaerobic gel filtration.

Activity Determination for Serine Deaminase. LSD1 was first diluted to a final concentration of 5 μM in Buffer B containing 50% glycerol. A typical reaction contained in a final volume of 1 mL: 0.2 mM NADH, 10 U of LDH, 0-20 mM L-serine, 100 mM EPPS, pH 8.0, and 55 nM LSD1. The reaction mixture was prepared inside of the anaerobic chamber; all of its components were anaerobic except for LDH. However, the volume of LDH added to the reaction mixture was 1% of the total volume. The reaction mixture, excluding LSD1, was incubated for 3-5 min at 37°C in a septum-sealed anaerobic cuvet (Starna; Atascadero, CA), and the reaction was initiated by injection of LSD1 via a gas-tight syringe. Enzyme turnover was monitored by a time-dependent decrease in absorption at 340 nm (ε_{340} = 6.22 x 10^3 M^{-1} cm^{-1}), which is due to NADH oxidation. One unit of activity is defined as 1 μmol of NAD^+ produced per minute. When turnover with L-threonine, L-cysteine, L-*allo*-threonine, or D-serine was monitored, the concentration of LSD1 in the assay was increased to 5.5 μM. The kinetic parameters K_M and V_{max} were obtained from fits of initial rate data as a function of serine concentration according to Equation 1. In some instances, data were fitted to Equation 2, which accounts for substrate cooperativity. When assays were carried out in the presence of inhibitors, the data were fitted to Equation 3 by multiple non-linear regression using the GraFit software program [253]. This equation describes competitive inhibition.

$$\vee = V_{max} \bullet [S] / (K_M + [S]) \quad (1)$$

$$\vee = V_{max} \bullet [S]^n / (K + [S]^n) \quad (2)$$

$$\vee = V_{max} \bullet [S] / (K_M + (1 + (I / K_I)) \bullet [S])) \quad (3)$$

Molecular Sieve Chromatography of LSD1. Molecular sieve chromatography of LSD1 was performed under anaerobic conditions with an ÄKTA (Amersham Biosciences) fast-performance liquid chromatography (FPLC) system, which was maintained inside of a Coy anaerobic chamber. The FPLC system was equipped with a HiPrep 16/60 Sephacryl S-200 HR column (Amersham Biosciences), and was controlled with the associated software program UNICORN, which was also used for data collection and analysis. The column was equilibrated in an anaerobic solution of Buffer B, and samples (250 μM) and standards (2-10 mg mL^{-1}) were chromatographed at a flow rate of 1 mL min^{-1} over a time span of 120 min. The proteins, cytochrome c (12.4 kDa), carbonic anhydrase (29 kDa), bovine serum albumin (66 kDa), alcohol dehydrogenase (150 kDa), and β-amylase (200 kDa), were used to generate a standard curve of known molecular weights, and the void volume (V_0) of the column was determined using blue dextran (2,000 kDa). The elution volumes (V_e) of the standards were obtained, and the ratios of V_e V_0^{-1} were plotted against the log of their respective molecular weights. The

standard curve was then used to extrapolate the apparent molecular weight of reconstituted LSD1 from its elution volume.

Preparation of Samples for EPR and Mössbauer Spectroscopy. Samples of LSD1 suitable for EPR or Mössbauer spectroscopy were prepared inside of the anaerobic chamber. EPR samples contained 200-300 μM enzyme in Buffer B, and were treated with 2 mM (final concentration) sodium dithionite, and frozen immediately in cold isopentane (-150°C) sitting in a dewar of liquid nitrogen. In some samples, L-serine, L-threonine, or L-cysteine (20 mM each) was added to the reduced protein before freezing. In all cases, the amount of time that elapsed between the addition of dithionite (and the substrate when appropriate) and the freezing of the sample was less than 30 s.

Mössbauer spectra were recorded on proteins that contained ^{57}Fe in place of natural-abundance iron. In all samples, the ^{57}Fe was incorporated into the protein via reconstitution, as described above, and samples contained 250-350 μM protein, and 20 mM L-threonine when appropriate. Samples were frozen within 30 s after adding the substrate to the enzyme.

A.4 Results

Purification and Characterization of Serine Deaminase. The iron-dependent serine deaminases have been reported to be unstable, losing activity quickly during purification, and to some extent, even in the cell [254-256]. In order to maximize purification of active enzyme, the protein was expressed as a fusion construct with a C-

terminal 6X histidine appendage, and purified under anaerobic conditions inside of an anaerobic chamber. The eluted protein was light brown in color, and its UV-visible spectrum displayed features–although not prominent–that are consistent with the presence of an Fe/S cluster (Figure 1.2, solid line). Among these features, the shoulder at 320 nm and the hump at 416 nm are the most defining, as is the broad tailing that extends beyond 700 nm.

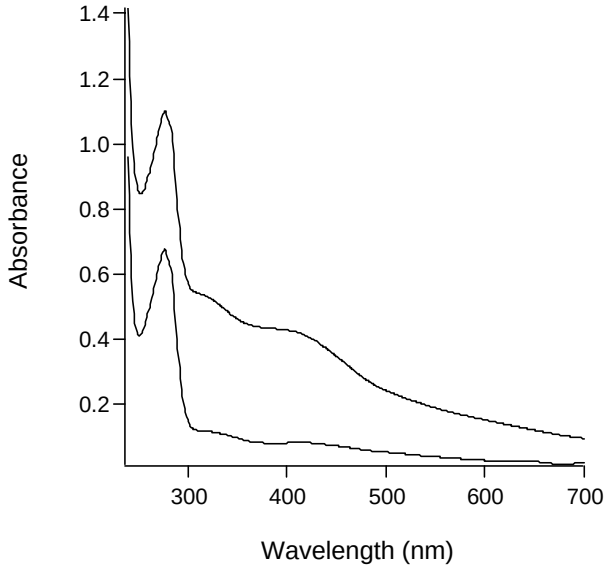

Figure 1.2: UV-visible Spectra of As-isolated (Bottom) and Reconstituted LSD (Top).

An extinction coefficient was determined using apo-LSD1 and the procedure of Gill and von Hippel, and was used to correct the Bradford dye-binding protein assay. It was found that the Bradford assay, using BSA as a standard, overestimates the concentration of LSD1 by a factor of 1.35. Analysis of subsequent aliquots of the as-isolated protein indicated the presence of 1.86 ± 0.46 equiv of iron and 0.670 ± 0.019 equiv of sulfide per polypeptide using the Bradford correction factor.

Reconstitution of Serine Deaminase. Treatment of as-isolated LSD1 with 5 mM DTT and 8 equiv each of $FeCl_3$ and Na_2S resulted in a pronounced change in its color after anaerobic gel-filtration, affording a protein that was intensely brown. Analytical methods revealed that the reconstituted protein contained (8.07 ± 0.03) Fe and (7.44 ± 0.46) S^{2-} per monomer. The quoted uncertainties are the standard deviation of 3 independent analyses, and reflect the individual uncertainties of the protein concentration and the iron and sulfide concentration. The UV-visible spectrum of the reconstituted protein is also shown in Figure 1.2 (dashed line). It displays prominent features at 316 nm and 407 nm. Importantly, the ratio of the feature at 278 nm to that at 407 nm (2.56) decreased significantly from its value in the as-isolated protein (8.33). These features, in combination with the overall spectral envelope of the protein, are most consistent with the formation of [4Fe-4S] clusters upon reconstitution, although it must be emphasized that the types and relative amounts of different Fe/S cluster species cannot be determined with great accuracy from UV-visible spectra. In order to quantitatively determine the composition of the Fe/S cluster(s) in reconstituted LSD1, Mössbauer and EPR spectroscopic experiments were carried out as described below.

Spectroscopic Characterization of Reconstituted Serine Deaminase. Shown in Figure 1.3 A is the Mössbauer spectrum of ^{57}Fe-reconstituted LSD1 recorded at 4.2 K in an externally applied magnetic field of 40 mT oriented parallel to the γ-beam. The prominent features of this spectrum are two sharp lines of similar intensity at -0.13 mm/s and +1 mm/s, and a broad peak at 2.7 mm/s. In addition, there is a featureless component extending from -6 mm/s to +6 mm/s, and a pronounced shoulder at 0.55 mm/s, which is

denoted by an arrow. The two lines at -0.13 mm/s and +1 mm/s belong to a quadrupole doublet of isomer shift, δ = 0.47 mm/s, and quadrupole splitting, ΔE_Q = 1.14 mm/s. These parameters are consistent with the presence of $[4Fe–4S]^{2+}$ clusters associated with the protein. The shoulder at +0.55 mm/s is at a position that is typical of the high energy line of a quadrupole doublet originating from $[2Fe\text{-}2S]^{2+}$ clusters, thus raising the possibility that this cluster form is also present in the sample. The broad component ranging from -6 mm/s to +6 mm/s, and the peak at 2.7 mm/s are often caused by adventitiously bound Fe species in samples of reconstituted Fe/S proteins. Alternatively, these features could arise from paramagnetic Fe/S cluster species, such as $[2Fe\text{-}2S]^{+}$, $[3Fe\text{-}4S]^{+}$, and $[4Fe\text{-}4S]^{+}$ clusters. It is not possible to distinguish and quantify small amounts of these Fe/S cluster forms using Mössbauer spectroscopy alone if they are present. However, the $[2Fe\text{-}2S]^{+}$, $[3Fe\text{-}4S]^{+}$, and $[4Fe\text{-}4S]^{+}$ clusters all have an S = 1/2 electronic ground state and exhibit characteristic EPR spectra. Consequently, we recorded the EPR spectrum of reconstituted LSD1 in the absence of dithionite. The spectrum reveals the presence of a small fraction of $[3Fe\text{-}4S]^{+}$ clusters, which amounts to 0.02 equiv of spin per polypeptide, corresponding to 0.7% of the total Fe in the sample (Figure 3, inset). Such small quantities are beyond the detection limit of Mössbauer spectroscopy and can be neglected for the data analysis. The characteristic features of $[2Fe\text{-}2S]^{+}$ and $[4Fe\text{-}4S]^{+}$ clusters are not observed in the EPR spectrum of reconstituted LSD1 in the absence of dithionite. Therefore, the broad absorption in the Mössbauer spectrum is attributed to adventitiously bound Fe.

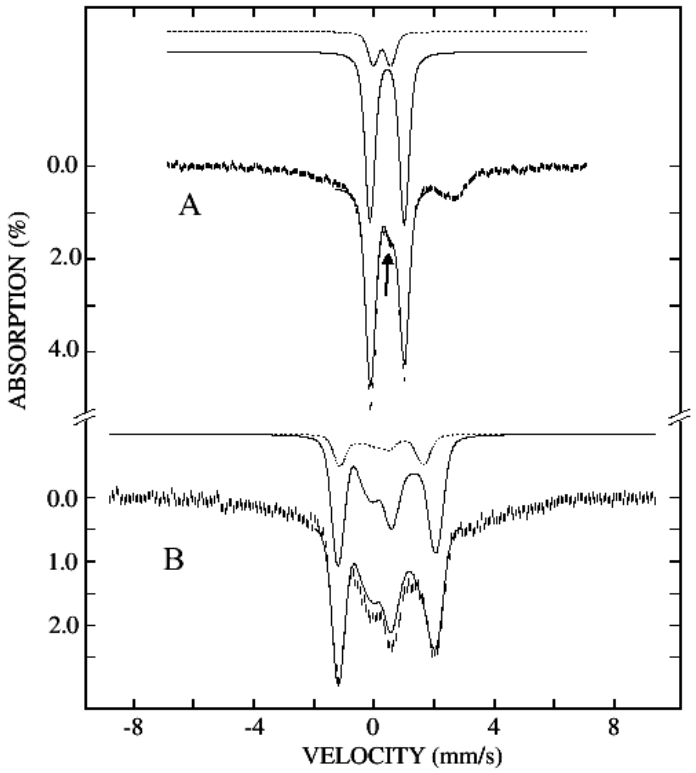

Figure 1.3: Mössbauer Spectra of Reconstituted LSD

In order to determine the parameters and relative amount of the $[4Fe\text{-}4S]^{2+}$ cluster, and to assess the presence of the $[2Fe\text{-}2S]^{2+}$ clusters more rigorously, the spectral envelope was analyzed by fitting the region from –1 mm/s to +2 mm/s. Initially, we fitted the data to only one quadrupole doublet; however, the fit becomes poor at ~0.5 mm/s, which corresponds to the location of the shoulder. Inclusion of a second quadrupole doublet significantly improves the quality of the fit. The more intense quadrupole doublet accounts for 50 ± 5% of the total absorption, and has parameters, δ = 0.47 mm/s and ΔE_Q = 1.14 mm/s, which are indicative of the configuration $[4Fe\text{-}4S]^{2+}$. The less intense quadrupole doublet (10 ± 5 % of the total absorption) has parameters, δ = 0.28 mm/s and ΔE_Q = 0.59 mm/s, which are indicative of the configuration $[2Fe\text{-}2S]^{2+}$.

We emphasize that the parameters for the latter component have a greater uncertainty, because its spectral features are overshadowed by the absorption features emanating from the $[4Fe\text{-}4S]^{2+}$ clusters as well as the adventitiously bound Fe, of which the exact shape is not known. Shown as a solid line overlaid with the experimental data in Figure 1.3A is the result of the least squares fit; the individual spectral components of the $[4Fe\text{-}4S]^{2+}$ and $[2Fe\text{-}2S]^{2+}$ clusters are plotted above the data as dashed and dotted lines, respectively.

To substantiate the presence of $[4Fe\text{-}4S]^{2+}$ and $[2Fe\text{-}2S]^{2+}$ clusters in reconstituted LSD1, we recorded a Mössbauer spectrum in an externally applied field of 8 T oriented parallel to the γ-beam (Figure 1.3B). $[4Fe–4S]^{2+}$ and $[2Fe–2S]^{2+}$ clusters have diamagnetic (S = 0) ground states, resulting in no internal magnetic fields at 4.2 K. Therefore, it is expected that the effective magnetic field at the ^{57}Fe nuclei would equal the externally applied field. The solid line overlaid with the experimental data in Figure 1.3 B is a simulation using the parameters described above and assuming diamagnetism ($S = 0$). The individual components are shown as dashed ($[4Fe\text{-}4S]^{2+}$) and dotted lines ($[2Fe\text{-}2S]^{2+}$) above the data. The quality of the simulation is excellent, and corroborates the presence of $[4Fe\text{-}4S]^{2+}$ and $[2Fe\text{-}2S]^{2+}$ clusters.

EPR spectra of the reconstituted enzyme are consistent with the configurations and stoichiometries of Fe/S species determined by Mössbauer spectroscopy. In the absence of dithionite, the enzyme displays a weak and fairly isotropic signal centered at g = 2.019, which accounts for 0.02 equiv of spin, and which is not observed at temperatures above 50 K at 5 mW power (Figure 1.4, inset), suggesting that the signal emanates from $[3Fe–4S]^{+}$ clusters. Other Fe/S cluster species are not detected. From the analyses of the Mössbauer and EPR spectra, it is possible to determine the stoichiometries of the Fe/S

clusters present in reconstituted LSD1: 1.25 ± 0.25 equiv of $[4Fe–4S]^{2+}$, 0.50 ± 0.25 equiv of $[2Fe–2S]^{2+}$, and 0.02 equiv of $[3Fe–4S]^{+}$ clusters per polypeptide. Upon reduction of LSD1 with dithionite, the spectrum of the $[3Fe–4S]^{+}$ cluster bleaches, and is replaced by a much broader axial signal, displaying $g_{\parallel} = 2.03$ and $g_{\perp} = 1.93$ (Figure 1.4). Quantification of the spin concentration of the signal indicates that it accounts for 78 μM spin, or 0.3 equiv with respect to the protein. A study of the temperature dependence of the signal at 5 mW microwave power (data not shown), indicates that it is maximal at 13 K, and then broadens considerably such that it is no longer visible at temperatures above 45 K. This behavior suggests that the paramagnetic signal derives from a $[4Fe–4S]^{+}$ cluster, and that the $[2Fe–2S]^{2+}$ clusters that are observed by Mössbauer spectroscopy are not reduced under the described experimental conditions. This conclusion stems from the inability to observe a signal above 45 K, and the generally accepted dictum that most [2Fe–2S] clusters are slow relaxing and observable by EPR at temperatures above 77 K [192].

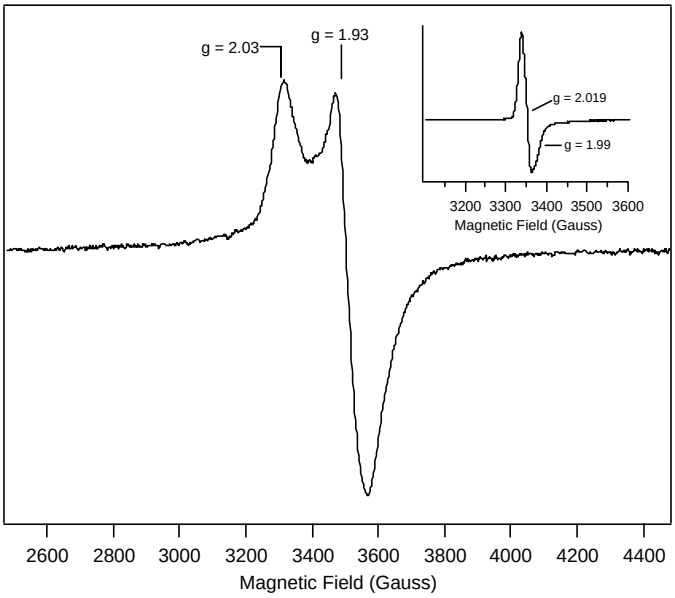

Figure 1.4: EPR of L-Serine Deaminase.

Quantification of Turnover of LSD1. Since the two products of the LSD1 reaction are pyruvate and ammonia, enzyme activity was measured by monitoring the LDH-dependent reduction of pyruvate to lactate at the expense of NADH. LDH will also act on α-ketobutyrate, producing 2-hydroxybutyrate [257], and allowing turnover of L-threonine or L-*allo*-threonine to be monitored by the same method. In the presence of 55 nM enzyme and varying concentrations of L-serine, the reactions were quite fast, and depending on the substrate concentration, were usually complete (all of the substrate was consumed) within 3 minutes of initiation. In some cases, small, but discernible lags were present; however, proper controls indicated that they did not derive from an insufficient amount of the coupling enzyme in the assay. We attribute the lags to either assembly of Fe/S clusters onto polypeptides that are insufficiently reconstituted, or a slow

oligomerization of polypeptides to the active quaternary structure, which is facilitated in the presence of substrate.

In Figure **1.5**, a plot of initial rate as a function of L-serine concentration is displayed, the inset depicting the Lineweaver-Burk representation of the data. A fit of the data to Equation 1 allowed extraction of the kinetic constants k_{cat} (436 s^{-1}) and K_M (2.67 ± 0.25 mM). In the presence of 20 mM substrate, LSD1 catalyzed deamination of L-threonine and L-*allo*-threonine with rates of 0.038 and 0.065 μmol min^{-1}, as compared with 128 μmol min^{-1} for L-serine under identical conditions. [Note that these rates are normalized for the enzyme concentration that was used in each study]. As expected, the enzyme did not catalyze the deamination of D-serine. L-Cysteine was an extremely poor substrate; its deamination took place at a rate that was only slightly above background NADH oxidation. By contrast, both D-serine and L-cysteine were reasonable competitive inhibitors, displaying K_I values of 1.41 ± 0.19 and 0.90 ± 0.09 mM, respectively (Figure **1.6**). L-alanine at concentrations below 25 mM did not inhibit the reaction to any significant extent, and in fact, produced a slight stimulatory effect (data not shown).

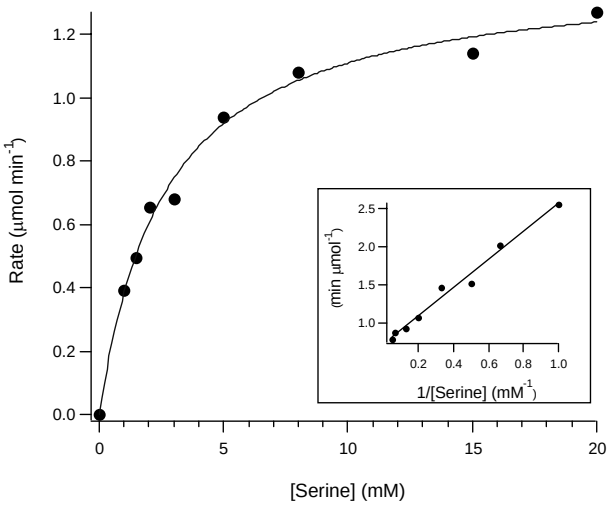

Figure 1.5: Turnover of LSD1 as a function of substrate concentration.

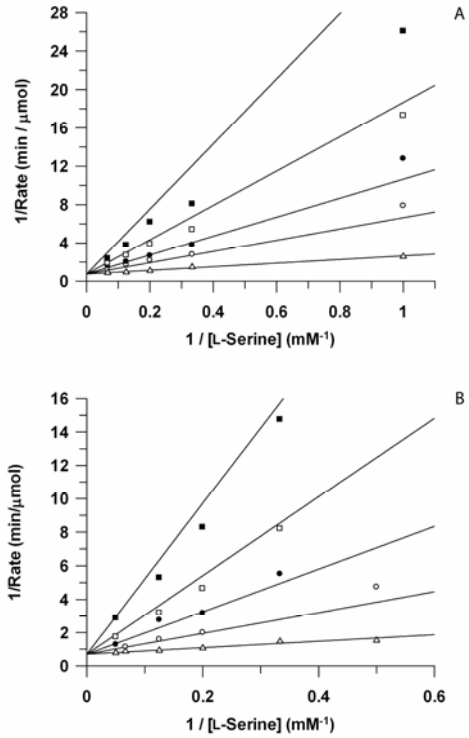

Figure 1.6: Inhibition of LSD1 by D-serine (A) and L-cysteine (B).

In contrast to the reconstituted enzyme, as-isolated LSD1 behaved erratically, making it difficult to obtain good kinetic data on this state of the enzyme. In general, however, its activity was more than 5-fold lower than that of the reconstituted enzyme. It was absolutely critical that dilutions of the reconstituted enzyme be made in Buffer B containing 50% glycerol. We discovered that at lower concentrations of glycerol, the enzyme rapidly lost activity (t1/2 ≈ 30 min), even while sitting on ice in the anaerobic chamber. When 50% glycerol was not part of the diluent, the kinetic profiles displayed cooperative behavior at low concentrations of substrate, followed by what appeared to be substrate inhibition. This behavior can be rationalized by a combination of the instability of the enzyme, and performing the assays in sequence from low substrate to high substrate. At concentrations of substrate near V_{max}, wherein the observed rate does not change significantly as a function of substrate concentration, what appears to be substrate inhibition is simply activity loss that is due to enzyme instability.

Molecular Sieve Chromatography of Serine Deaminase. An analysis of the quaternary structure of LSD1 was undertaken by molecular-sieve chromatography on Superose 200 under anaerobic conditions. The primary sequence of the His-tagged protein indicates a molecular weight of ~51 kDa, consistent with its analysis by SDS-PAGE electrophoresis. A plot of log $V_e\ V_0^{-1}$ versus molecular weight for a series of protein standards was used to generate a standard curve from which the molecular weight of LSD1 was extracted. Peak 1 in the chromatogram elutes with a retention time that corresponds to a protein of 252 kDa, and accounts for a minor (~5%) fraction of the total protein (Figure 1.7). All remaining LSD1 is accounted for in Peak 2, which is highly

uniform and symmetrical in shape. Peak 2 elutes at a retention time that corresponds to a protein of 107 kDa, which is consistent with a dimeric quaternary structure for the overwhelming majority of LSD1 under the conditions outlined in Experimental Procedures. Note that our LSD1 contains a C-terminal 6X histidine tag. Whether the His-tag influences dimerization has not been assessed.

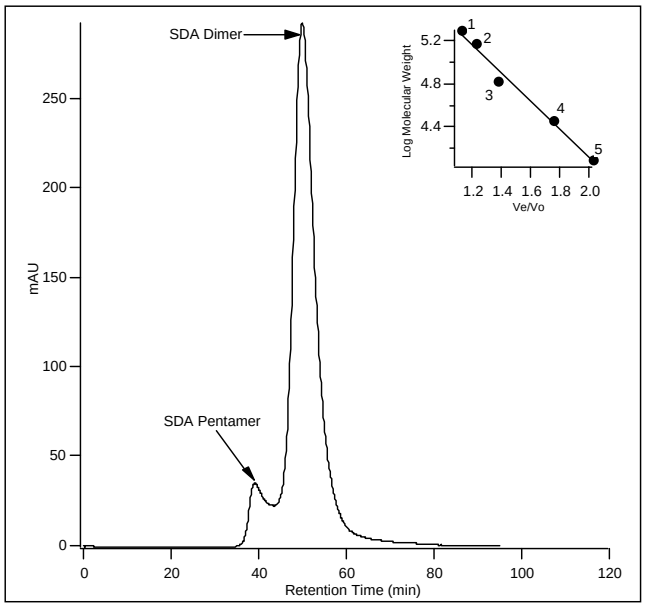

Figure 1.7: Anaerobic molecular sieve chromatography of LSD1.

Interaction of the [4Fe-4S] Cluster with Substrate and Substrate Analogs. In order to determine whether the [4Fe–4S] cluster participates in catalysis or simply acts as a structural element of the protein, we assessed whether the addition of substrate would perturb the Mössbauer or EPR spectra of the samples. Unexpectedly, upon addition of 20 mM L-serine to dithionite-reduced LSD1, the intensity of the EPR spectrum drastically decreased in the < 30 s that it took to freeze the sample (Figure 1.8A); the residual

spectrum shows a very slight broadening of the feature at g = 2.03 (Figure 1.8B, inset). By contrast, the spectra in the presence of L-cysteine, L-threonine, and D-serine are not significantly reduced in intensity, but also show the slight broadening in their features at g = 2.03, which is indicated by the arrows in Figures 1.8B and 1.8B. The spectrum in the presence of L-cysteine is not displayed, since it is identical to those in the presence of L-threonine and D-serine. The marked change in spectral intensity upon addition of the true substrate, but not upon addition of inhibitors or poor substrates, suggests that the amino acid binds to or near the Fe/S cluster, and that the reduction in spectral intensity might be related to turnover.

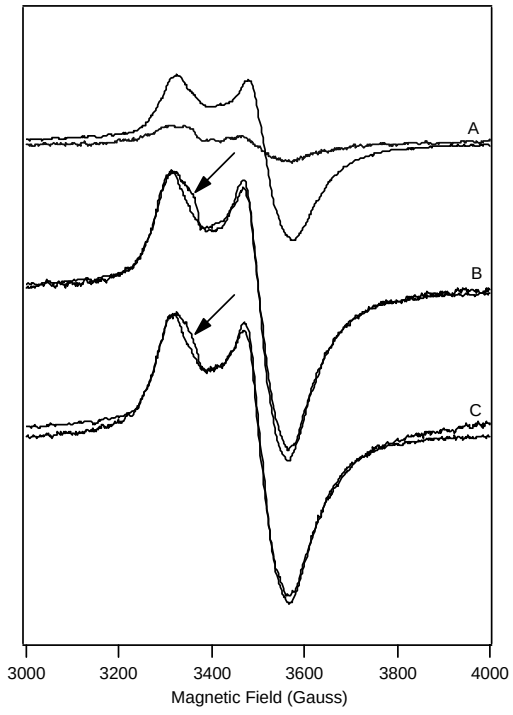

Figure 1.8: X-band EPR spectra of RCN LSD1 in the presence of L-serine (A), L-threonine (B), and D-serine (C).

Mössbauer spectroscopy was also used to probe for interactions between the substrate and the Fe/S cluster. Because small substrate-induced perturbations in the spectrum of the Fe/S cluster are more easily detected in species giving rise to a quadrupole doublet rather than a magnetically split spectrum, the experiment was carried out using reconstituted LSD1 that was not treated with dithionite, and which contained 50 ± 5% of the Fe in the form of $[4Fe–4S]^{2+}$ clusters. L-threonine was employed as the added substrate, because it is turned over significantly slower than L-serine (vide supra), but gives rise to the same perturbation of the EPR spectrum of the $[4Fe–4S]^{+}$ cluster. The Mössbauer spectrum of reconstituted LSD1 (350 μM) in the presence of 20 mM L-threonine was identical to the spectrum of reconstituted LSD1 in the absence of substrate (i.e. the Mössbauer spectrum is not perturbed by L-threonine).

A.5 Discussion

In this study we described the biochemical and biophysical characterization of *E. coli* L-serine deaminase containing an N-terminal 6X His-tag. When overexpressed in *E. coli*, the isolated protein contained small amounts of iron and sulfide (1.86 ± 0.46 Fe and 0.670 ± 0.019 S^{2-} per monomer), and displayed a weak UV-visible spectrum in the 300–700-nm region that is consistent with the presence of [4Fe–4S] clusters. Anaerobic treatment of the protein with $FeCl_3$ and Na_2S in the presence of DTT resulted in the uptake of substantial amounts of iron and sulfide, as well as a dramatic increase in the activity of the protein. We used a combination of UV-visible, EPR, and Mössbauer spectroscopies together with analytical methods to assess the configuration of all species

of iron on the protein subsequent to reconstitution, as well as their relative stoichiometries. We found that the predominant configuration was $[4Fe\text{-}4S]^{2+}$ (1.25 ± 0.25 equiv per polypeptide), accounting for greater than 50% of the total iron associated with the protein. Other Fe/S-cluster forms detected included 0.5 ± 0.25 equiv of $[2Fe\text{-}2S]^{2+}$, and ~0.02 equiv of $[3Fe\text{-}4S]^{+}$ clusters per polypeptide. The large uncertainty in each value reflects the individual errors of three different methods, which are the determination of protein and iron concentrations, and the quantification of various configurations of iron by Mössbauer spectroscopy.

We argue, as has been previously proposed [239, 240], that the catalytically active form contains one $[4Fe–4S]^{2+}$ cluster, and that the other cluster species are artifacts of the reconstitution procedure.[2] Indeed, the protein contains 9 cysteine residues, which can contribute to the coordination of adventitious iron, especially if any of the cysteines are on the surface of the protein. The thermodynamic stability of Fe/S clusters is well documented, and [4Fe–4S] and most likely [2Fe–2S] clusters, which are coordinated by exogenous thiolate ligands (e.g. DTT) are present in solution under reconstitution conditions [258]. Spectroscopically, such species are not expected to be discernible from genuine Fe/S cofactors. Potentially, these clusters may bind to surface-exposed cysteine residues of the protein, forming clusters of the general formula $[4Fe–4S]DTT_nCys_{4-n}$, which may not be separated from the protein by gel filtration chromatography.

We demonstrated that the reconstituted enzyme is catalytically active, converting L-serine to pyruvate and ammonia with a k_{cat} of 436 s^{-1}. L-threonine and L-*allo*-threonine were also turned over, albeit significantly slower, whereas L-cysteine and D-serine were found to be competitive inhibitors. In contrast, the as-isolated enzyme did not yield

reliable kinetic data, which we attribute to its lability and cofactor deficiency. These studies support our contention that the catalytically active state of LSD1 contains a [4Fe–4S] cluster.

Our model for the deamination of L-serine by LSD1 is based on the elegant work of Beinert, Kennedy, Emptage, Münck and collaborators on the enzyme aconitase [250], which catalyzes the interconversion of citrate and isocitrate. The first step involves the dehydration of citrate to form *cis*-aconitate, which is subsequently rehydrated, affording isocitrate. In its resting state, the enzyme contains a $[4Fe–4S]^{2+}$ cluster that is ligated to the protein via three cysteine residues that are coordinated to three of the irons of the cluster, termed Fe_b. The fourth iron, Fe_a, is not coordinated by a cysteine residue, but contains a bound hydroxyl (water) group. In addition, the hydroxyl group of the substrate, as well as one of the substrate carboxylate groups, ligate iron Fe_a in a bidentate fashion, resulting in hexacoordination at this site. The Fe/S cluster is thought to facilitate loss of the hydroxyl group by acting as a Lewis acid [250].

A similar role has been proposed for the Fe/S cluster of LSD1 [239, 240], and a mechanism for deamination of L-serine is shown in Figure 1.9. Coordination of the hydroxyl group of L-serine (**1**) to the unique iron of the Fe/S cluster (**2**) allows elimination of the hydroxyl group–presumably with general-acid assistance–and formation of 2-amino-2-propenoic acid. Tautomerization of this species gives rise to 2-imino-propionic acid (**3**), which is subsequently hydrolyzed to ammonia and pyruvate.

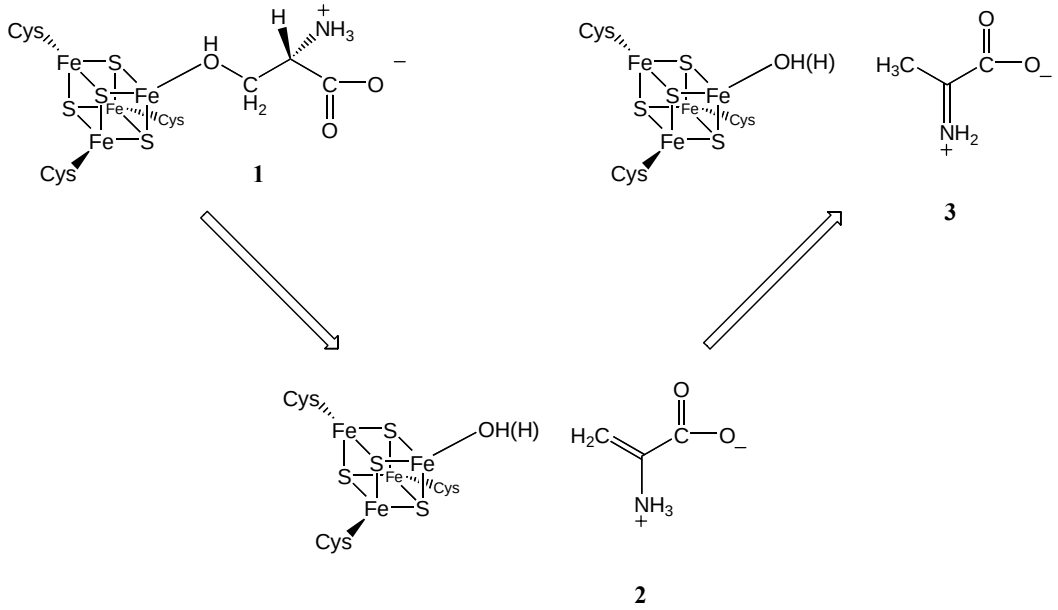

Figure 1.9: Proposed Role for the [4Fe-4S] Cluster of LSD1 in Catalysis.

In aconitase, a wealth of spectroscopic evidence supports the role of the unique Fe site in binding substrate and facilitating loss of the hydroxyl group. Upon addition of substrate, the electronic structure of the $[4Fe–4S]^{2+}$ cluster changes significantly, as evidenced by changes of the Mössbauer parameters of site Fe_a, which depend on the nature of the substrate bound: $\delta = 0.44$ mm/s and $\Delta E_Q = 0.83$ mm/s (no substrate), $\delta = 0.84$ mm/s and $\Delta E_Q = 1.26$ mm/s (isocitrate), and $\delta = 0.89$ mm/s and $\Delta E_Q = 1.83$ mm/s (citrate) [250, 259-261]. In addition, the EPR spectrum of the $[4Fe–4S]^{+}$ cluster changes significantly upon substrate addition, with the principal g-values shifting from 2.06, 1.93, and 1.86, to 2.04, 1.85, and 1.78, respectively [250, 260]. The exact mode of binding of substrates to the Fe/S cluster was established by ^{57}Fe, ^{33}S, ^{15}N, and ^{17}O electron-nuclear double-resonance spectroscopy (ENDOR) [220, 262-264], and was subsequently confirmed by x-ray crystallography [265]. Other enzymes containing a [4Fe–4S] cluster,

in which only three Fe sites are coordinated by cysteinate ligands from the protein, include the enzymes of the radical SAM superfamily. The co-substrate or cofactor, S-adenosyl-L-methionine (SAM), coordinates to the fourth Fe site in a bidentate fashion via the amino and carboxylate substituents of the molecule [155, 266], causing significant changes of the EPR and Mössbauer spectroscopic properties of the cluster. For example, in pyruvate formate–lyase (PFL) activase, the Mössbauer parameters of Fe_a of the $[4Fe–4S]^{2+}$ cluster change from $\delta = 0.42$ mm/s and $\Delta E_Q = 1.12$ mm/s to $\delta = 0.72$ mm/s and $\Delta E_Q = 1.15$ mm/s upon addition of SAM. Binding of SAM also perturbs the EPR spectrum of the $[4Fe–4S]^{+}$ cluster of PFL activase; the observed g-values shift from 2.01 and 1.94 to 2.01, 1.89, and 1.88 [118, 195]. In biotin synthase (BioB), another member of the radical SAM superfamily, addition of SAM perturbs the Mössbauer parameters of two Fe sites of the $[4Fe–4S]^{2+}$ cluster. In the absence of SAM, both sites have $\delta = 0.47$ mm/s and $\Delta E_Q = 1.10$ mm/s, which convert to $\delta = 0.40$ mm/s and $\Delta E_Q = 0.86$ mm/s, and $\delta = 0.64$ mm/s and $\Delta E_Q = 1.26$ mm/s, respectively, in the presence of SAM. In analogy to PFL activase and aconitase, the EPR spectrum of the $[4Fe–4S]^{+}$ cluster of BioB is sensitive to the presence of SAM; the principal g-values shift from 2.04 and 1.94 to 2.00, 1.93, and 1.85 [267].

In contrast to the significant changes in the EPR and Mössbauer spectra of aconitase and the radical SAM enzymes upon binding of substrate, we observe comparatively small changes in the EPR spectra of the $[4Fe–4S]^{+}$ cluster in the presence of L-serine, L-threonine, L-*allo*-threonine, or D-serine. The changes, however, are nearly identical for all of these substrates, suggesting that they interact with the [4Fe–4S] cluster

in a similar way. The Mössbauer spectrum of LSD1 in the presence of L-threonine revealed no discernable changes compared to the spectrum of reconstituted LSD1. We point out, however, that for aconitase and the radical SAM enzymes, the unique Fe site has coordination numbers of 6 and 5, respectively, when the substrate is bound. In the absence of substrate, their Mössbauer parameters for Fe_a are similar to those typically observed for cysteinate-ligated Fe sites of $[4Fe–4S]^{2+}$ clusters. The changes in the Mössbauer parameters upon substrate binding are thus likely to be a consequence of the increased coordination number. Our combined EPR and Mössbauer spectroscopic studies suggest that L-serine might displace the fourth ligand coordinated to Fe_a in LSD1, which is presumably a water (hydroxide) molecule, and coordinates the iron in a monodentate fashion (Figure 1.9). In support of this hypothesis, it has been proposed that coordination of L-serine to the Fe/S cluster of LSD1 is most likely monodentate, involving only the hydroxyl group of the substrate, because simultaneous coordination of the hydroxyl group and either the amino or the carboxylate group would not permit proper orbital alignment for effective elimination of water (hydroxide) from the substrate [239].

Three related serine deaminases have been described in some detail. These are the enzymes from *Peptostreptococcus asaccharolyticus* [239], *Clostridium propionicum* [248], and *Clostridium sticklandii* [268]. Each of these proteins is activated by iron and DTT; however, the nature of the iron-containing cofactor has been demonstrated only in the enzyme from *P. asaccharolyticus*. Upon purification of the enzyme under anaerobic conditions, it displayed a rhombic EPR signal (g_1 = 2.001, g_2 = 2.014, g_3 = 2.028) in phosphate buffer at pH 5, and a fairly axial signal around g = 2.01 in Tricine–KOH buffer

(pH 8.0). Both signals broadened considerably as the temperature was raised, such that they were no longer visible above 30 K. These g-values and temperature-dependent properties were taken to indicate the presence of $[3Fe–4S]^{+}$ clusters [249]. Interestingly, the addition of high concentrations of L-serine in each case caused the two signals to converge into signals of similar shape. The authors concluded that the substrate must bind in proximity to the cluster, protecting it from buffer solutes, which affect the properties of the EPR spectrum of the protein [249]. We emphasize that this form of the Fe/S cluster is believed not to be catalytically relevant, and that effects of substrate on the cluster probably are unrelated to direct interaction, since the missing iron is presumably the one to which the substrate binds. Efforts to observe the catalytically relevant form of the Fe/S cluster were unsuccessful; the cluster was not amenable to reduction to the $[4Fe–4S]^{+}$ state by chemical methods (sodium dithionite) or by photoreduction.

In conclusion, we have demonstrated for the first time, and thereby confirmed the hypothesis that catalytically active LSD1 requires [4Fe–4S] clusters for catalysis. The proposed role of the [4Fe–4S] cluster is coordination of the hydroxyl group of the substrate, thus facilitating its elimination. Tests of this model are currently under investigation. In particular, the finding that LSD1 can be reduced to the $[4Fe–4S]^{+}$ state renders the protein amenable to study by other forms of spectroscopy that can unequivocally establish the exact nature of the interaction between the substrate and the Fe/S cluster.

A.6 References

1. Mudd, S.H., J.D. Finkelstein, F. Irreverre, and L. Laster, Threonine dehydratase activity in humans lacking cystathionine synthase. *Biochem Biophys Res Commun*, 1965. **19**(5): p. 665-70.
2. Ogawa, H., T. Gomi, K. Konishi, T. Date, H. Nakashima, K. Nose, Y. Matsuda, C. Peraino, H.C. Pitot, and M. Fujioka, Human liver serine dehydratase. cDNA cloning and sequence homology with hydroxyamino acid dehydratases from other sources. *J Biol Chem*, 1989. **264**(27): p. 15818-23.
3. Umbarger, H.E., Threonine deaminases. *Adv Enzymol Relat Areas Mol Biol*, 1973. **37**: p. 349-95.
4. Dowhan, W., Jr. and E.E. Snell, D-serine dehydratase from Escherichia coli. 3. Resolution of pyridoxal 5'-phosphate and coenzyme specificity. *J Biol Chem*, 1970. **245**(18): p. 4629-35.
5. Dowhan, W., Jr. and E.E. Snell, D-serine dehydratase from Escherichia coli. II. Analytical studies and subunit structure. *J Biol Chem*, 1970. **245**(18): p. 4618-28.
6. Marceau, M., E. McFall, S.D. Lewis, and J.A. Shafer, D-serine dehydratase from Escherichia coli. DNA sequence and identification of catalytically inactive glycine to aspartic acid variants. *J Biol Chem*, 1988. **263**(32): p. 16926-33.
7. Brown, E.A., R. D'Ari, and E.B. Newman, A relationship between L-serine degradation and methionine biosynthesis in Escherichia coli K12. *J Gen Microbiol*, 1990. **136 (Pt 6)**: p. 1017-23.

8. Yanofsky, C. and I.P. Crawford, in *The Enzymes*, P.D. Boyer, Editor. 1972, Academic Press: New York. p. 1-31.

9. Davis, L. and D.E. Metzler, in *The Enzymes*, P.D. Boyer, Editor. 1972, Academic Press: New York. p. 33-74.

10. Grabowski, R., A.E. Hofmeister, and W. Buckel, Bacterial L-serine dehydratases: a new family of enzymes containing iron-sulfur clusters. *Trends Biochem Sci*, 1993. **18**(8): p. 297-300.

11. Flint, D.H. and R.M. Allen, Iron–Sulfur Proteins with Nonredox Functions. *Chem Rev*, 1996. **96**(7): p. 2315-2334.

12. Hesslinger, C., S.A. Fairhurst, and G. Sawers, Novel keto acid formate-lyase and propionate kinase enzymes are components of an anaerobic pathway in Escherichia coli that degrades L-threonine to propionate. *Mol Microbiol*, 1998. **27**(2): p. 477-92.

13. Su, H.S., B.F. Lang, and E.B. Newman, L-serine degradation in Escherichia coli K-12: cloning and sequencing of the sdaA gene. *J Bacteriol*, 1989. **171**(9): p. 5095-102.

14. Shao, Z. and E.B. Newman, Sequencing and characterization of the sdaB gene from Escherichia coli K-12. *Eur J Biochem*, 1993. **212**(3): p. 777-84.

15. Su, H., J. Moniakis, and E.B. Newman, Use of gene fusions of the structural gene sdaA to purify L-serine deaminase 1 from Escherichia coli K-12. *Eur J Biochem*, 1993. **211**(3): p. 521-7.

16. Newman, E.B., C. Walker, and K. Ziegler-Skylakakis, A possible mechanism for the in vitro activation of L-serine deaminase activity in Escherichia coli K12. *Biochem Cell Biol*, 1990. **68**: p. 723-728.

17. Carter, J.E. and R.D. Sagers, Ferrous ion-dependent L-serine dehydratase from Clostridium acidiurici. *J Bacteriol*, 1972. **109**(2): p. 757-63.

18. Grabowski, R. and W. Buckel, Purification and properties of an iron-sulfur-containing and pyridoxal-phosphate-independent L-serine dehydratase from Peptostreptococcus asaccharolyticus. *Eur J Biochem*, 1991. **199**(1): p. 89-94.

19. Hofmeister, A.E., R. Grabowski, D. Linder, and W. Buckel, L-serine and L-threonine dehydratase from Clostridium propionicum. Two enzymes with different prosthetic groups. *Eur J Biochem*, 1993. **215**(2): p. 341-9.

20. Hofmeister, A.E., S.P. Albracht, and W. Buckel, Iron-sulfur cluster-containing L-serine dehydratase from Peptostreptococcus asaccharolyticus: correlation of the cluster type with enzymatic activity. *FEBS Lett*, 1994. **351**(3): p. 416-8.

21. Beinert, H., M.C. Kennedy, and C.D. Stout, Aconitase as Iron-Sulfur Protein, Enzyme, and Iron-Regulatory Protein. *Chem Rev*, 1996. **96**: p. 2335-2373.

22. Bradford, M.M., *Anal Biochem*, 1976. **72**: p. 248-254.

23. Kennedy, M.C., T.A. Kent, M. Emptage, H. Merkle, H. Beinert, and E. Münck, Evidence for the Formation of a Linear [3Fe-4S] Cluster in Partially Unfolded Aconitase. *J Biol Chem*, 1984. **259**(23): p. 14463-14471.

24. Beinert, H., Micro Methods for the Quantitative Determination of Iron and Copper in biological Material. *Methods Enzymol*, 1978. **54**: p. 435-445.

25. Beinert, H., Semi-micro Methods for Analysis of Labile Sulfide and of Labile Sulfide plus Sulfane Sulfur in Unusually Stable Iron-Sulfur Proteins. *Anal Biochem*, 1983. **131**: p. 373-378.

26. Gill, S.C. and P.H. von Hippel, Calculation of protein extinction coefficients from amino acid sequence data. *Anal Biochem*, 1989. **182**(2): p. 319-26.

27. Leatherbarrow, R.J., *GraFit Version 5*. 2001, Horley, UK: Erithacus Software Ltd.

28. Hofmeister, A.E.M., S. Textor, and W. Buckel, Cloning and Expression of the Two Genes Coding for L-Serine Dehydratase from *Peptostreptococcus asaccharolyticus*: Relationship of the Iron–Sulfur Protein to Both L-Serine Dehydratases from *Escherichia coli. J Bacteriol*, 1997. **179**(15): p. 4937-4941.

29. Newman, E.B. and V. Kapoor, In vitro studies on L-serine deaminase activity of *Escherichia coli* K12. *Can J Biochem*, 1980. **58**: p. 1292-1297.

30. Newman, E.B., D. Dumont, and C. Walker, In Vitro and In Vivo Activation of L-Serine Deaminase in *Escherichia coli* K-12. *J Bacteriol*, 1985. **162**(3): p. 1270-1275.

31. Orme-Johnson, W.H. and N.R. Orme-Johnson, *Iron-sulfur proteins: The problem of determining cluster type.*, in *Iron-Sulfur Proteins*, T.G. Spiro, Editor. 1982, John Wiley & Sons: New York.

32. Meister, A., Reduction of β-γ-Diketo and γ-Keto Acids Catalyzed by Muscle Preparations and by Crystalline Lactic Dehydrogenase. *J Biol Chem*, 1950. **184**: p. 117-129.

33. Venkateswara Rao, P. and R.H. Holm, Synthetic Analogues of the Active Sites of Iron–Sulfur Proteins. *Chem Rev*, 2004. **104**: p. 527-559.

34. Kent, T.A., M.H. Emptage, H. Merkle, M.C. Kennedy, H. Beinert, and E. Munck, Mossbauer studies of aconitase. Substrate and inhibitor binding, reaction intermediates, and hyperfine interactions of reduced 3Fe and 4Fe clusters. *J Biol Chem*, 1985. **260**(11): p. 6871-81.

35. Emptage, M.H., T.A. Kent, M.C. Kennedy, H. Beinert, and E. Munck, Mossbauer and EPR studies of activated aconitase: development of a localized valence state at a subsite of the [4Fe-4S] cluster on binding of citrate. *Proc Natl Acad Sci U S A*, 1983. **80**(15): p. 4674-8.

36. Moura, J.J., I. Moura, T.A. Kent, J.D. Lipscomb, B.H. Huynh, J. LeGall, A.V. Xavier, and E. Munck, Interconversions of [3Fe-3S] and [4Fe-4S] clusters. Mossbauer and electron paramagnetic resonance studies of Desulfovibrio gigas ferredoxin II. *J Biol Chem*, 1982. **257**(11): p. 6259-67.

37. Werst, M.M., M.C. Kennedy, H. Beinert, and B.M. Hoffman, 17O, 1H, and 2H electron nuclear double resonance characterization of solvent, substrate, and inhibitor binding to the [4Fe-4S]+ cluster of aconitase. *Biochemistry*, 1990. **29**(46): p. 10526-32.

38. Werst, M.M., M.C. Kennedy, A.L. Houseman, H. Beinert, and B.M. Hoffman, Characterization of the [4Fe-4S]+ cluster at the active site of aconitase by 57Fe, 33S, and 14N electron nuclear double resonance spectroscopy. *Biochemistry*, 1990. **29**(46): p. 10533-40.

39. Telser, J., M.H. Emptage, H. Merkle, M.C. Kennedy, H. Beinert, and B.M. Hoffman, 17O electron nuclear double resonance characterization of substrate binding to the [4Fe-4S]1+ cluster of reduced active aconitase. *J Biol Chem*, 1986. **261**(11): p. 4840-6.

40. Kennedy, M.C., M. Werst, J. Telser, M.H. Emptage, H. Beinert, and B.M. Hoffman, Mode of substrate carboxyl binding to the [4Fe-4S]+ cluster of reduced aconitase as studied by 17O and 13C electron-nuclear double resonance spectroscopy. *Proc Natl Acad Sci U S A*, 1987. **84**(24): p. 8854-8.

41. Lauble, H., M.C. Kennedy, H. Beinert, and C.D. Stout, Crystal structures of aconitase with isocitrate and nitroisocitrate bound. *Biochemistry*, 1992. **31**(10): p. 2735-48.

42. Walsby, C.J., W. Hong, W.E. Broderick, J. Cheek, D. Ortillo, J.B. Broderick, and B.M. Hoffman, Electron-Nuclear Double Resonance Spectroscopic Evidence That S-Adenosylmethionine Binds in Contact with the Catalytically Active [4Fe-4S]$^{+}$ Cluster of Pyruvate Formate-Lyase Activating Enzyme. *J Am Chem Soc*, 2002. **124**(12): p. 3143-3151.

43. Chen, D., C. Walsby, B.M. Hoffman, and P.A. Frey, Coordination and mechanism of reversible cleavage of S-adenosylmethionine by the [4Fe-4S] center in lysine 2,3-aminomutase. *J Am Chem Soc*, 2003. **125**(39): p. 11788-9.

44. Krebs, C., W.E. Broderick, T.F. Henshaw, J.B. Broderick, and B.H. Huynh, Coordination of Adenosylmethionine to a Unique Iron Site of the [4Fe–4S] of Pyruvate Formae–Lyase Activating Enzyme: A Mössbauer Spectroscopic Study. *J Am Chem Soc*, 2002. **124**(6): p. 912-913.

45. Krebs, C., T.F. Henshaw, J. Cheek, B.H. Huynh, and J.B. Broderick, Conversion of 3Fe–4S to 4Fe–4S Clusters in Native Pyruvate Formate-Lyase Activating Enzyme: Mössbauer Characterization and Implications for Mechanism. *J Am Chem Soc*, 2000. **122**(50): p. 12497-12506.

46. Cosper, M.M., G.N.L. Jameson, R. Davydov, M.K. Eidsness, B.M. Hoffman, B.H. Huynh, and M.K. Johnson, The [4Fe–4S]2+ Cluster in Reconstituted Biotin Synthase Binds S-Adenosyl-L-methinine. *J Am Chem Soc*, 2002. **124**(47): p. 14006-14007.

47. Zinecker, H., J.R. Andreesen, and A. Pich, Partial purification of an iron-dependent L-serine dehydratase from Clostridium sticklandii. *J Basic Microbiol*, 1998. **38**(2): p. 147-155.

Footnotes

[1]Abbreviations: BSA, bovine serum albumin; DTT, dithiothreitol; EPPS, N-(2-hydroxyethyl)piperazine-N'-3-propanesulfonate; EPR, electron paramagnetic resonance; Fe/S, iron–sulfur; HEPES, N-(2-hydroxyethyl)piperazine-N'-2-ethanesulfonate; IPTG, isopropyl-β-D-thiogalactopyranoside; LDH, lactate dehydrogenase; LSD, L-serine deaminase; NAD, nicotinamide adenine dinucleotide; NADH, nicotinamide adenine dinucleotide (reduced form); Ni-NTA, nickel nitrilotriacetic acid; PLP, pyridoxal 5'-phosphate; SAM, S-adenosyl-L-methionine; S/T, serine/threonine.

[2]In accord with this hypothesis, site-directed mutagenesis studies indicate that only three of the nine cysteine residues are essential for catalysis, since their substitution with non-sulfur containing amino acids results in abolishment of catalytic activity. These cysteines presumably are those that ligate the [4Fe–4S] cluster. Similar substitutions of the remaining cysteine residues either produce relatively slight decreases or increases in activity (Zhao et al, manuscript in preparation).

Figure legends

Figure 1. UV-visible spectra of as-isolated LSD1 (solid line) and reconstituted LSD1 (dashed line). Both proteins were diluted into Buffer B to final concentrations of 16.4 μM (as-isolated LSD1) and 10.8 μM (reconstituted LSD1).

Figure 2. Mössbauer spectra of ^{57}Fe-reconstituted LSD1 recorded at 4.2 K in an externally applied field (oriented parallel to the γ-beam) of (A) 40 mT and (B) 8 T. The solid line overlaid with the experimental data (hashed marks) are simulations representing the contribution from the $[4Fe\text{-}4S]^{2+}$ and $[2Fe\text{-}2S]^{2+}$ clusters. The individual spectral components of these two clusters are plotted as dashed ($[4Fe\text{-}4S]^{2+}$) and dotted ($[2Fe\text{-}2S]^{2+}$) lines above the experimental data for clarity. The parameters used for the simulation are given in the text.

Figure 3. X-band EPR spectra of reconstituted LSD1 reduced with 2 mM dithionite. Conditions of measurement were: microwave power, 5 mW; receiver gain, 2×10^4; modulation amplitude, 10 G; temperature, 13 K; microwave frequency, 9.65 GHz. Inset. Reconstituted LSD1 before reduction with dithionite, obtained under identical conditions.

Figure 4. Turnover of LSD1 as a function of substrate concentration. Assays were carried out as described in Materials and Methods. The concentration of LSD1 in each assay was 55 nM, and the concentration of L-serine was varied between 0 and 20 mM. The solid line represents a fit to Equation 1, yielding V_{max} = 1.41 μmol min^{-1} and K_M = 2.67 ± 0.25 mM. The inset is a Lineweaver-Burk plot of the data.

Figure 5. Inhibition of LSD1 by D-serine (top panel) and L-cysteine (bottom panel). Assays were carried out as described in Experimental Procedures. The concentration of LSD1 in each assay was 55 nM. Bottom panel, L-serine was varied between 2 and 20 mM at 0 (open triangles), 2 (open circles), 5 (closed circles), 10 (open squares) and 20 (closed squares) mM cysteine. Top panel, L-serine was varied between 1 and 15 mM at 0 (open triangles), 3 (open circles), 6 (closed circles), 12 (open squares), and 24 (closed squares) mM D-serine. Lineweaver–Burk plots were constructed by multiple non-linear regression analysis of the data to Equation 3 using the GraFit software program.

Figure 6. Molecular Sieve Chromatography of LSD1. Gel-filtration experiments were carried out as described in Materials and Methods. The void volume (V_0) of the column was determined using blue dextran. The elution volumes (V_e) of standards were obtained, and the log of their respective molecular weights were plotted versus the ratio of V_e V_0^{-1}. The standard

curve was used to extrapolate the apparent molecular weight of reconstituted LSD1 from its elution volume. Peak 1 corresponds to a mass of 253 kDa (pentamer). Peak 2 corresponds to a mass of 107 kDa (dimer). Inset. Standard curve. **1**, amylase (200 kDa); **2**, alcohol dehydrogenase (150 kDa); **3**, bovine serum albumin (66 kDa); **4**, carbonic anhydrase (29 kDa); **5** (cytochrome c, 12.4 kDa).

Figure 7. X-band EPR spectra of reconstituted LSD1 in the presence of (A) L-serine (B) L-threonine, and (C) D-serine. Conditions of measurement were: microwave power, 5 mW; receiver gain, 2 x 104; modulation amplitude, 10 G; temperature, 13 K; microwave frequency, 9.65 GHz. In each case, the dashed line is reconstituted LSD1 reduced with 2 mM dithionite in the absence of added amino acids, which is shown for comparison. Spectra obtained in the presence of L-threonine and D-serine were multiplied by 1.75 to make their intensities similar to that of the dashed spectrum in order to better compare the broadening in the feature at 2.03 (arrows). The spectrum in the presence of L-cysteine is not displayed, since it is identical to those in the presence of D-serine and L-threonine.

Appendix B

Quinolinate Synthetase Binds a [4Fe-4S] cluster that is Requisite for Catalysis

B.1 Abstract

Quinolinic acid is an intermediate in the biosynthesis of nicotinamide-containing redox cofactors. The ultimate step in the formation of quinolinic acid in prokaryotes is the condensation of IS and dihydroxyacetone phosphate, which is catalyzed by the product of the *nadA* gene in *Escherichia coli*. A combination of UV-visible, Mössbauer, and EPR spectroscopies, along with analytical methods for the determination of iron and sulfide, demonstrate for the first time that anaerobically purified quinolinate synthetase (NadA) from *E. coli* contains one [4Fe-4S] cluster per polypeptide. The protein is active, catalyzing the formation of quinolinic acid with a V_{max} $[E_T]^{-1}$ of 0.01 s^{-1}.

B.2 Introduction

The initial steps in the biosynthesis of nicotinamide adenine dinucleotide (NAD), the primary biological cofactor for oxidation–reduction (redox) reactions, vary considerably between prokaryotes and eukaryotes, although both pathways involve the common intermediate, quinolinic acid [1]. In most eukaryotic organisms, quinolinic acid is produced via degradation of the amino acid L-tryptophan via an "aerobic" pathway, requiring the activities of several enzymes that use molecular oxygen as a substrate [1, 2]. Alternatively, *Escherichia coli* and most other prokaryotes generate quinolinic acid via a

unique condensation reaction between dihydroxyacetone phosphate (DHAP) and iminosuccinate (IS) in an "anaerobic" pathway (Figure 2.1) [3, 4]. This reaction requires the concerted efforts of two proteins, quinolinate synthetase (NadA) and aspartate oxidase (NadB). The mechanism of NadB has been studied in fair detail; the enzyme contains a flavin cofactor, which accepts a hydride equivalent from *L*-aspartate, affording IS, one of the substrates for NadA [5-8]. In contrast to NadB, there has been very little characterization of the NadA-dependent reaction or the enzyme itself, attributable in part to the sensitivity of the protein to molecular oxygen, as well as its production in inclusion bodies upon overexpression of the gene in *E. coli*,[9] characteristics that have led to the proposal that the enzyme might harbor an oxygen-sensitive iron–sulfur (Fe/S) cluster[4]. Moreover, the protein contains nine cysteine residues, three of which reside in a CX_2CX_2C motif,[10] a common pattern observed in proteins that contain [4Fe–4S] clusters, and deletion of the *E. coli iscS* gene, which is believed to mobilize sulfur for Fe/S cluster biosynthesis, renders the bacterium auxotrophic for nicotinic acid [11]. Herein we show that coexpression of the *nadA* gene with plasmid pDB1282, which contains the *isc* operon from *Azotobacter vinelandii*, allows for production of ample amounts of soluble protein. Characterization of the protein by UV-visible, electron paramagnetic resonance (EPR), and Mössbauer spectroscopies shows unequivocally that it contains one [4Fe–4S] cluster per polypeptide.

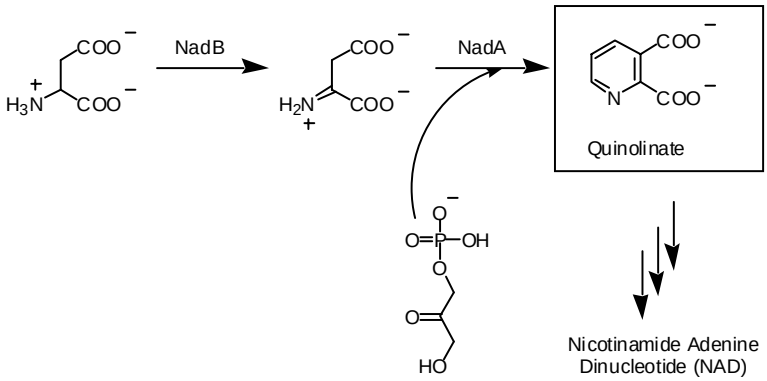

Figure 2.1: Anerobic pathway towards NAD^+ biosynthesis.

B.3 Results and Disscussion

The *nadA* gene was cloned by PCR into plasmid pET-28A (confers kanamycin resistance)–which is IPTG-inducible and under the control of the T7 promoter–such that the protein is produced with an N-terminal hexahistidine tag that is separated from the natural N-terminal methionine residue by a linker of 10 amino acids. The plasmid was transformed into *E. coli* BL21(DE3) that also harbored plasmid pDB1282 (confers ampicillin resistance), which contains the genes of the *A. vinelandii isc* operon under the control of an arabinose-inducible promoter. The isc-related genes were induced first by addition of arabinose (0.05% final concentration) at an OD_{600} of 0.3, followed by induction of the *nadA* gene by addition of IPTG (200 μM final concentration) at an OD_{600} of 0.6. The protein was then isolated in a Coy anaerobic chamber (≤1 ppm O_2) as described previously for the isolation of lipoyl synthase [12].

NadA, overproduced and purified in this fashion, is brown in color, and its UV-vis spectrum (Figure 2.2A) is consistent with the presence of [4Fe-4S] (Fe/S) clusters. In

order to verify the presence of Fe/S clusters and accurately determine their nature and stoichiometry, anaerobically isolated NadA was characterized using a combination of Mössbauer and EPR spectroscopies, and chemically analyzed for its iron and sulfide content.

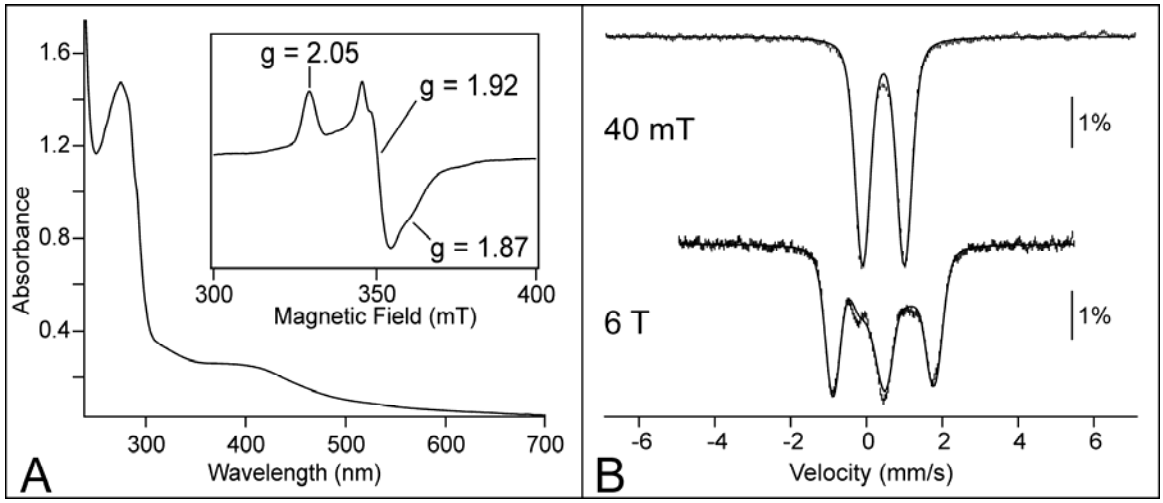

Figure 2.2: (A) UV-visible Spectrum of as-isolated NadA. (B) Mössbauer spectrum of as-isolated NadA. (A-inset) EPR spectrum of as-isolated NadA.

The Mössbauer spectrum (Figure 2B, top spectrum, hash marks), obtained at 4.2 K and 40 mT, is a broad quadrupole doublet with parameters that are typical of a $[4Fe\text{-}4S]^{2+}$ cluster species; the isomer shift (δ) is 0.45 mm/s and the quadrupole splitting parameter (ΔE_Q) is 1.10 mm/s (Figure 2.2B, top spectrum, solid line). The spectrum recorded in a 6-T parallel magnetic field (Figure 2.2B, bottom spectrum) can be simulated assuming a diamagnetic (S = 0) ground state, thereby corroborating the assignment of the quadrupole doublet to a $[4Fe\text{-}4S]^{2+}$ cluster species. The EPR spectrum of anaerobically isolated NadA (not shown) reveals the presence of a small amount (< 1% of total Fe) of a $[3Fe\text{-}4S]^{+}$ cluster species, which is beyond the detection limit of

Mössbauer spectroscopy. The protein contains 5.0 ± 1.4 Fe and 2.8 ± 0.3 S^{2-} per polypeptide (average and standard deviation obtained from four independent determinations). Taken together, the data suggest a stoichiometry of one [4Fe-4S] cluster per polypeptide.

Reconstitution of NadA with additional iron and sulfide under anaerobic conditions followed by anaerobic gel-filtration chromatography results in 7.6 ± 0.9 Fe and 5.7 ± 0.5 S^{2-} per polypeptide. Analysis of the reconstituted protein by Mössbauer spectroscopy (data not shown), however, reveals that only 40 ± 5% of the associated iron is in the form of $[4Fe\text{-}4S]^{2+}$ clusters, corresponding to a stoichiometry of 3.1 ± 0.7 irons per polypeptide in this configuration. Moreover, EPR analysis of reconstituted NadA in the absence of dithionite reduction reveals the presence of 0.1 equiv of $[4Fe\text{-}4S]^{+}$ clusters per polypeptide, corresponding to 0.4 Fe per polypeptide in this configuration. Therefore, the total stoichiometry of $[4Fe–4S]^{+,2+}$ clusters on reconstituted NadA is ~0.85 ± 0.20 per polypeptide, demonstrating that despite the presence of nine cysteines on the protein, the total number of clusters on the protein does not exceed one per polypeptide. The EPR spectrum of dithionite-reduced NadA is broad (Figure 2A, inset), and broadens further to the extent of being almost unobservable at temperatures above 50 K, consistent with its assignment as a $[4Fe–4S]^{+}$ cluster species. Spin quantification indicates that the signal accounts for 0.6 equiv of spin per polypeptide. Very little perturbation of the spectrum was observed in the presence of dihydroxyacetone phosphate or oxaloacetate, a mimic of IS, or a combination of both compounds.

The ability of both as-isolated and reconstituted NadA proteins to catalyze formation of quinolinic acid was assessed by HPLC using authentic quinolinic acid as a

standard. IS, a required but unstable substrate for NadA, has a half-life of 2.5 min at 37°C and pH 8.0,[13] and therefore was generated from *L*-aspartate by action of NadB, using fumarate as the electron acceptor. At pH 7.5 and 37°C, the reconstituted enzyme catalyzed formation of quinolinic acid with a specific activity of 0.015 μmol min^{-1} mg^{-1} (V_{max} $[E_T]^{-1}$ = 0.01 s^{-1}) in an assay that was linear over 20 min (data not shown). IS could also be generated nonenzymatically via Schiff's base formation between oxaloacetate and NH_3, added to the reaction mixture as $(NH_4)_2SO_4$;[13] however, the rate of quinolinic acid formation was 5-fold slower. In order to verify that quinolinic acid was indeed formed in the assay, the relevant peak from the HPLC chromatogram was collected and derivatized to allow for analysis by GC-MS. Peaks corresponding to silylated quinolinic acid and silylated nicotinic acid were observed. Nicotinic acid is a known decomposition product of quinolinic acid, which forms under the conditions of the derivatization procedure [14]. Although the apparent turnover number of the enzyme is low, it is significantly faster than the turnover number observed for the rate-limiting step in the biosynthesis of quinolinic acid via the degradation of L-tryptophan, which appears to be a nonenzymatic conversion of 2-amino-3-carboxymuconic semialdehyde to the final product via a pericyclic reaction (k = 1.8 x 10^{-4} s^{-1} – 2.0 x 10^{-3} s^{-1}) [15, 16].

Our results appear to be at variance with a previously published study, in which recombinant NadA was isolated from inclusion bodies.[9] The inclusion bodies were subsequently resolubilized, purified, and refolded in the absence of added iron, affording protein that was purported to catalyze formation of quinolinic acid with a specific activity of 0.6 U mg^{-1} in the presence of EDTA, wherein one unit was defined as the amount of protein catalyzing the production of 1 mmol of NADPH per min in the assay. Given the

amount of protein (60 μg) employed in the assay and the concentration of the limiting reagent (DHAP, 1 mM), we estimate that all of the substrate would have been consumed in much less than one minute; however, the assay was conducted over a time period of 45 min. Presumably this is simply a typographical error; however, we cannot yet draw firm comparisons between our differing activities in the absence of the true unit definition.

Two mechanisms that account for the synthesis of quinolinic acid from the condensation of DHAP and IS have been advanced, both involving the formation of species **1** (Figure **2.3**) as the direct precursor to quinolinic acid (species **2**) [3, 8]. We propose that this dehydration, which is similar to those carried out by Fe/S-containing enzymes within the hydro–lyase family,[17] is facilitated by coordination of the hydroxyl group to one of the irons of the [4Fe–4S] cluster.

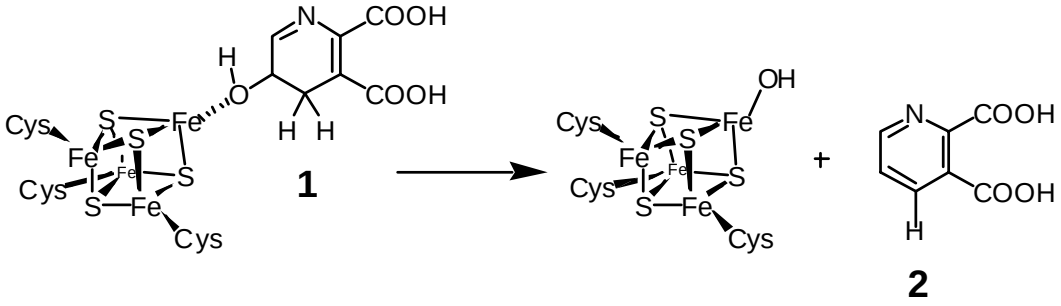

Figure 2.3**:** Proposed role for the [4Fe-4S] cluster in quinolinic acid formation.

The presence of distinctly different pathways in most prokaryotes and eukaryotes for the biosynthesis of quinolinic acid suggests that NadA might prove to be a key target for the design of antibacterial agents. The studies described herein show clearly that the enzyme can be obtained in sufficient amounts for both biochemical and spectroscopic characterization when handled under anaerobic conditions.

B.4 References

1. Magni, G., A. Amici, M. Emanuelli, N. Rafaelli, and S. Ruggieri, Enzymology of NAD^+ synthesis. *Adv. Enzymol. Relat. Areas Mol. Biol.*, 1999. **73**: p. 135-182.
2. Kurnasov, O., V. Goral, K.L. Colabroy, S. Gerdes, S. Anantha, A. Osterman, and T.P. Begley, NAD biosynthesis: identification of the tryptophan to quinolinate pathway in bacteria. *Chem. Biol.*, 2003. **10**: p. 1195-1204.
3. Begley, T.P., C. Kinsland, R.A. Mehl, A. Osterman, and P. Dorrestein, The biosynthesis of nicotinamide adenine dinucleotides in bacteria. *Vitamins Hormones*, 2001. **61**: p. 103-119.
4. Penfound, T. and J.W. Foster, *Biosynthesis and recycling of NAD*, in *Escherichia coli and Salmonella*, F.C. Neidhardt, Editor. 1996, American Society for Microbiology: Washington D. C. p. 721-730.
5. Tedeschi, G., N. Rafaelli, T. Simonic, C. Treu, A. Mattevi, and A. Negri, Probing the active site of *L*-aspartate oxidase by site-directed mutagenesis: role of basic residues in fumarate reduction. *Biochemistry*, 2001. **40**: p. 4738-4744.
6. Bossi, R.T., A. Negri, G. Tedeschi, and A. Mattevi, Structure of FAD-bound *L*-aspartate oxidase: insight into substrate specificity and catalysis. *Biochemistry*, 2002. **41**: p. 3018-3024.
7. Mortarino, M., A. Negri, G. Tedeschi, T. Simonic, S. Duga, H.G. Gassen, and S. Ronchi, *L*-Aspartate oxidase from *Escherichia coli*. I. Characterization of coenzyme binding and product inhibition. *Eur. J. Biochem.*, 1996. **239**: p. 418-426.

8. Nasu, S., F.D. Wicks, and R.K. Gholson, *L*-Aspartate oxidase, a newly discovered enzyme of *Escherichia coli*, is the B protein of quinolinate synthetase. *J. Biol. Chem.*, 1982. **257**(2): p. 626-632.

9. Ceciliani, F., T. Camori, S. Ronchi, G. Tedeschi, M. Mortarino, and A. Galizzi, Cloning, overexpression, and purification of *Escherichia coli* quinolinate synthetase. *Prot. Express. Purif.*, 2000. **18**: p. 6-70.

10. Flachmann, R., N. Kunz, J. Seifert, M. Gutlich, F.J. Wientjes, A. Laufer, and G. Gassen, Molecular biology of pyridine mucleotide biosynthesis in *E. coli*: cloning and characterization of quinolinate synthesis gene *nadA* and *nadB*. *Eur. J. Biochem.*, 1990. **175**: p. 221-228.

11. Lauhon, C.T. and R. Kambampati, The *iscS* gene in *Escherichia coli* is required for the biosynthesis of 4-thiouridine, thiamin, and NAD. *J. Biol. Chem.*, 2000. **275**(26): p. 20096-20103.

12. Cicchillo, R.M., D.F. Iwig, A.D. Jones, N.M. Nesbitt, C. Baleanu-Gogonea, M.G. Souder, L. Tu, and S.J. Booker, Lipoyl Synthase Requires Two Equivalents of S-Adenosyl-L-Methionine to Synthesize One Equivalent of Lipoic Acid. *Biochemistry*, 2004. **43**: p. 6378-6386.

13. Nasu, S. and R.K. Gholson, Replacement of the B protein requirement of the *E. coli* quinolinate synthetase system by chemically-generated iminoaspartate. *Biochem. Biophys. Res. Commun.*, 1981. **101**(2): p. 533-539.

14. McDaniel, H.G., An improved method for measuring quinolinic acid in biological specimens. *Methods Enzymol*, 1980. **66**: p. 91-95.

15. Keys, I.L.D. and G.A. Hamilton, The mechanism for the conversion of α-amino-β-carboxymuconate ε-semialdehyde to quinolinate, an apparent nonenzymic step in the biosynthesis of the nicotinamide coenzymes from tryptophan. *J. Am. Chem. Soc.*, 1987. **109**: p. 2156-2163.

16. Colabroy, K.L. and T.P. Begley, The pyridine ring of NAD is formed by a nonenzymatic pericyclic reaction. *J. Am. Chem. Soc.*, 2005. **127**: p. 840-841.

17. Flint, D.H. and R.M. Allen, Iron–sulfur proteins with nonredox functions. *Chem Rev*, 1996. **96**(7): p. 2315-2334.

VITA

Robert M. Cicchillo (Ph.D.)

Education: Youngstown State University, Youngstown, Ohio 44555, **B.S. Biology**, 1998

Youngstown State University, Youngstown, Ohio 44555, **M.S. Chemistry**, 2000

The Pennsylvania State University, University Park, Pennsylvania 16802, **Ph.D.** (2006)

Youngstown State University**:**

Undergraduate Research Training - Molecular Biology (B.S.)

Synthesis of Sugar Derived *C*-Glycosides *via* Dithiane Chemistry (M.S.)

The Pennsylvania State University**:** Biochemical, Biophysical, and Mechanistic Investigations of Lipoyl Synthase from *Escherichia coli*: A Member of the "Radical SAM" Family of Enzymes. (Ph.D.)

Publications:

1. **Cicchillo R.M.**, Tu L., Stromberg, J.S., Hoffart L.M., Krebs, C., and Booker S.J. (2005) *Escherichia coli* Quinolinate Synthetase Does Indeed Harbor a [4Fe–4S] Cluster. *J. Am. Chem. Soc.* 127 (20): 7310-7311.
2. **Cicchillo R.M.** and Booker S.J. (2005) Mechanistic Investigations of Lipoic Acid Biosynthesis in Escherichia coli: Both Sulfur Atoms in Lipoic Acid are Contributed by the Same Lipoyl Synthase Polypeptide. *J. Am. Chem. Soc.* 127(9): 2860-2861.
3. Nesbitt N.M., Baleanu-Gogonea C., **Cicchillo R.M.**, Goodson K., Iwig D.F., Broadwater J.A., Haas J.A., Fox B.G., Booker S.J. (2005) Expression, Purification, and Physical Characterization of *Escherichia coli* Lipoyl(Octanoyl) Transferase. *Protein Expr. Purif.,* 39(2):269-82.
4. **Cicchillo R.M.**, Baker M.A., Schnitzer E.J., Newman E.B., Krebs C., Booker S.J. (2004) *Escherichia coli L*-Serine Deaminase Requires a [4Fe-4S] Cluster in Catalysis. *J. Biol Chem.* 279, 32418-25.
5. **Cicchillo R.M.**, Lee K.H., Baleanu-Gogonea C., Nesbitt N.M., Krebs C., Booker S.J. (2004) *Escherichia coli* Lipoyl Synthase Binds Two Distinct [4Fe-4S] Clusters per Polypeptide. *Biochemistry*, 43, 11770-81.
6. **Cicchillo R.M**., Iwig D.F., Jones A.D., Nesbitt N.M., Baleanu-Gogonea C., Souder M.G., Tu L., Booker S.J. (2004) Lipoyl Synthase Requires Two Equivalents of S-adenosyl-*L*-Methionine to Synthesize One Equivalent of Lipoic Acid. *Biochemistry*, 43, 6378-86.
7. McCartney J.L., Meta C.T.**, Cicchillo R.M.**, Bernardina M.D., Wagner T.R., Norris P. (2003) Addition of Lithiated C-Nucleophiles to 2,3-O-isopropylidene-D-erythronolactone: Stereoselective Formation of a Furanose *C*-disaccharide. *J. Org. Chem.*, 68, 10152-5.
8. **Cicchillo R.M.**, Norris P. (2000) A convenient synthesis of glycosyl chlorides from sugar hemiacetals using triphosgene as the chlorine source. *Carbohydr. Res.*, 328, 431-4.

Awards: NSF-RTG Travel Award (2002) and The Pennsylvania State Alumni Dissertation Award (2006)